Investigating the Roles of Zinc Finger Homeobox Gene 3 in Circadian Rhythms

Jessica Kate Edwards (BA Oxon.)

Magdalen College

The Nuffield Laboratory of Ophthalmology

Medical Sciences Division

University of Oxford

Mammalian Genetics Unit, Medical Research Council, Harwell

A thesis submitted for the degree of Doctor of Philosophy

Michaelmas 2012

Abstract

This thesis describes a program of investigation carried out by the author at MRC Harwell that shows, for the first time, that the gene *Zfhx3* plays a role in modulating the circadian clock. The work has used the short circuit (*Sci*) mouse model to assess the molecular and genetic role of *Zfhx3* in circadian behaviour and visual processing.

The *Sci* mutant was identified in an ENU mutagenesis dominant screen at MRC Harwell. The causative mutation was found in a highly conserved region of zinc finger homeobox 3 (*Zfhx3*), previously not known to play a role in the function of the circadian clock.

This study has shown that *Zfhx3* RNA is specifically expressed in the adult SCN. Additionally, co-immunoprecipitation has shown that ZFHX3 can interact with core clock proteins, CRY1, CRY2 and PER2 and the *Sci* mutation causes differential effects on the RNA expression of *Cry1, Cry2* and *Per1*. Genetic interaction experiments identified an interaction between *Sci* and *Cry2* under constant darkness and a potential interaction between *Sci* and *Cry1* and *Cry2* under constant light. Together, these data indicate that *Zfhx3* has a role in modulating the core circadian oscillator, in particular through cryptochromes.

A role for *Zfhx3* has also been identified in visual processing and retinal function. *Zfhx3* RNA was shown to be highly expressed in the ganglion, inner and outer nuclear layers of the retina. *Sci* mutants have increased retinal sensitivity by 20 fold, which may be attributed to a decrease in GABA neurotransmission in the retina.

From this study, novel functions for *Zfhx3* within the circadian and visual systems have been identified. This exemplifies that molecular components of the circadian oscillator may remain to be identified and forward genetic approaches are facilitating advancements in this field.

Acknowledgements

First I would like to take this opportunity to express my sincere thanks to Dr Patrick Nolan for the opportunity to work within his lab on this exciting project. To work within his lab at MRC Harwell has been a wonderful opportunity and privilege. I have been able to learn new and challenging techniques, develop many scientific and personal skills and importantly make extremely valuable friendships which will remain with me into the future.

I would like to thank everyone I have worked with during the course of producing this thesis, especially all members of the neurobehavioural and neurodegeneration labs. Everyone has contributed to my enjoyment in working at Harwell and producing the data that has formed this thesis – both on a personal and professional level. I would also like to thank Professor Russell Foster for his external supervision of my thesis and the members of his laboratory, in particular Dr Stuart Peirson, who have made an enormous contribution to this work.

I would like to thank the Medical Research Council, Oxford University and Magdalen College for their funding and support of my DPhil. I have spent 8 very enjoyable years with Oxford University, and have been very fortunate to complete both my Bachelors degree and DPhil with Magdalen. I am very grateful that my DPhil has enabled me to travel to exciting conferences in Poland, Switzerland, San Diego and Florida where I have had the opportunity to present my work, meet new people and experience new places.

I would like to acknowledge the vital contribution of all my family and friends. They have given me constant love and support throughout. They have all given me endless motivation and enthusiasm and their involvement has been essential in my enjoyment of these last 4 years of this DPhil. A final special thank you goes to my husband Tom, who has supported, helped and encouraged me throughout, as we worked alongside each other at MRC Harwell.

Contents

Abstract i

Contents iii

List of Tables x

List of Figures xii

Chapter I xv

Introduction xv

1.1. Circadian Rhythms 1

1.1.1. Introduction 1

1.1.2. Circadian rhythms are endogenously generated 2

1.1.3. Entrainment of circadian rhythms 4

1.1.4. Mammalian Photoreceptors and Identification of Melanopsin 6

1.1.5. Synaptic Input to the SCN 7

1.1.6. Molecular basis of the circadian clock 10

1.1.7. Mammalian circadian oscillator 11

1.1.8. Temperature compensation of the circadian clock 14

1.2. ENU mutagenesis and mouse genetics 16

1.2.1. The mouse as a model organism in behavioural research 16

1.2.2. Forward genetics 17

1.2.3. Clock knock-out vs Clock ENU point mutation 19

1.2.4. ENU mutagenesis dominant and recessive screens 20

1.2.5. Screening ENU mutants for circadian phenotypes 23

1.2.6. Mapping and cloning of ENU mutations 26

1.2.7. Reverse genetics 27

1.3. Zinc Finger Homeobox 3 28

1.3.1. Identification of Zfhx3, structure and function 28

1.3.2. Conservation of *Zfhx3* 31

1.3.3. Known functions of *Zfhx3* 33

1.3.4. *Zfhx3* and disease 36

1.3.5. Other *Zfhx3* mutants 38

1.3.6. Conclusions 39

Chapter II 41

Materials and Methods 41

2. Materials and Methods 42

2.1. Materials List 42

2.2. Buffers and Solutions 46

2.3. Primers 49

2.4. Antibodies 51

2.5. Plasmids 52

2.6. Methods 53

2.6.1. Animal Husbandry 53

2.6.2. Circadian Behavioural Phenotyping 53

2.6.3. Startle and Pre-Pulse Inhibition 54

2.6.4. Pupilometry 55

2.6.5. Optokinetic Drum 56

2.6.6. Genotyping 56

2.6.7. Agarose gel electrophoresis 60

2.6.8. Protein Extraction 61

2.6.9. Protein Quantification 62

2.6.10. Immuno-precipitation 62

2.6.11. SDS-PAGE 63

2.6.12. Western Blotting 64

2.6.13. HRP Chemi-luminescence Detection 64

2.6.14. Culture of Adherent Cell Lines: Hek293, Cos7 and U2OS 65
2.6.15. Culture and differentiation of P19 cells 65
2.6.16. Freezing Cells for Storage 66
2.6.17. Counting and Plating Cells 67
2.6.18. Transfection of Cell Lines 67
2.6.19. Isolation and culture of Mouse Embryonic Fibroblasts (MEFs) 68
2.6.20. Stable isotope labelling by amino acids in cell culture (SILAC) 68
2.6.21. Nuclear and Cytoplasmic Fractionation and Protein Extraction 69
2.6.22. Immuno-fluorescence 70
2.6.23. Tissue Collection 70
2.6.24. RNA Extraction 71
2.6.25. cDNA Synthesis 72
2.6.26. Generation of Riboprobe Template by PCR 72
2.6.27. QIAGEN Gel Extraction and PCR Purification 74
2.6.28. Preparation of Lysogeny Broth (LB) plates for bacterial growth 75
2.6.29. TOPO™ Cloning 75
2.6.30. Transformation in Escheria Coli 76
2.6.31. Plasmid Purification 76
2.6.32. DIG Labelled RNA Riboprobe Synthesis 78
2.6.33. *In Situ* Hybridisation 81
2.6.34. Haematoxylin and eosin (H&E) staining 82
2.6.35. Expression and purification of HIS tagged proteins 82
Chapter III 85
Characterisation of the Short Circuit Circadian Phenotype 85
3. Short circuit Circadian Phenotype 86
3.1. Introduction 86
3.2. Circadian wheel running activity of Short circuit Mutants 91

3.3. Phase shifting and light pulses 95
3.4. Entrainment under dim light-dark cycles 100
3.5. Discussion 108
3.5.1. Identification of short circuit 108
3.5.2. Short circuit Wheel Running Phenotyping 109
3.5.3. Circadian phenotypes detected under light conditions 111
3.5.4. Conclusions 117
Chapter IV 119
Molecular Characterisation of *Zfhx3* 119
4. *Zfhx3* molecular characterisation 120
4.1. Introduction 120
4.2. RNA expression analysis 121
4.2.1. RT-PCR expression studies 121
4.2.2. *In situ* hybridisation in the adult SCN 123
4.2.3. *In situ* hybridisation in embryonic development 125
4.3. Over-expression and Co-immuno-precipitation 127
4.4. ZFHX3 protein expression 135
4.5. Stable Isotopically Labelled Amino Acids in Cells Culture assay 148
4.6. Discussion 155
4.6.1. RNA expression 155
4.6.2. Protein interactions 158
4.6.3. Protein expression 160
4.6.4. Conclusions 165
Chapter V 167
***Sci*^{Zfhx3} Genetic Interaction with Cryptochromes** 167
5. *Zfhx3* interaction with cryptochromes 168
5.1. Introduction 168

5.2. Generation of *Sci ; Cry1* and *Sci ; Cry2* Double Mutants 169

5.3. *Sci ; Cry1* Circadian Phenotype in Constant Darkness 173

5.4. *Sci ; Cry1* Circadian Phenotype in Constant Light 177

5.5. *Sci ; Cry2* Circadian Phenotype in Constant Dark 180

5.6. *Sci ; Cry2* Circadian Phenotype in Constant Light 184

5.7. Discussion 187

5.7.1. Purpose of this chapter 187

5.7.2. Hypotheses 188

5.7.3. *Zfhx3*$^{Sci/+}$ *; Cry1*$^{-/-}$ and *Zfhx3*$^{Sci/+}$ *; Cry2*$^{-/-}$ double mutant phenotypes 192

Chapter VI 196

Characterisation of Ophthalmological Phenotypes and Functions of *Zfhx3* in the Visual System 196

6. *Zfhx3* Interaction with the Visual System 197

6.1. Introduction 197

6.2. *Zfhx3* expression in the adult eye 199

6.2.1. *In situ* hybridisation 199

6.2.2. Retinal RNA expression analysis by quantitative real-time PCR 202

6.2.3. Startle and Pre-pulse Inhibition Assessment 207

6.3. Morphological analysis of *Sci* eyes 214

6.3.1. Retinal Histology 214

6.3.2. Corneal histological assessment 219

6.4. Visual and image forming capabilities in *Sci* animals 224

6.4.1. Slit lamp, ophthalmoscope and optokinetic drum head tracking 224

6.4.2. Pupillary Response of *Sci* Animals 229

6.4.3. Electroretinogram assessment in *Sci* animals 233

6.5. Discussion 236

6.5.1. Expression analysis 237

6.5.2. Corneal dystrophy and associated phenotypes 240
6.5.3. Pupilometry and ERG phenotypes 243
6.5.4. Conclusions 245
Chapter VII 247
Discussion 247
7. Introduction 248
7.1. Summary of main aims 248
7.2. Summary of the main results 248
7.3. Short circuit Phenotype 251
7.3.1. Short circadian period and reduced circadian amplitude 251
7.3.2. Post-transcriptional modification by ZFHX3 on the circadian clock 252
7.3.3. Transcriptional manipulation by ZFHX3 on circadian clock gene expression 253
7.4. Phenotypes under altered lighting conditions 255
7.4.1. Effects of *Zfhx3* on photic signalling cascades to the SCN 255
7.4.2. Involvement of *Zfhx3* in retinal neurotransmission 258
7.4.3. *Zfhx3* as a candidate gene for Keratoconus phenotypes 260
7.4.4. *Sci* mutants display less plasticity of the SCN in responses to light 261
7.4.5. Involvement of *Zfhx3, Cry1* and *Cry2* in light mediated circadian responses 262
7.5. Wider roles of *Zfhx3* 264
7.5.1. Retinoic acid signalling and Hox gene expression 265
7.5.2. *Zfhx3* functions in DNA damage responses through ATM signalling 266
7.5.3. Circadian control of the cell cycle through *Zfhx3* signalling 268
7.5.4. Circadian responses to genotoxic and chemotoxic stress 270
7.6. Future work 271
7.6.1. Protein based studies 271
7.6.2. Transcriptional-based assays 272
7.6.3. Alternative models and mutant resources 272

7.7. Final Conclusions 274

Chapter VIII 276

Bibliography 276

List of Tables

Table 1: Description of the annotated domains and motifs identified within the *Zfhx3* transcript. 30

Table 2: Short circuit PCR genotyping set up. 57

Table 3: Short circuit genotyping RT-PCR thermal cycling conditions. 58

Table 4: *Cry2* PCR genotyping set-up. 59

Table 5: *Cry2* genotyping PCR thermal cycling conditions. 59

Table 6: *Per2-Luc* PCR genotyping set-up. 60

Table 7: *Per2-Luc* genotyping PCR thermal cycling conditions. 60

Table 8: Immuno-fluorescence protocol. 70

Table 9: cDNA synthesis reaction set-up 72

Table 10: cDNA synthesis thermal cycling. 72

Table 11: Primer sequences used for *Zfhx3* riboprobe synthesis. 73

Table 12: PCR reaction mix for riboprobe synthesis. 73

Table 13: Thermal cycling conditions for riboprobe synthesis PCR. 73

Table 14: Gel extraction and PCR purification protocol. 74

Table 15: TOPO cloning protocol. 75

Table 16: QIAGEN miniprep plasmid purification. 77

Table 17: QIAGEN midi prep plasmid purification. 78

Table 18: Restriction digest of plasmid DNA. 79

Table 19: DIG labelled riboprobe transcription reaction. 80

Table 20: Calculated period length (τ) in hours at “lights off” during entrainment. 103

Table 21 A-C: Phase angle calculations of entrainment at 10 lux (lights off at 7pm) 105

Table 22: Calculation of Alpha (α) as a measure of total length of activity during 12:12 LD cycle at 10 lux) 106

Table 23: Top associated networks across all SILAC experimental conditions. 150

Table 24: Top associated diseases across all SILAC experimental conditions. 151

Table 25: Top molecular and cellular functions across all SILAC experimental conditions. 152

Table 26: Top associated canonical pathways across all SILAC experimental conditions.. 154

Table 27: Punnett square cross for *Sci ; Cry1* original outcross. 170

Table 28: Punnett square cross for *Sci ; Cry1* double heterozygote intercross. 171

Table 29: Punnett square cross for *Sci ; Cry1* double heterozygote backcross to homozygous $Cry^{-/-}$ knock-out..... 172

Table 30: Total number of double mutant animals and litter mate controls obtained from *Sci ; Cry* crosses..... 173

Table 31: Period length (hours) recorded for all *Sci ; Cry1* animals analysed by monitoring wheel running activity..... 175

Table 32: 2 way ANOVA to test for an interaction between *Sci* and *Cry1* based upon τDD..... 177

Table 33: Distribution of behaviours under constant light in *Sci ; Cry1* mutants. 179

Table 34: Period length (hours) recorded for all *Sci ; Cry2* animals analysed by monitoring wheel running activity..... 182

Table 35: 2 way ANOVA to test for an interaction between *Sci* and *Cry2* based upon τDD..... 184

Table 36: Distribution of behaviours under constant light in *Sci ; Cry2* mutants 185

Table 37: Comparison of the startle reflex response between $Zfhx3^{+/+}$ and $Zfhx3^{Sci/+}$.. 209

Table 38: Raw data for the startle reflex response to a 110 dB tone with or without being preceded by a pre-pulse. 211

Table 39: Pre-pulse inhibition calculated as a percentage of the initial startle response..... 212

Table 40: Combined data of INL and ONL retinal thickness and INL:ONL ratio in Sci animals..216

Table 41: Comparison of corneal thickness from H&E stained adult eye sections..... 221

Table 42: Visual acuity (cycles/degree ; c/d) of each eye in $Zfhx3^{+/+}$ and $Zfhx3^{Sci/+}$ animals..... 227

List of Figures

Figure 1: Photic phase response curve. 5

Figure 2: Neurotransmission at the pre/postsynaptic neuron in response to a light induced action potential from the retino-hypothalamic tract. 8

Figure 3: Schematic of neural efferents and afferents of the SCN. 9

Figure 4: General requirements of a transcriptional / translational molecular oscillator. 11

Figure 5: Schematic of the molecular basis of the mammalian circadian oscillator 14

Figure 6: ENU mutagenesis breeding scheme. 22

Figure 7: Representative double plotted actogram of circadian wheel running activity of a wild-type mouse 25

Figure 8: Schematic of the ZFHX3 transcript. 29

Figure 9: Identification and preliminary wheel running characterisation of the *Sci* mutant 88

Figure 10: Location and conservation of the *Sci* mutation in *Zfhx3*. 90

Figure 11: *Sci* circadian phenotype assessed by wheel running activity 93

Figure 12: Actograms of three representative animals screened for ability to phase shift in response to an acute light pulse.. 97

Figure 13: Generation of *Sci* phase response curve. 98

Figure 14: Representative actograms for $Zfhx3^{+/+}$ and $Zfhx3^{Sci/+}$ under shifted 12:12 LD cycles with increasingly scotopic light intensities. 102

Figure 15: Bar chart representation of period length at “lights off” during entrainment of $Zfhx3^{+/+}$ and $Zfhx3^{Sci/+}$ animals at 100 lux, 10 lux and 1 lux.. 104

Figure 16: Analysis of duration of activity during a 12:12 light dark cycle, with 10 lux light intensity 106

Figure 17: Representative actograms of *Sci* animals screened for ability to shift activity in response to a shifted 12:12 light-dark cycle at lowering levels of light intensity. 107

Figure 18: RNA expression pattern of *Zfhx3* and known clock genes in $Zfhx3^{+/+}$ and $Zfhx3^{Sci/+}$ liver 122

Figure 19: *In situ* hybridisation on *Sci* SCN using a *Zfhx3* DIG-labelled riboprobe 124

Figure 20: *In situ* hybridisation on whole and sectioned mouse WT embryos using a DIG labelled *Zfhx3* riboprobe. 126

Figure 21: Co-immuno-precipitation reactions between ZFHX3 and known clock proteins. ... 130

Figure 22: Co-localisation and FRET between MYC-ZFHX3 and CRY2-HA, over-expressed in HEK293 cells. ... 131

Figure 23: Sub-cellular co-localisation of ZFHX3 and CRY2 within the nuclei of HEK293 cells.. 133

Figure 24: Location of peptide sequences generated for antibody production within the ZFHX3 amino acid sequence. ... 136

Figure 25: Co-immunofluorescence of U2OS cells transfected with *Zfhx3*-HA full length human construct and labelled with α-HA and α-ZFHX3.. ... 137

Figure 26: Detection of ZFHX3 in transfected cell lines by western blotting. ... 138

Figure 27: Detection of ZFHX3 in undifferentiated and retinoic-acid differentiated P19 cells. ... 139

Figure 28: Detection of ZFHX3 in adult tissues across ZT points. ... 140

Figure 29: Detection of ZFHX3 in embryonic tissue across developmental stages 12.5 dpc – 16.5dpc ... 142

Figure 30: Detection and identification of low molecular weight protein identified by α-ZFHX3. ... 144

Figure 31: Generation of purified antigenic peptide for α-ZFHX3 generation. ... 145

Figure 32: Western blot analysis on adult and embryonic tissue protein lysates using unpurified α-ZFHX3 sera from one injected rabbit. ... 146

Figure 33: A model of a signalling pathway from ATM to ZFHX3 required for activation of ATM in response to oxidative stress. ... 164

Figure 34: Representative actograms depicting the circadian phenotypes of *Sci ; Cry1* double mutants ... 174

Figure 35: Graphical representation of the period length in constant darkness for Sci-Cry1 mutants. ... 176

Figure 36: Representative actograms illustrating various behaviours under constant light conditions. ... 178

Figure 37: Bar chart of behaviours exhibited by *Sci ; Cry1* mutants under constant light conditions ... 180

Figure 38: Representative actograms depicting the circadian phenotypes of *Sci ; Cry2* double mutants. ... 181

Figure 39: Graphical representation of the period length in constant darkness for *Sci ; Cry2* mutants. 183

Figure 40: Bar chart of behaviours exhibited by *Sci ; Cry2* mutants under constant light conditions..... 186

Figure 41: Bioinformatic analyses of the 10kb region upstream of the promoters of known clock genes to identify putative *Zfhx3* AT motif binding sites.. 190

Figure 42: Schematic to illustrate the location of retinal and corneal *in situ* hybridisation images in relation to the entire eye. 200

Figure 43: RNA expression of *Zfhx3* in adult retina and cornea.. 201

Figure 44: Relative expression of mammalian opsins in *Sci* retinas.. 203

Figure 45: Comparison of relative expression of *Opn3* in the retina between $Opn4^{-/-}$ and *Sci* animals.. 204

Figure 46: Relative expression of retinal candidate genes in *Sci* retinas.. 206

Figure 47: Bar chart representation of the average startle response for $Zfhx3^{+/+}$ and $Zfhx3^{Sci/+}$. 210

Figure 48: Bar chart representation of the percentage pre-pulse inhibition. 213

Figure 49: Bright-field image taken of H&E stained whole eye section. 215

Figure 50: Representative images taken of $Zfhx3^{+/+}$ and $Zfhx3^{Sci/+}$ retinas on X20 objective. .. 215

Figure 51: Bar-chart comparison of INL and ONL between $Zfhx3^{Sci/+}$ and $Zfhx3^{+/+}$ retinas 217

Figure 52: Bar chart representation of INL: ONL ratio between $Zfhx3^{Sci/+}$ and $Zfhx3^{+/+}$ retinas. 218

Figure 53: Images taken of H&E stained corneas from *Sci* animals.. 220

Figure 54: Measurements of corneal thickness in *Sci* mutants. 222

Figure 55: Photograph of the Optokinetic drum and computer set up. 226

Figure 56: Comparison of visual acuity between $Zfhx3^{+/+}$ and $Zfhx3^{Sci/+}$ using the Optokinetic drum to monitor head tracking..... 228

Figure 57: Pupillary light reflex pathway. Arrow heads indicate the structure where axons terminate 230

Figure 58: Characterisation of the pupillary light reflex response in *Sci* animals. 232

Figure 59: Dark and light adapted electroretinogram (ERG) and flash visual evoked potential (VEP) recordings taken from *Sci* animals. 236

Chapter I

Introduction

1. Introduction

1.1. Circadian Rhythms

1.1.1. Introduction

The circadian system is a complex behavioural mechanism which has evolved across all light-sensitive organisms. It is a behaviour that has developed to allow organisms to anticipate changes in the environment in order to improve evolutionary fitness. Therefore under conditions of an entraining external environment (such as a daily light-dark cycle or temperature fluctuations), the benefits of possessing an endogenous circadian clock are highest.

The term "circadian" is derived from the Latin "*circa*" meaning "about" and "*diem*" meaning "day". This simply defines circadian rhythms as those which display an oscillation of approximately 24 hours. As early as the 1700's it was first recorded that circadian rhythms were endogenously generated and not a passive response to the external environment. In 1729, Jean-Jacque d'Ortous De Mairan, identified that heliotropism in *Mimosa pudica* persists under constant darkness and is not controlled by external light (De Mairan, 1729). De Mairan went on to discuss that experiments with other species should be conducted, with further manipulation of light-dark cycles and anticipated a link to human subjects with sleep-wake disorders. This preliminary work eventually precipitated studies into the field of "chronobiology" and the subsequent demonstration of the existence of an endogenous oscillator.

Further support for an endogenous circadian oscillator came from the identification that the "free-running" circadian period, that observed under constant conditions, deviated from 24 hours (Edmunds, et al. 1987). This deviation varied between individuals, species and

experimental conditions and this provided further corroboration that endogenous rhythms could exist without exogenous factors.

It is generally accepted that for a biological rhythm to be circadian, it must follow 4 general criteria: (1) the rhythm is endogenously generated, (2) the rhythm can be entrained by external cues such as light, temperature, food, (3) the period is approximately 24 hours, repeating once a day, (4) the rhythm can be compensated over a range of temperatures. These four criteria are discussed in more detail below.

1.1.2. Circadian rhythms are endogenously generated

Individual circadian clock cells are able to rhythmically persist in constant conditions, in the absence of all time cues. The genetic and molecular components which generate this 24 hour rhythm are well characterised and will be discussed in more detail. In order for these cells *in vivo* to be functional, they must all be coordinated such that they are individually synchronised in their phase of the circadian clock, although individual cells may fire out of phase from each other. The suprachiasmatic nucleus (SCN) of the hypothalamus is the site of the "master oscillator" in mammals. Here, ≈20,000 individual clock cells are orchestrated to produce an organised neuronal firing rate which in turn coordinates peripheral clocks in other tissues. The SCN therefore acts to produce a stable endogenous clock in both the core oscillator and peripheral tissues.

In the mouse, SCN neurogenesis occurs approximately five days before birth, in a ventrolateral to dorsomedial progression (VanDunk, et al. 2011). The mature SCN is a complex heterogeneous structure. In broad anatomical terms, the SCN comprises 2 major subdivisions – the dorsomedial SCN known as the "shell" and the ventrolateral SCN known as the "core" (Welsh, et al. 2010). The core and the shell can be defined based upon neurotransmitter and neuropeptide expression. The majority of neurons comprising the SCN shell use arginine

vasopressin (AVP) (Ingram, et al. 1998; Ingram, et al. 1996) and those of the core utilise vasoactive intestinal polypeptide (VIP) (Nagai, et al. 1996), gastrin releasing peptide (GRP) (Battey, et al. 1991; Battey and Wada 1991) and neuromedins (Mori, et al. 2005). The subdivisions of the SCN and the paired nuclei need to be synchronised with each other in order to produce a unified rhythm to synchronise peripheral oscillators. Cell-cell communication is required for a robust rhythm that is precise and resistant to perturbations (e.g. by temperature or genetic mutation). This is achieved through coupling mechanisms of the SCN neurons (Welsh, et al. 1995).

In comparison to the stable structure of the SCN, isolated SCN neurons in culture are visibly less robust, exhibiting a range of molecular periods and more variable rhythms (Herzog, et al. 2004; Welsh, et al. 1995). Dispersed SCN neurons from circadian mutants, such as *Per1*$^{-/-}$ or *Cry1*$^{-/-}$ have weak, low amplitude rhythms in culture. In comparison, the intact SCN from these mutants can preserve a more stable rhythm due to the coupling of these weakly rhythmic cells despite their genetic mutations (Liu, et al. 2007). The SCN as a whole uses coupling to provide local synchrony to set a common period amongst all oscillatory neurons (Colwell 2000). A number of neurotransmitters have been identified for their involvement in this process. The predominant neurotransmitters include VIP, GRP and GABA (gamma aminobutyric acid) – with VIP being the most abundant and well characterised in terms of SCN function and synchrony. Mice with down-regulated *Vip* or its associated receptor display weak rhythms in locomotor activity (Aton, et al. 2005; Colwell, et al. 2003; Harmar, et al. 2002). This is an indirect measure in which to monitor the intact synchronizer function of the SCN. A complete loss of VIP results in de-synchrony within the SCN and SCN organotypic explants are arrhythmic in culture (Brown, et al. 2007). Due to this coupling mechanism, the SCN is a less sensitive tissue to manipulate either genetically or by external signals, in comparison to peripheral tissues.

1.1.3. Entrainment of circadian rhythms

Circadian entrainment is utilised by organisms to adapt to an external environment to allow for maximal fitness and improve survival. Entrainment to an external cue (*zeitgeber*) results in coordinated activation of molecular and genetic events which ultimately drive changes in behaviour. Aschoff termed the word "*zeitgeber*" (German, meaning "time-giver") to describe the relationship between the endogenous oscillator and the variable external environment (Aschoff 1960). The endogenous oscillator will continually adjust to the *zeitgeber* on a 24 hour basis.

Adaptation, anticipation and economisation of energy-consuming processes are fundamental to natural selection and evolution and as proposed by Pittendrigh, evolved strategies of circadian entrainment provide a mechanism for this to occur (Daan 2000; Pittendrigh 1993). The circadian clock can be entrained by many factors, including temperature, food availability, predator/prey cycles, and social contact (Herzog and Huckfeldt 2003; Mendoza 2007; Mrosovsky 1988). Some of these *zeitgeber*s, such as food, are able to entrain an oscillator ("food entrainable oscillator") distinct from the master pacemaker itself (Carneiro and Araujo 2009), or temperature which is under both homeostatic (thermoregulatory) and circadian regulation. These listed factors have only a moderate influence on the circadian clock in comparison to the effects of external light on entrainment.

In circadian research, a phase-response curve (PRC) describes the relationship between the effects of a z*eitgeber* on the circadian clock and the time at which the z*eitgeber* is given (Decoursey 1960; Smeal, et al. 2010). Different z*eitgeber*s (such as light, food, exercise) have their own unique PRC due to their differential effects on the circadian clock (Minors, et al. 1991; Reebs and Mrosovsky 1989). Additionally, each species will have its own unique PRC (Golombek and Rosenstein 2010). With light as a z*eitgeber*, there are periods within the PRC where a light pulse may cause a phase delay, a phase advance or no effect at all. Producing a

PRC can therefore be used to study the sensitivity of the circadian system to light and the degree to which an organism responds to a light stimulus with a phase shift. In humans, exposure to light in the early subjective night will induce a phase delay, a later sleep onset and wake-up time. Exposure to light in the late subjective night will have the opposite effect and cause a phase advance, an earlier wake-up time and an earlier sleep onset. At other times during the circadian cycle, the effect of a light pulse is minimal (Minors, et al. 1991). This is depicted in the PRC diagram in Figure 1.

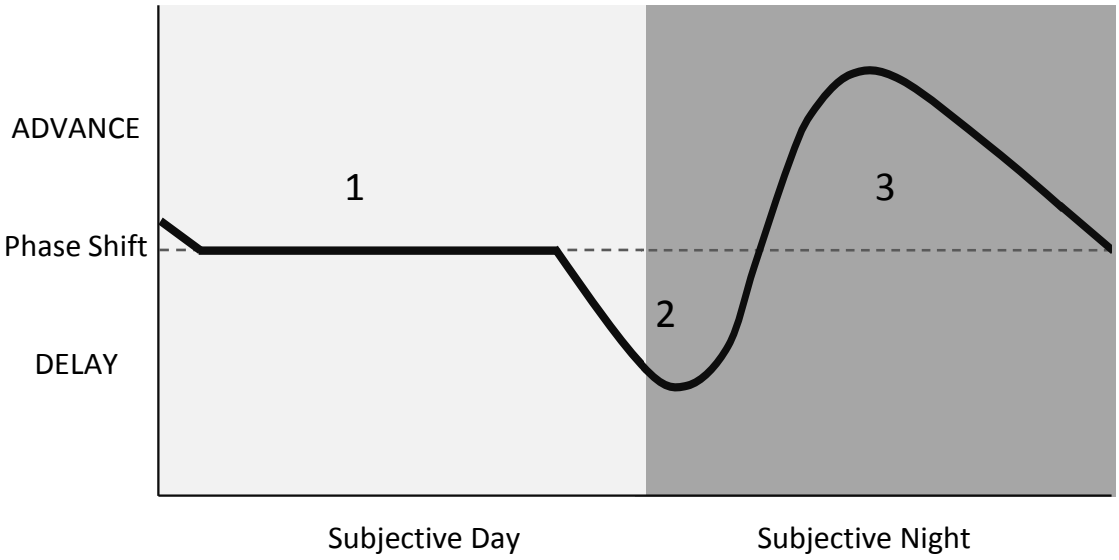

Figure 1: Photic phase response curve. A phase response curve depicts phase shifts in response to light, or any other *zeitgeber*, and is unique to each individual depending upon their "chronotype". The schematic represents a typical phase response curve to light exposure. During the subjective day (1) the effects of bright light exposure has little or no effect on the phase response curve, i.e. no phase shift occurs. As evening and night approaches (2), the effect of bright light exposure causes a phase delay. The result is a later sleep onset and sleep arousal time. This effect becomes stronger as the night progresses until approximately five hours into subjective night (3). At this point, the effect of bright light exposure reverses the effect on the phase response curve and causes phase advances. The result is an earlier arousal and earlier sleep onset. The point at which the PRC switches from phase delays to phase advances coincides with the lowest point in body temperature (Wehr, et al. 2001).

1.1.4. Mammalian Photoreceptors and Identification of Melanopsin

Light is one of the strongest *zeitgeber*s on the circadian clock and is dependent on a sophisticated visual system and photoreceptor signalling cascade to the SCN in mammals. The predominant pathway by which photic information is transmitted to the SCN is discussed in 1.1.5. Until the early 1990's, it was thought that rods and cones were the only photoreceptors in the mammalian eye. However, when mice with retinal degeneration (rd/rd) were observed to phase shift their circadian rhythms and display a pupillary reflex in response to external light stimuli, it became evident that another photoreceptor may exist to govern non-image forming visual processes (Foster, et al. 1991). These mice however did have a proportion of remaining functional cones which could have been sufficient for these responses. Transgenic mice lacking all rods and cones were generated to prove that they were not participating in the observed response (Freedman, et al. 1999). These animals were blind, lacking all image forming perception, however were still able to shift their circadian rhythms in response to light. Complete removal of the eye abolished this process as proof that there was an additional ocular-residing photoreceptor (Nelson and Zucker 1981). It was later that a novel opsin, melanopsin *(Opn4)*, was cloned and found to be expressed in distinct populations of the retinal ganglion cells (RGC's) (Provencio, et al. 2000). The axons of these cells project directly to the SCN, regulating circadian entrainment to light and the olivary pretectal nucleus (OPN), responsible for the pupillary reflex (Moore, et al. 1995). Other projections from the RGC's include afferents to the ventrolateral preoptic nucleus (VLPO) involved in sleep regulation.

This specific subclass of RGCs, *Opn4*-containing intrinsically photosensitive RGCs (ipRGC's), are thought to be common to all mammalian species. ipRGC's are most sensitive to irradiances at 480nm and in response to light, depolarize with characteristically slower kinetics than those of rod cells (Panda, et al. 2005; Van Hook and Berson 2010). This depolarization continues over a long period of time, allowing for a sustained response to bright light. Genetic deletion of *Opn4*

resulted in a loss of signal transduction from the ganglion cells retro-labelled from the SCN and subsequent deficiencies in the pupillary reflex and photoentrainment (Panda, et al. 2003).

1.1.5. Synaptic Input to the SCN

The SCN receives synaptic inputs from three major pathways which synchronise (entrain) the circadian oscillator. As previously discussed, the first and predominant pathway for circadian entrainment is through the ipRGC's via the retino-hypothalamic tract (RHT). Lesion studies have shown that the RHT is sufficient for circadian entrainment, or "circadian vision", as opposed to cognitive vision (Johnson, et al. 1988). Surgical transection of pathways leaving the optic chiasm results in blindness but individuals are still able to entrain to light. Lesions to the RHT however, do not affect vision but abolish circadian entrainment. This monosynaptic pathway predominantly uses the neurotransmitters and neuropeptides glutamate and pituitary adenylate cyclise-activating polypeptide (PACAP) which are released directly at the ventral SCN upon light stimulation at the retina (Ebling 1996). Light is relayed to the ipRGC's containing *Opn4*, via the photoreceptor cells (rods and cones) and interneuron's (amacrine and bipolar cells). The axons of the ipRGC's form the RHT which upon stimulation by light, release glutamate and PACAP onto the post-synaptic SCN neurons. Binding of these neurotransmitters to their receptors results in membrane depolarisation and an influx of Ca^{2+} (Wang, et al. 2008). This triggers a kinase cascade which results in the phosphorylation of CREB. Phosphorylated CREB activates immediate early genes (IEGs) including *Per1*, by binding CRE elements in IEG promoters. This leads to a shift in circadian phase of neural activity (Figure 2) (Shiromani, et al. 1995; Tischkau, et al. 2003). Approximately 40% of SCN neurons respond in this way and change in electrical excitability upon photic stimulation by the RHT (Golombek and Rosenstein 2010).

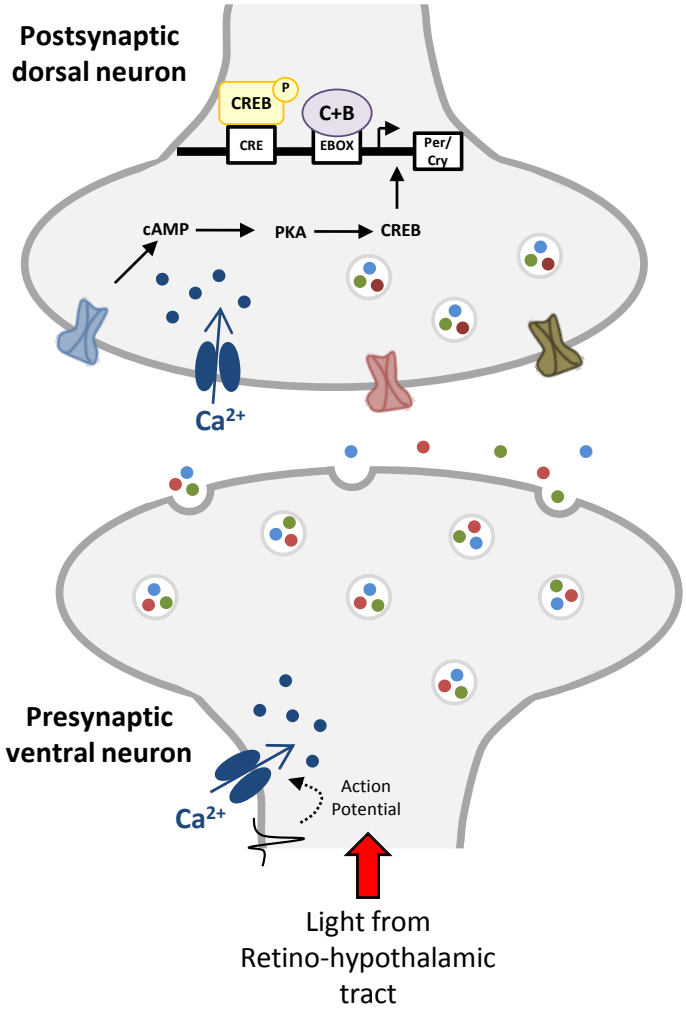

Figure 2: Neurotransmission at the pre/postsynaptic neuron in response to a light induced action potential from the retino-hypothalamic tract. Photic input from the RHT causes a change in action potential at the pre-synaptic ventral neurons of the SCN. Calcium influx into the pre-synaptic ventral neuron results in neurotransmitter release, including glutamate, PACAP, VIP, GABA and GRP. Binding of neurotransmitter to the corresponding receptor on the postsynaptic dorsal neuron membrane of the SCN shell occurs resulting in postsynaptic membrane depolarization and calcium influx. Elevated cAMP and the activation of a kinase cascade results in phosphorylation of CREB. Phosphorylated CREB binds CRE elements in gene promoter regions and activates IEG expression. (Figure adapted from Welsh, et al. 2010).

The geniculo-hypothalamic tract (GHT) and the raphe-hypothalamic pathway comprise the two other pathways inputting to the SCN. Both convey non photic and indirect photic information. The GHT connects the intergeniculate leaflet (IGL) to the SCN, with neuronal terminals overlapping in the same areas of the SCN as the RHT (Reghunandanan and

Reghunandanan 2006). The IGL receives direct input from the retina, and the GHT pathway relays some of this photic input indirectly to the SCN. Lesions to the GHT block activity induced phase-shifts, suggesting an important role in entrainment (Janik and Mrosovsky 1994). The raphe nuclei also receive retinal afferents to relay indirect photic input to the SCN. A reverse projection from the SCN to the raphe nuclei is also observed. Lesions to the raphe nuclei reduce the amplitude of the circadian molecular oscillation, but rhythmicity still remains. A schematic of these SCN afferents and efferents and neurotransmitters involved are shown in Figure 3.

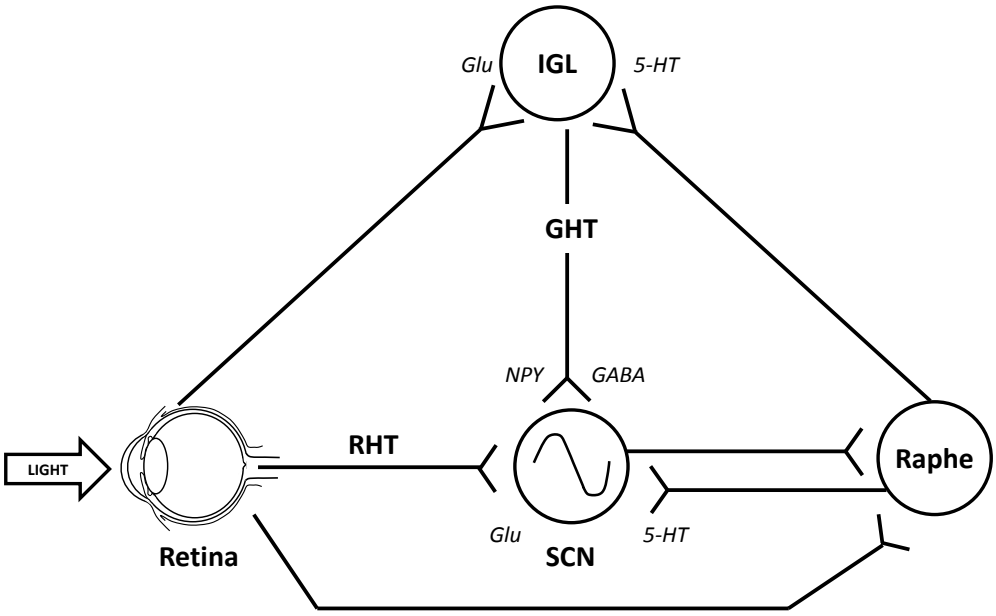

Figure 3: Schematic of neural efferents and afferents of the SCN. The RHT is the major entrainment pathway for photic input to the SCN, relaying light information directly from the retina. The RHT also projects to the IGL. Both these pathways predominantly use Glutamate (Glu) as their neurotransmitter. The GHT relays secondary photic information (originally from the retina) from the IGL. This pathway predominantly releases the neurotransmitter GABA and neuropeptide Y (NPY). The final major input to the SCN comes from the raphe nuclei. This pathway may also provide secondary photic information to the SCN due to an additional efferent from the retina to the raphe nuclei. Serotonin (5-HT) is the predominant neurotransmitter. Figure adapted from Ohdo 2010).

1.1.6. Molecular basis of the circadian clock

The molecular components of the circadian oscillator act together to produce a positive and negative feedback loop of transcription and translation, which take approximately 24 hours. Although there is large sequence diversity in clock proteins between the 5 kingdoms, similar evolutionarily conserved mechanisms of action are evident.

There is considerable homology between species in how the circadian oscillator is produced despite there being a number of ways in which it can be achieved biochemically. Figure 4 shows one generalised mechanism which is commonly observed in circadian molecular oscillators in a number of species, involving transcriptional and translational feedback loops (TTFL) (Dunlap 1999). This is not a requirement, as has been demonstrated for cyanobacteria, such as *S. elongatus*. A transcription-translation feedback loop was postulated in which the *kaiBC* gene is transcribed and subsequently KaiB and KaiC proteins are translated. KaiA and KaiB proteins act antagonistically on KaiC phosphorylation, and phosphorylated KaiC protein inhibits *KaiBC* transcription in a negative feedback loop. This circadian oscillator was later recapitulated *in vitro* using purified KaiA, B and C proteins and ATP. Rhythmic phosphorylation of KaiC was detected suggesting that a biochemical interaction drives the circadian oscillations and does not depend on transcription/translation.

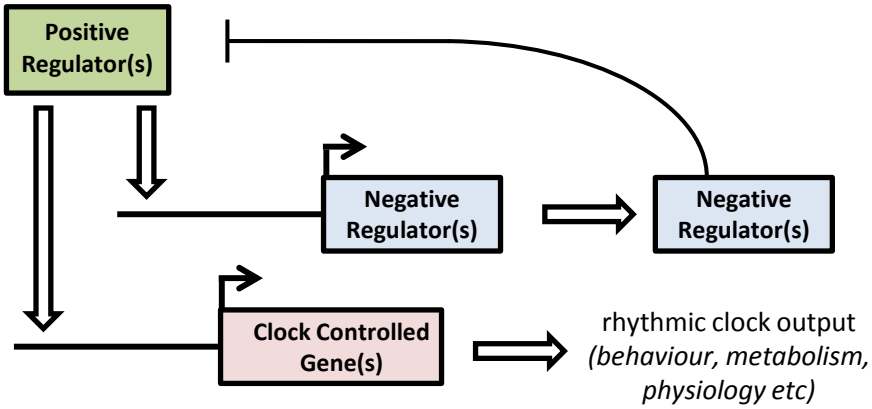

Figure 4: General requirements of a transcriptional / translational molecular oscillator. The figure illustrates some of the common elements observed between species which use a transcriptional / translational mechanism to generate a circadian rhythm. Known positive regulators include: KaiA (*Synechococcus*), White-collar 1 & 2 (*Neurospora*), CLK & CYC (*Drosophila*), CLOCK & BMAL1 (mammals). Negative regulators include: KaiC (*Synechococcus*), Frequency (*Neurospora*), PER & TIM (*Drosophila*), PER & CRY (mammals). Figure adapted from Dunlap 1999.

1.1.7. Mammalian circadian oscillator

Components of the molecular circadian clock have been elucidated through the use of various model organisms and both forward and reverse genetic approaches (Dunlap 1999). In mammals, the master circadian clock resides in the SCN of the anterior hypothalamus. The SCN is comprised of 8,000-10,000 neurons possessing an internal molecular clock consisting predominantly of a negative feedback loop and interconnected ancillary loops. The negative feedback loop consists of the two cryptochrome (*Cry1* and *Cry2*) and three period (*Per1, Per2,* and *Per3*) genes and their protein products. *Cry1/2* and *Per1/2/3* transcription is activated by positive regulators circadian locomotor output cycles kaput (CLOCK) and brain and muscle aryl hydrocarbon receptor nuclear translocator (ARNT)-like (BMAL1). CLOCK and BMAL1 are both basic helix-loop-helix-PAS (Per-Arnt-Single-minded) transcription factors which heterodimerise

and initiate transcription of target genes containing E-box *cis*-regulatory elements in their promoters. These target genes include *Cry1/2* and *Per1/2/3* (Ko and Takahashi 2006).

At the start of the subjective day, the core loop of the molecular circadian oscillator begins with CLOCK and BMAL1 forming a heterodimer and binding to the E-box motif (CANNTG, with a palindromic canonical consensus of CACGTG) within the *Cry1/2* and *Per1/2/3* promoters. CLOCK/BMAL1 binding initiates transcription of *Cry1/2* and *Per1/2/3* and CRY1/2 and PER1/2/3 proteins accumulate in the cytoplasm over the course of the day. CRY and PER proteins can heterodimerise in the cytoplasm and undergo post-translational modification. PER proteins are phosphorylated by casein kinases (CK1 ε and δ) (Dey, et al. 2005; Lowrey, et al. 2000; Meng, et al. 2008) and glycogen synthase kinase-3 (GSK-3) (Iitaka, et al. 2005) and CRY proteins are ubiquitinated by F-box proteins including FBXL3 and FBXL21 (Busino, et al. 2007; Dardente, et al. 2008; Godinho, et al. 2007; Siepka, et al. 2007). These post-translational modifications introduce a point of delay into the feedback loop in order for it to take 24 hours to complete. By circadian night, the PER-CRY complex translocates to the nucleus and interacts with CLOCK-BMAL1 at the E-box element causing a repression on transcription. CRY and PER protein levels deplete as they undergo degradation and CLOCK-BMAL1 transcriptional repression. As CRY and PER protein levels fall throughout the night, repression of CLOCK-BMAL1 mediated transcription is lifted and the cycle repeats (Gallego and Virshup 2007).

Additional feedback loops and post-translational modifications exist to fine-tune the molecular oscillator and maintain a robust circadian period under environmental fluctuations. There are also levels of redundancy within the circadian core clock to ensure that mutations that may occur do not have severe effects on the circadian oscillator. One known stabilizing loop involves the retinoic acid-related orphan nuclear receptors REV-ERBα and RORα, which act to repress or stabilize (respectively) *Bmal1* expression. *Rev-erb*α and *Ror*α rhythmical transcription is initiated by the CLOCK-BMAL1 complex. REV-ERBα inhibits *Bmal1* transcription

by binding retinoic acid-related orphan receptor response elements (ROREs) at the *Bmal1* promoter (Preitner, et al. 2002). RORα counter-balances the action of REV-ERBα and promotes *Bmal1* transcription at the RORE of the Bmal1 promoter (Ueda, et al. 2002). This results in transcriptional activation of *Bmal1* at specific times of circadian day. Transcription of *Rev-erbα* is inhibited by the CRY-PER interaction with CLOCK-BMAL1 at the *Cry* and *Per* promoters (Preitner, et al. 2002). A schematic of the mammalian circadian clock is shown in Figure 5.

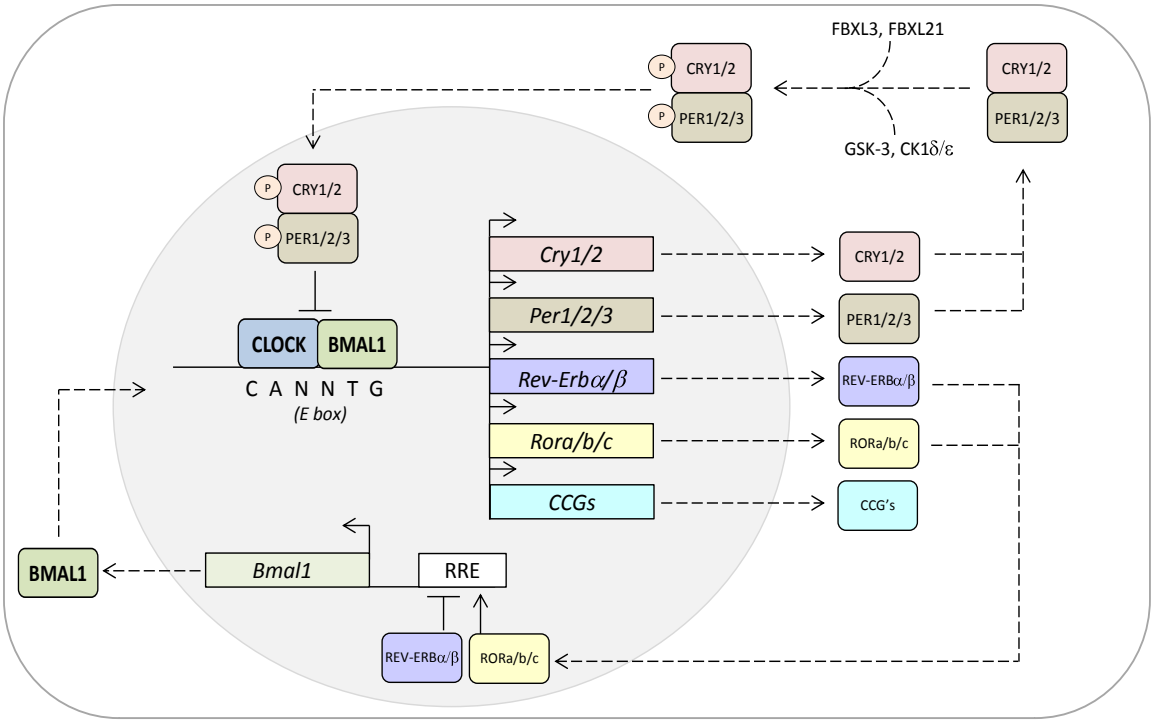

Figure 5: Schematic of the molecular basis of the mammalian circadian oscillator. CLOCK and BMAL1 proteins heterodimerise in the cell nucleus and bind to E box elements within the promoters of *Cry1/2, Per1/2/3, Rev-erbα, Rora/b/c* and other clock-controlled genes (CCG). Transcription of these genes is activated, thus constituting the positive limb of the molecular oscillator. PER and CRY proteins are translated in the cytoplasm and heterodimerise. The PER/CRY complex undergoes post-translational modification, including ubiquitination of CRY by F-box proteins and phosphorylation of PER by GSK-3 and CK1δ/ε. The PER/CRY complex translocates to the nucleus where it inhibits the transcriptional activity of CLOCK/BMAL1. This constitutes the negative limb of the molecular feedback loop. Over-time, abundance of CRY and PER proteins decreases in the nucleus and therefore results in a lift of the repression on CLOCK/BMAL1. CLOCK/BMAL1 can re-initiate transcription and the molecular oscillator repeats the cycle. In an additional feedback loop, RORa/b/c and REV-ERBα/β antagonistically regulate transcription of Bmal1.

1.1.8. Temperature compensation of the circadian clock

Most biological processes increase in rate with increasing temperature. It is essential that circadian rhythms are maintained across varying endogenous and exogenous temperatures as encountered in nature, and therefore complex molecular feedback mechanisms exist by which to fine tune the molecular circadian oscillator to dynamic changes in temperature. The

mechanisms for temperature compensation are still under investigation using a number of model systems (Edwards, et al. 2006; Gould, et al. 2006). Evidence suggests that both transcription dependent and transcription/translation independent mechanisms are required.

As mentioned, due to coupling, the SCN is less sensitive to manipulation compared with peripheral tissues. An example of this is temperature resistance. The SCN has been demonstrated to free-run through a 24 hour cycle with 12 hours of 36^{o}C and 12 hours 38.5^{o}C (Buhr, et al. 2010). In comparison, peripheral tissues such as the lung and the pituitary will entrain to this temperature cycle. Further evidence has come from experiments that block cell-cell signalling and therefore inhibit coupling within the SCN. After using tetrodotoxin (TTX) to block voltage-gated sodium channels, temperature pulses can reset the circadian rhythm, thus creating a temperature sensitive SCN (Buhr, et al. 2010).

1.2. ENU mutagenesis and mouse genetics

1.2.1. The mouse as a model organism in behavioural research

In the early 21st century, the Human Genome Project completed its aim to sequence all genes of the human genome. The focus on these ca. 25,000 genes is now to understand their function and dysfunction in disease. This has been driven forward by the parallel sequencing projects of other model organisms which are allowing researchers to study human gene homologues in accessible model systems. Commonly utilised model organisms encompass species from all phyla, including eukaryotes and prokaryotes. Rodents, such as *Mus musculus* or *Rattus norvegicus*, share highly homologous genomes to *Homo sapiens*, with similar gene number and extensive synteny. *M. musculus* in particular is a valuable tool due to the density to which the genome of many inbred lines have been sequenced which allows for genetic mapping of spontaneous and mutagenesis-induced mutations through use of single nucleotide polymorphisms (SNPs). Together with a short gestation period and relative ease of maintenance and cost, rodents provide an ideal model system by which to understand the human genome. Other species, such as *Drosophila melanogaster*, are also widely used in genetic research. Although the genome is significantly reduced and less conserved in comparison to *Homo sapiens*, this allows for rapid manipulation and ease of mutant generation. In the context of circadian research, the first systematic screens to identify clock genes were conducted in *D. melanogaster*, *C. reinhardtii* and *N. crassa* since the 1970's (Bruce 1972; Konopka and Benzer 1971; Loros, et al. 1989). Since the late 1990's, with the development of mutagenesis and screening strategies in rodents, mammalian models have been increasingly utilised in circadian research.

The mouse is commonly used in neuroscience and behavioural research as an organism in which to model disease. The mouse displays measurable endophenotypes of complex

behaviours including anxiety, depression and fear. Physiologically, the mouse is a comparative model to humans and this allows for disorders during development, adulthood and aging to be analysed and assumptions made regarding associated human conditions. Circadian phenotypes can be readily analysed and assessed in the mouse. Many of the core clock circadian genes have been identified in mouse by forward and reverse genetic screens, as will be discussed in more detail.

1.2.2. Forward genetics

One method for understanding gene function is to identify an abnormal trait or phenotype and work back to determine the causative mutation. This approach is un-biased, requiring no *a priori* assumptions and is hypothesis generating, such that novel genes or specific DNA residues may be attributed to known pathologies and behaviours. Most behaviours are complex traits, relying upon genetic and environmental interactions. This is true for the circadian system.

The molecular basis of the circadian clock has expanded over the last decade through implementation of forward genetic screens and analysis of phenodeviants. As previously described, the central circadian oscillator, driving rhythms through a transcriptional – translational feedback loop, consists of a small set of known core clock genes including *Cry 1/2, Per 1/2/3, Clock, Bmal1* and *Rev-erb*α (Ko and Takahashi 2006; Wager-Smith and Kay 2000). However, it is evident that there must be additional genetic components to circadian rhythm generation and unsurprisingly, the number of newly characterised genes involved in the molecular circadian system is continually expanding. Recent examples of new genes identified from forward genetic screens include F-box and leucine-rich repeat protein 3 (*Fbxl3*) in *M. musculus* (Godinho, et al. 2007; Siepka, et al. 2007), Quasimodo (*Qsm*) in *D. melanogaster* (Chen, et al. 2011a) and type II protein arginine methyltransferase 5 (*Prmt5*) in

A. thaliana (Hong, et al. 2010), which have been shown to have important roles within the molecular circadian oscillator.

Spontaneous mutations occur at a low rate of approximately 5 x 10^{-6} per locus. As such, methods of mutagenesis are used in order to increase the frequency of finding mutations that effect behaviour, including circadian behaviours. It is of note however that one of the most well characterised circadian mutants, the hamster *tau* mutant, was a spontaneous mutation identified in *CK1ε* (Ralph and Menaker 1988a). Although at the time of the identification of this mutant the genetic component was not known, this became the first single-gene mutation affecting the circadian system to be identified in mammals.

X-ray mutagenesis was one of the first mutagen candidates to be used which can increase mutation rate from 20 – 100 times (Cordes 2005). The disadvantage of X-ray mutagenesis is that it commonly induces chromosomal rearrangements which inevitably affect multiple genes. Chemical mutagenesis, such as *N*-ethyl-*N*-nitrosourea (ENU) however, induces predominantly point mutations. It acts through direct alkylation of nucleic acids, at a dosage dependent controlled rate of 1 mutation every 1 – 1.5 Mb (Quwailid, et al. 2004). A key feature of ENU is that it displays a high affinity for spermatogonial germ cells allowing for mutations to occur in the germ line which can be inherited. Crucially, it does not cause complete sterility in males, rather, after administration it results in a period of temporary sterility as spermatogonia are depleted but then re-populate the testes (Justice, et al. 1999), allowing offspring carrying inherited mutations to be assessed.

The most common ENU-induced point mutations are transversions (A-T → T-A) or transitions (A-T → G-C) (Cordes 2005). The resultant mutations are diverse, including missense or non-sense, loss or gain of STOP codons, or those which affect splicing or transcriptional activity. As a result, hypermorphs, neomorphs and antimorphs may all be generated. In this way, ENU can create an allelic series, to finely dissect gene function. ENU may therefore be considered a

complementary approach to reverse genetic strategies, since issues such as redundancy or pleiotropy may be avoided if the induced mutation still allows for the gene to function. Additionally, ENU induced mutations are expressed endogenously, under the genes' normal promoter activity, thus overcoming potential artefactual data due to artificially up or down-regulated gene expression.

1.2.3. Clock knock-out vs Clock ENU point mutation

An illustrative example of the advantages of ENU and how its compares to reverse genetic strategies is evident when comparing the *Clock* knock-out mouse to the *Clock* ENU mutant. The *Clock* gene was identified in an ENU mutagenesis forward genetics screen (Antoch, et al. 1997; King, et al. 1997b). A phenodeviant was identified with abnormal wheel running activity, with a period of ≈24.3 hours in constant darkness. Inter-crossing G1 phenodeviants identified a period of 27 hours in the homozygous mutant. Mapping of the mutation led to a novel circadian locus and subsequently an A → T transversion was indentified in the 5' splice donor site of intron 19 in the gene now known as *Clock*. Molecular analysis showed that splicing was affected with the mutation resulting in exon 19 skipping, causing a 51 amino acid deletion in the clock protein. It was hypothesized that *Clock* may serve as a master regulator of the circadian transcriptional – translational feedback loop. Later work set about to delete *Clock* in a reverse genetic strategy by generating a null mutant using the Cre – LoxP system (Debruyne, et al. 2006). The prediction was that the circadian oscillator would be severely compromised and circadian rhythmicity would be lost. Unexpectedly, circadian rhythmicity was maintained in the homozygous null mutants. Only a mild phenotype was observed - a shortening of the period length in constant darkness by approximately 20 minutes and an advanced onset of activity of 2 hours. This demonstrates that ENU mutagenesis may be used to identify novel genes, and elucidate gene function by compromising gene activity. In the case of the *Clock* mutant, the point mutation produced a protein which had impaired function,

but not so severe that a phenotype was masked due to redundancy. Through the use of a *Clock*/deletion model (where only one allele of the *Clock* gene was expressed and was carrying the ENU mutation) the *Clock* ENU-induced mutation was shown to be antimorphic, a dominant negative mutation that competed with the wild type allele. Based on these genetic studies, it was concluded that the *Clock* gene was a component of the normal circadian system (King, et al. 1997a).

Additionally, in cases of functional redundancy, a knock-out may not illustrate the function or necessity of a gene, as is apparent for the *Clock* knock-out in which neuronal PAS domain-containing protein 2 *(Npas2)* is thought to compensate (DeBruyne, et al. 2007). As is clear from this example, the use of both approaches has helped define the role of *Clock* in the circadian system.

1.2.4. ENU mutagenesis dominant and recessive screens

Breeding schemes that follow ENU mutagenesis of male mice may use either dominant or recessive strategies. For a dominant screen, mutations must show a dominant or semi dominant phenotype in the first generation progeny from the mutagenised founder (G1). This approach is quick, since only one generation of breeding is required before phenodeviants may be identified. The ENU treated male is mated to a wild-type female of either the same or a different genetic background. Each G1 individual carries its own unique set of ENU induced mutations and can be phenotyped for dominant mutations either using a high throughput strategy or for specific phenotypes using a specialized phenotyping pipeline (Nolan, et al. 2000).

Dominant mutations however, are recovered less frequently, on average ten times less than recessive mutations. To detect recessive mutations, the screen requires two more generations of breeding before aberrant phenotypes may be observed. In a recessive screen,

the G1 progeny are mated to another wild-type animal to produce the G2 offspring. The ENU mutations will still be in a heterozygous state and so these offspring are finally inter-crossed to produce G3 animals, homozygous for ENU induced mutations. Alternatively, G2 female progeny may be back-crossed to the male founder (G1) and again, the ENU induced mutations will now be homozygous (Balling 2001). G1 dominant and G3 recessive breeding schemes are outlined in Figure 6.

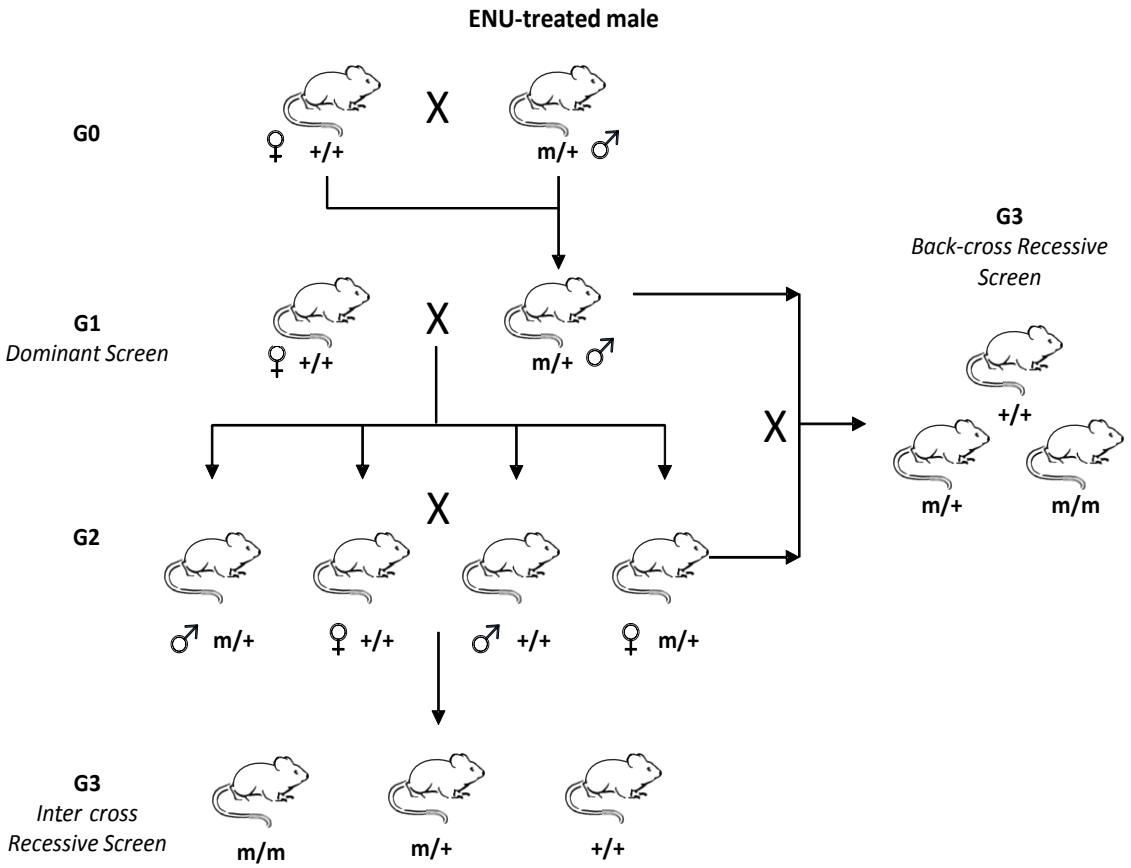

Figure 6: ENU mutagenesis breeding scheme. Male mice are injected with *N*-ethyl-*N*-nitrosourea (ENU), causing random point mutations through-out the genome, including in spermatogonial germ cells. After a period of temporary sterility, mutagenised males are mated to wild-type females. The G1 progeny may be assessed for phenotypes as a result of dominant mutations inherited from the mutagenised male. Each G1 offspring carries a unique set of mutations and therefore will exhibit different phenotypes. At the chosen dose, there will be approximately 30 – 50 functional mutations, but phenotypes are usually due to one mutation. In order to detect phenotypes as a result of recessive mutations, G1 male mice, heterozygous for ENU-induced mutations, are mated to wild-type females. The offspring from this cross (G2) are then either inter-crossed to each other or mated back to the original G1. Both these methods will homozygose ENU induced mutations. The G3 progeny can be phenotyped for both recessive and dominant mutations. It is common to use wild-type females of a different genetic background in the breeding scheme in order to facilitate genetic mapping of any phenodeviant.

1.2.5. Screening ENU mutants for circadian phenotypes

Circadian phenodeviants can be identified using many different methods by recording regular measurable behaviours including food/water intake, temperature, or activity to name a few. One commonly used method is a low through-put screen based upon wheel-running activity under an automated lighting regime (Bacon, et al. 2004). Each individual phenodeviant, from either G1 or G3 litters, is singly housed in a cage fitted with a running wheel. Each revolution of the wheel is recorded and plotted as a measure of the animal's activity throughout the entire screen to produce a double-plotted actogram (Figure 7). Wheel running activity provides a precise data output with less variation compared to measurements of total activity. Data is consolidated to produce a clean circadian biomarker although this is a reduced depiction of the total behavioural activity.

A typical primary screen consists of an initial one week period under a 12:12 light-dark (LD) schedule to entrain the animals. A wild-type animal is expected to show high levels of activity during the 12 hours of darkness and minimal to no activity during the light period, due to the masking effect of light. Aberrant phenotypes detected at this stage of the screen may suggest a deficit in the detection and interpretation of the external light cue to synchronize the circadian oscillator. The animals are then exposed to a period of constant darkness for up to five weeks. This allows for an assessment of the endogenous circadian clock, to persist in the absence of an external *zeitgeber*. The period of wheel running activity is calculated as an indicator of the internal circadian period. A wild-type animal should display a period (τ) of approximately 23.5 hours, and phenodeviants can be detected based on their deviations from this expected behaviour. Phenotypes observed under these conditions may implicate an intrinsic aberration to the molecular basis of the circadian oscillator. The screen may then continue with a period of constant light, under which a wild-type animal will normally lengthen its period. Again, phenodeviants can be identified compared to litter mate controls

and deficits here may be suggestive of abnormal photic detection and relay of entrainment signals to the SCN. Other lighting schedules may include light pulses to assess masking or phase shifting, or returning to a 12:12 LD cycle to assess re-entrainment after exposure to constant light conditions. As well as period, levels of activity, phase angle, and responses to light intensity may also be analyzed to further dissect the circadian phenotype on a behavioural level. A representative actogram from a typical screen is shown in Figure 7.

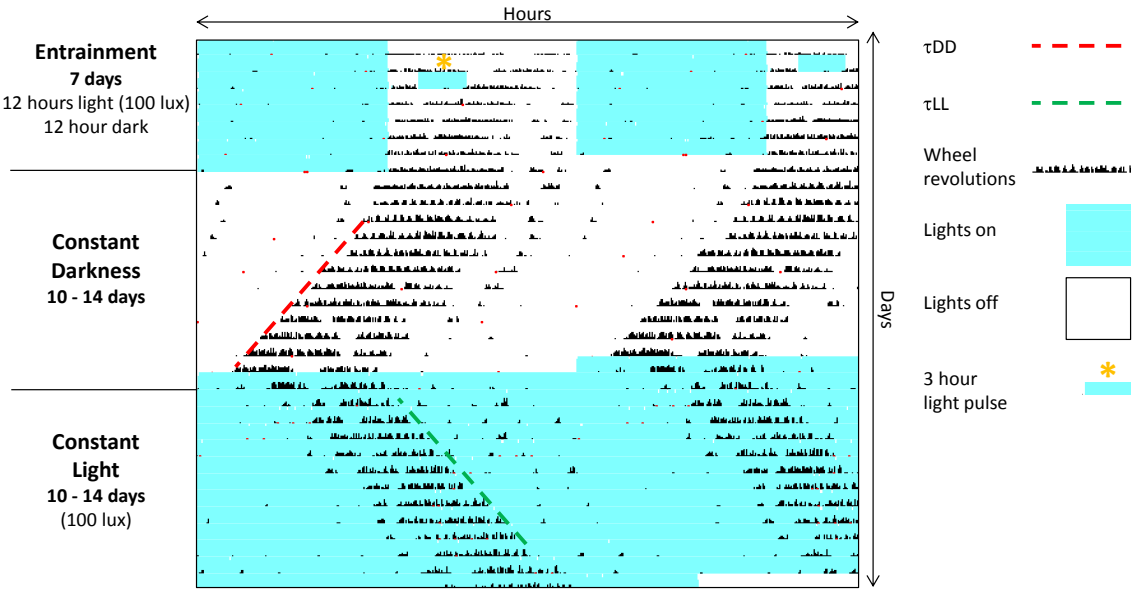

Figure 7: Representative double plotted actogram of circadian wheel running activity of a wild-type mouse. Mice are individually housed within cages equipped with running wheels. The revolutions of the wheel are automatically recorded and plotted as shown above. The initial phase of the screen consists of a 12:12 LD cycle to allow for circadian entrainment. Nocturnal animals will become active and run on the wheel once the lights are switched off, as depicted by the vertical black bars representing wheel revolutions. Screens may include brief light pulses during the dark period of the entrainment phase in order to look at the direct effects of light on activity. In a wild-type animal, activity should be suppressed during the light pulse, a phenomenon known as "masking". Aberrations to the wild-type phenotype during LD may indicate a deficit in photic input to the SCN and/or the detection of light. In the second phase of the screen, the animals are subjected to constant dark conditions. This allows for a direct assessment of the free-running ability of the molecular oscillator in the absence of any *zeitgeber*. The period (τDD) is measured as the gradient of activity, expected to be approximately 23.5 hours in a wild-type animal. Deviations from this gradient are used as an indicator for a circadian phenodeviant with a disturbance to the molecular clock. The third phase of the screen consists of constant light. This may be used to assess the stability of the circadian clock and the ability of the SCN neurons to remain synchronised. A wild-type animal will lengthen the period (τLL) by 1.5 hours or more. Phenodeviants may exhibit "splitting" of the circadian rhythm (implicating decoupling of the two SCN nuclei), "arrhythmia" (decoupling of the SCN neurons), or abnormalities in the lengthening of the circadian period. During all phases of the screen, activity levels may also be determined as well as the amplitude of the circadian rhythm. Screens may become more complex by using additional light pulses, different lighting conditions or different day lengths (T-cycles).

1.2.6. Mapping and cloning of ENU mutations

Following identification of phenodeviants, the mutation is tested for inheritance and penetrance. Phenodeviants are mated to wild-type animals on a different inbred background to the mutant founder, and the progeny are tested for the observed phenotype. This continues through sequential generations to ensure that the phenotype is inherited as expected and expressed as observed in the original founder. Those mutations which are inherited and maintain high levels of penetrance (the proportion of individuals with the mutated allele displaying the associated phenotype) are then selected for mapping and positional cloning of the mutation.

The first step in identifying a causative mutation is to generate a low resolution map of the mutant locus. Typically, 10 – 20 phenodeviants are selected for mapping. All mutant animals must share one region of linkage in common which corresponds to the abnormal phenotype, and different regions of recombination that result from the differing genetic backgrounds of the two parents. By using approaches such as a genome-wide scan, which uses a panel of genetic markers such as SNPs, a genetic map can be produced in which the common region of linkage can be identified. Using SNPs, a short common region emerges between the phenodeviants and this resultant locus is known as a "candidate region". Technological advances now make it possible for the whole genome to be sequenced following a genome-wide scan, such that all sequences within a critical region can be aligned and the functional mutation may be identified. With this method, if more than one mutation is identified in the candidate region, the causative mutation has to be elucidated through further analyses. For ENU mutations however, phenotypes are usually the result of just one causative mutation (Shibuya and Morimoto 1993). Once a mutation has been identified, it is important to prove that the mutation identified is causative of the phenotype. Techniques such as bacterial artificial chromosome (BAC) rescue may be used (Antoch, et al. 1997; Justice, et al. 1999).

1.2.7. Reverse genetics

Reverse genetic studies provide a complementary approach to forward genetic screens such as those described above. Reverse genetics relies upon prior knowledge about a candidate gene and studying its function in its endogenous state or artificially creating mutant alleles and examining the effects on the phenotype of interest. This has been made possible since the advent of whole genome sequencing. This is a technique that has been employed in circadian genetics since the first clock genes were identified across various model systems. Through extrapolation of data and mining for homologous genes in other models, components of the circadian oscillator have been identified and confirmed in various model systems based upon these reverse genetic approaches (Takahashi, et al. 1994; Wager-Smith and Kay 2000). There are a number of strategies in which reverse genetic studies are pursued, both *in vitro* and *in vivo*. These may include techniques such as gene knock-down by RNAi, knock-out or gene-trap technology, over-expression studies, reporter gene assays and mutagenesis archive screening.

All these techniques provide complementary approaches to each other and to forward genetic screens. They can provide additional information about the role and function of a gene and the consequences on phenotypes when gene and protein expression is altered. Many of these techniques may be used to verify the identity of mutations from mutagenesis screens and the type of mutation produced (e.g. loss or gain of function). In addition, approaches such as generating conditional knock-outs allows for mutations or knock-outs that would normally cause homozygous lethality during development, to be spatially and temporally controlled. The combination of these approaches with forward genetics allows for an allelic series of mutations to be produced in order to further understand gene function.

1.3. Zinc Finger Homeobox 3

1.3.1. Identification of Zfhx3, structure and function

Zinc finger homeobox 3 (*Zfhx3*) is one of the largest known DNA binding proteins characterised to date. It was first identified in the early 1990's as a protein which acted to suppress alpha-feto protein (AFP) expression in hepatocytes (Li, et al. 2009; Morinaga, et al. 1991a). It was shown that ZFHX3 binds an AT rich consensus sequence in the AFP enhancer (Yasuda, et al. 1994b). As such, *Zfhx3* was originally named as AT-binding factor 1 (*Atbf1*), but later phylogenetic analysis identified that *Atbf1* was closely related to *Zfhx2* and *Zfhx4* and was renamed to reflect this relationship (Holland, et al. 2007). There are two characterised isoforms of *Zfhx3*. The first to be identified was the smaller of the two transcripts, encoding a protein of 306 kDa (Morinaga, et al. 1991a). This protein contains 4 homeodomains and 18 zinc fingers. A larger transcript was later isolated which encoded a 404kDa protein (Ido, et al. 1996). This protein has a 902 amino acid extension at the N-terminus. The two transcripts are due to alternative promoter usage and alternative splicing of exon 2. The larger of the two transcripts contains an additional five zinc fingers, two acidic domains and a serine-threonine rich region.

The transcript of *Zfhx3* is highly complex, encoding multiple domains allowing it to perform different functions. Obvious roles of *Zfhx3* are in transcriptional regulation, however, a number of motifs within the *Zfhx3* transcript suggest other roles in enzymatic-based activity in DNA metabolism. *Zfhx3* has been annotated as peaking in expression at E12.5 during murine development. High expression is observed in the central nervous system, and in particular in regions undergoing cellular differentiation. Furthermore, *Zfhx3* is expressed in the differentiating field of the brain where cells are not expressing nestin (Jung, et al. 2005), a neural stem cell marker. The characterised features of *Zfhx3* are illustrated in Figure 8 and are detailed in Table 1.

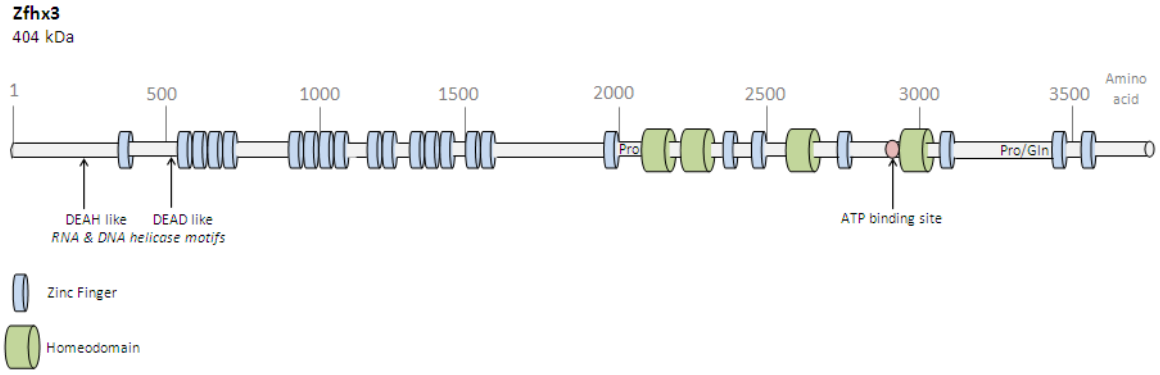

Figure 8: Schematic of the ZFHX3 transcript. The largest transcript encodes a 404 kDa protein with multiple motifs and domains. There are 23 zinc fingers, predominantly clustered towards the N-terminus and 4 homeodomains towards the C-terminus. The collinear organisation of the 23 zinc fingers and 4 homeodomains are conserved throughout evolution, suggesting an interaction between the domains.

Domain / Motif	Number in *Zfhx3*	Function
Homeodomain	**4**	Sequence-specific DNA binding motif usually acting within the promoters of target genes. ZFHX3 is involved in transcriptional regulation of a number of genes including *c-Myb, AFP, MUC5AC, Pit1* and *Pias3*.
Zinc finger	**23**	*Zfhx3* has C2H2 and zinc-knuckle type zinc fingers likely to be involved in binding DNA, RNA and protein.
DEAH box	**1**	DEAH box-like sequence often found in the helicase II super-family. Helicases use hydrolysis of a nucleotide triphosphate to relinquish energy required for nucleic acid strand separation allowing for nucleic acid metabolism processes.
DEAD box	**1**	As above for DEAH box-like sequence.
RNA binding motif	**1**	May implicate *Zfhx3* in RNA translation and metabolism, splicing and editing.
ATPase-A motif	**1**	Site of energy production by hydrolysis of ATP to ADP. Required for change in protein conformation or catalytic activation. In *Zfhx3*, ATP hydrolysis is DNA or RNA dependent and requires homeodomains and zinc fingers for its activity.
Nuclear Localisation Signals (NLS)	**7**	5 known nuclear import signals and 3 nuclear export signals and other less highly conserved NLS signals are found in the *Zfhx3* transcript. Acts to regulate transcriptional activity and has roles in cell cycle progression.
Acidic domains	**8**	Protein interactions and protein solubility.
Leucine-rich helix motif	**1 + 31 variants**	LXXLL motif may be responsible for forming complexes with nuclear receptors to affect target gene expression.
Serine/Threonine rich region	**3**	Regulation of cellular localisation, protein degradation, protein interactions. May be involved in regulating mRNA splicing at the nuclear speckle.
PolyQ region	**8**	Formation and stabilisation of protein-protein interactions, transcriptional regulation and nuclear localisation. *Zfhx3* is the first protein in which a CAA repeat has been identified in a protein coding region.
PolyP region	**5**	Rapid, non-specific ligand binding. PolyP regions often contain glutamine residues which together form a conformationally restricted polypeptide chain (as is the case for *Zfhx3*). Often associated with a transcriptional repressor domain.
PolyG region	**1**	Protein-protein interactions.

Table 1: Description of the annotated domains and motifs identified within the *Zfhx3* transcript. The transcript of *Zfhx3* encodes numerous domains and motifs, some of which remain to be assigned specific functions in Zfhx3 biochemistry. The most well characterised and dominant domains of *Zfhx3* are the homeodomains and zinc fingers which are highly conserved in *Zfhx3* homologues, paralogues and orthologues.

1.3.2. Conservation of *Zfhx3*

The zinc finger homeobox gene family was previously described as two members, *Zfh3* and *Zfh4*. In vertebrates, the *Zfhx* gene has undergone multiple duplications resulting in 3 homologues in humans, *ZFHX2, ZFHX3* and *ZFHX4*. A second more distantly related family has come from *ZFH1/2*. This includes *ZEB1* and *ZEB2*, previously known as *ZFHX1a* and *ZFHX1b,* however this was considered misleading in their degree of relatedness to the other *Zfhx* genes (Holland, et al. 2007). *Zeb1* and *Zeb2* are distinguished by their known ability to bind E box elements (Genetta, et al. 1994; Postigo and Dean 1997). E-box elements are a common DNA control mechanism in transcriptional regulation. They are common in circadian genes, found in the promoters of *Cry1, Cry2, Per1,* and *Per2* (Gekakis, et al. 1998; Hao, et al. 1997; Kume, et al. 1999; Yoo, et al. 2005) and are therefore crucial in the circadian transcriptional feedback loop. It is therefore interesting to note that there is an ancestral ability of the *Zfh* family, which includes *Zfhx3*, in regulating gene transcription via the E-box.

Zfhx3 is highly conserved across different species, including primates, rodents, insects (*D. melanogaster*) and nematodes (*C.elegans*). The *D. melanogaster Zfhx3* homologue, *Zfh2*, encodes 3005 amino acids to produce a 332 kDa protein with 16 zinc fingers and 3 homeodomains. It was first isolated in 1991, together with *Zfh1*, as the first transcriptional regulatory protein with both homeodomains and zinc fingers (Fortini, et al. 1991; Hashimoto, et al. 1992). All the homologous domains between *D. melanogaster Zfh2* and mammalian *Zfhx3* are collinearly arranged, implicating a similar function and a selective pressure has maintained this order. Co-localisation of ZFH2 with dopa-decarboxylase (*Ddc*) in the *D. melanogaster* CNS suggests that *Zfh2* may be involved in the regulation of *Ddc*-containing neuronal lineages. Immuno-precipitation assays identified that homeodomain 2 of ZFH2 bound an AT rich binding site within the distal enhancer of *Ddc* (Lundell and Hirsh 1992).

ZFH2 has been previously observed to bind an evolutionarily conserved cis-element present in the four Drosophila opsin genes known as Rhodopsin Conserved Sequence I (RCSI) (Fortini, et al. 1991). This element is similar to the *Ddc* regulatory element by the presence of an AT rich motif (CTAATTGAATT) and both share a similar sequence composition to the homeodomain consensus binding sequence, TCAATTAAAT (Hoey and Levine 1988). It is possible that both the *Ddc* promoter and RSCI element may be bound and regulated by a number of homeobox proteins. Whilst *Ddc* is bound by ZFH2 homeodomain 2, in contrast, the RCSI element is bound by homeodomain 3 (Fortini, et al. 1991), suggesting that there is a specificity between the homeodomains in which elements they bind and regulate despite homologous binding motifs. It is known however, that homeodomains can relatively easily bind AT rich motifs in competitive assays which do not reflect the specificity and less "promiscuous" binding *in vivo* (Hoey and Levine 1988; Mann 1995). Taking all the evidence together however, these results support a role for ZFH2 in the regulation of *Ddc* as well as opsin and photoreceptor genes and this may be extrapolated to *Zfhx3*.

The *R. norvegicus Zfh4* transcript produces a protein of 392 kDa which has 50% amino acid identity with mouse and human *Zfhx3* (Nogami, et al. 2005). The homeodomains and zinc fingers are highly conserved (85-97% and 44-100% respectively). Localisation studies of ZFH4 showed a high degree of overlap in the expression pattern of ZFHX3, which has been useful in further identifying and understanding the function and roles of *Zfhx3* (Nogami, et al. 2005). ZFH4 is highly expressed in the developing mid-brain and diencephalon as well as the arcuate nucleus and pre-optic area of the hypothalamus, as well as the substantia nigra and subthalamic nucleus of the basal ganglia. Furthermore, ZFH4 co-localises with tyrosine hydroxylase immuno-reactive cells, consistent with expression studies of ZFHX3 and Drosophila ZFH2. This suggests an evolutionarily conserved role for *Zfhx3* in the dopaminergic system – either in its development, as indicated by high expression in the developing embryo, or in transcriptional regulation, already shown by the binding of ZFH2 homeodomain 2 to the

AT motif binding site in the *Ddc* promoter (Lundell and Hirsh 1992). Moderate expression of *Zfh4* and *Zfhx3* has also been identified in the developing oculomotor nucleus, lateral geniculate nucleus and post-mitotic neurons of the retina (including the ganglion cell layer). Together with the discussed role of ZFH2 in opsin regulation and also in lens differentiation, this may suggest a role for these paralogous proteins in the visual system.

In all species studied, *Zfhx3* expression peaks in the developing CNS and has relatively lower expression in the mature adult. High expression in regions of the hypothalamus may implicate a role of *Zfhx3* in the establishment of neural networks to/from the hypothalamic nuclei, including the SCN. In support of this, two important studies have performed an analysis of the transcription factors expressed in the putative SCN of the developing mouse hypothalamus. In an initial study, 220 transcription factors were found to be restricted to distinct populations within the hypothalamus of E13.5 or P0 mice (Gray, et al. 2004). In a later study, 72 transcription factors were found to have discrete expression patterns in the anterior hypothalamus which would include the developing SCN (VanDunk, et al. 2011). *Zfhx3* was one of these transcription factors expressed highly at both E13.5 and P0. From this, a potential role of *Zfhx3* in SCN development and an involvement in the circadian system could be hypothesised.

1.3.3. Known functions of *Zfhx3*

Based upon analysis of the structure of the *Zfhx3* functional domains, it is conceivable that *Zfhx3* plays many roles across a range of aspects of physiology. The majority of publications have focused on the role that *Zfhx3* plays in the cell cycle and as a tumour suppressor and many have identified pathogenic mutations in *Zfhx3* from genome wide association studies (GWAS) (Benjamin, et al. 2009b; Burgner, et al. 2009; Cho, et al. 2007; Sun, et al. 2007).

Cellular differentiation and proliferation – AT motif binding and E box elements

The first study on *Zfhx3* described the role it had in suppressing AFP expression through binding the AT motif in the AFP enhancer (Ido, et al. 1996). AFP is often used as a biomarker for certain cancer types, with elevation of AFP levels often indicative of cancer. One study showed that *Zfhx3* mRNA levels are reduced in AFP-gastric cancer cells (Miura, et al. 2004b). Upon treatment of these cells in dissociated culture with mitomycin-C (MMC), a DNA cross-linker often used as a chemotherapeutic agent, *Zfhx3* mRNA expression increased. It was also shown that concurrently, p21 (Waf1/Cip1) gene expression increased 7 fold as well as cellular levels of p53. Further work identified that ZFHX3 was binding the p21 promoter in a heterodimer with p53 to activate p21 transcription. The result of activated p21 transcription was inhibition of cell growth.

MyoD proteins comprise a family of muscle regulator factors (MRFs). They are bHLH transcription factors that heterodimerise with other bHLH E-proteins, which together can bind and regulate E-boxes in muscle specific genes to determine muscle cell fate (Ludolph and Konieczny 1995; Yun and Wold 1996). The activity of MyoD proteins has been shown to be enhanced by Myocyte enhancer factor-2, MEF2. MEF2 and MyoD family MRFs bind A-T rich elements of muscle specific genes, to control transcription (Molkentin, et al. 1995). Inhibitor of DNA binding (Id) family proteins reciprocally inhibit this action by interacting with E-proteins or MyoD to form a complex that is unable to interact with the E-box (Atherton, et al. 1996; Benezra, et al. 1990). Other factors, including ZEB proteins, also inhibit the E-box and the access of MyoD's to the E-box (Postigo and Dean 1997; Postigo and Dean 1999).

Given that MEF2 and MRFs bind AT motifs, a shared feature of ZFHX3, and the role that *Zfhx3* has in the cell cycle and differentiation, it is reasonable to suggest that *Zfhx3* may also be involved in this gene network in muscle cell differentiation. In a myoblast cell line, C2C12, induction of myogenic differentiation with DMSO causes a decrease in the larger isoform of

Zfhx3 mRNA (Berry, et al. 2001). It is possible that *Zfhx3* may function to inhibit MRF genes to prevent *MyoD* dependent myogenesis. The *Mrf4* promoter contains two E-boxes, a *Mef2* site and an AT motif (2 bp adjacent to the first E-box) (Naidu, et al. 1995). In cells transfected with *Zfhx3*, *MyoD* activation of *Mrf4* was inhibited (Berry, et al. 2001). Further analysis showed that this may be achieved through the binding of ZFHX3 to the AT motif of MRF4 via the 4th homeodomain. It is therefore suggested that the binding of ZFHX3 to the AT motif may restrict binding of other factors, including MYOD, to the *Mrf4* E-box (Berry, et al. 2001). It is not uncommon for AT motifs to lie very close to E-box elements. It is therefore reasonable to suggest that in some cases, including MRF4, binding of ZFHX3 or other factors to AT motifs may not directly affect E-box mediated transcription, but may mask E-box elements, therefore indirectly affecting transcriptional activation of the target gene. This is an important consideration in the context of circadian gene regulation which is dependent upon E-box activation.

Further analysis in this study aimed to identify whether a series of fragments of *Zfhx3* or homeodomain 4 alone could also bind the E-box element. So far, binding by ZFHX3 to the E-box sequence has not been detected by mobility shift assays. Additionally, ZFHX3 was not shown to be able to drive a luciferase construct consisting of a 5 X tandem repeat of the E-box element (Berry, et al. 2001). This suggests that ZFHX3 does not have the ability to bind E-box elements under these conditions, although it remains to be conclusively determined using an intact full length *Zfhx3* construct. It is also possible that ZFHX3 can interact with E-boxes in conjunction with other proteins. This is the case with ZEB, which exerts repression on the E-box together with the co-repressor CtBP (Postigo and Dean 1999). Similarly seen in the circadian system, both CLOCK and BMAL1 heterodimerise before interacting with the *Cry/Per* E-boxes. Motif analysis of the *Zfhx3* transcript has identified a number of potential co-factor binding sites.

1.3.4. *Zfhx3* and disease

Cancer

A number of studies have implicated mutations in *Zfhx3* being causative of cancers. As previously mentioned, a number of GWAS studies have linked *Zfhx3* to prostate, gastric and breast cancers. It has been frequently identified that the long arm of human chromosome 16, where human *Zfhx3* is positioned, is often lost in many cancers (Caligo, et al. 1998; Cleton-Jansen, et al. 2008).

To date, the majority of studies involving *Zfhx3* have focused on its potential role as a tumour suppressor candidate gene. Many of these studies have identified differences in *Zfhx3* mRNA expression between normal and cancerous cells. *In vitro*, treatment with *Zfhx3* siRNA in *Zfhx3* positive cell lines causes an increase in cellular proliferation and decreased *Zfhx3* mRNA expression levels have been identified in cancerous cells. Many molecular mechanisms have been identified for how *Zfhx3* acts as an anti-mitotic factor including protein and genetic interactions with *p21, Runx3, Tgfβ* and *Smads* (Mabuchi, et al. 2010).

A study investigating the role of *Zfhx3* in contributing to breast cancer phenotypes identified a mechanism by which *Zfhx3* acts through inhibiting estrogen receptor (ERα) function (Dong, et al. 2011; Dong, et al. 2010). Many breast cancers are known as estrogen receptor positive breast cancers, where regulated control over estrogen receptor expression and activity is altered. Estrogen receptors are part of the type 3 nuclear receptor family, which become catalytically active and able to exert effects on target gene transcription upon binding to a ligand. In this way, nuclear receptors are sensors of hormones, steroids or other cytosolic molecules, and upon ligand and co-factor binding, are able to regulate transcription in processes such as metabolism, homeostasis or immune response. The known regulators of ERα contain nuclear receptor boxes, an LXXLL motif which mediates the substrate and ligand binding. In this study, ZFHX3 was shown to have one LXXLL motif and 31 variants, LXXXL. It

was shown that ZFHX3 directly binds to ERα, and may competitively exclude other ligands and co-factors from binding. In ER positive cancerous cells, *Zfhx3* RNA has been shown to be up-regulated as a mechanism to prevent un-controlled cell proliferation by binding ERα.

Interestingly the core molecular circadian clock includes two nuclear receptors, Rev-erbα and RORα. As with ERα, *Rev-erbα* also contains an LXXLL binding site, and acts as a REDOX sensor by binding HEME to induce activity. Upon binding co-factors including NCoR, HDAC3 and a Heme ligand, REV-ERBα exerts transcriptional inhibition on the *Bmal1* promoter. Additionally, nuclear receptor binding sites, including LXXLL motif variants, have been identified in the *Per* genes and PER2 has been shown to be able to bind to nuclear receptors and then the complex rhythmically binds to target gene promoters (Ripperger, et al. 2010). It may be significant that nuclear receptors/nuclear co-factor binding appear to be a central component of the circadian clock transcriptional mechanism and that ZFHX3 has been shown to have the ability to bind nuclear receptors through its own LXXLL and LXXL motifs.

Cardiac Disorders

The diversity of the roles of *Zfhx3* is further exemplified in the frequency of SNPs being identified from GWAS studies for various disorders and diseases. In 2009, two back to back papers were published identifying variants in *Zfhx3* as a new risk allele for atrial fibrillation (AF) (Benjamin, et al. 2009a; Gudbjartsson, et al. 2009; Li, et al. 2011). AF is an electrical disorder of the upper chambers of the heart, producing an irregular heart rhythm. The disease is inherited in a Mendelian ratio, therefore inferring a genetic predisposition. Initial GWAS studies identified sequence variants located close to the *PitX2* gene, on human chromosome 4q25. In replicate GWAS studies, this risk locus has been confirmed together with a new risk locus on 16q22. Two intronic SNPs were independently identified within an intron of *Zfhx3*. *PitX2* and *Zfhx3* may be genetically linked. It has been previously shown that ZFHX3 binds an enhancer element of the *Pit1* promoter for transcriptional activation regulating pituitary

development. PIT1 itself forms a heterodimer with PITX2 (AF risk allele) to become an active DNA binding complex regulating transcription (Qi, et al. 2008a).

Neurodegenerative and Psychiatric disease

Zfhx3 has recently been implicated in neuronal cell death in Alzheimer's disease (AD) (Jung, et al. 2011). Aβ-induced neurotoxicity in AD likely occurs through apoptotic pathways including ATM and p53, which ZFHX3 is known to interact with and regulate. *Zfhx3* has been shown to be up-regulated in AD affected brains and in APP transgenic mice (APP is the Aβ precursor protein). *In vitro*, rat primary cortical neurons were targeted with genotoxic compound to stimulate and replicate the pathogenesis observed in AD and apoptotic events. In these cells, *Zfhx3* was again shown to be up-regulated. Application of *Zfhx3* siRNA attenuated the apoptotic response. Further work went on to demonstrate that in cells exposed to ionizing radiation, ZFHX3 became phosphorylated which could interact with ATM to initiate the ATM apoptosis pathway.

There is preliminary evidence that *Zfhx3* gene expression is affected in schizophrenia. A study of mRNA expression in a small sample of human schizophrenic post-mortem brain samples identified large genome wide changes in expression levels in mRNA in the superior temporal gyrus. The study identified 428 genes to be down-regulated >1.5 fold and 191 up-regulated > 1.5 fold. Out of these, *Zfhx3* was shown to be one of the most significantly up-regulated by 2.39 fold (Bowden, et al. 2008).

1.3.5. Other *Zfhx3* mutants

Although *Zfhx3* is predominantly expressed in the developing CNS, studies have also identified *Zfhx3* in other organs, predominantly the lung and intestine. The larger *Zfhx3* isoform was initially isolated from human embryonic lung fibroblast cDNA (Ido, et al. 1996). Although most of the regional expression of *Zfhx3* mRNA peaks in development and drops in the mature

adult, mRNA expression of *Zfhx3* has been shown to persist in the adult lung. *In situ* hybridisation has shown that *Zfhx3* mRNA is expressed in the epithelial cell layer of the bronchioles in the developing and adult mouse lung. Support for a role of *Zfhx3* in the development and maintenance of the bronchiolar epithelium comes from unpublished data (Noguchi et al, 20th Annual Meeting of Molecular Biology Society of Japan) that showed that *Zfhx3*$^{-/-}$ mice die at birth due to dysmorphologies and malfunction of the lung and a subsequent lack of respiratory activity. The neonates display a phenotype similar to neonatal respiratory distress syndrome. More recently, a published conditional allele of *Zfhx3* has been generated using the Cre-LoxP system (Sun, et al. 2012) where approximately 70% of the amino acid sequence is lost. Heterozygous animals display significant pre-weaning mortality, with those surviving being smaller and lighter in weight as well as prolonged weaning and hypo-activity. As will be discussed later, both these alleles show phenotypes consistent with the *Zfhx3* mutant described in this thesis.

1.3.6. Conclusions

Zfhx3 is a large transcription factor consisting of a diverse array of sequence motifs which render it capable of performing a wide range of roles and functions genetically and molecularly. *Zfhx3* has consistently been identified as being predominantly expressed in the developing embryo, with localisation studies in rodents identifying *Zfhx3* expression in the CNS, peaking in the mouse at E13.5. Work on *Zfhx3* homologues and orthologues have implicated roles for *Zfhx3* in neuronal development but also suggest general roles in cellular differentiation and mitotic control. Specific DNA and protein targets for *Zfhx3* have been identified and GWAS and mutation studies continue to associate *Zfhx3* variants with a number of diseases including cancers, heart diseases and psychiatric conditions as described. *Zfhx3* is yet to be associated with behavioural processes such as circadian rhythms, sleep and visual perception. It is an interesting candidate gene for a role in these areas due to the nature of

the domains it possesses, its expression pattern and from extrapolation of the known roles of other *Zfhx* family members and related genes.

The aim of this thesis is to identify whether *Zfhx3* plays a role in the circadian system, either directly at the level of the molecular clock, or in input or output pathways. This study identified *Zfhx3* using a forward genetics strategy, and together with reverse genetic approaches is using the mouse as a model system to evaluate the function and role of *Zfhx3* in circadian behaviour. The identification of the short circuit mutant and the corresponding point mutation within the coding region of *Zfhx3* will be discussed. An assessment of circadian and ophthalmological phenotypes and an investigation into the molecular action of *Zfhx3* within these systems is presented.

Chapter II

Materials and Methods

2. Materials and Methods

2.1. Materials List

Reagents and Consumables	Manufacturer	Catalogue Number
10 ml Serological Pipettes	Greiner Bio-One	607180
100 mm Tissue Culture Dish	Greiner Bio-One	664160
100 bp Ladder	NEB	N0467S
1kb Ladder	NEB	N3232
25 ml Serological Pipettes	Greiner Bio-One	760180
5ml Serological Pipettes	Greiner Bio-One	606180
60mm Tissue Culture Dishes	Greiner Bio-One	628160
Acetic anhydride	MP Biomedicals	154680
Agarose	Sigma	A9539
Albumin from Bovine Serum	Sigma	A2153
αMEM (Minimum Essential Medium Alpha)	Invitrogen / GIBCO	22561021
Amersham ECL Plus™ Western Blotting Detection Reagent	GE healthcare	RPN2132
Ampicilin	Sigma	A9518
Anti-Digoxigenin-AP, Fab fragments	Roche	11 093 274 910
β-mercaptoethanol	Sigma	M3148
Bacterial Grade Petri Dishes	VWR	82050-910
BIOTAQ Core Kit	Bioline	BIO-21071
Blocking reagent	Roche	11096176001
Blotting Paper, Extra Thick	Bio rad	1703966
Bradford Reagent	Sigma	B6916
Calf Serum	Invitrogen / GIBCO	16010-159
Cell Scrapers	Greiner Bio-One	541070
Chelating sepharose resin	GE Healthcare	17-0575-01
Chloramphenicol	Sigma	R4408
Chloroform	BDH Chemicals	277106P
Cobalt Chloride hexahydrate, ACS reagent, 98%	Sigma	255599
Complete, EDTA-free (Protease Inhibitor Cocktail Tablets)	Roche	11873580001
Cover-slips 22 X 22 mm	VWR	631-0124
Cyclohexamide (CHX)	Sigma	C7698-1G
dNTP 100mM Set	Invitrogen	10297-018
Denhardt's Solution	Serum Biotech	304205
Dexamethasone	Sigma	D4902-25MG
Dextran Sulfate Sodium Salt	MP Biomedicals	160110
DH5α Competent Cells	Invitrogen	18265-017
DIG RNA Labelling Kit	Roche	11175025910

DMEM (Dulbecco's Modified Eagle´s Medium)	GIBCO	3196-021
Dimethyl sulfoxide (DMSO)	SIGMA	D2650
dNTP Mix 40mM	Bioline	BIO-39043
DPBS (Dulbecco's Phosphate Buffered Saline)	Lonza	LONZ17-512F/12
DPX Mountant for Histology	BDH Chemicals	360294H
Ethanol (EtOH)	Fisher Scientific	E/0650DF/17
Ethylenediaminetetraacetic Acid 99.995% (EDTA)	Sigma	431788
Foetal Bovine Serum	PAA Laboratories Limited	A15-010
Formamide	Sigma	F7508
Forskolin	Sigma	F6886
Fugene6	Roche	11814443001
GelRed	Biotium	41003-1
GlutaMAX™-I Supplement, 200 mM	Invitrogen	35050038
Glycerol	Fisher Scientific	G/0650/17
Glycine	Sigma	G7126
HindIII	NEB	R0104
HiMark Prestained Protein Standard	Invitrogen	LC5699
Hybond Blotting Paper	GE healthcare	RPN6101M
Hydrochloric Acid	Fluka	84436
Immidazole	Sigma	I5513
Innoculation Loops	Sarstedt	203-10
Isopentane	Acros Organics	126470010
Isopropanol	Fisher	P/7490/17
jetPRIME	POLYPLUS TRANSFECTION	114-15
Lysing Matrix D Beads	MP Biomedicals	6913-100
Magnesium Chloride Hexhydrate	Sigma	M270
McCoy´s 5A Culture Media	PAA Laboratories Limited	E15-022
MEM Non-essential Amino Acid Solution (100 X)	Sigma	M7145
Methanol, MeOH	Fisher Scientific	M/3950/17
MG132	Sigma	C2211
MicroAmp FastOptical qRT-PCR plates	Applied Biosystems	403012
Midi Gel Adaptors	Invitrogen	WA0999
NaCl	Sigma	S3014
NBT/BCIP Stock Solution	Roche	11 681 451 001
NE-PER* Nuclear and Cytoplasmic Extraction Kit	Thermo Scientific	78833
Newborn Calf Serum, Heat Inactivated	Invitrogen / GIBCO	26010074
Nonidet P40 Substitute	Sigma	74385
NotI	NEB	R0189
Novablue Gigasingles Competent Cells	Merck	71227-3
NuPAGE® Antioxidant	Invitrogen	NP0005
NuPAGE® LDS Sample Buffer (4X)	Invitrogen	NP0007
NuPAGE® MOPS SDS Running Buffer (20X)	Invitrogen	NP0001
NuPAGE® Novex 3-8% Tris-Acetate Gel 1.0 mm, 10 well	Invitrogen	EA0375BOX
NuPAGE® Novex 3-8% Tris-Acetate Gel 1.0 mm, 12	Invitrogen	EA03752BOX

well		
NuPAGE® Novex 3-8% Tris-Acetate Midi Gel, 20W	Invitrogen	WG1602A
NuPAGE® Novex 4-12% Bis-Tris Gel 1.0 mm, 12W	Invitrogen	NP0322
NuPAGE® Novex 4-12% Bis-Tris Midi Gel, 12+2W	Invitrogen	WG1401A
NuPage® Sample Reducing Agent 10X	Invitrogen	NP0004
NuPAGE® Tris-Acetate SDS Running Buffer (20X)	Invitrogen	LA0041
OrangeG Loading Dye	NEB	B70225
Pap Pen	Vector labs	H-4000
PCR plate Adhesive Seals	ThermoScientific	ab0558
Penicillin/Streptomycin	Lonza	DE17602E
PhosSTOP (Phosphatase Inhibitor Cocktail Tablets)	Roche	4906837001
Phusion Flash Polymerase Master Mix	Fisher Scientific	F-548L
Prolong gold Antifade Reagent with DAPI	Invitrogen	P-36931
Protein G Sepharose	Sigma	P3296
PureYield Plasmid Miniprep System 250	Promega	A1222
QIAfilter Plasmid Midi Kit	Qiagen	12243
Qiagen cDNA Synthesis Kit	Qiagen	210212
QIAquick Gel Extraction Kit	Qiagen	28704
QIAquick PCR Purification Kit	Qiagen	28104
QIAquick PCR Purification Kit	Qiagen	28104
Qiazol Reagent	Qiagen	79306
Rapid DNA Dephos & Ligation Kit	Roche	4898117001
Restore Plus Stripping	Thermo Scientific	46430
Retinoic Acid	Sigma	R2625
RNAse Zap	Ambion	9780
SeeBlue® Plus2 Pre-Stained Standard	Invitrogen	LC592
SimplyBlue™ SafeStain	Invitrogen	LC6060
Skim Milk Powder	Sigma	70166-500G
SNAPid	Millipore	WAVDBASE
SNAPid Single Blot Holder	Millipore	WBAVDBH01
Sodium Acetate	Sigma	S2889
Sodium Deoxycholate > 97%	Sigma	D6750
Sodium Dodecyl Sulphate > 97%	Schwarz Mann Biotech	811036
Sodium Hydroxide ACS reagent, ≥97.0%, pellets	Sigma	221465
Superscript III First Strand QPCR Supermix	Invitrogen	11752050
T175 Flask with Filter Cap	Greiner Bio-One	660175
T25 Flask with Filter Cap	Greiner Bio-One	690175
T4 Ligase	NEB	M0202S
T4 Ligase Buffer	NEB	B0202S
T75 Flask with Filter Cap	Greiner Bio-One	658175
Taq Master Mix II	Biogene	PCRM002D
Taqman Mastermix, Platinum	Invitrogen	11743-500
Thermo-Fast 96 Well Non-skirted, Natural PCR plate	Abgene	TUL-962-011N
TissueTek	Sakura Finetek	4583

TOPO TA Cloning kit (pCR® 2.1-TOPO®)	Invitrogen	K4600-01
Triethanolamine Free Base	MP Biomedicals	152163
Tris Base	Bio rad	161-0716
Tris-HCL	Promega	H5121
tRNA; from E. coli MRE 600 (RNAse negative)	Roche	10109541001
Trypan Blue	Invitrogen	15250-061
Trypsin-Versene (EDTA)	Lonza	733-1806
Tween®20	Sigma	P137-9
UltraPure DEPC-Treated Water	Invitrogen	750023
X-gal (5-Bromo-4-chloro-3-indolyl β-D-galactopyranoside)	Sigma	B6024

2.2. Buffers and Solutions

2.3.1 Ripa Buffer

Reagent	Amount
1M Tris pH 7.5	10 ml
NaCl	1.753 gram
10% SDS	2 ml
10% Na-Deoxycholate	10 ml
NP-40	2 ml
H_2O	176 ml

2.3.2 Ripa Buffer complete

Reagent	Amount
Ripa Buffer	10 ml
Protease Inhibitors (25 X)	500 µl
Phosphatase Inhibitors (10 X)	1 ml

2.3.3 Transfer Buffer for Western Blotting

Reagent	Amount
Tris	11.64 grams
Glycine	5.88 grams
10% SDS solution	7.5 ml
100% MeOH	400 ml
H_2O	1592.5 ml

2.3.4 Blocking Solution (for western blotting)

Reagent	Amount
Skim milk powder	5 grams
PBS	100 ml
Tween-20	200 µl

2.3.5 PBST Wash Solution (for western blotting)

Reagent	Volume
PBS	100 ml
Tween-20	200 µl

2.3.6 SNAPid Blocking Solution (for western blotting)

Reagent	Amount
Skim milk powder	0.2 grams
PBS	100 ml
Tween-20	200 µl

2.3.7 Western Blotting HRP detection mix

Reagent	Amount
ECL solution "A"	975 µl
ECL solution "B"	25 µl

2.3.8 4% PFA in PBS

Reagent	Amount
Paraformaldehyde	20 grams
PBS	500 ml

Warm at 60^{o}C whilst stirring until fully dissolved. Filter before use.

2.3.9 Hybridisation Solution (for *in situ* hybridisation)

Reagent	Amount
100% Deionised Formamide	2.5 ml
E.Coli tRNA (10mg/ml)	100 µl
50 X Denhardts	100 µl
Dextran sulphate	0.5 g
NaCl	0.175 g
SDS	0.012 g
0.5 M EDTA pH 8 (RNAse free)	10 µl
DEPC treated H_2O	2.3 ml

Warm at 60^{o}C to dissolve Dextran Sulphate.

2.3.10 Acetylation mix (for *in situ* hybridisation)

Reagent	Volume
Triethanolamine	5.69 ml
37% HCl	780 µl
Acetic Anhydride	1 ml
DEPC H_2O	442 ml

Acetic Anhydride added drop-wise over 4 minutes.

2.3.11 Buffer B1 (for *in situ* hybridisation)

Reagent	Volume
5M NaCl	30 ml
1M Tris-HCl pH 7.6	100 ml
H_2O	870 ml

2.3.12 Buffer B2 (for *in situ* hybridisation)

Reagent	Volume
5M NaCl	10 ml
1M Tris-HCl pH 9.5	50 ml
1M $MgCl_2$	25 ml
H_2O	415 ml

2.3.13 Blocking Solution (for *in situ* hybridisation)

Reagent	Amount
Buffer B1	50 ml
Blocking powder	0.5 g

2.3.14 Detection Mix (for *in situ* hybridisation)

Reagent	Volume
Buffer B2	50 ml
NBT/BCIP	1 ml

2.3.15 DMEM (complete) for Cell Culture

Reagent	Volume
DMEM	500 ml
Penicilin/Streptomycin	5 ml
FBS	50 ml
Glutamax (for MEF culture)	5 ml

2.3.16 McCoys (complete) for Cell Culture

Reagent	Volume
McCoys 5A	500 ml
Penicillin/Streptomycin	5 ml
FBS	50 ml

2.3.17 Cell Freezing Media

Reagent	Volume
DMEM or McCoys 5A	16 ml
DMSO	2 ml
FBS	2 ml

2.3.18 P19 Culture Media

Reagent	Volume
αMEM	500 ml
Calf serum	12.5 ml
Foetal bovine serum	7.5 ml
Non essential amino acids	5 ml
Glutamax	5 ml
Penicillin/Streptomycin	5 ml

2.3.19 P19 Induction Media

Reagent	Volume
αMEM	500 ml
Calf serum	25 ml
Non essential amino acids	5 ml
Glutamax	5 ml
Penicillin/Streptomycin	5 ml

2.3.20 Sonication Buffer (protein expression)

Reagent	Volume
Tris	20 mM pH 8
NaCl	100 mM

2.3. Primers

1.1.1. Genotyping Primer Sequences (20 μM)

Primer Name	Sequence 5' → 3'
Sci FW	TCCACGCATTGCTTCAGATG
Sci Rev	TGTGCCTTCTGCTTGTTCTCA
Sci VIC (probe) MGB	VIC – TTTGAGCTCTTCATTCA
Sci FAM (probe) MGB	FAM – CTTTGAGCTCGTCATT
Per2Luc FW1	CTGTGTTTACTGCGAGAGT
Per2Luc FW2	GGGTCCATGTGATTAGAAAC
Per2Luc Rev1	TAAAACCGGGAGGTAGATGAG
Cry2 FW1	CCAGAGACGGGAAATGTTCTT
Cry2 FW2	GAGATCAGCAGCCTCTGTTCC
Cry2 Rev1	GCTTCATCCACATCGGTAACTC

1.1.2. RT-PCR Primer Sequences (2 μM)

Primer Name	Sequence 5' → 3'
Rpli3a FW	GGAAGCGGATGAATACCAAC
Rpli3a Rev	GGATCCCATCCAACACCTT
Dbp FW	GAGCCTTCTGCAGGGAAACA
Dbp Rev	GCCTTGCGCTCCTTTTCC
Cry1 FW	GCTATGCTCCTGGAGAGAACGT
Cry1 Rev	TGTCCCCGTGAGCATAGTGTAA
Cry2 FW	TGACCTAGACAGAATCATCGAACTG
Cry2 Rev	GGCTGATGAGGGCCTGAA
Per1 FW	CCCCTGCCTCCCAGTGA
Per1 Rev	CTGAAAGTGCATCCTGATTGGA
Per2 FW	AGCTACACCACCCCTTACAAGCT
Per2 Rev	GACACGGCAGAAAAAAGATTTCTC
Clock FW	TGTCTCAAGCTGCAAATTTACCA
Clock Rev	TTTAGATGCTGCATGGCTCCTA
Bmal1 FW	CCGTGCTAAGGATGGCTGTT
Bmal1 Rev	TTGGCTTGTAGTTTGCTTCTG
Reverba FW	CGTTCGCATCAATCGCAACC
Reverba Rev	GATGTGGAGTAGGTGAGGTC
Zfhx3 FW	CCAATAGCCTGGAGAAGCTG
Zfhx3 Rev	AGTTGCACAGGACACAGTGG
Rod opsin FW	TGTTCCTGCTCATCGTGCTGG
Rod Opsin Rev	GGAAGTTGCTCATCGGCTTGC
UVS FW	TCTTCACAGTCTTCATCGCCAGC
UVS Rev	GTTCAAAAGCCAGGAAAGCCAATG
MWS FW	ATGGTGGTGGTGATGGTCTTCG
MWS Rev	TGTCTTGGAGGTGCTGGAAAGTTC
Encephalopsin FW	AAGGTGACTCCGAACAGGGATACC
Encephalopsin Rev	GCTGGTGCTGCTTCTCTACTCCAAG
RGR FW	CGAGGGGTGACAGAAACTTCATCAG
RGR Rev	CCAGCCAAGCAGCAGCATTC
cFos FW	ATCGGCAGAAGGGGAAAGTAG
cFos Rev	GCAACGCAGACTTCTCATCTTCAAG
Tyrosine Hydroxylase FW	GATTGCAGAGATTGCCTTCC
Tyrosine Hydroxylase Rev	GGTAGCAATTTCCTCCTTTGTG
PACAP FW	CCCTGCTGGTGTATGGGATA
PACAP REV	TGGTCGTAAGCCTCGTCTTC
GAD2 FW	AGGTGGCCCAAAAGTTCAC
GAD2 REV	CCGGAGTCTCCATAGAGCAG
GAD1 FW	ACTGGGCCTGAAGATCTGTG
GAD1 Rev	CAGGAAAGCAGGTTCTTGGA

2.4. Antibodies

		Concentration / Dilution		
Primary Antibodies	**Company**	**Western Blot**	**Immuno-precipitation**	**Immuno-fluorescence**
α-MYC (rabbit)	Sigma, C3956	1:2000	2 μg / reaction	1:200
α -MYC (mouse)	Invitrogen, 13-2500	1:2000	3 μg / reaction	1:200
α -HA (rabbit)	Sigma, H6908	1:1000	1:150	1:200
α -HA (mouse)	Covance, MMS101R	1:1000	1:150	1:200
α -V5 (mouse)	Invitrogen, R96025	1:5000	1:500	1:200
α -FLAG (mouse)	Sigma, F3165	1:3000	1:150	1:200
α -Actin (rabbit)	Autogen, ACTB22-A	1:80,000	N/A	N/A
α -Actin (mouse)	Abcam, 8226	1:80,000	N/A	N/A
α -P84 (rabbit)	Abcam, 5E10	1:2000	N/A	N/A
α -ZFHX3(A) (rabbit)	Custom	1:3000	N/A	1:200
α -SC35 (mouse)	Abcam, 11826	N/A	N/A	1:200
α -cFos (rabbit)	NEB, 9F6	N/A	N/A	1:200
α -Histone H3 (rabbit)	Sigma, H9289	N/A	N/A	1:200
Secondary Antibodies	**Company**	**Western Blot**	**Immuno-precipitation**	**Immuno-fluorescence**
α -Rabbit HRP	Biorad, 170-6515	1:10,000	N/A	N/A
α -Mouse IgG peroxidase	Sigma, A4416	1:10,000	N/A	N/A
AlexaFluor 488 (mouse, rabbit)	Invitrogen, A10684 & A11070	N/A	N/A	1:400
AlexaFluor 568 (rabbit, goat)	Invitrogen, A21069 & A11057	N/A	N/A	1:400
AlexaFluor 647 (mouse, goat)	Invitrogen, A21235 & A21447	N/A	N/A	1:400

2.5. Plasmids

Plasmid name	cDNA species	Vector backbone	Tags	Source
Cry1-HA	Full length mouse cDNA	pcDNA3.1	HA	Michael Hastings lab University of Cambridge.
Cry2 - HA	Full length mouse cDNA	pcDNA3.1	HA	Michael Hastings lab.
Rev-erba-V5-HIS	Full length mouse cDNA	pcDNA3.1	V5, HIS	Nolan lab MRC Harwell
Epas1-MYC	Full length mouse cDNA	pcDNA3	MYC	Celeste Simon lab University of Pennsylvania.
Per2-HA	Full length mouse cDNA	pcDNA3 vers.b	HA	Bert van der Horst lab ErasmusMC Rotterdam
Bmal1-V5-HIS	Full length mouse cDNA	pcDNA3.1	V5, HIS	Michael Hastings lab.
Zfhx3-V5-HIS	Full length mouse cDNA	pcDNA3.1	V5, HIS	Michael Parsons MRC Harwell
Zfhx3-MYC	Full length human cDNA	pCI (modified)	MYC	Yutaka Miura lab Nagoya City University
Zfhx3-HA	Full length human cDNA	pCI (modified)	HA	Yutaka Miura lab.
EV-MYC	MYC epitope only	pCI(modified)	MYC	Yutaka Miura lab.
EV-HA	HA epitope only	pCI(modified)	HA	Yutaka Miura lab.
TRX-HIS-Zfhx3	750bp 3' mouse cDNA fragment	pET32b	TRX, HIS	Michael Parsons.

2.6. Methods

2.6.1. Animal Husbandry

Mice were maintained in accordance with the Animals Scientific Procedures Act (ASPA) 1986. Colonies were bred and housed in individually ventilated cages (IVCs) in a pathogen-free environment. All procedures carried out were according to the personal and project license, permitted by the Home Office. All animal work was performed under project license 30/2686 and personal license 30/8580. All animals were culled in accordance with the Schedule 1 method of cervical dislocation, in a designated area.

2.6.2. Circadian Behavioural Phenotyping

Wheel-running: Wheel-running activity was used to identify circadian phenodeviants following ENU mutagenesis. Mice were individually housed in cages within light-tight chambers, kept under environmentally controlled conditions. Cages contained running wheels in which the revolutions were monitored and plotted as activity on double-plotted actograms. Initially, cages were exposed to a week-long entrainment period of a 12:12 light-dark cycle. Constant conditions followed entrainment, with two weeks of constant darkness followed by constant light, assessing the free-running ability. In some screens, a second 12:12 LD cycle followed the period of constant light to assess re-entrainment. A light intensity of 100 lux using a fluorescent light source was used for all screens unless otherwise stated. Food and water were provided *ad libitum*. Littermate controls were run alongside phenodeviants. After data collection, animals were either returned to normal housing conditions or culled. Animals did not remain singly housed for wheel running analysis for more than ten consecutive weeks. Animals were analysed from 8 weeks of age.

Light pulses: A 15 minute 100 lux light pulse was given to animals housed in constant darkness. Tissues were collected at circadian time points (CTs) 15 minutes following the light

pulse. Animals were housed as described above and CT values were calculated from the onset of wheel running activity. Circadian times were calculated in relation to CT 12, the first onset of activity. All animals were culled in the dark.

2.6.3. Startle and Pre-Pulse Inhibition

Male mice were assessed for startle response and pre-pulse inhibition (PPI) at ten weeks of age. The mice were allowed to acclimatise to the phenotyping room for 30 minutes prior to the test. Following this, the mice were placed in individual sound-proofed startle boxes (Med Associates Inc Equipment). The startle boxes consisted of an outer chamber containing a sound proofed acoustic chamber with a load cell platform and amplifier, regulated by a sound generator (Med Associates Inc Equipment). Sound and movement sensor calibration were completed monthly. Each mouse was placed onto the load cell platform within the acoustic chamber and the door closed. The automated acoustic programme lasted approximately 50 minutes. Once the test was completed, the mouse was returned to the home cage and the acoustic chamber was wiped clean with ethanol and allowed to dry before running subsequent sessions with other animals. The startle and PPI protocol, modified from EMPRESS Phenotyping (empress.har.mrc.ac.uk) was as follows:

- An initial acclimatisation of 5 minutes without a pre-pulse stimulus, an inter-trial interval of 50 msec and a pulse of white noise 110 (dB)/40 msec.
- A pre-pulse inhibition session of ten different trial types presented in a pseudorandom order with an inter-trial delay of 20 – 30 seconds.
- A trial in which only an acoustic startle pulse is presented as white noise 110 dB/ 40 msec.
- Eight different pre-pulse trials, of 10 msec duration, of 70, 80, 85, or 90 dB white noise stimuli presented alone or preceding the pulse by 50 msec.

- A trial in which only background noise 65 dB is presented to measure baseline movement of the animal in the chamber.
- The startle response was recorded every millisecond for 65 msec after the onset of startle.

2.6.4. Pupilometry

Pupillary light reflex responses were assessed by Dr. Stuart Peirson and Carina Pothecary at the University of Oxford and carried out as previously described (Hughes, et al. 2012). Animals were housed on a 12:12 light-dark cycle and were tested between *zeitgeber* time (ZT) 4 and 8 and were dark adapted for 1–2 hours prior to testing. A xenon arc lamp (150 W solar simulator, Lot Oriel, UK) with a 480 nm monochromatic filter (Andover, 10 nm half-bandwidth) was used to produce a light intensity of 14.6 log quanta / cm^2 / s (173 lW/ cm^2 / s) (bright light) or 11.6 log quanta / cm^2 / s (0.17 lW/ cm^2 / s) (dim light). Light was transmitted to the eye via a liquid light pipe as an irradiant light stimulus using a two inch integrating sphere (Pro-lite Technology, UK). Images of the pupillary light response were collected with a Prosilica near infrared sensitive charge couple device video camera (BRSL) at a rate of 10 frames / s. The camera was positioned perpendicular to the contra-lateral eye, which was illuminated by infra-red light emitting diodes (850 nm, 10 nm half-bandwidth). In this way, consensual pupil responses could be measured in response to an irradiant light stimulus. Five minutes prior to recording, 1% tropicamide was applied to the stimulated eye. Animals remained un-anaesthetized during the procedure but were temporarily restrained by “scruffing”, using normal husbandry techniques for the duration of the recording (29 secs). After brief baseline measurements of the dark-adapted pupil (2 secs), the left eye was exposed to the light stimulus for 10 secs. Recovery data were collected for a post-stimulus period of 17 secs. Each animal was tested on multiple occasions to minimize any artifacts due to handling. To assess the ability of the pupil to constrict fully, a topical solution of 1 M carbachol (Sigma) in sterile

phosphate buffered saline (PBS) (pH 7.4) was applied to the cornea. Pupil size was measured after 1 hour of dark adaptation before carbachol was administered, and again at 15 min after application of the miotic agent. Images were analysed using ImageJ.

2.6.5. Optokinetic Drum

Male mice aged 10–12 weeks were tested for optomotor responses using a visual tracking drum. Mice were acclimatised for 30 minutes to the phenotyping room prior to starting the test. Mice were then individually placed onto a raised circular platform of 8 cm diameter in the centre of four screens each displaying a moving black and white vertical bar pattern. The mouse was allowed to settle for 30 seconds before starting the test. The frequencies of the stripes used were 0.25 cycles / degree (subtending an angle of 2^{o} when viewed from the centre of the drum), 0.125 cycles / degree (4^{o}), or 0.0625 cycles / degree (8^{o}). The pattern was rotated anticlockwise for 30 seconds at a rotation speed of two revolutions per minute (12^{o}/sec) to assess right eye ability and repeated clockwise to assess left eye ability. During the rotations, the mouse was observed for its head tracking response. The test started with the 2^{o} stripe and if no head tracking response was observed, the stripe was increased to 4^{o} and 8^{o}.

2.6.6. Genotyping

All genotyping primer and probe sequences are listed in Table 1.1.1.

Ear biopsy digestion using NaOH: 100 μl 50 mM NaOH was added to each ear biopsy and incubated at 95°C for 90 minutes. 10 μl 1 M Tris pH7.5 was then added to each sample. This method of DNA extraction was used for *Sci* and *Cry2* genotyping.

DNeasy Blood and Tissue DNA Extraction (QIAGEN): DNA extraction from ear biopsies was carried out as described in the manufacturers protocol. Briefly, 180 μl lysis buffer ATL and 20

μl Proteinase K was added to each ear biopsy and vortexed. The samples were incubated overnight at 55°C. 200 μl buffer AL and 200 μl 100% ethanol were added to each sample, vortexed, and added to a spin column within a collection tube. The samples were centrifuged at 6000 *x g* for 1 minute and the flow through was discarded. 500 μl buffer AW1 was added and centrifuged and discarded as before. 500 μl buffer AW2 was added and centrifuged at 20,000 *x g* for 3 minutes. The column was transferred to a new micro-centrifuge tube and 200 μl elution buffer AE was added and incubated for 2 minutes before centrifuging at 20,000 *x g* for 1 minute. The flow through contained the eluted DNA ready for use. This method of DNA extraction was used for *Per2*-Luciferase (*Per2-Luc*) and *Cry1* genotyping.

***Sci*:** The mutation for *Sci* was genotyped using a real time PCR (RT-PCR) Taqman assay. DNA was diluted 1:20 in H_2O for the reaction. The following reaction in Table 2 was then set up on ice in a RT-PCR plate: Genotyping primer and probe sequences are listed in Table 1.1.1.

Reagent	**Volume**
20 μM forward primer	1.25 μl
20 μM reverse primer	1.25 μl
100 μM VIC® dye-labelled MGB probe	0.05 μl
100 μM FAM™ dye-labelled MGB probe	0.05 μl
2 X Platinum QPCR SuperMix-UDG with ROX	10 μl
H_2O	5.4 μl
DNA	2 μl

Table 2: Short circuit PCR genotyping set up.

The programme was run on an ABI 7500 Fast Real Time System. The cycling programme was run as shown in Table 3.

Temperature	Duration
50°C	2 minutes
95°C	10 minutes
START X40 CYCLES	
95°C	15 seconds
60°C	1 minute

Table 3: Short circuit genotyping RT-PCR thermal cycling conditions.

The allelic discrimination genotyping method is a multiplexed end-point assay that detects variants of a single nucleic acid sequence. The VIC labelled probe recognises the mutant allele and the FAM labelled probe recognises the wild type allele. The probe contains a fluorescent dye and a quencher. The quencher is removed by exonuclease activity if there is a perfect match between the probe and the recognised sequence and fluorescence is released. The relative amounts of the fluorescence and consequently the presence of either allele, is determined by analysing the resultant dissociation curve plots.

***Cry1*:** Genotyping of *Cry1* knock-out animals was carried out by Ms. Jo Chesham at the MRC Laboratory of Molecular Biology, University of Cambridge.

***Cry2*:** A PCR based assay was used to distinguish between the *Cry2* deletion allele and wild type. DNA was diluted 1:4 in H_2O for the reaction. The following reaction in Table 4 was set up on ice in a PCR plate.

Reagent	Volume
Hot Shot PCR master mix	7.5 μl
20 μM shared reverse primer	0.3 μl
20 μM forward primer 1	0.15 μl
20 μM forward primer 2	0.15 μl
H_2O	4.9 μl
DNA	2 μl

Table 4: *Cry2* PCR genotyping set-up.

The samples were then run on a thermal cycling programme as shown in Table 5.

Temperature	Duration
94°C	2 minutes
START X35 Cycles	
95°C	30 seconds
55°C	30 seconds
72°C	90 seconds
End Cycles	
72°C	10 minutes

Table 5: *Cry2* genotyping PCR thermal cycling conditions.

The sizes of the PCR products were then analysed by agarose gel electrophoresis (2.6.7). *Cry2*$^{+/+}$ band size was 550 base pairs (bp), *Cry2*$^{-/-}$ band size was 310 bp.

Per2-Luc: A PCR based assay was used to distinguish between the *Per2-Luc* mutant and wild type allele. The PCR reaction in Table 6 was set up on ice in a PCR plate:

Reagent	Volume
10 X NH_4 Buffer	5 μl
dNTP (40 mM total)	1.25 μl
20 μM FW primer 1	1 μl
20 μM FW primer 2	1 μl
20 μM REV primer	1 μl
50 mM $MgCl_2$ Solution	2 μl
H_2O	37.6 μl
BIOTAQ DNA Polymerase (5U/μl)	0.4 μl
DNA	1 μl

Table 6: *Per2-Luc* PCR genotyping set-up.

The samples were then run on a thermal cycling programme as shown in Table 7.

Temperature	Duration
95°C	1 minute
START X32 Cycles	
95°C	1 minute
52°C	1 minute
72°C	1 minute
End Cycles	
72°C	7 minutes

Table 7: *Per2-Luc* genotyping PCR thermal cycling conditions.

The sizes of the PCR products were then analysed by agarose gel electrophoresis (2.6.7). *Per2* wild-type band size was 230 bp, *Per2-Luc* band size was 680 bp.

2.6.7. Agarose gel electrophoresis

DNA and RNA samples were analysed by agarose gel electrophoresis. Gels of 0.8% - 2% were made by dissolving 0.8 g – 2 g agarose in 100 ml 1 X TAE buffer, by heating for 60–120 seconds

in a conventional microwave. Once dissolved, the agarose was allowed to cool before adding GelRed™ nucleic acid stain at a 1:20,000 dilution from the 10,000 X stock. The agarose was then poured into a cast with a well comb, and allowed to set at room temperature (RT). After removal of the well comb, the gel was transferred to a gel tank and 1 X TAE solution was added until it submerged the gel. 5–25 μl sample was loaded into each well. Samples already containing loading dye from the PCR reaction could be added directly to the wells. For samples not containing loading dye, Orange G dye was added at a 1:3 ratio before loading. Gels were typically run at 80 – 130 volts (0.12 – 0.18 Amps) for 0.5–3 hours, depending on the percentage of the agarose, the separation required and expected amplicon size. Following electrophoresis, gels were visualised using a GelDoc UV light source system.

2.6.8. Protein Extraction

From tissue: RIPA lysis buffer, 1 ml with 1 X protease and phosphatase inhibitors, was added to a prepared micro-centrifuge tube containing a homogenizing matrix of 1.4 mm ceramic spheres. Snap frozen tissue (approximately 10 mg) was then added to the lysis buffer. It was then homogenised with 15 second pulses, using a FastPrep Homogenizer, at 4^{o}C until the tissue was completely disrupted. The samples were then centrifuged at 10,000 x *g*, 4^{o}C for 5 minutes. The supernatant was transferred to a new micro-centrifuge tube and was quantified using Bradford reagent (2.6.9). Lysates were stored at -20^{o}C for 24 hours and -80^{o}C long term.

From cells: Cells were washed twice with PBS at 4^{o}C. 500 μl RIPA buffer (with 1 X protease and phosphatase inhibitors) was then added to a 10 cm dish of confluent cultured cells on ice. The amount of RIPA buffer was scaled up or down depending on the size of the culture dish. The cells were left to incubate for 30 minutes on ice before being collected by scraping and transferring to a micro-centrifuge tube. The samples were then centrifuged at 10,000 x *g,* 4^{o}C, for 30 minutes and the supernatant was transferred to a new micro-centrifuge tube and

quantified using Bradford reagent (2.6.9). Lysates were stored at -20°C for 24 hours and -80°C long term.

2.6.9. Protein Quantification

Protein standards were made through serial dilution using a 10 mg / ml BSA stock. 20 µl of BSA was added to a micro-centrifuge tube with 80 µl of 1:5 diluted RIPA buffer in H_2O. The 2 µg final concentration solution was vortexed and briefly centrifuged for 30 seconds at 10,000 x *g* at RT. 50 µl of the 2 mg / ml stock was transferred to a micro-centrifuge tube containing 50 µl 1:5 diluted RIPA buffer for the 1 mg / ml standard. The process was repeated until a standard of 0.125 mg/ml was reached. 5 µl of each standard was loaded in triplicates into a 96 well plate as well as an H_2O blank and 1:5 diluted RIPA buffer alone. 5 µl of each protein sample, diluted 1:5 in H_2O, was then loaded in triplicates into the plate. Bradford reagent was mixed and brought to RT before adding 200 µl to each well. The plate was then left on a rocker at low speed at RT for 5 minutes to allow for complete homogenisation of the samples. Protein concentrations were determined using a KCjunior™ spectrophotometer and data analysis software at 595 nm wavelength. The concentrations of protein generated were accepted as accurate if the standard curve produced had an R^2 value greater or equal to 0.98.

2.6.10. Immuno-precipitation

All protein samples were kept on ice and all centrifugation was performed at 4°C unless otherwise stated. 1 mg protein lysate was made up to 1 ml with RIPA buffer (with 1X protease and phosphatase inhibitors). 25 µl protein G sepharose beads were added to a micro-centrifuge tube with 500 µl of RIPA buffer. The beads were centrifuged at 2,000 x *g* for 1 minute. The supernatant was removed and the protein sample was added for pre-clearing by incubating at 4°C, rotating for 1 hour. The protein lysate and beads were then centrifuged at 2,000 x *g* for 1 minute at 4°C. The supernatant (soluble protein lysate) was removed from the

beads and transferred to a new micro-centrifuge tube and the beads were discarded. Primary antibody was then added to the lysate (Table 2.4) and incubated rotating at 4°C overnight. The sample was then briefly centrifuged at 2,000 x *g* for 1 minute at 4°C and added to a fresh aliquot of 25 µl protein G sepharose beads, pre-washed in RIPA buffer. The sample was then incubated for 2 hours at 4°C rotating. Following the immuno-precipitation reaction, the sample was briefly centrifuged and the supernatant removed. 50 µl sample buffer and 5 µl reducing agent was added, briefly vortexed and then heated to 95°C for 5 minutes. 20 µl of the sample (avoiding the beads) was then loaded onto an SDS-PAGE gel (2.6.11) or stored at -80°C until required.

2.6.11. SDS-PAGE

Protein samples for SDS-PAGE were prepared on ice. For mini pre-cast Novex gels, up to 20 µg of protein was mixed with 5 µl sample buffer and 2 µl sample reducing agent in a total volume of 20 µl. For midi Novex gels, up to 50 µg of protein was mixed with 12.5 µl sample buffer and 5 µl sample reducing agent in a total volume of 45 µl. Samples were briefly vortexed before incubation at 95°C for 5 minutes. Samples were then centrifuged at RT before loading onto the gel. Large proteins (more than 200 kDa) were separated on 3 – 8% Tris-Acetate gels alongside the HiMark™ protein standard and NuPage Tris-Acetate running buffer. Smaller proteins (less than 200 kDa) were separated on 4 – 12% Bis-Tris gels alongside the SeeBlue® Plus2 protein standard and NuPage MOPs running buffer. 500 µl NuPage anti-oxidant was added to the inner chamber (cathode) of the mini gel tank and 435 µl to the midi gel tank. Gels were run at 120 - 200 volts (80 – 110 mA) for 60 – 120 minutes, depending on the separation required and the gel used.

2.6.12. Western Blotting

Semi-dry transfer: Following protein separation by SDS-PAGE, the precast Novex gels were removed from their cassettes and incubated for 10 minutes in transfer buffer (2.3.3). PVDF membrane was cut to the size of the gel, briefly activated by immersion in 100% methanol and incubated in transfer buffer along with two pieces of thick filter paper. The transfer stack was assembled on the semi-dry blotter first with filter paper, then the PVDF membrane, the gel and the second piece of filter paper on top. The transfer was set to 12 volts (2 amps) for two hours in all instances.

Antibody incubation: Following transfer of the protein from the gel to the membrane, the membrane was blocked for 2 hours (2.3.4) at RT with gentle rocking. The membrane was then rinsed in washing reagent (2.3.5), three times for 5 minutes. The membrane was then transferred to a pre-wetted blot holder (SNAPid) using MilliQ H_2O to use with the Millipore SNAPid vacuum based western blotting system. The membrane, within the blot holder, was placed within the SNAPid unit and 3 mls SnapID blocking solution (2.3.6) with primary antibody (Table 2.6) was added to the membrane and left to incubate for 10 minutes at RT. The vacuum source was then applied (20 psi) and 30 mls of washing reagent was added to the membrane and left to drain. This was repeated three times. The vacuum source was then switched off and 3 mls of SnapID blocking solution with HRP conjugated secondary antibody was added to the membrane and left to incubate for 10 minutes at RT. The membrane was washed three times using the vacuum source as before.

2.6.13. HRP Chemi-luminescence Detection

Following western blotting, the membrane was left to incubate with 1 ml ECL-Plus reagent for 3 minutes (2.3.7). The ECL was then drained and the membrane placed between 2 acetate sheets and rolled to remove air bubbles. The membrane was then developed using the ChemiDocIT system, using the auto-expose function. The exposure time varied depending on

the protein sample being studied, the amount of protein loaded on the gel and the efficiency of the antibody labelling.

2.6.14. Culture of Adherent Cell Lines: Hek293, Cos7 and U2OS

All cell types described were maintained in a humidified incubator at 37^{o}C with 5% CO_2 in the presence of 0.1% benzalkonium chloride. To maintain sterility, all cell culture work was carried out in containment under class II biological safety cabinets and all surfaces and reagents were sterilised with 70% ethanol before contact with the cells. Hek293 and Cos7 cells were maintained in complete DMEM (2.3.15) and U2OS cells were maintained in complete McCoys 5A media (2.3.16). All culture media and reagents were pre-warmed to 37^{o}C before use with cells for all cell culture protocols. Cells were passaged using trypsin-EDTA every alternate day, or when more than 70% confluent. To passage cells, media was removed from the culture vessel and the cells were washed twice with 5 mls Dulbecco's phosphate buffered saline (DPBS). For a T75 culture flask or 10 cm dish, 3 ml Trypsin-EDTA was added to the culture vessel and incubated at 37^{o}C for 5 minutes or until cells were visibly detached. This was scaled up or down depending on the size of the culture vessel. 7 ml culture media was added to the cell suspension and pipetted up and down to ensure even cell distribution. Cells were then transferred to a new culture vessel containing culture media, in a ratio depending on their subsequent use. For maintaining cells, 1 ml suspended cell solution was added to 19 ml fresh media. Alternatively, cells would be counted using a haemocytometer and plated accordingly (2.6.17).

2.6.15. Culture and differentiation of P19 cells

Undifferentiated P19 cells were cultured in P19 culture media (2.3.18) and passaged as described in 2.6.14 prior to differentiation into neuronal cell types using retinoic acid. For differentiation, P19 cells were washed with 5 ml DPBS then incubated with 1 ml Trypsin at

37°C for 10 minutes. Once the cells detached, 10 ml P19 induction media (2.3.19) was added to the trypsin and cell solution. 1 ml suspended cells were transferred to a bacterial grade petri dish (for low adherence) containing 9 ml P19 induction media. Retinoic acid was added to the cells at a final concentration of 5 x 10^{-7} M. Aggregates of cells formed in suspension between 24 – 48 hours. Once aggregates had formed, the suspension was collected and transferred to a Falcon tube. Cells were centrifuged at 1000 x *g* for 5 minutes and the media was removed from the cell pellet. The cell pellet was resuspended in 10 ml P19 induction media with retinoic acid and transferred to a new bacterial grade dish. Cell aggregates were harvested again after 24 – 48 hours by centrifugation. The cells were then washed with αMEM, and centrifuged at 1000 x *g*. The media was discarded and the cell pellet was resuspended in 2 ml trypsin with 100 μg DNAse. The cells were incubated in a 37°C water bath for 10 minutes with occasional agitation. 4 ml P19 culture media was added to the cell solution and centrifuged at 1000 x *g* for 5 minutes. The media was removed and the cell pellet was resuspended in 5 ml P19 culture media. Cells were then counted as described in 2.6.17. 2.1 x 10^6 cells in 5.7 ml P19 culture media were cultured in a 10 cm cell culture grade dish to adhere. Cells were incubated at 37°C for 2 – 4 days for optimal differentiation. The media was changed every 36 hours and cells collected once at desired confluency.

2.6.16. Freezing Cells for Storage

Cells were regularly frozen down for storage in order to maintain stocks. Cells were trypsinised and resuspended in complete media as described (2.6.14). Following this, the cell solution was transferred to a Falcon tube and centrifuged at 1,000 x *g* for 5 minutes at RT. The supernatant was then removed and the cell pellet was resuspended in 4 ml freezing media (2.3.17). 1 ml was then transferred to a cryovial and snap frozen on dry ice before being stored in a liquid nitrogen storage tank.

2.6.17. Counting and Plating Cells

Cells were counted using a haemocytometer prior to plating for transfection. Cells were trypsinised and made up to 10 ml with complete media as described (2.6.14). 500 μl cells were then added to 500 μl 0.4% trypan-blue diluted 1:4 in DPBS and vortexed to mix. 10 μl of the cell solution was then added to a haemocytometer beneath a cover-slip, which created a 1.0 mm x 0.1 mm total volume over each square in the haemocytometer grid. The total number of cells in the grid was then counted, with clumps being considered as one cell and those on the outside boundary being ignored. The total number of cells per ml was then calculated as $2(n/4) \times 10^4$. The total volume required of the cell suspension was then transferred to a Falcon tube and centrifuged at 1000 *x g* for 5 minutes at RT. The supernatant was removed and the cell pellet was resuspended in the total volume of media required (either with or without additives, depending on the experimental requirement) before being added to the culture vessel. Cells were then incubated and cultured as normal.

2.6.18. Transfection of Cell Lines

Cells were transfected using jetPRIME™ reagent according to the manufacturers conditions. 10 μg total plasmid DNA was added to 500 μl jetPRIME™ buffer, pulse vortexed and briefly centrifuged at 1000 x *g* at RT. 20 μl of jetPRIME™ transfection reagent was then added to the DNA solution, pulse vortexed, centrifuged 1000 x *g* and incubated for 10 minutes at RT. The transfection mix was then added drop wise to a 10 cm dish of 70% confluent cells in complete media. Cells were then analysed or harvested after a minimum of 24 hours. The transfection mix was scaled up or down depending on the size of the culture vessel, however the 1:2 ratio of DNA concentration (μg) : jetPRIME reagent (μl) remained the same.

2.6.19. Isolation and culture of Mouse Embryonic Fibroblasts (MEFs)

Embryos were harvested at E13.5 – E14.5 for preparation of MEFs. Prior to embryo isolation, 10 cm cell culture dishes containing 10 mls DPBS with 0.1% glycine, were incubated at 37^{o}C until ready for use. The pregnant female was culled and the uterus was harvested using sterilized forceps and scissors. The embryo sacs were transferred into PBS on ice. Each embryo was removed from its yolk sac and then culled immediately by removing the head. Under a microscope, the limbs, tail, and all internal organs were removed and could be used for DNA extraction and genotyping as required (2.6.6). Under sterile conditions, the remaining embryo body was transferred to a fresh dish of DPBS to rinse the embryo and then transferred to a dish containing 5 ml trypsin. The embryo body was roughly chopped using scalpel blades and mixed by pipetting up and down with a 5 ml serological pipette. The trypsin / embryonic cell solution was transferred to a 50 ml Falcon tube and incubated in a 37^{o}C water bath for 5 minutes, with constant agitation. The DPBS + glycine solution was discarded from the plates that had incubated at 37^{o}C and 10 ml fresh complete DMEM was added to the dish. The trypsin-containing cell solution was added directly to the DMEM and homogenized further by pipetting. The dishes were incubated over night at 37^{o}C and the media changed the following day. The cells were passaged at a 1:3 or 1:2 ratio as described in 2.6.14, depending on confluency and growth rate.

2.6.20. Stable isotope labelling by amino acids in cell culture (SILAC)

SILAC was carried out on freshly isolated MEFs as described in 2.6.19. SILAC “heavy” and “light” media were made fresh by addition of either normal or heavy isotopically labelled Lysine and Arginine (L-Lysine-2HCl; L-Arginine-HCl; 13C6, 15N2 L-Lysine-2HCl 50mg; 13C6 15N4 L-Arginine-2HCl), 1% Penicillin-Streptomycin antibiotic and 10% FBS. Wild-type MEFs were isolated and directly cultured in DMEM containing light lysine and arginine whilst mutant MEFs were cultured in DMEM containing heavy lysine and arginine. The MEFs were passaged four

times (P4) across 14 days in the appropriate SILAC media in order to allow for maximal incorporation of the heavy or light amino acids before the MEFs became senescent. For experiments requiring synchronisation of the cells, a final concentration of 10 μM forskolin was added to the cultured MEFs and left for 14 – 24 hours. For experiments requiring proteasome inhibition, proteasome inhibitor MG132 was added at a final concentration of 5 μg / ml and incubated for 4 hours prior to collection. Cells were then collected at the desired time according to their synchronisation or proteasome inhibition. The cells were counted as described in 2.6.17 and an equal number of wild-type and mutant MEFs were combined and the cells pelleted for protein extraction and nuclear and cytoplasmic fractionation as described in 2.6.21 below.

2.6.21. Nuclear and Cytoplasmic Fractionation and Protein Extraction

Adherent cells were harvested by trypsinisation and pelleted by centrifugation at 2000 *x g* for 5 minutes. The cell pellet was washed by re-suspension in cold PBS and pelleted by centrifugation as before. The PBS was removed and discarded and the cell pellet was left as dry as possible and kept on ice. The nuclear and cytoplasmic protein extraction was then followed as per the manufacturers protocol (Thermo Scientific, NE-PER® Nuclear and Cytoplasmic Extraction, 78833). Briefly, 200 μl of ice cold CER I buffer (containing protease and phosphatase inhibitors) was added to the cell pellet of an approximate packed cell volume of 20 μl. The cells were vortexed rigorously to fully resuspend the pellet and then incubated on ice for 10 minutes. 11 μl of ice cold CER II buffer was then added to the cells, briefly vortexed to mix and incubated on ice for a further minute. The cells were again briefly vortexed and then pelleted for 5 minutes at 16,000 *x g* at 4^{o}C. The supernatant containing the cytoplasmic fraction was transferred to a pre-chilled micro-centrifuge tube and stored at -80^{o}C until required. The nuclear fraction was resuspended in 100 μl NER buffer (containing protease and phosphatase inhibitors). The pellet was vortexed for 15 seconds every 10

minutes for a total of 40 minutes. The sample was then pelleted for 10 minutes as before and the supernatant containing the nuclear fraction was transferred to a pre-chilled micro-centrifuge tube and stored at -80^{o}C until required for western blotting, immuno-precipitation or mass spectrometry analysis.

2.6.22. Immuno-fluorescence

Immuno-fluorescence was performed on cells or tissue sections (cut at 12 μm) on slides. All steps were performed at RT. The protocol is outlined in Table 8.

Step	Reagent	Duration
Fixation	4% pfa	15 minutes
Wash	PBS	1 minute
Permeabilisation	100% MeOH (cold)	20 minutes
Wash	PBS + 0.2 % Tween (PBST)	2 X 5 minutes
Blocking	PBST + 10% goat serum	1 hour
Primary Antibody	PBST + 5% goat serum + 1:200 – 1:400 antibody	1 hour
Wash	PBST	4 X 10 minutes
Secondary Antibody	PBST + 2.5% goat serum + 1:400 antibody	1 hour (in the dark)
Wash	PBST	4 X 10 minutes

Table 8: Immuno-fluorescence protocol.

Slides were briefly dried before mounting media containing DAPI was added to the slides and sealed with a cover-slip and left to incubate in the dark, at RT until hardened. Slides were then stored in the fridge in a humidified chamber until visualisation by fluorescence microscopy.

2.6.23. Tissue Collection

Tissue samples were collected for processes such as protein, RNA or DNA extraction or for sectioning. For all processes, animals were culled according to Schedule 1 in a designated

area. Tissues were dissected as quickly as possible using pre-chilled equipment which had been washed and decontaminated with RNAse ZAP to avoid any degradation. For RNA or protein extraction, harvested tissues were placed into micro-centrifuge tubes on dry ice and snap frozen. They were then stored at -80^{o}C until required. Whole tissues for sectioning were carefully dissected and rinsed in PBS. Tissues were fresh-frozen by positioning in optimal cutting temperature (OCT) freezing medium within an embedding mould, over isopentane on dry ice. Once frozen, the samples were stored at -80^{o}C before being sectioned at 12 μm using a cryostat. For whole eye sections, eyes were first punctured through the lens before being submerged in 4% PFA at 4^{o}C overnight. Eyes were then transferred to 30% sucrose at 4^{o}C overnight before embedding in OCT medium.

2.6.24. RNA Extraction

Approximately 100 mg of frozen tissue was homogenized in 1 ml Qiazol reagent using a pestle or syringe. Samples were then incubated for 5 minutes at RT before adding 0.2 ml chloroform. The sample was then repeatedly inverted to mix for 15 seconds and then incubated for 25 minutes at RT. The sample was then centrifuged for 15 minutes at 12,000 x *g*, 4^{o}C. The aqueous phase was transferred to a new micro-centrifuge tube and 500 μl isopropyl alcohol was added and incubated for 10 minutes at RT. Again, the sample was centrifuged for 10 minutes at 12,000 x *g*, 4^{o}C. The supernatant was removed and the RNA pellet was washed with 1 ml 75% ethanol. The sample was vortexed and then centrifuged for 5 minutes at 7,500 x *g* at 4^{o}C. The supernatant was removed and the pellet was briefly allowed to air dry. The RNA pellet was then resuspended in 100 μl DEPC treated H_2O and quantified and analysed using a Nanodrop spectrophotometer. A 260/280 ratio of 2.0 and 260/230 ratio of 2.0 – 2.2 was expected for pure RNA.

2.6.25. cDNA Synthesis

cDNA was prepared under RNAse free conditions using the Invitrogen SuperScript™ III First Strand cDNA Synthesis SuperMix. The pipettes, bench area and equipment were decontaminated and treated with RNAse Zap and filter tips were used throughout. The reaction in Table 9 was set up on ice in a PCR plate.

Reagent	Volume
RNA	X μl (1 μg)
RT enzyme mix	2 μl
RT 2X reaction mix (containing Oligo dT)	10 μl
DEPC H_2O	Up to 20 μl

Table 9: cDNA synthesis reaction set-up.

The reaction then went through the following thermal cycling programme shown in Table 10.

Temperature	Duration
25 °C	10 minutes
50 °C	30 minutes
85 °C	5 minutes
1 μl of E.Coli RNAse H was added and mixed	
37°C	20 minutes

Table 10: cDNA synthesis thermal cycling.

The cDNA synthesis was checked by electrophoresis (2.6.7) to qualitatively assess cDNA quality and quantity. It was then stored at -20 °C until further use.

2.6.26. Generation of Riboprobe Template by PCR

Constructs for *in situ* hybridisation were amplified by PCR from genomic DNA. Constructs were designed for exonic probes within exon 9 and exon 2 of the *Zfhx3* transcript using the following primer pairs in Table 11.

Primer Name	Sequence 5' → 3'
Zfhx3 ex9 FW	GTGCCCAGAACCAGTTCATT
Zfhx3 ex9 Rev	CAACCTGACTCTGTCTGCCA
Zfhx3 ex2 FW	GGACCTGTCCAAATTCGATG
Zfhx3 ex2 Rev	GAGAAAGTAGAGCCAGCCGA

Table 11: Primer sequences used for *Zfhx3* riboprobe synthesis.

The following PCR reaction in Table 12 was set up in a PCR plate on ice:

Reagent	Volume
Taq Master Mix (Biogene)	7.5 μl
Zfhx3 FW primer (10 μM)	1 μl
Zfhx3 REV primer (10 μM)	1 μl
Genomic DNA (100 ng / μl)	0.5 μl

Table 12: PCR reaction mix for riboprobe synthesis.

The reaction went through the following thermal cycling programme shown in Table 13.

Temperature	Duration
94°C	2 minutes
X35 Cycles	
94°C	30 seconds
55.2°C	30 seconds
68°C	30 seconds
End Cycles	
72°C	10 minutes

Table 13: Thermal cycling conditions for riboprobe synthesis PCR.

The PCR product was separated and analysed by agarose gel electrophoresis (2.6.7). The expected amplicon sizes were 585 bp (exon 9 probe) and 591 (exon 2 probe). PCR products were then immediately purified by gel extraction (2.6.27) followed by TOPO™ cloning (2.6.29). This was to ensure the integrity of the A-overhang produced by amplification with *Taq* polymerase which was required for the TOPO™ cloning technique. Following TOPO™ cloning

and amplification and purification of plasmid DNA, plasmids were sequenced to confirm the orientation and the sequence of the PCR cloned inserts. Sequencing was carried out by GATC-biotech using stock primers for the T7 and M13 promoters, present in the TOPO™ vector.

2.6.27. QIAGEN Gel Extraction and PCR Purification

Template DNA, produced by PCR or restriction digest technique from plasmid vectors, were isolated from other DNA products by gel extraction, or cleaned up using a PCR purification kit. This was required prior to cloning or sequencing. For gel extraction, DNA products were loaded in a 0.8% agarose gel containing 1:20,000 GelRed, and separated for up to 3 hours at 80 volts (0.12 amps) (2.6.7). The gel was then visualised using a UV source and the band of the correct molecular weight was excised using a clean blade and transferred to a micro-centrifuge tube. This was carried out rapidly to avoid UV cross-linking of the DNA to the agarose gel. Up to 400 mg of gel weight could be processed in one reaction. The following protocol in Table 14 was then followed. All centrifugation steps were performed at 13,000 x g for 1 minute at RT and all flow through was discarded. For PCR purification, 3 X reaction volume buffer QG was added to the sample and purified on a column as for gel extraction.

Step	Reagent	Process
Solubilisation	3 X gel volume QG buffer	Added to gel slice and Incubated at 50^{o}C for 10 minutes.
pH balancing	10 μl 3M NaAc pH5.0	Invert to mix.
Column purification	800 μl sample loaded on to column	Centrifugation
	500 μl buffer QG added to column	Centrifugation
	750 μl buffer PE	Centrifugation
	N/A	Centrifugation
Elution	30 – 50 μl buffer EB	Column transferred to a micro-centrifuge tube, incubated with EB for 1 minute and centrifuged.

Table 14: Gel extraction and PCR purification protocol.

2.6.28. Preparation of Lysogeny Broth (LB) plates for bacterial growth

Thick LB was dissolved by heating in a bench top autoclave. The liquid LB was then transferred to a fresh bottle and cooled in a 55^{o}C water bath for 1 hour. Antibiotics or chemical additives could then be added to the LB media before pouring. LB plates were poured and allowed to cool before short term storage at 4^{o}C.

Ampicilin: 100 mg / ml ampicilin stock was prepared by dissolving 1 gram in 10 mls H_2O. The stock solution was filtered through a 0.22 μm filter and aliquoted and stored at -20^{o}C. Ampicilin was added at a 1:1000 dilution to liquid LB before pouring plates.

Chloramphenicol: For bacterial expression constructs with chloramphenicol resistance, chloramphenicol was added to liquid LB media before pouring plates. Chloramphenicol was added at a 1:1000 dilution from a 34 mg / ml stock prepared in water.

X-gal: For plasmids containing a LacZ reporter, blue-white screening could be performed when growing transformants in the presence of X-gal substrate. 1 X-gal tablet was dissolved in 250μl N,N-dimethylformamide, at 37^{o}C with occasional mixing. 40 μl was spread onto each plate and allowed to dry before plating the transformation mix as described in section 2.6.30.

2.6.29. TOPO™ Cloning

TOPO™ cloning proceeded immediately after amplification and purification of a DNA template using to ensure integrity of A-overhangs. The following reaction in Table 15 was set up on ice:

Reagent	Volume
PCR product	3 μl
Salt solution	1 μl
H2O	2 μl
pCR2.1®-TOPO vector	1 μl
Mix by stirring with a pipette tip	

Table 15: TOPO cloning protocol.

The reaction was incubated at RT for 5 minutes for fragments less than 1kb or up to 2 hours for larger fragments. The reaction was then transformed as described in 2.6.30. Due to the presence of a LacZ reporter in the pCR®2.1 vector, X-gal was added to the LB-amp plates in order to select successful clones using blue-white screening (2.6.30).

2.6.30. Transformation in Escheria Coli

Plasmid DNA was transformed into chemically competent *E.coli* cells. Between 1 – 10 ng DNA was added to a 50 μl vial of Novablue gigasingles competent cells on ice, stirred gently using a pipette tip and incubated from 5 minutes to 30 minutes (for larger inserts). The cells were then incubated for 30 seconds in a 42^{o}C water bath and then put back on ice for 2 minutes. 250 μl SOC media pre-warmed to 37^{o}C was then added to the cells and incubated in a shaking incubator at 225 rpm for 1 hour at 37^{o}C. During this incubation, selective LB plates were pre-warmed to 37^{o}C. After the incubation, an appropriate volume of the transformation mix was streaked using aseptic technique onto the agar plate. The transformation mix was left to settle into the agar for 10 minutes at RT before being inverted and incubated at 37^{o}C overnight. If X-gal was used for blue / white screening after ligation, single white colonies indicated positive clones where the insert had disrupted the production of β-galactosidase. If colonies were blue, the insert had not ligated into the vector and hence the lacZ cassette remained functional and the β-galactosidase produced was able to hydrolyse X-gal to produce a blue colour.

2.6.31. Plasmid Purification

Individual Colony Growth: Single colonies grown on LB-amp plates were picked using a pipette tip and added to 5 ml LB media + 100 μg / ml ampicilin in a 50 ml Falcon tube. The Falcon tube was partly sealed to allow air flow into the tube, and incubated at 37^{o}C in a shaking incubator at 225 rpm. For a midi-preparation of the plasmid, the culture was left to

incubate for 8 hours before a further 20 ml of LB media + ampicilin was added. It was then left to incubate over night at 37^{o}C in a shaking incubator at 225 rpm for further growth. For a mini-preparation of the plasmid, the 5 ml culture was left to incubate for approximately 12 hours before harvesting.

QIAGEN Mini Prep: Plasmid purification was performed according to the manufacturer's protocol. The protocol is outlined in Table 16.

Process	
Centrifugation of sample	4^{o}C, 6000 x *g*, 5 minutes
Resuspend pellet in 250 μl buffer P1	
Transfer to new micro-centrifuge tube	
250 μl buffer P2	Invert X 6
350 μl buffer N3	Invert X 6
Centrifugation	RT, 13,000 x *g*, 10 minutes
Transfer supernatant to spin column	
Centrifugation	RT, 13,000 x *g*, 1 minute
500 μl buffer PB	RT, 13,000 x *g*, 1 minute
750 μl buffer PE	RT, 13,000 x *g*, 1 minute
Transfer dry column to new collection tube	RT, 13,000 x *g*, 1 minute
Transfer dry column to a micro-centrifuge tube and add 30 ml H_2O	5 minute incubation, RT
Centrifugation Eluted DNA in the flow-through.	RT, 13,000 x *g*, 1 minute

Table 16: QIAGEN miniprep plasmid purification.

QIAGEN Midi Prep: Plasmid purification was performed according to the manufacturer's protocol. The protocol is outlined in Table 17.

Process	
Centrifugation of sample	4°C, 6000 x *g*, 15 minutes
Resuspend pellet in 4 ml buffer P1	Invert X 6
Add 4 ml buffer P2	Invert X 6, Incubate RT 5 minutes
Add 4 ml buffer P3 (cold)	Invert X 6
Transfer solution to filter cartridge	Incubate RT 10 minutes
Equilibrate QIAGEN-tip 100 with 4 ml buffer QBT	Empty by gravity flow
Filter solution from filter cartridge into QIAGE-tip (using syringe plunger without force)	Empty by gravity flow
Wash tip with 10 ml buffer QC	Empty by gravity flow
Elute into 15 ml collection tube with 5 ml buffer QF	Empty by gravity flow
Precipitate with 3.5 ml isopropanol	Invert X 6, centrifuge at 4°C, 30 minutes, 15,000 x *g*
Remove supernatant	
Add 2 ml 70% EtOH	Centrifuge 4°C 10 minutes, 15,000 x *g*
Air-dry pellet and resuspend in 100 μl H2O	

Table 17: QIAGEN midi prep plasmid purification.

The eluted DNA was analysed by electrophoresis and quantified using the Nanodrop™ 8000.

2.6.32. DIG Labelled RNA Riboprobe Synthesis

Template preparation by restriction digest: 30 μl (100 ng / ml) plasmid DNA was linearised by restriction digest. HindIII was used to linearise plasmids where the insert cloned in the antisense orientation to the T7 primer and NotI was used to linearise plasmids where the insert was cloned in the sense orientation to the T7 primer. The following reaction in Table 18 was set up in a micro-centrifuge tube on ice.

Reagent	Volume
NEB enzyme buffer	5 μl
100 X BSA	0.5 μl
DEPC treated H2O	12.5 μl
Restriction Enzyme	2 μl
Plasmid DNA	30 μl

Table 18: Restriction digest of plasmid DNA.

The solution was mixed by pipetting and centrifuged for 30 seconds, at 13,000 x *g*, at RT and incubated at 37°C overnight. The reaction was then analysed by agarose gel electrophoresis (2.6.7) alongside an undigested control to check for complete linearisation. The digested plasmid was then precipitated by adding 5 μl 3 M sodium acetate, pH 4.5, and 125 μl 100% ethanol, flicking the tube to mix. The sample was incubated on dry ice for 1 hour and then centrifuged at 4°C, 12,000 x *g* for 30 minutes. The ethanol was removed by pipetting and 200 μl of 70% ethanol was added to wash the pellet. The sample was centrifuged again for 10 minutes. The supernatant was carefully removed from the pellet and briefly allowed to air-dry (less than 1 minute) before re-suspending in 6 μl DEPC treated H_2O. The sample was then quantified using the Nanodrop™ 8000.

Transcription: The following reaction in Table 19 was set up in an RNA-grade micro-centrifuge tube.

Reagent	Volume
DNA template	4 μl
10 X Transcription Buffer	2 μl
10 X DIG RNA Labelling Mix	2 μl
DEPC treated H_2O	10 μl
Reaction was mixed by pipetting and centrifuged at 13,000 x g for 30 seconds.	
RNA polymerase (20U/μl T7 or SP6)	2 μl
RNAse inhibitor	1 μl
The reaction was incubated for 2 hours in a 37°C water bath	
10U/ml DNAse I	10 μl
Reaction was incubated for 20 minutes at 37oC.	
200 mM EDTA	2 μl
4M LiCL	2.5 μl
100% EtOH	75 μl

Table 19: DIG labelled riboprobe transcription reaction.

The precipitation reaction was left at -20°C overnight. The reaction was then centrifuged at 4°C, 12,000 x *g* for 30 minutes. The supernatant was carefully removed from the pellet by pipetting and washed with 200 μl ice cold 70% EtOH. The sample was centrifuged at 4°C, maximum speed for 5 minutes and the supernatant was again removed from the pellet. The sample was briefly allowed to air dry (less than 1 minute) before being resuspended in 100 μl DEPC treated H_2O. 5 μl of the probe was analysed by agarose gel electrophoresis (2.6.7) and the Nanodrop™ 8000 was used to check the purity of the RNA. The probes were stored at -20°C short term.

2.6.33. *In Situ* Hybridisation

In Situ Hybridisation was performed as described by Wilkinson, 1999. The procedure was carried out under RNAse free conditions. All glassware was baked prior to use and all solutions were made using DEPC-treated H_2O and then autoclaved. Surfaces and apparatus were regularly cleaned with RNAse-Zap and rinsed with DEPC treated H_2O and filter tips were used throughout.

Probe Hybridisation: Cryopreserved tissue sections (12 μm thickness) were stored at -20°C. Prior to *in situ* hybridisation, slides were brought to RT for 1 hour. Slides were then fixed in 4% PFA in PBS at RT for 15 minutes followed by 3 X 3 minute washes in PBS. The slides were then placed into acetylation mix (2.3.10) for 10 minutes, with 1 ml acetic anhydride added drop-wise for the first 4 minutes of the incubation. The slides were then washed 3 X 5 minutes in PBS. The back of the slides were then wiped and left on a slide rack for 1 minute and the sections were outlined with a PAP pen. 500 μl hybridisation solution (2.3.9) was added to each slide and left to incubate for 1 hour at RT. During the incubation, 160 ng of probe was added to 500 μl hybridisation solution in a micro-centrifuge tube (this was multiplied by the number of slides being processed) and left to mix by rotating at RT for 1 hour. The slides were then drained onto tissue and the probe was added to each slide. A piece of parafilm was laid over the top of the sections and the slides were transferred to the *in situ* chamber humidified with 5 X SSC and 50% formamide, and incubated over night at 70°C.

Blocking and Primary Antibody: Each slide was placed into a 50 ml Falcon tube containing 30 ml 5 X SSC. The Falcon tubes were then left to incubate for 5 minutes at 70°C or until the parafilm started to detach from the slides. The parafilm was removed and the slides were incubated in 0.2 X SSC at 70°C for 1 hour. The slides were then placed in fresh 0.2 X SSC and incubated for 5 minutes at RT followed by another 5 minute incubation in buffer B1 (2.3.11) at RT. The backs of the slides were then wiped and 500 μl blocking solution was added to each

slide (2.3.13) and left to incubate for 1 hour at RT. During this incubation, anti-DIG antibody was diluted 1:5000 in blocking reagent and left to mix at 4°C on a rotator for 1 hour prior to use. After the blocking incubation, the slides were drained and 500 µl anti-DIG solution was added to each slide and incubated overnight at 4°C.

Developing: The slides were washed 3 X 5 minutes in buffer B1 at RT. The slides were then left to incubate in buffer B2 (2.3.12) for 5 minutes at RT. During this incubation, the detection mix was prepared (2.3.14). In a dark-room, the slides were drained and 500 µl detection mix was added to each slide. The slides were then placed in an incubation chamber, humidified with water and left for 12 – 48 hours in the dark at RT until the colour development was complete. Following this, slides were washed 2 X 5 minutes in PBS before visualising.

2.6.34. Haematoxylin and eosin (H&E) staining

Cryopreserved tissue sections cut at 12 µm were stained by H&E in order to visualise the nuclei and cytoplasm and most histological structures. Staining was performed by the histology service at MRC Harwell using a Shandon Varistain 24 autostainer. Slides were then mounted in glycerol and were visualized by light microscopy.

2.6.35. Expression and purification of HIS tagged proteins

Pilot Expression Test: pET-32 (a or b) bacterial expression constructs were transformed into BL21 pLysS *E.Coli* competent cells as described in 2.6.30. 100 µl of the transformants were plated onto LB plates containing ampicilin and chloramphenicol and incubated overnight at 37°C as described in 2.6.30. A starter culture was set up by transferring 1 bacterial colony to 20 ml LB + 75 µg / ml ampicilin and 34 µg / ml chloramphenicol and growing for 16 hours at 37°C, shaking at 225 rpm. 1ml of this culture was then used to inoculate a fresh 10 ml LB + ampicilin and chloramphenicol, and grown for 2 – 3 hours at 37°C, 225 rpm. OD_{600} readings were taken using 1 ml of culture and 1 ml LB as a blank. Once OD_{600} readings greater than 0.6

were reached, Isopropyl β-D-1-thiogalactopyranoside (IPTG) was added to a final concentration of 1 mM to induce protein expression. The cultures were grown for a further 2 hours. 1 ml pre-IPTG and 1 ml post-IPTG treatment samples were taken and used for western blot analysis. Briefly, each 1 ml sample was centrifuged at 13,000 x *g* for 2 minutes. The supernatant was discarded and the cell pellet was resuspended in 100 μl PBS. 100 μl 2 X SDS-PAGE sample buffer and 10 μl β-mercaptoethanol was added. Samples were briefly sonicated and left to cool on ice. The samples were then denatured at 95°C for 5 minutes and 20 μl was loaded onto an SDS-PAGE gel as described in 2.6.11. The gel was then rinsed three times with 20 ml distilled water and then incubated for 1 hour with 20 ml SimplyBlue™ Safe Stain (Coomassie). The gels were then de-stained in distilled water overnight at 4°C.

Pilot Solubility Test: 8 ml of bacterial culture (from the pilot expression test) was harvested by centrifugation at 5,000 x *g* for 15 minutes at RT. The cell pellet was resuspended in 500 μl sonication buffer (SB) (2.3.20) and sonicated for 1 minute. Samples were centrifuged at 13000 *x g* for 3 minutes and the supernatant containing soluble proteins was transferred to a fresh micro-centrifuge tube. The remaining cell pellet was resuspended in 500 μl SB containing 8M urea. The sample was centrifuged at 13000 *x g* for 3 minutes at 4°C and the supernatant containing insoluble (but urea soluble) proteins was stored. The pellet was resuspended again in 500 μl SB with 8M urea and stored. 100 μl of all three fractions was mixed with 100 μl 2 X SDS-PAGE sample buffer with 10 μl β-mercaptoethanol, denatured for 5 minutes at 95°C and 20 μl loaded onto an SDS-PAGE gel as described in 2.6.11. The gel was then stained and visualised as described in "pilot expression test".

Protein purification: 5 ml LB + ampicilin and chloramphenicol was inoculated with a single bacterial colony and grown overnight at 37°C shaking at 225 rpm. The following day 500 ml of fresh LB + antibiotic and chloramphenicol was inoculated with the 5 ml overnight culture. The culture was grown until OD_{600} was between 0.4 to 0.5 (approximately 2 – 3 hours). When the

desired OD was reached, 1 ml of un-induced sample was removed and 1 mM IPTG was added to the remaining culture. The cultures were grown for a further 3 hours. Again, 1ml culture post protein induction was removed. The bacterial pellets were harvested by centrifugation at 8000 x *g* for 15 minutes at 4°C. The pellets were resuspended in 20 ml SB (2.3.20) and sonicated on ice for 5 – 10 cycles for 10 seconds. The crude lysate was transferred into a micro-centrifuge tube and centrifuged at 15000 x *g* for 30 minutes at 4°C. The cleared lysate was saved for purification and 100 μl of the sample was saved for SDS-PAGE analysis. 2 ml packed volume of chelating sepharose resin was prepared by washing with five volumes de-ionised H_2O on a collection column and allowed to empty by gravity flow. Two volumes of 50 mM cobalt chloride was added to the column and mixed by rotation for 5 minutes at RT. The column was washed with 3 X 5 volumes of water and allowed to empty by gravity flow. The column was then equilibrated with two volumes of SB buffer and allowed to empty by gravity flow. The end of the column was plugged and the cleared lysate was added to the column. The column was sealed and allowed to mix by rotation for 30 minutes at RT. After the incubation, the cap and plug were removed and the lysate allowed to flow through by gravity flow. This flow-through was collected for future use and a sample kept back for SDS-PAGE analysis. The column was washed with 3 X 3 volumes of SB buffer. The protein was then eluted with one volume of SB + 100 mM imidazol and 10 μl was set aside for SDS-PAGE. Remaining protein was then eluted in two volumes of SB + 100 mM imidazole, again keeping 10 μl for SDS-PAGE. The final elution was performed with 1 volume of SB + 100 mM imidazole and 10 μl set aside for SDS-PAGE. All collected samples were then analysed by SDS-PAGE and Coomassie blue staining as before and eluted proteins were quantified by comparison to BSA protein standards, of known concentration, on an SDS-PAGE gel.

Chapter III

Results I

Characterisation of the Short Circuit Circadian Phenotype

3. Short circuit Circadian Phenotype

3.1. Introduction

The short circuit (*Sci*) phenodeviant was identified in Dr Patrick Nolan's laboratory at MRC Harwell. It was identified in an ENU mutagenesis screen for dominant circadian phenotypes. The original *Sci* founder, on a C3H/BALB/c background, displayed reduced amplitude, a short circadian period length under constant darkness and a reduced or absent phase shift in response to a light pulse in constant darkness. The mutant phenotype was tested for inheritance, crossing to a C3H in-bred animal and the behavioural phenotype was completely penetrant on this background. The mutation was back crossed further onto C3H for 10 generations until congenic, and although penetrant, the mutation produced variable phenotypes in the colony. The original phenotypes and preliminary characterisations of the *Sci* mutant are shown in Figure 9.

Low resolution mapping identified a novel mutant locus to be associated with circadian rhythms, from 101.86 Mb to 110.46 Mb on distal chromosome 8. Positional cloning refined the mutant locus further between 107.3 and 110.46 Mb. Candidate genes were sequenced and a G → T transition was identified in exon 9 of the novel circadian gene zinc finger homeobox 3 (*Zfhx3*). This mutation causes a valine 1963 phenylalanine amino acid substitution in a highly conserved region of the protein. Figure 10 shows the critical region, location and conservation of the *Sci* mutation in *Zfhx3*. Following the identification of the causative mutation, genotype and phenotype correlation demonstrated that the mutation caused homozygous lethality during embryonic development, therefore only $Zfhx3^{Sci/+}$ adult animals have been phenotypically assessed.

The identification of the *Sci* mutant and the causative mutation was carried out prior to the start of this DPhil project by Drs Sofia Godinho, Alun Barnard and Michael Parsons. This

chapter describes the subsequent behavioural analyses that have been performed for this thesis to characterise the circadian phenotype of the *Zfhx3*$^{Sci/+}$ mutant. Wheel running activity has been used as an endogenous marker of *in vivo* circadian rhythmicity to analyse and annotate the circadian behaviour of the *Zfhx3*$^{Sci/+}$ animals.

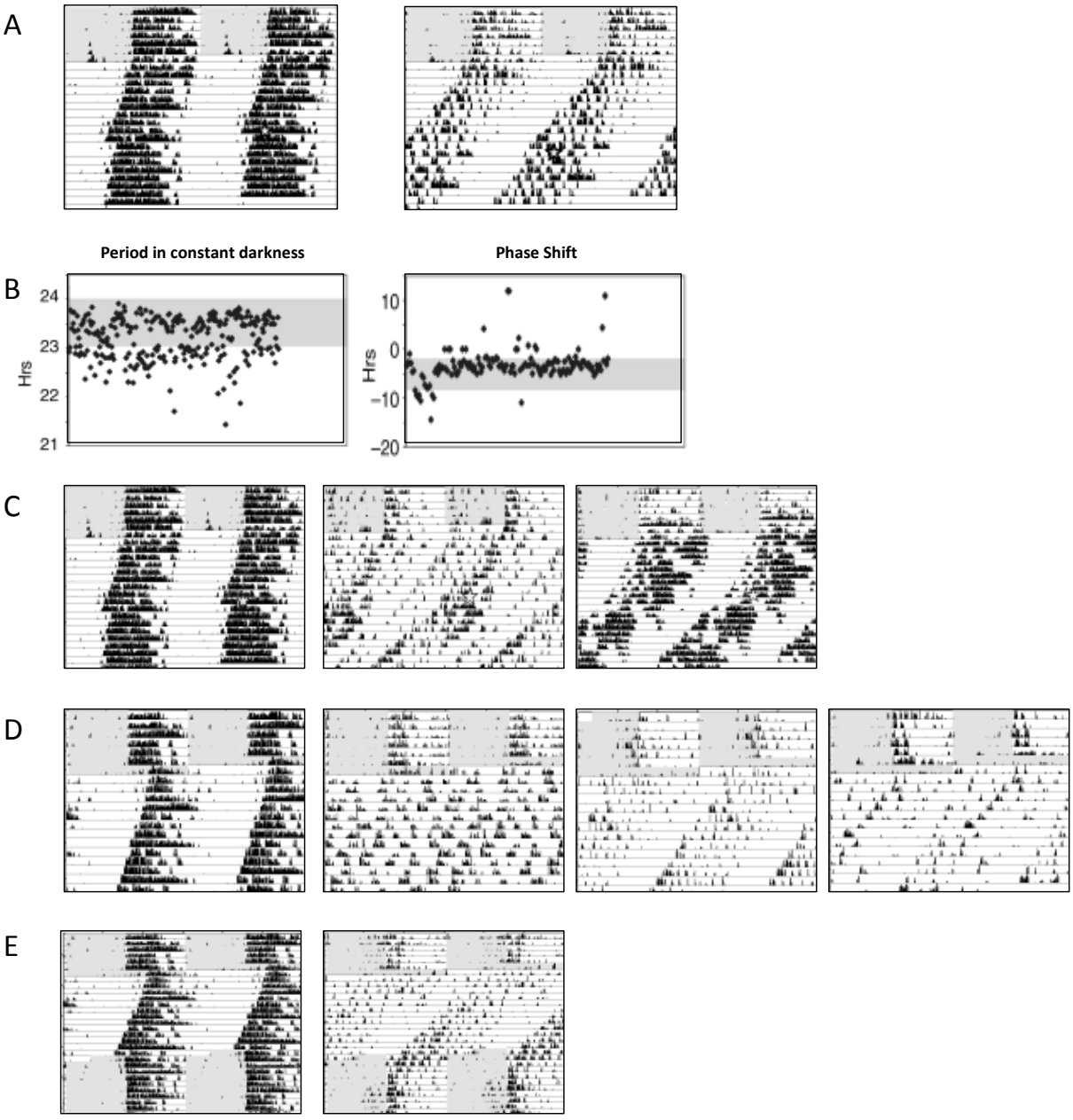

Figure 9: Identification and preliminary wheel running characterisation of the *Sci* mutant. Circadian locomotor activity has been represented as a double plotted actogram. Shaded regions indicate lights on at 100 lux and white regions indicate darkness. (A) Double plotted actogram of a *Zfhx3*$^{+/+}$ (left) and a representative *Sci* phenodeviant. The *Sci* phenodeviant showed a short circadian period length, reduced amplitude and reduced or absent phase shift in response to a light pulse at CT16. (B) Scatter plots showing the variation in period length under constant darkness (left) and phase shift following a 15 minutes light pulse at CT16 (right) in the *Sci* colony. The shaded area represents the mean values ± 3 standard deviations for the first generation (F1) population. (C) Double plotted actogram of *Zfhx3*$^{+/+}$ (left) and two *Sci* phenodeviants (middle, right). Animals were exposed to a 12:12 light dark

(LD) cycle for 7 days followed by 10 days constant darkness. A light pulse at CT16 was given to assess phase shift ability and a further 10 days constant darkness to assess free-running ability. *Sci* phenodeviants showed an advanced phase angle, reduced or absent phase shift, reduced amplitude and high daytime activity levels. (D) Double plotted actogram for *Zfhx3*$^{+/+}$ (left) and three *Sci* phenodeviants. As with (C), mice were exposed to a 12:12 LD cycle for 7 days followed by an additional 12 hours of light. Animals were then maintained under constant darkness for up to 14 days. Variable expression of the phenotype was detected (middle and right) including arrhythmic behaviour and advanced phase angle. (E) Assessment of re-entrainment to a 12:12 LD cycle following constant darkness. *Zfhx3*$^{+/+}$ (left) re-entrains to lights-off stimulus, *Sci* phenodeviant (right) shows incomplete re-entrainment with elements of free-running. (Bacon, et al. 2004).

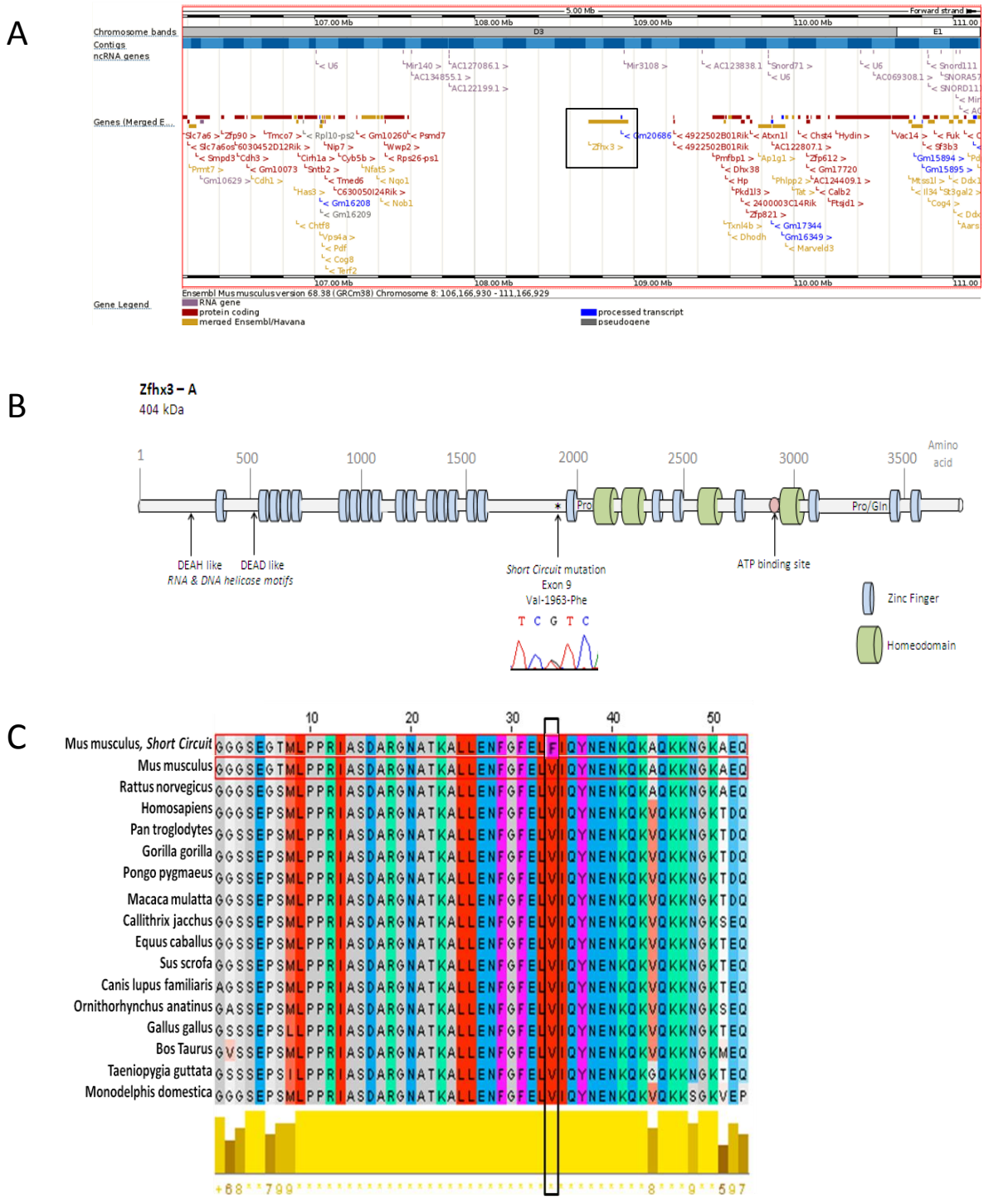

Figure 10: Location and conservation of the *Sci* mutation in *Zfhx3*. (A) Overview of the *Sci* critical region from 107.3 to 110.5 Mb on mouse chromosome 8, showing the location of *Zfhx3* neighbouring genes. (Image taken from ensembl.org) (B) Schematic showing protein domains of ZFHX3. The *Sci* mutation causes a mutation in exon 9 resulting in a valine to phenylalanine substitution at amino acid 1963. (C) Conservation of the *Sci* amino acid residue across species. The *Sci* mutation lies within a highly conserved region of *Zfhx3* across species suggesting evolutionary conservation of this amino acid.

3.2. Circadian wheel running activity of Short circuit Mutants

The *Sci* animals were bred onto both C57BL/6J and C3H backgrounds and backcrossed for 10 generations until congenic, ensuring that other functional ENU induced mutations were removed. Breeding difficulties however were encountered on the C57BL/6J congenic line, and retinal degeneration inherent from the *Pde6b* locus in the C3H congenic strain interfered with circadian phenotyping. To circumvent these problems, the *Sci* animals were maintained on a mixed F1 background between C3H and C57BL6/J. This ensured that breeding viability was maintained and the proportion of $Pde6b^{rd/rd}$ in the population was at 1/8 frequency and could be genotyped and removed from subsequent breeding and phenotyping. As a result, more variability was produced in all behaviours because of genetic heterogeneity.

Cohorts of *Sci* animals were regularly assessed for their wheel running behavioural phenotypes under automated light dark cycles in order to ensure a genotype with phenotype correlation. The majority of phenotypes that were identified in the original *Sci* founder, and G1 offspring, remained after back-crossing *Sci* onto C57BL/6J, C3H and the mixed F1 background between C57BL/6J and C3H. The shortened period phenotype was observed in all $Zfhx3^{Sci/+}$ animals screened, and lies between 21.4 – 23 hours. A significant reduction in circadian amplitude (the difference between the peak and average value of a wave) was also observed in all $Zfhx3^{Sci/+}$ animals. Both these phenotypes have been confirmed *ex vivo* in SCN slices using a Per2-LUC reporter gene assay (Prof. Michael Hastings). There is therefore an intrinsic SCN phenotype, supporting a disruption to the core circadian clock, without the influence of SCN input, due to the *Sci* mutation. Normal synchronisation within the SCN implies that neuronal coupling and signalling within the SCN is not affected. This correlation additionally supports that wheel running activity is an accurate measure of endogenous circadian phenotype and is evident at the tissue level at the site of the core circadian oscillator.

Phenotypes detected under light conditions showed variable expression in *Zfhx3*$^{Sci/+}$ mutants. Many animals showed increased day-time activity during a 12:12 LD cycle and variable phenotypes under constant light. Although a proportion of animals showed expected period lengthening under constant light conditions, many animals showed splitting of the circadian rhythm and a tendency to arrhythmic behaviour after prolonged light exposure. Animals failed to re-entrain following constant light, instead either continuing to free run or showing two periods of activity through the LD cycle. These phenotypes under light conditions suggest that the *Sci* mutants are more sensitive and susceptible to the de-coupling effects of light on the SCN or an aberrant light input signalling pathway, which is discussed further in Results Chapter 4. All these phenotypes observed throughout the entirety of the circadian screen are shown in the actograms in Figure 11.

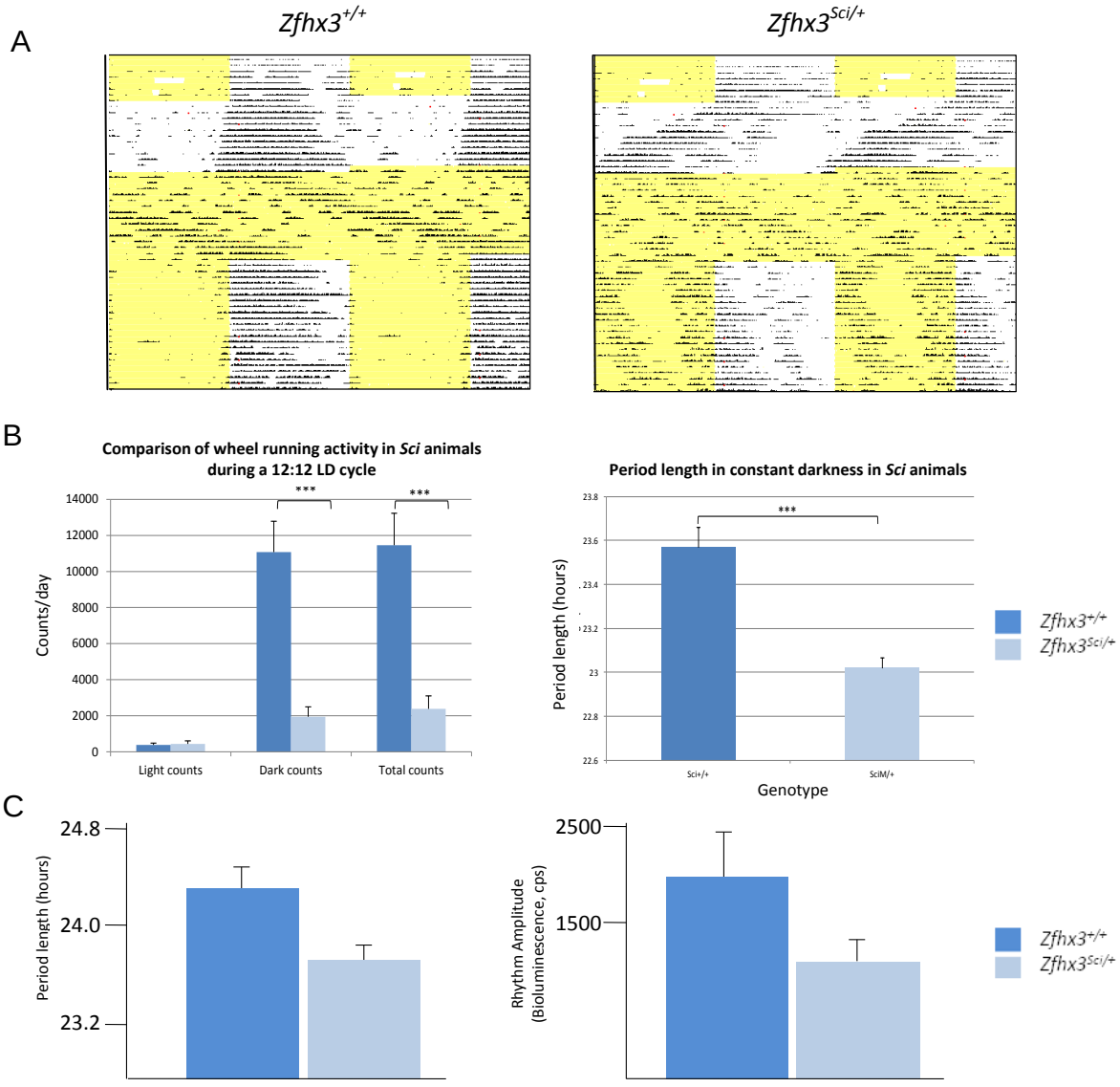

Figure 11: *Sci* circadian phenotype assessed by wheel running activity. (A) Representative double-plotted actograms for $Zfhx3^{+/+}$ and $Zfhx3^{Sci/+}$ animals. Animals were exposed to a 7 day 12:12 LD entrainment period. Animals were then housed in constant darkness for 10 – 14 days for an assessment of free-running parameters. This was followed by 10 – 14 days constant light and then a 12:12 LD cycle to assess re-entrainment. A fluorescent light source at 100 lux was used for all screens. $Zfhx3^{Sci/+}$ show a short circadian period in DD, low amplitude of the circadian rhythm in DD and LL, increased day-time activity and poor re-entrainment. (B - Left) $Zfhx3^{Sci/+}$ showed comparable wheel running activity to $Zfhx3^{+/+}$ in lights-on during an entrainment period, but significantly less wheel running counts during darkness and in total throughout the entrainment period (2-way T-TEST, p = 0.0012 and p = 0.0017 respectively, n = 6 per genotype). Proportionally, the $Zfhx3^{Sci/+}$ animals show higher wheel counts during day-time, considering total wheel counts, compared to $Zfhx3^{+/+}$. (B – Right) $Zfhx3^{Sci/+}$ have a significantly shorter circadian period length in constant darkness compared to $Zfhx3^{+/+}$ (2-way T-TEST, p = 0.0009, n = 6 per genotype).

(C) *Ex vivo Sci* phenotype shown in isolated SCN using a PER2-Luciferase reporter (data courtesy of Prof. Michael Hastings, University of Cambridge). The short circadian period and reduced rhythm amplitude as observed in wheel running activity was also detected in the *Zfhx3*$^{Sci/+}$ SCN.

3.3. Phase shifting and light pulses

In the natural environment, the endogenous circadian rhythm must be continually shifted towards the external environment time since the endogenous rhythm has a slight deviation from 24 hours. This ensures that the correct phase relationship between the external environment and the endogenous oscillator is maintained. If an animal becomes active during the early subjective night, this results in a shift of activity later in time on the next circadian oscillation, a phase delay. Activity in the late subjective night will result in a shift in activity earlier in the next circadian oscillation, a phase advance. This behavioural mechanism allows for a re-alignment of the circadian phase in response to a change in the external environment. This can be recapitulated artificially using light pulses during constant darkness and assessing the phase shift effect.

The original cohorts of *Sci* phenodeviants showed aberrant phase shift responses to a light pulse during constant darkness (Figure 9). As such, the *Sci* animals (generated by crossing successively to F1 hybrid animals) were re-assessed for the ability to adjust the phase of the free-running circadian rhythm in response to a light pulse. By monitoring wheel running activity through constant darkness, a measure between the activity onsets before and after a given light pulse allowed for the associated adjustment in the phase to be calculated. The actograms in Figure 12 show the wheel running activity throughout this screen, with the red arrows indicating the application of the 15 minute 100 lux light pulse. The shift in wheel running behaviour provided an endophenotype to indirectly observe the phase change of the SCN.

Initially, light pulses at CT16 and CT 22 were intended in order to observe phase advances and delays at the times at which the maximal phase-shifting effect of light is observed. However, due to the highly variable activity onsets across the *Zfhx3*$^{Sci/+}$ cohort, accurate activity onsets for these CT values could not always be calculated across a whole cohort. As such, wide

coverage was obtained and a preliminary phase response curve (PRC) could be constructed. The activity onsets of the *Zfhx3*$^{+/+}$ cohort were more predictable and consistent and therefore a more narrow range of CT values were targeted. A PRC however, could still be produced for comparison with *Zfhx3*$^{Sci/+}$. The preliminary PRC data showed that although the *Zfhx3*$^{Sci/+}$ mutants had a normal phase delay in response to early subjective night light pulses (CT 12 – 18), they had an exaggerated phase advance in response to late subjective night light pulses (CT 19 – 24). Figure 13 shows the method by which the phase shift was calculated, the averaged data across the two genotypes and the subsequent PRC.

A

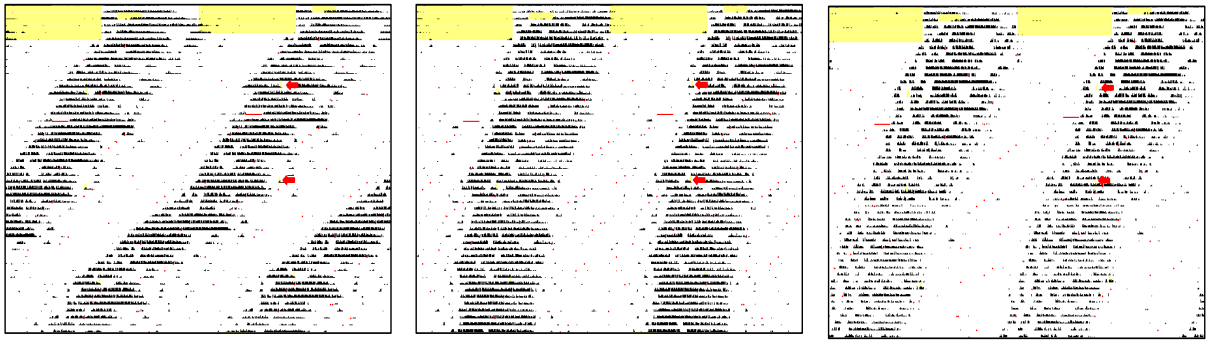

B

Figure 12: Actograms of three representative animals screened for ability to phase shift in response to an acute light pulse. A cohort of (A) 7 *Zfhx3*$^{+/+}$ and (B) 7 *Zfhx3*$^{Sci/+}$ females aged between 7 - 10 weeks were assessed for ability to phase shift in response to a 15 minute 100 lux light pulse during constant darkness. Animals were entrained to a 12:12 LD cycle and then exposed to constant dark conditions. Once a stable period was observed, a light pulse was given to all cages within the same light-tight chamber. An average CT was calculated for the entire coffin and could not be given individually to each cage. As such, although specific CT values were targeted, a range of CT values were reached because of the variability of activity onsets within each chamber. The CT calculation was based upon the first peak of activity being CT12. This was averaged across all cages and the light pulse was given 4 hours later. The same protocol was completed for the CT22 light pulse. A 14 day period was left between the two light pulses to give time for the period length to stabilise following the first light pulse. The red arrows denote when the light pulse was given.

A

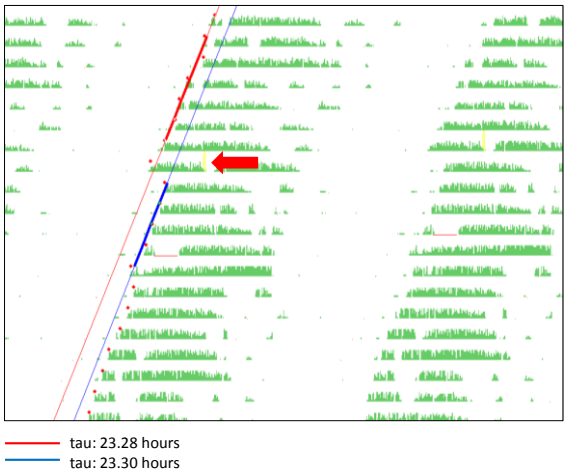

B

CT	*Sci*$^{+/+}$ phase shift	*Sci*$^{M/+}$ phase shift
2	-	1.320
3	-	0.645
4	-	0.650
10	-	-0.560
11	-	-0.440
12	-1.490	-1.760
14	-1.555	-2.700
15	-2.555	-2.450
16	-1.955	-
17	-1.645	-1.053
18	-0.730	-0.310
20	-	1.635
21	0.410	3.130
22	0.772	3.350
23	0.370	-

C

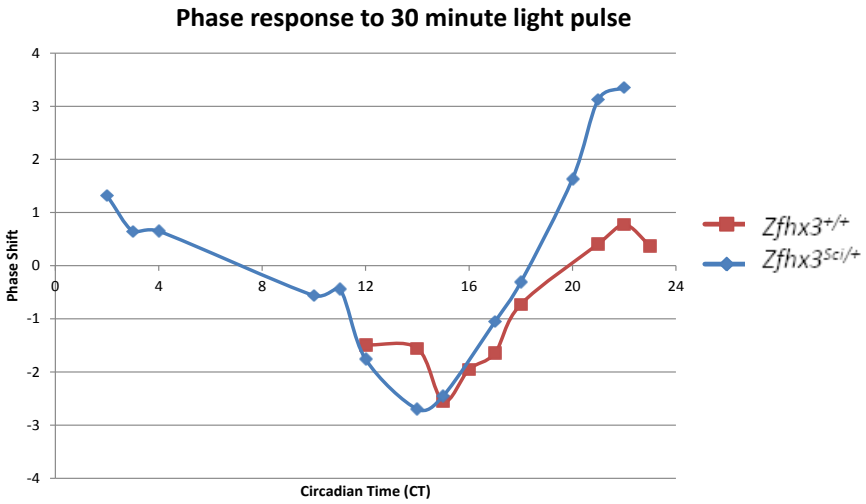

D

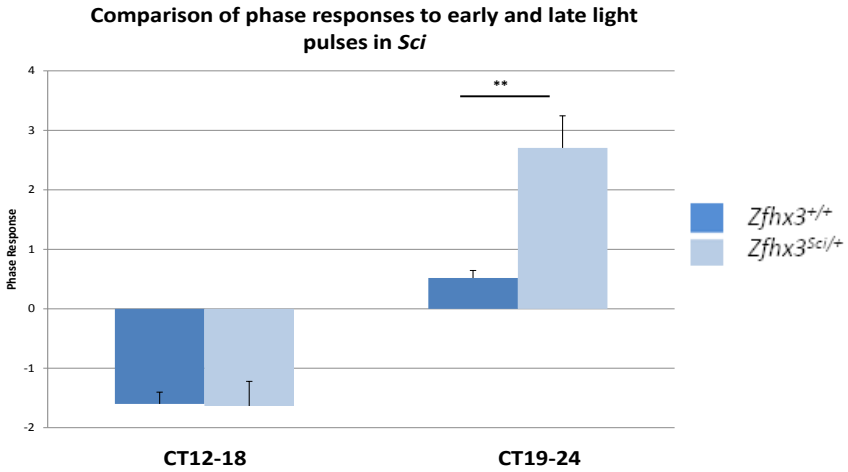

Figure 13: Generation of *Sci* phase response curve. (A) Annotated actogram to show the calculation of the phase shift. The stable τ before and up to the light pulse was calculated and is depicted by the red line. The stable τ following the light pulse was estimated and is depicted by the blue line. The two lines should be near parallel, indicating a constant τ regardless of the light pulse. The horizontal distance between the two parallel lines provides

the measure of phase shift. A negative value is generated when the blue line lies to the right of the red and a positive value is generated when the blue line lies to the left of the red line. Data analysis was produced using ClockLab (Actimetrics Software, Evanston, IL). (B) Calculated phase shift across estimated CT times. Although only two light pulses were given per animal, the timing of the light pulse was averaged and estimated across 10 cages. Due to variable activity onsets, light pulses were given across various CT points across the circadian cycle. (C) Phase response curve (PRC) generated based upon the tabulated data shown in (B). *Zfhx3*$^{+/+}$ PRC shown in red and *Zfhx3*$^{Sci/+}$ shown in blue. A broader coverage was generated for the *Zfhx3*$^{Sci/+}$ animals due to wider variation in activity onsets and therefore less accuracy in the timing of the desired light pulse. This provided more data points across the circadian cycle. *Zfhx3*$^{Sci/+}$ show a significantly exaggerated phase advance in response to a light pulse in the late subjective night (2-way T-TEST, p = 0.017). The phase delay in response to a light pulse in the early subjective night is comparable between *Zfhx3*$^{+/+}$ and *Zfhx3*$^{Sci/+}$. (C) Averaged phase delay and phase advance across early (CT 12 – 18) and late (19 – 24) subjective night. There is a significant exaggeration of the phase advance response at CT 19 – 24 in *Zfhx3*$^{Sci/+}$ animals (2-way T-TEST, p = 0.016).

3.4. Entrainment under dim light-dark cycles

Mice were subjected to a protocol of shifted LD cycles at decreasing light intensity. This was used to further dissect the phenotypes observed in wheel running under standard light conditions. This protocol mimicked a jetlag experiment and could assess whether *Zfhx3*$^{Sci/+}$ animals could effectively shift their circadian phase. This protocol was also used to provide an assessment as to whether the *Sci* animals could entrain to low light intensities, thus providing an indicator of light sensitivity.

The screen started with a 7 day 12:12 LD cycle using a light intensity 100 lux. The 12:12 LD cycle was shifted forward by 4 hours and the light intensity was reduced to 10 lux. The animals were maintained in this new 12:12 LD cycle until entrained. The lighting conditions then returned to the original setting to re-start the experiment. Once re-entrained, the 12:12 LD cycle was again shifted forward 4 hours and the light intensity was reduced to 1 lux. The screen ended at 1 lux irradiance since it was at this level that a significant difference was observed between *Zfhx3*$^{+/+}$ and *Zfhx3*$^{Sci/+}$ mutant animals. Representative actograms are shown in Figure 14.

The screen was performed on 7 *Zfhx3*$^{Sci/+}$ and 7 *Zfhx3*$^{+/+}$ female animals, aged between 4 – 5 months. Analysis was performed using ClockLab (Actimetrics Software, Evanston, IL). To analyse the differences in activity between genotypes at 1 lux, a τ could be measured for *Zfhx3*$^{Sci/+}$ as the mutant animals appeared to free-run through the LD cycle. To analyse the differences observed at 10 lux, the phase angle of entrainment was calculated during each 12:12 LD cycle.

A significant difference between *Zfhx3*$^{Sci/+}$ and *Zfhx3*$^{+/+}$ was detected when comparing the period lengths during entrainment at 1 lux (2-way T-TEST, $p = 0.004$). A significant difference was also detected when comparing between the period length in *Zfhx3*$^{Sci/+}$ at 1 lux to 100 lux

(2-way T-TEST, p = 0.00002) confirming a change in τ from the original conditions. *Zfhx3*$^{+/+}$ animals did not statistically differ in period length between 1 lux and 100 lux (2-way T-TEST, p = 0.99) confirming that they did not free-run but maintained normal entrainment. This data is shown Table 20 and Figure 15.

Although no overall significant difference by T-TEST statistic was observed in the phase angle of entrainment at 10 lux, when categorising animals into "normal" and "abnormal" entrainment behaviour, chi-squared analysis indicated a significant difference in the number of animals displaying normal entrainment between the *Zfhx3*$^{Sci/+}$ and the *Zfhx3*$^{+/+}$(χ^2 = 6.3, 1 d.f, p = 0.012). The data are shown in Table 21. There was no difference in the total length of time spent active (Alpha, α) between *Zfhx3*$^{Sci/+}$ and *Zfhx3*$^{+/+}$ during the 10 lux 12:12 LD cycle (Table 22 and Figure 16). Representative actograms are shown in full in Figure 17.

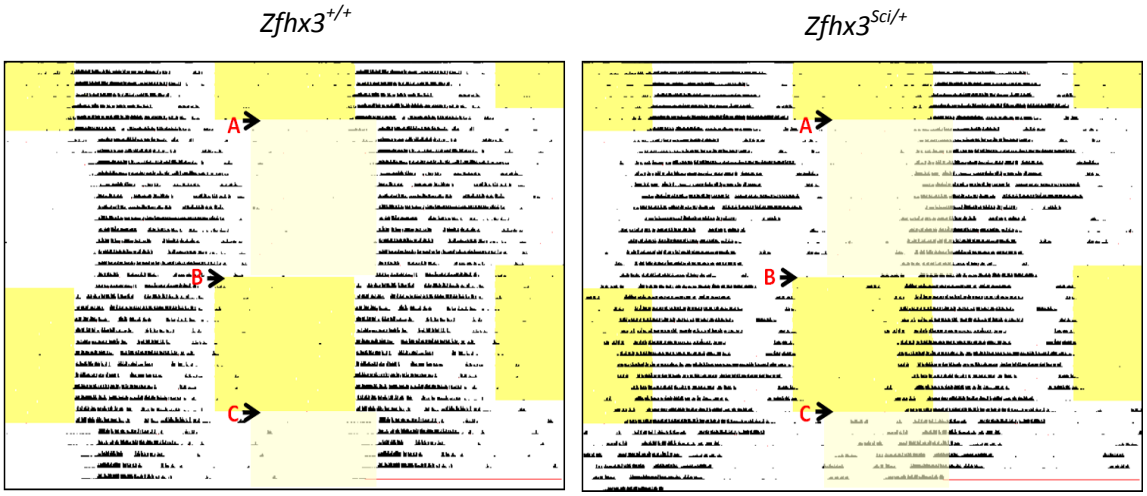

A. Shifted LD cycle and change from 100 → 10 lx.
B. Shifted LD cycle and change from 10 → 100 lx.
C. Shifted LD cycle and change from 100 → 1 lx.

Figure 14: Representative actograms for *Zfhx3*$^{+/+}$ and *Zfhx3*$^{Sci/+}$ under shifted 12:12 LD cycles with increasingly scotopic light intensities. Animals originated in a 12:12 LD cycle with 100 lux light intensity. After entrainment, the LD cycle was shifted forward 4 hours and the light intensity decreased to 10 lux (A). An advanced phase angle was observed in the *Zfhx3*$^{Sci/+}$ animals whereas the *Zfhx3*$^{+/+}$ showed normal entrainment. The LD cycle was then returned to the starting condition and entrainment was again assessed (B). The advanced phase angle remained in the *Zfhx3*$^{Sci/+}$ animals. Finally, the LD cycle was shifted forward 4 hours and the light intensity decreased to 1 lux (C). Under these conditions, the *Zfhx3*$^{Sci/+}$ appeared to free-run and displayed a shortened τ. The *Zfhx3*$^{+/+}$ animals showed normal entrainment to the lights off cue. This suggests that *Zfhx3*$^{Sci/+}$ animals are unable to entrain to low light intensities of 1 lux.

A

Zfhx3$^{+/+}$	Period length (τ) in hours		
ID	**100 lux**	**10 lux**	**1 lux**
29.3b	24	24	24.01
29.2c	24.06	23.81	23.49
29.3g	24.01	23.89	23.64
28.5b	23.73	24.16	24.24
28.6a	23.95	24.1	24.11
28.6b	24	24.02	24.01
29.2d	23.89	24.02	24.15
AVERAGE	**23.95**	**24.00**	**23.95**

B

Zfhx3$^{Sci/+}$	Period length (τ) in hours		
ID	**100 lux**	**10 lux**	**1 lux**
28.6d	n/a	n/a	n/a
28.6e	24	24.03	23.56
29.3a	24	24.05	23.17
29.3c	23.92	23.81	23.5
29.3d	24.04	n/a	n/a
29.3e	24	24.02	23.5
29.3f	23.97	24.11	23.48
AVERAGE	**23.99**	**24.00**	**23.44**

C

T-TEST	**p-value**
Zfhx3$^{+/+}$ τ 1 lux vs *Zfhx3*$^{+/+}$ τ 100 lux	0.99013
Zfhx3$^{Sci/+}$ τ 1 lux vs *Zfhx3*$^{Sci/+}$ τ 100 lux	0.00002
Zfhx3$^{+/+}$ τ 1 lux vs *Zfhx3*$^{Sci/+}$ τ 1 lux	0.00436

Table 20: Calculated period length (τ) in hours at "lights off" during entrainment. The period of activity onsets in a 12:12 LD cycle should be 24 hours, implying activity robustly occurs once lights are switched off. This does not take into account an advanced or delayed phase angle but a maintained circadian rhythmicity. A 2 way T-TEST statistic has been used to calculate the p-value for differences within each genotype, comparing 1 lux to 100 lux and to calculate the p-value for differences between genotypes at 1 lux. There was a significant difference in τ between *Zfhx3*$^{Sci/+}$ at 1 lux and 100 lux, therefore showing a change in τ with decreased light intensity. Additionally there was a significant difference in τ between *Zfhx3*$^{+/+}$ and *Zfhx3*$^{Sci/+}$ at 1 lux, showing that the *Zfhx3*$^{+/+}$ had not changed τ with decreased light intensity.

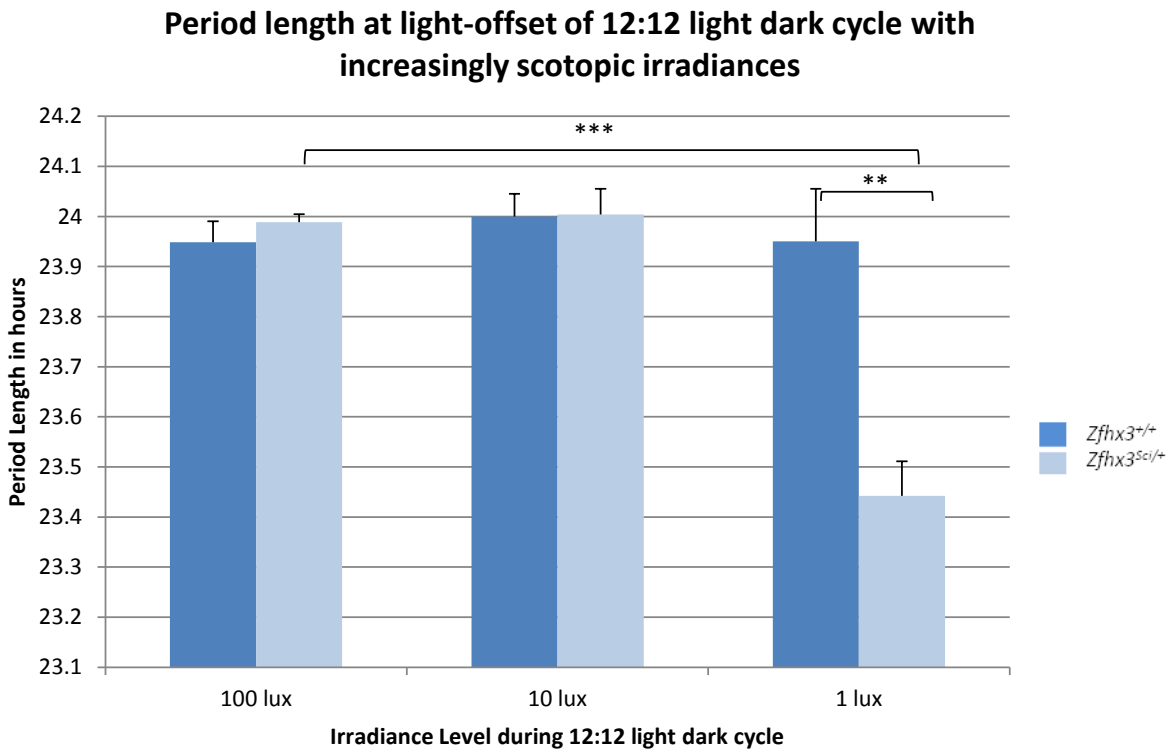

Figure 15: Bar chart representation of period length at "lights off" during entrainment of *Zfhx3*$^{+/+}$ and *Zfhx3*$^{Sci/+}$ animals at 100 lux, 10 lux and 1 lux. Period length values were calculated using ClockLab at the onset of activity during each 12:12 LD cycle. There were no significant differences between genotypes at 100 lux or 10 lux. There was a significant difference between genotypes at 1 lux illustrating that the *Zfhx3*$^{+/+}$ animals maintain a normal period length at 1 lux compared to *Zfhx3*$^{Sci/+}$ which lose their ability to entrain and free-run with an average period length of 23.44 hours. Significance values are show in Table 20 (C).

Analysis of Phase Angle of entrainment at 10 lux:

A

	Phase Angle (°)		
	***Zfhx3*$^{+/+}$**	***Zfhx3*$^{Sci/+}$**	
	171	133	*
	168	176	
	168	133	*
*	131	131	*
*	130	arrhythmic	*
	158	173	
	156	103	*
Average	**154.57**	**141.50**	
STERR	**6.55**	**11.43**	
T TEST	**0.33**		

B

	Onset of Activity (Hours)		
	***Zfhx3*$^{+/+}$**	***Zfhx3*$^{Sci/+}$**	
	7.13	5.54	*
	7.00	7.33	
	7.00	5.54	*
*	5.46	5.46	*
*	5.42	arrhythmic	*
	6.58	7.21	
	6.50	4.29	*
Average	**6.44**	**5.90**	
STERR	**0.27**	**0.48**	
T TEST	**0.25**		

*Consider animals with onset < 6 .5 hours or phase angle < 156 ° as abnormal

C

	(*Zfhx3*$^{Sci/+}$) **Observed**	(*Zfhx3*$^{+/+}$) **Expected**
normal	2	5
abnormal	5	2

χ^2 6.30 (1 d.f)

p-value 0.012

Table 21 A-C: Phase angle calculations of entrainment at 10 lux (lights off at 7pm). (A) Phase angle was calculated at the first day of entrainment to the shifted 12:12 light-dark cycle. (B) Onset of activity was calculated as (phase angle) / 24. On average, there was no significant difference between *Zfhx3*$^{+/+}$ and *Zfhx3*$^{Sci/+}$ animals. (C) When considering animals with a phase angle of entrainment of < 156° or < 6.5 hours as abnormal, a chi-squared statistic could be calculated. The "expected" values were taken from the *Zfhx3*$^{+/+}$ data. There was a significant difference between the proportion of abnormal animals observed in the *Zfhx3*$^{Sci/+}$ cohort, compared to the *Zfhx3*$^{+/+}$.

Duration of activity (Alpha, α) at 10 lux:

α at 10 lux (Hours)

	wt	het
	9.61	8.12
	8.82	7.33
	8.34	8.19
	6.17	7.93
	7.44	arrhythmic
	8.73	6.06
	6.88	10.18
Average	**8.00**	**7.97**
STERR	**0.46**	**0.55**
T TEST	**0.97**	

Table 22: Calculation of Alpha (α) as a measure of total length of activity during 12:12 LD cycle at 10 lux. Alpha was calculated as the difference between onset and offset of activity. Despite differences in phase angle between *Zfhx3*$^{+/+}$ and *Zfhx3*$^{Sci/+}$, there was no difference in the total duration of activity. (2-Tail T-TEST p > 0.05).

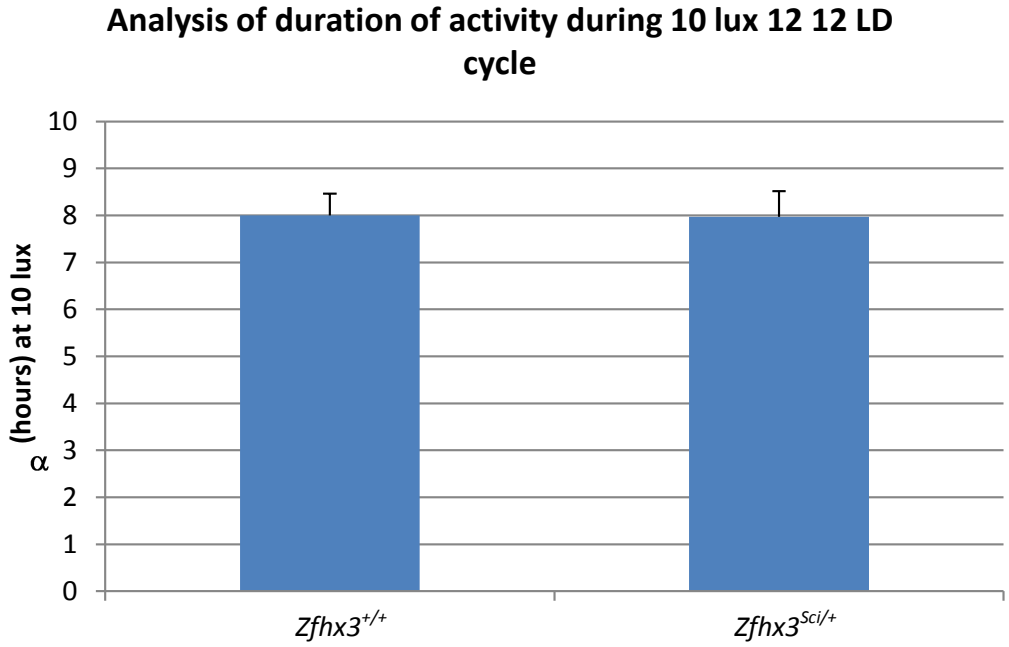

Figure 16: Analysis of duration of activity during a 12:12 light dark cycle, with 10 lux light intensity. The duration of activity (α) was calculated as the difference between activity onset and offset. There was no significant difference in duration of activity despite different activity onsets between *Zfhx3*$^{+/+}$ and *Zfhx3*$^{Sci/+}$. (2-Tail T-TEST p > 0.05).

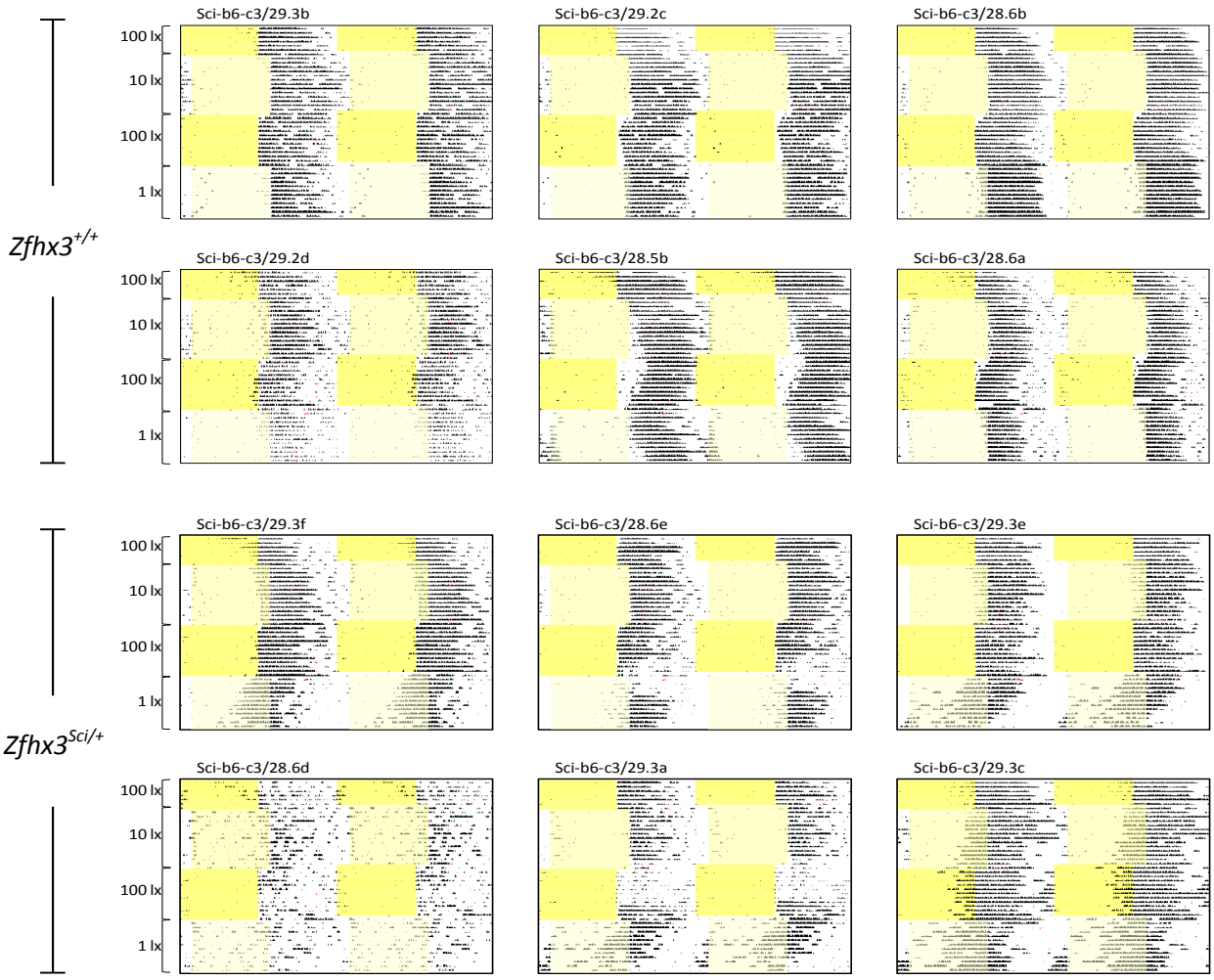

Figure 17: Representative actograms of *Sci* animals screened for ability to shift activity in response to a shifted 12:12 light-dark cycle at lowering levels of light intensity. A cohort of 7 *Zfhx3*$^{+/+}$ females and 7 *Zfhx3*$^{Sci/+}$ females aged 14 weeks were screened for ability to entrain to a light-dark cycle of 100 lux, 10 lux and 1 lux. The LD cycle was shifted forward 4 hours from the original time of "lights on" and decreased to 10 lux intensity. After animals had entrained, the LD cycle shifted back to the original settings. Once re-entrained, the LD cycle was shifted forward 4 hours and was decreased to 1 lux intensity.

3.5. Discussion

3.5.1. Identification of short circuit

The short circuit *(Sci)* mutant was identified in an ENU mutagenesis screen for dominant circadian phenodeviants. The mutant was from a cohort of ENU mutagenised G1 males which were assessed for phenotypes based on wheel running activity under an automated lighting schedule. The original phenodeviant displayed a complex circadian phenotype which was shown to be inherited and fully penetrant. These phenotypes included a shortened period in constant darkness, reduced amplitude of the circadian rhythm, increased day time activity during a 12:12 LD cycle and reduced or absent phase shift in response to a light pulse. The shortest period under constant darkness detected in the original progeny was 21.8 hours compared to 23.5 hours in a wild type animal housed under the same conditions. The causative mutation was mapped to a novel circadian locus, with a region of common linkage among phenodeviants lying between 107.3 and 110.5 Mb on mouse distal chromosome 8. Candidate gene sequencing identified a G → T transition in exon 9 of the gene zinc finger homeobox 3 (*Zfhx3*), resulting in a valine → phenylalanine substitution. This work was carried out prior to commencing this DPhil, by Drs Michael Parsons, Sofia Godinho and Alun Barnard. Genotype – phenotype correlation indicated that the mutation was homozygous lethal, and as such all behavioural screens presented have been carried out using $Zfhx3^{Sci/+}$ animals and $Zfhx3^{+/+}$ littermate controls.

Further circadian phenotyping has been performed to assess the *Sci* phenotype on a congenic genetic background without other functional ENU induced mutations. The *Sci* mutant was backcrossed 10 generations onto C3H and C57BL6/J backgrounds, and therefore deemed

congenic. Breeding problems on the congenic C57BL6/J background and the influence of the *Pde6b*rd locus on the C3H background led to the generation and maintenance of the *Sci* mutant on a mixed F1 background. Litter mate controls were used for all behavioural analyses because of genetic variation between animals being on this mixed strain background.

3.5.2. Short circuit Wheel Running Phenotyping

The *Zfhx3*$^{Sci/+}$ animals showed a consistently short circadian period under constant darkness, significantly shorter than *Zfhx3*$^{+/+}$ animals. A short circadian period would implicate an aberration in the molecular oscillator such that it is running faster than external environmental time. Numerous circadian gene knock-out mice show short period phenotypes, including *Clock*$^{-/-}$, *Per1*$^{-/-}$, *Cry1*$^{-/-}$ and *Reverb*$\alpha^{-/-}$. Fewer knock-out and mutant mice with long circadian periods have been generated, but known mutants include *Cry2*$^{-/-}$ and *Fbxl3*$^{Afh/Afh}$ (van der Horst, et al. 1999; Godinho, et al. 2007). The mutation in *Zfhx3* has either a direct effect on the circadian clock within the molecular feedback loop, or indirectly in a genetic cascade that impacts on the molecular oscillator. The wheel running circadian phenotype identified in *Sci* was recapitulated in isolated SCN slices. A shortened period and reduced amplitude was detected using a luciferase based assay which indicates that the phenotype is evident at the site of the core oscillator and not just in the peripheral clock or in the output of the circadian clock, observed in wheel running activity. In the absence of light input to the SCN, the short circadian period remains in *Zfhx3*$^{Sci/+}$ SCN slices. This provides further support that the *Zfhx3* mutation is affecting the circadian clock directly. Additionally the rhythmic wave of neuronal activity through the SCN, visualised by the PER2:LUC luminescence, appeared normal. Therefore on the gross neuronal level in the SCN, neuronal communication and coupling appeared unaffected in *Zfhx3*$^{Sci/+}$. It is therefore likely that the

phenotype is due to a deficit in the molecular oscillator, and implicates *Zfhx3* as a novel circadian clock gene.

Due to the pleiotropic roles of *Zfhx3*, including crucial functions during development, homozygous *Sci* animals have not been obtained. Further work remains to determine the phenotype in the homozygous condition. Since only $Zfhx3^{Sci/+}$ adult animals have been behaviourally phenotyped, a genetic cross between *Sci* and a PER2-Luciferase reporter line has been established. $Zfhx3^{Sci/+}$; Per2:Luc MEFs will be generated from embryos of all three genotypes such that the $Zfhx3^{Sci/Sci}$ may be analysed in a cellular system. The expectation would be a further deterioration of circadian rhythmicity if *Zfhx3* is essential within the accurate running of the circadian clock.

Additionally, attempts have been made to generate animals carrying either gene-trapped or conditional null alleles. A gene trap would produce a knock-down of *Zfhx3* genome wide. Since it would be a knock-down and not a knock-out, it is hypothesised that these animals would be viable and the adult circadian phenotype could be assessed and compared to the *Sci* mutant. Attempts had been made to generate *Zfhx3* gene-trapped animals; however karyotypic analysis of targeted ES cells detected 100% anueploidy (ES cell targeting performed by Dr Lydia Teboul and karyotic analysis by Dr Martin Fray). This gene trap (RRJ548, BayGenomics) has been previously published which used the *Zfhx3* gene trap to show a genetic interaction between *Zfhx3* and *Pit1* (Qi, et al. 2008b). However, our experience showed that this gene-trap was not viable in producing normal targeted ES cells.

A conditional knock-out would also be valuable in determining the nature of the *Zfhx3* mutation and the effect on the molecular clock. A conditional knock-out would be required to circumvent the essential role of *Zfhx3* during development and an SCN specific CRE line would allow for the circadian phenotype to be assessed in isolation of the pleiotropic roles of *Zfhx3* in the adult. A

conditional knockout strategy was designed based around the exclusion of exon 3 which would cause a frame shift and a premature stop codon. The construction of the targeting vector was initiated however the nature of the highly repetitive intronic sequence for homologous arms made the cloning process technically difficult. A conditional knockout targeting construct was later made available by KOMP which was using the same strategy to remove exon 3. Anomalies were detected in this targeting construct upon sequence verification and therefore it was not pursued further for ES cell injection. Technical limitations have therefore hindered this progress however these efforts will be continued in order to assess the circadian phenotype further and the mechanism behind the action of *Zfhx3* on the circadian oscillator.

3.5.3. Circadian phenotypes detected under light conditions

The *Sci* mutants show additional phenotypes under constant light conditions and during the light phase of a 12:12 LD cycle. These may be distinct from the phenotype and mechanism of the short circadian period in constant darkness. Firstly, the *Zfhx3*$^{Sci/+}$ animals have higher activity levels during the day compared to *Zfhx3*$^{+/+}$, showing reduced masking effects of light on activity. Although light is the predominant zeitgeber, other factors such as food intake, social interaction and temperature, may influence entrainment either positively or negatively. However, the controlled environment in which the *Sci* animals are housed may rule out these additional effects on entrainment in the data presented. Normal masking has been observed in response to a short light pulse given during the 12 hours of darkness (data not shown). The acute effects of light exposure are therefore maintained in *Zfhx3*$^{Sci/+}$ however across a 12 hour light period, the effect of masking is less robust. This requires further investigation, however it may suggest that *Zfhx3*$^{Sci/+}$ animals become desensitised to the effects of light after long periods of exposure. This may be attributed to disrupted signalling from the retina, including the rods, cones and intrinsically

photosensitive retinal ganglion cells (ipRGC) signalling pathway; or at the SCN level. An investigation into the neural coupling under light conditions at the level of the SCN may be informative to determine whether light sensitivity is affecting photic entrainment. As will be discussed in Chapter VI, a role for retinal *Zfhx3* in photic input and light processing may be causative of the effects of light on the entrainment of the circadian oscillator.

Zfhx3$^{Sci/+}$ animals fail to show normal re-entrainment to a 12:12 LD cycle following constant light or dark conditions. This provides further support that the effects of constant light acts to decouple more readily the circadian oscillator in *Zfhx3*$^{Sci/+}$. Although the phenotype is variable across the *Sci* cohort, many animals show two periods of activity to a 12:12 LD cycle following constant light exposure. This may be a similar effect to what is observed when the circadian rhythm "splits" into two components under constant light, suggesting a separation of the circadian rhythm into two independent oscillations. Failure to re-entrain in *Zfhx3*$^{Sci/+}$ suggests that the effect of continuous light exposure has had perhaps a semi-permanent decoupling effect on the circadian oscillators between the two nuclei of the SCN which are no longer in synchrony with each other. This would implicate an increased sensitivity to light in *Zfhx3*$^{Sci/+}$, and because of this finding, further investigations into light intensity sensitivity were investigated in this chapter. This may again be attributed to either a retinal or a neuronal signalling deficit in the *Zfhx3*$^{Sci/+}$ animals and further work is required to understand the mechanism. The use of a conditional knockout using retinal and SCN CRE lines may facilitate the understanding of these phenotypes to identify the origin of the role of *Zfhx3* in producing these abnormal circadian behaviours.

Light is the most prominent cue to be able to entrain the circadian clock and exposure to light during the subjective night will produce phase shifts of locomotor activity rhythms (Daan 2000). The mechanism of how differential effects on phase are produced depending on the circadian

time of application of the light pulse still remains to be understood. To determine whether photic entrainment may have been altered by the *Zfhx3* mutation, the resetting effects of single light pulses given to *Sci* mice free-running in constant darkness was investigated. The phase delays in the early subjective night were shown to be comparable between $Zfhx3^{+/+}$ and $Zfhx3^{Sci/+}$. A high amplitude phase advance however, was observed in $Zfhx3^{Sci/+}$ mice in response to light pulses in the late subjective night.

It is known that phase resetting of the mammalian circadian clock involves the acute induction of *Per1* and *Per2* (Shearman, et al. 1997; Shigeyoshi, et al. 1997; Tischkau, et al. 2003). It is well characterised that light information is directly related to the SCN via the RHT, primarily using glutamate. Light pulses will stimulate glutamate release and causes a signalling cascade involving the phosphorylation of CREB and CRE-mediated transcription. There are two CRE sites within the promoter region of the *Per1* gene and one within *Per2* (Bae, et al. 2001; Reppert and Weaver 2001). Light induced phosphorylated CREB has been detected in the core region of the SCN containing VIP neurons (Ding, et al. 1997; von Gall, et al. 1998) and this is where light induced *Per1* and *Per2* expression is first observed. It is therefore hypothesised that *Per1* and *Per2* expression is initiated in VIP neurons of the core SCN by light induced phosphorylated CREB. *Zfhx3* also has a CRE activation site within its promoter region and can be activated by phosphorylated CREB signalling pathways (Kim, et al. 2010). It would be informative to determine whether *Zfhx3* RNA is also expressed in the core SCN, together with *Per1* and *Per2* and whether induction of *Zfhx3* expression is observed following a light pulse.

Phase shifting experiments have been performed in *Per1* and *Per2* knock-out animals and differential effects have been identified. In a type II Aschoff protocol, it has been shown that *Per1* mutants show a normal phase delay and no phase advance. *Per2* mutants were shown to have no

phase delay but an exaggerated phase advance. The implication, from data produced under this protocol, is that *Per1* is required for the phase advance response and *Per2* for the phase delay (Albrecht, et al. 2001; Zheng, et al. 2001; Zheng, et al. 1999)

Current data would suggest that *Per1* RNA activation is required for the light and glutamate induced phase advance in the late subjective night (JBC, Gillette, 2002). It is also hypothesised that this is the primary role for *Per1*, in photic entrainment. Given the *Sci* phenotype of an exaggerated phase advance, it may be that there is an over-expression of *Per1* following the light pulse. The amplitude of *Per1* and *Per2* RNA expression following a light pulse should now be investigated in the *Sci* mutant in order to determine whether the *Sci* mutation is directly affecting the function of *Per1* in photic entrainment. Additionally, other clock gene RNA expression should be investigated in order to indicate whether the aberrations in the *Sci* PRC are caused by changes on the circadian pacemaker. This has been determined in other mutant models. In the *Rev-erb*$\alpha^{-/-}$ *; Per1*^{Brdm1} double knockout, a high amplitude resetting was observed in the late subjective night. Analysis of clock gene RNA expression detected a light induced activation of *Cry1* and *Per2* after a CT22 light pulse. Light-induction of *Cry* expression had not previously been observed in mammals and its involvement in light mediated responses in mammals is highly debated. The light induction of *Cry1* and *Per2* in this mutant is consistent to what is observed in invertebrates such as Zebrafish where *Cry1* is normally a light signalling molecule (Weger, et al. 2011).

There are numerous second messenger cascades which are involved in the photic signalling transduction pathway and light induced phase responses. Phase delays in the early night utilise ryanodine receptors to release Ca^{2+}. Blocking of these receptors inhibited light induced phase delays (Ding, et al. 1998). cGMP-dependent protein kinase (PKG) appears necessary for light induced phase advances in the late subjective night, with PKG inhibitors attenuating the phase

advance response (Mathur, et al. 1996; Weber, et al. 1995). An investigation into calcium release following a light pulse in the SCN neurons would help determine whether there is an involvement of *Zfhx3* in this signalling cascade and if the exaggerated phase advance response is due to effects on Ca^{2+} release.

It is known that neuro-modulators such as NPY, GABA and serotonin, are involved in photic signalling and artificial manipulation can have direct effects on the photic PRC. *Zfhx3* has known reported expression in adult dopaminergic neurons, and additionally effects on GABA signalling has been identified in $Zfhx3^{Sci/+}$ which is discussed later in Chapter VI. Therefore an investigation into neuro-modulators involved in photic integration at the SCN and photic resetting should be investigated further. The majority of SCN neurons are GABAergic and both GABA(A) and GABA(B) receptors are found in the SCN (Novak and Albers 2004). Activation of GABA receptors in the SCN has been shown to induce phase shifts and GABA is known to modulate phase shifts by light *in vivo*. Application of a GABA agonist and injection of the SCN with NMDA to mimic light-induced responses has been shown to cause a suppression of phase shifts (Mintz, et al. 2002). Specifically, a GABA(B) receptor agonist has been shown to reduce phase advance responses. As will be discussed in later chapters, a reduction in *Gad1* and *Gad2* has been identified in the retina of $Zfhx3^{Sci/+}$ animals and would likely cause a reduction in GABA neurotransmission in the retina. It remains to be determined whether this reduction is also evident in the SCN, however a reduction in GABA neurotransmission may be consistent with an exaggerated phase advance.

Further investigation into light sensitivity and the plasticity of the circadian clock to shift in response to light was performed in *Sci* animals. A jet-lag modelled experiment was set up using 12:12 LD cycles that were shifted and the re-entrainment was assessed. Additionally, as the LD cycle was shifted, the light intensity was decreased to determine the intensity threshold by which

Sci animals could detect and entrain to the ZT. As the light intensity was decreased from 100 lux to 10 lux and the 12:12 LD cycle shifted back 4 hours, *Zfhx3*$^{Sci/+}$ showed an advanced phase angle. This persisted when the 12:12 LD cycle was returned to the original conditions.

By shifting the 12:12 LD cycle forward 4 hours, the last day of the first LD cycle would have 16 hours of light before the next 12 hours of darkness. The *Zfhx3*$^{Sci/+}$ animals although were entrained and displayed the same duration of total activity, were unable to shift their circadian rhythm as readily as *Zfhx3*$^{+/+}$ and showed an advanced phase angle in response to this long day length. However, since the total period of activity (α) and calculated τ through the activity onsets was equivalent to *Zfhx3*$^{+/+}$, this is thought not to be due to the effects of decreased light intensity but rather the plasticity of the circadian clock to shift the behavioural rhythm. Additionally, since total duration and phase of activity during the circadian cycle was the same between the two genotypes, it can be proposed that there was no significant defect in the functioning of the core clock or locomotor activity output of the clock to be causing this phenotype. Since the *Zfhx3*$^{Sci/+}$ mutants could not re-shift their circadian phase when returning back to the original starting conditions, the implication is that the *Zfhx3*$^{Sci/+}$ circadian system is less readily manipulated and modulated by the external environment as it is in *Zfhx3*$^{+/+}$. This would have consequences in correlating the circadian clock to the external environment in relation to changes in day length and time zone (jetlag).

When the 12:12 LD cycle was shifted forward and the light intensity was decreased to 1 lux, *Zfhx3*$^{Sci/+}$ appeared to free run. *Zfhx3*$^{Sci/+}$ acted behaviourally as if in constant darkness. From this result it can be determined that the photic sensitivity in *Zfhx3*$^{Sci/+}$ is decreased such that scotopic light intensity is not a strong enough *zeitgeber* to entrain and adjust the circadian rhythm as it is in

Zfhx3$^{+/+}$. This may be indicative of a signalling defect within the ipRGCs, rods and cones or in the transduction of photic information to the SCN which is later discussed in Chapter VI.

3.5.4. Conclusions

The *Sci* mutant has been comprehensively assessed for circadian phenotypes using wheel running based activity screens. Activity under different lighting conditions was used as a biomarker for the endogenous circadian rhythm. Data collected in this way provided an accurate representation of the circadian clock and in the case of *Sci*, correlated accurately to the phenotype observed at the SCN level. The *Sci* mutant has been shown to have a complex behavioural phenotype, with various aberrant behaviours detected through the basic circadian screen. These phenotypes were identified in the original founder male from the G1 ENU mutagenesis screen and persisted after back-crossing the mutant onto congenic backgrounds.

The phenotypic data provides a strong support that *Zfhx3* is involved at many levels of the circadian behavioural system. Various phenotypes have been detected under light conditions. During entrainment *Zfhx3*$^{Sci/+}$ show heightened day time activity, suggesting that the long term effect of light is not sufficient to maintain the negative effect of masking as observed in *Zfhx3*$^{+/+}$. Additionally, *Zfhx3*$^{Sci/+}$ show less robust circadian behaviour under prolonged constant light with *Zfhx3*$^{Sci/+}$ showing deterioration in circadian rhythmicity more readily than *Zfhx3*$^{+/+}$. Furthermore, following constant light, *Zfhx3*$^{Sci/+}$ show abnormal re-entrainment, again indicating that the effects of constant light caused a long term effect on the SCN and after 3 weeks of a normal 12:12 LD cycle, animals still failed to entrain. Taken together, *Zfhx3*$^{Sci/+}$ animals show a complex behavioural phenotype which suggests a role of this novel circadian gene, *Zfhx3*, to act within the input, core clock and output of the circadian system. Further experimentation is required to assess the role of *Zfhx3* at each level of the circadian clock. This will be facilitated by the use of other mutants,

including conditional knockouts and other genetic crosses. Additionally, the circadian phenotype of *Zfhx3*$^{Sci/Sci}$ remains to be determined, which is expected to show an even further breakdown of circadian behaviour if *Zfhx3* is required as a core clock gene.

Chapter IV

Results II

Molecular Characterisation of *Zfhx3*

4. *Zfhx3* molecular characterisation

4.1. Introduction

The *Zfhx3* gene has numerous complex functions which have been annotated since its identification 1991 (Morinaga, et al. 1991a). These predominantly include its involvement within the cell cycle as an anti-mitotic factor and in neurogenesis and nervous system development (Ido, et al. 1994; Jung, et al. 2005; Miura, et al. 1995; Yasuda, et al. 1994a). A role for *Zfhx3* has so far not been investigated or identified in the circadian system. As such, this chapter aimed to determine whether *Zfhx3* may have a circadian function given the phenotype of the *Sci* animals. Of particular importance, this chapter aimed to identify whether *Zfhx3* was expressed in the suprachiasmatic nucleus (SCN) of the hypothalamus in the adult mouse brain. This would support a role within the core circadian clock. Additionally, work was performed to identify whether there are any direct genetic or protein interactions between ZFHX3 and known clock proteins.

This chapter has used molecular, genetic and proteomic approaches to further characterise the function of *Zfhx3* and determine the role that it plays in defining and manipulating circadian behaviours. Optimisation has been required for several ZFHX3 antibodies in order to assess the protein products as well as the optimisation for expression of several *Zfhx3* over-expression constructs. As will be discussed, further experimental approaches are required to isolate the mechanism by which *Zfhx3* acts upon the core circadian clock however results from this chapter support a strong involvement of *Zfhx3* in the molecular oscillator.

4.2. RNA expression analysis

4.2.1. RT-PCR expression studies

In addition to the work presented in this thesis, further characterisation of the molecular role and function of *Zfhx3* within the context of circadian biology has been performed by Dr. Michael Parsons (MRC Harwell). Results obtained from his studies have shown that the *Zfhx3* RNA transcript oscillates with a 24 hour period in extra-SCN tissues. Additionally, it has been shown that the phase of *Zfhx3* RNA expression in $Zfhx3^{Sci/+}$ is shifted compared to $Zfhx3^{+/+}$ and the effect of the *Zfhx3* mutation also has effects on the amplitude and phase of known circadian RNA transcripts. The most affected transcripts in the presence of the *Sci* mutation are *Cry1, Cry2* and *Per1*. *Cry2* and *Per1* show a reduced peak amplitude of expression whereas *Cry1* shows an increased peak amplitude of expression. Only subtle shifts in the phase of expression are observed. A summary of these results are shown in Figure 18 (data courtesy of Dr Michael Parsons) and should be considered together with the other results presented in this and other chapters.

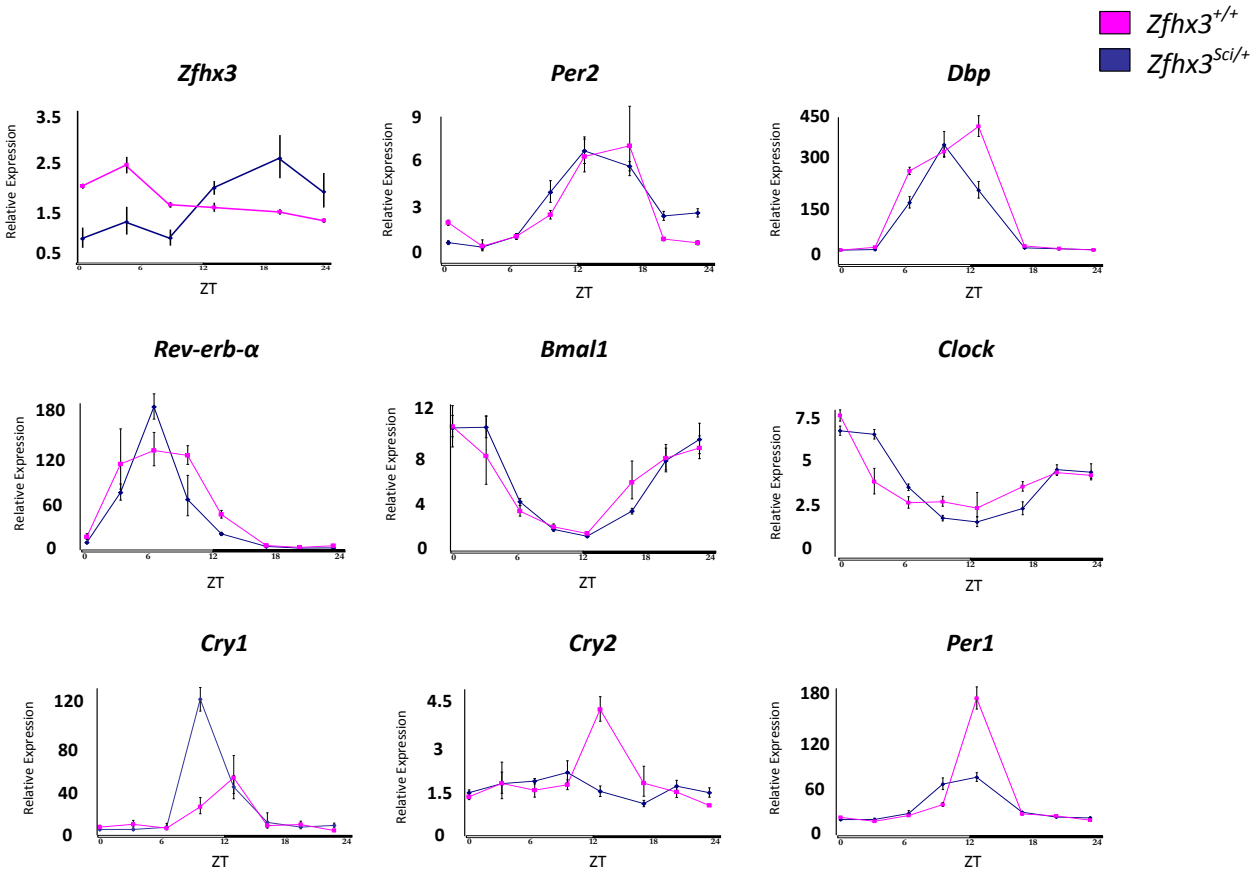

Figure 18: RNA expression pattern of *Zfhx3* and known clock genes in *Zfhx3*$^{+/+}$ and *Zfhx3*$^{Sci/+}$ liver. The panels show the relative expression of *Zfhx3* and eight known clock transcripts in *Sci* liver across ZT points. The phase of expression of *Zfhx3* is shifted in *Zfhx3*$^{Sci/+}$ compared to *Zfhx3*$^{+/+}$, however there is no difference in the peak amplitude of expression. *Per2, Dbp* and *Bmal1* show little change in RNA oscillation in the presence of the *Sci* mutation. There is a small increase in the peak of expression of *Rev-erb-α* RNA and a slight phase advance in *Clock* RNA expression. The most severe effects are evident in *Cry1, Cry2* and *Per1* RNA expression. Both *Cry2* and *Per1* have a dampened peak of expression, with *Cry2* in particular showing little circadian oscillation in *Zfhx3*$^{Sci/+}$ liver. *Cry1* shows highly increased amplitude in the peak of RNA expression. This may be compensatory to the *Cry2* RNA expression pattern or *vice versa*.

4.2.2. *In situ* hybridisation in the adult SCN

In situ hybridisation was performed to assess whether *Zfhx3* RNA was expressed in the adult SCN and therefore may function at the site of the core circadian oscillator. Sense and antisense DIG labelled RNA probes generated against the *Zfhx3* transcript were hybridised against cryopreserved adult mouse coronal brain sections which included the SCN and optic chiasm. Animals were culled across ZT times at four hourly time intervals (ZT 3, 7, 11, 15, 19 and 23). *In situ* hybridisation was then performed and qualitative RNA expression was assessed across a 24 hour period. $Zfhx3^{+/+}$ and $Zfhx3^{Sci/+}$ brain sections were harvested and sections were processed together along with negative controls. A minimum of three independent experiments were performed. Representative images of *in situ* hybridisation on the SCN are shown in Figure 19.

From Figure 19 it is evident that within this coronal section through the adult brain, the *Zfhx3* RNA transcript is expressed specifically in the SCN. Although a quantitative analysis is not possible from these studies, the transcript is constitutively expressed across ZT points. This suggests that *Zfhx3* has a specific role and function at the site of the core circadian oscillator. There is little evidence of RNA expression outside of the SCN at this level of the brain, sectioned through the SCN. RT-PCR (performed by Dr. Michael Parsons) has shown that the *Zfhx3* RNA transcript does oscillate in extra-SCN tissues such as hypothalamus, liver and MEFs as discussed previously and shown in Figure 18. Further work continues to characterise the oscillation of *Zfhx3* in the SCN. It also remains to be assessed whether ZFHX3 protein is expressed in the SCN and whether it oscillates. This work is dependent upon a reliable antibody suitable for both immuno-histochemistry and western blotting, which is discussed later in this chapter. The data so far however, strongly suggests that there is a specific role for *Zfhx3* at the site of the core circadian oscillator in the adult brain.

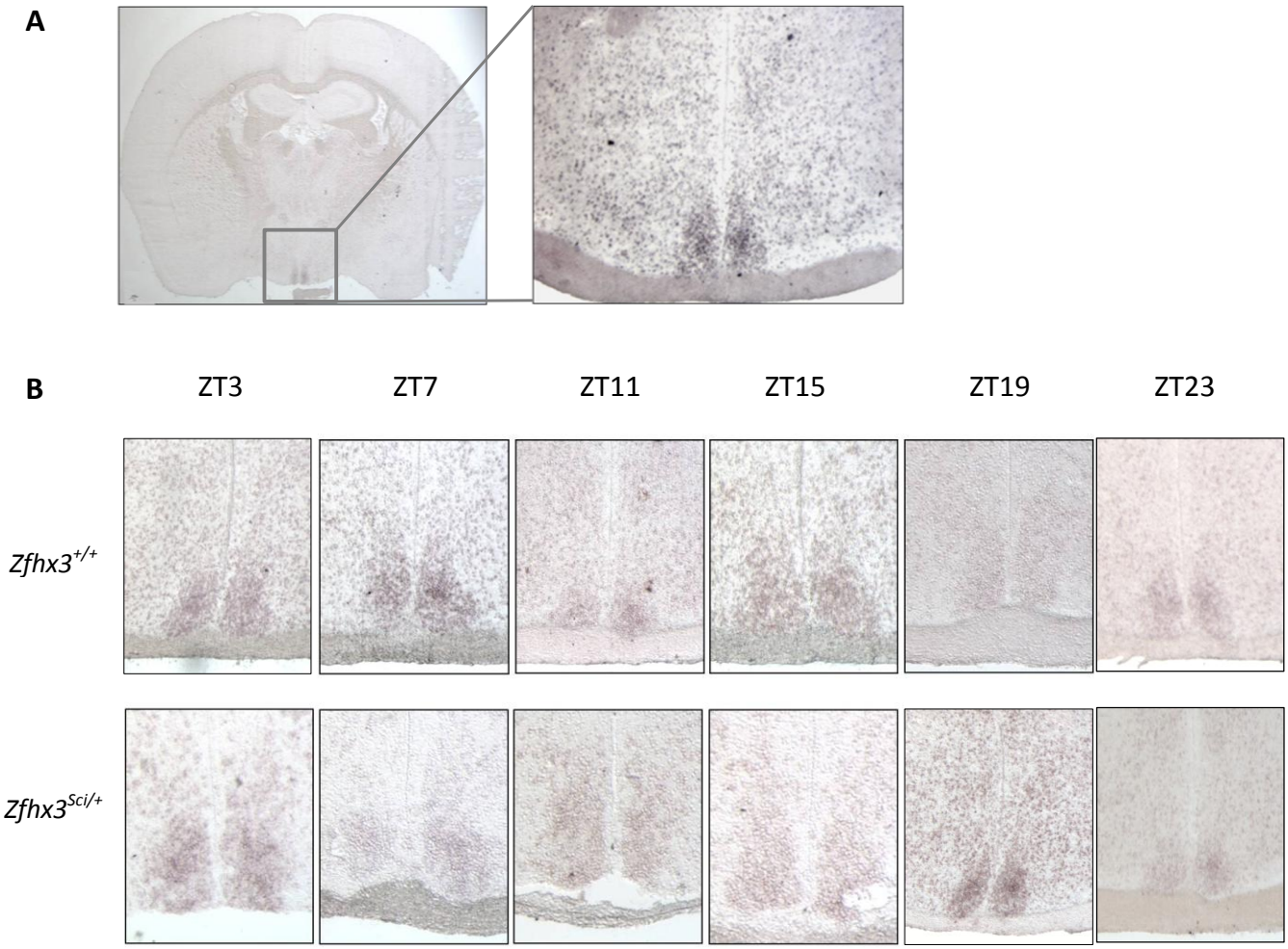

Figure 19: *In situ* hybridisation on *Sci* SCN using a *Zfhx3* DIG-labelled riboprobe. Age matched whole adult brains, were collected across ZTs and fresh frozen in OCT. 12 μm coronal sections were cut through the SCN and used for *in situ* hybridisation. A *Zfhx3* DIG-labelled riboprobe was used to assess the expression of *Zfhx3* RNA in the SCN of the adult mouse brain across ZT points. NBT/BCIP staining produced a purple stain where there was hybridisation of the probe to the endogenous RNA transcript. (A) Whole coronal brain section through the optic chiasm and SCN. The enlarged region shows the region encompassing the SCN where there is positive staining. The only positive staining for *Zfhx3* within the entire section is detected in the SCN, indicating a specific localisation of the *Zfhx3* RNA to the site of the core circadian oscillator. (B) The top panel of images show *in situ* hybridisation in $Zfhx3^{+/+}$ SCN across four hourly time points. The bottom panel of images show *in situ* hybridisation in $Zfhx3^{Sci/+}$ SCN across four hourly time points. In both, it is observed that the RNA expression of *Zfhx3* is constitutively expressed across all ZT points.

4.2.3. *In situ* hybridisation in embryonic development

Zfhx3 is known to be a transcriptional regulator during embryonic development. This is supported by the homozygous lethality in *Sci* mutants, potentially supporting impaired activity or non-functionality during development. Homozygous *Sci* animals fail to survive past late gestation which may suggest that this is not brain-related developmental lethality. *In situ* hybridisation was used to confirm the expression pattern of *Zfhx3* in mouse embryos across a developmental time course. *Zfhx3* has been reported to be expressed in the putative SCN region of the developing hypothalamus in the mouse brain, therefore experimental efforts focused on detection of *Zfhx3* in the developing brain to confirm this result.

Zfhx3 RNA expression was detected from E10.5 dpc and persisted until E16.5 dpc. The expression was confined predominantly to the nervous system, with expression detected in the somites and frontal brain, but also in the limb buds. In late gestation, *Zfhx3* RNA was seen to be expressed throughout the mid and hind brain, with strong staining in the pre-optic area, hypothalamus and thalamus. Additionally, specific staining was observed in the olfactory epithelium and spinal cord. Given that *Zfhx3* has also been shown to be specifically expressed almost exclusively in the adult SCN, the data shows that *Zfhx3* is more broadly expressed in development during the establishment of neural networks but its function persists more specifically at the site of the core circadian oscillator in the adult brain. Representative images from *in situ* hybridisation on embryonic tissues are shown in Figure 20.

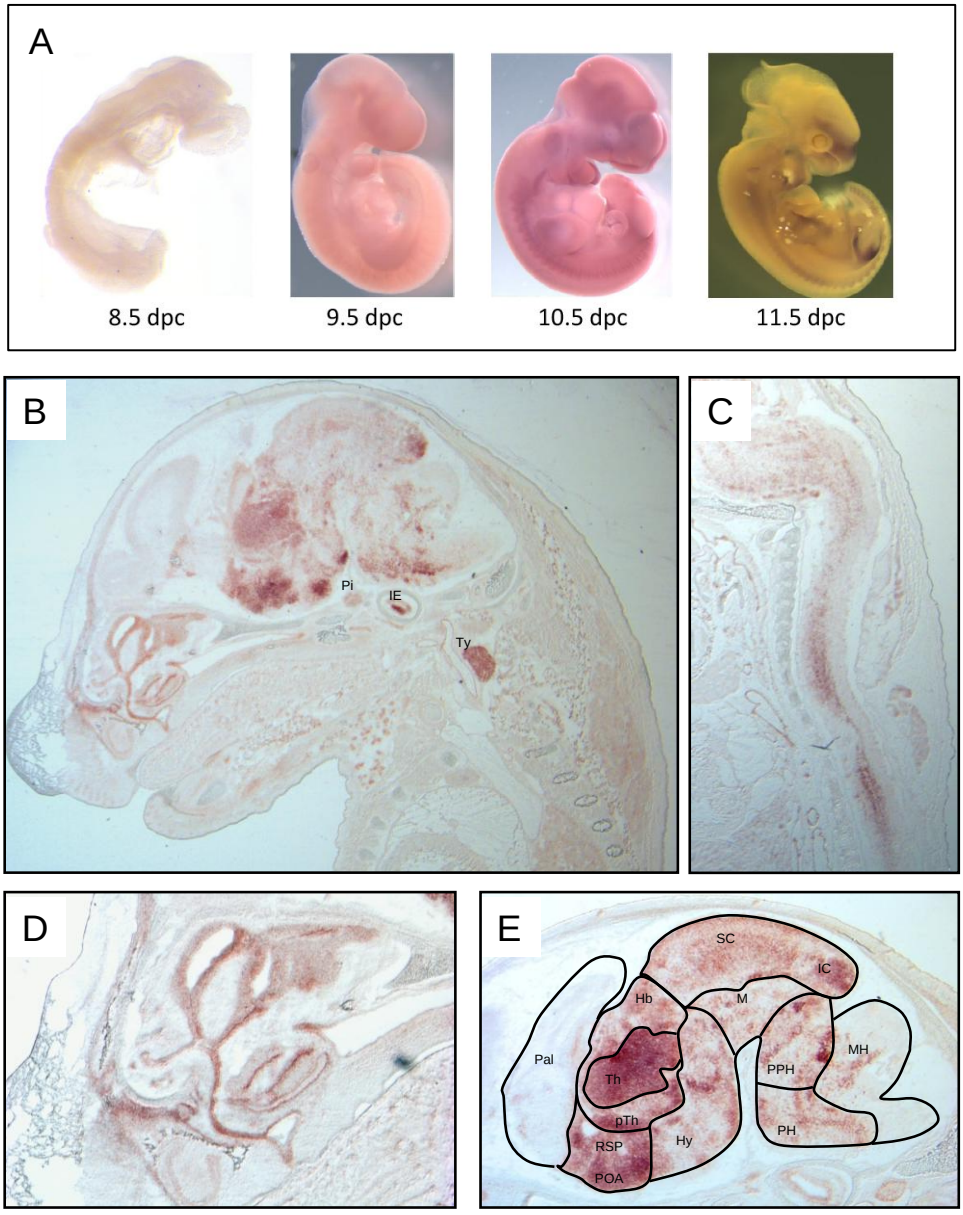

Figure 20: *In situ* hybridisation on whole and sectioned mouse WT embryos using a DIG labelled *Zfhx3* riboprobe. *In situ* hybridisation was used to visualise the RNA expression pattern of *Zfhx3* through embryonic development. (A) Whole mount *in situ* hybridisation on embryos from 8.5 dpc – 11.5 dpc. *Zfhx3* RNA was detected from 10.5 dpc in the frontal brain, spinal cord and limb buds. This staining pattern was observed from 10.5 dpc – 13.5dpc. (B) 16.5 dpc mouse embryonic mid-line sagittal section. This staining pattern was observed from 14.5 dpc – 16.5 dpc. (C) Spinal cord at E16.5 dpc. (D) Olfactory epithelium at E16.5dpc. (E) Brain regions at 16.5 dpc: Th: Thalamus. pTh: Pre-thalamus. Hb: Habenula. Hy: Hypothalamus. RSP: Rostral Secondary Prosencephalon. POA: Preoptic Area. SC: Superior Colliculus. IC: Inferior Colliculus. M: Midbrain. PPH: Prepontine Hindbrain. PH: Pontine Hindbrain. Pal: Pallium. MH: Medullary Hindbrain. IE: Inner Ear. Ty: Thymus.

4.3. Over-expression and Co-immuno-precipitation

In order to assess whether ZFHX3 interacted physically with any known clock proteins, a system of over-expression followed by co-immuno-precipitation was used. Full-length, human cDNA *Zfhx3* expression constructs with V5, HA and MYC tags were optimised for expression and used depending on the epitope tag of the co-transfected full length mouse cDNA clock gene expression constructs. Having optimised the transfection efficiency and expression of each fusion protein, mammalian expression constructs were co-transfected in HEK293 cells. 24 – 48 hours following transfection, cells were harvested and extracted proteins were co-immunoprecipitated. In each case, the antibody to the epitope tag for the *Zfhx3* expression construct was used in the immuno-precipitation and the antibody to the epitope tag of the clock protein was used for western blotting. In this way a positive interaction was detected between ZFHX3 and CRY1, CRY2, EPAS1 and PER2. An interaction was not identified between ZFHX3 and REVERBα. These interactions have been shown in three independent experiments, together with negative controls. Work continues to identify whether an interaction co-exists in over-expression between ZFHX3 and CLOCK, PER1 and BMAL1 however preliminary experiments suggest that there is no interaction between these proteins. Representative western blots showing these interactions are shown in Figure 21.

These protein interactions have only been demonstrated in this one orientation of the immuno-precipitation reaction. Positive interactions failed to be detected when using an antibody to the epitope tag of the clock genes expression construct and probing the western blot with an antibody to the epitope tag for ZFHX3. This may be due to the size of ZFHX3 protein, 404 kDa and the clock proteins may be too small or weak to immunoprecipitate this larger protein. Attempts at cross-linking the proteins to stabilise any interaction also failed to produce a positive result in this

orientation. Further work is therefore required to conclusively prove these protein interactions. To further assess this, preliminary co-localisation and Forster Resonance Energy Transfer (FRET) were completed. Co-localisation between CRY2 and ZFHX3, co-transfected in HEK293 cells, has been consistently observed. Preliminary FRET analysis has shown that the two over-expressed proteins are within close enough distance to physically interact (less than 10 nm apart) however this has so far only been demonstrated once. Representative images for these co-localisation and FRET results between ZFHX3 and CRY2 are shown in Figure 22.

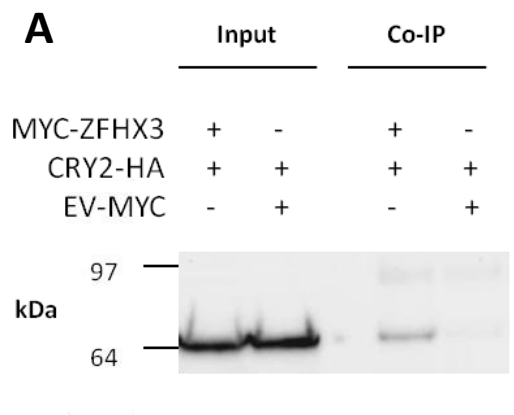

CRY2: 67 kDa

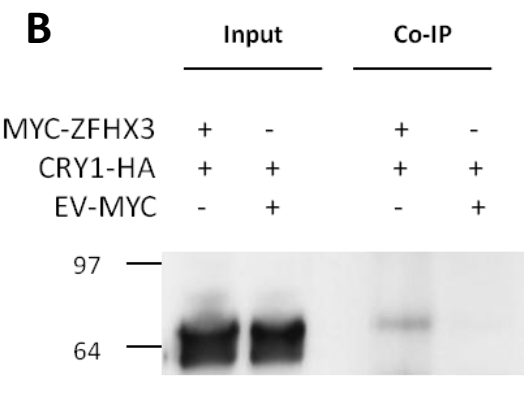

CRY1: 67 kDa

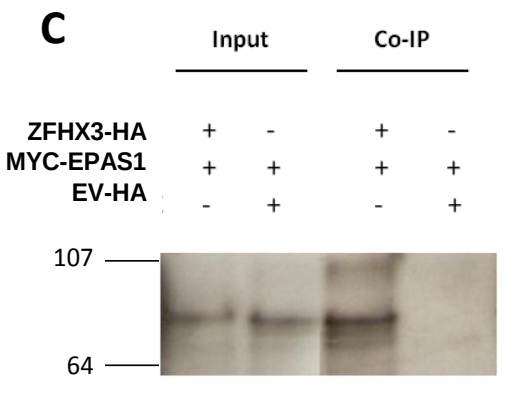

EPAS1: 96.4 kDa

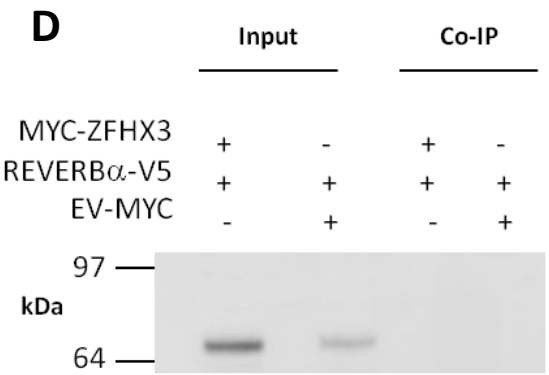

REVERBα: 66.8 kDa

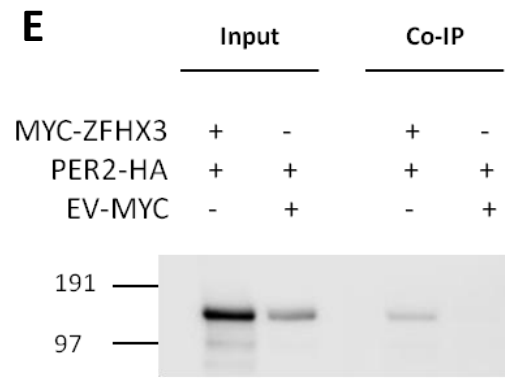

PER2: 136 kDa

Figure 21: Co-immuno-precipitation reactions between ZFHX3 and known clock proteins. HEK293 cells were transiently transfected with *Zfhx3* and clock gene mammalian expression constructs with epitope tags. Cells were harvested between 24 – 48 hours later and extracted proteins were used for immuno-precipitation. Each panel first shows the protein input by western blotting with either both transfected expression constructs or an empty construct (EV-MYC) with the clock expression construct. This showed that the construct had been successfully transfected and expressed. The following two lanes in each western blot show the CO-IP result. (A) MYC-ZFHX3 and CRY2-HA or CRY2-HA and EV-MYC were co-transfected into HEK293 cells. The ZFHX3 over-expressed protein was pulled down with an α-MYC antibody and the protein lysates probed by western blotting using α-HA antibody. In this way ZFHX3 was shown to interact with CRY2 when pulling down the MYC-ZFHX3 fusion protein. (B) In the same way as (A), ZFHX3 was shown to interact with CRY1 when pulling down the MYC-ZFHX3 fusion protein. (C) ZFHX3-HA and MYC-EPAS1 or MYC-EPAS1 and EV-HA were co-transfected into HEK293 cells. The ZFHX3 over-expressed protein was pulled down with an α-HA antibody and the protein lysates probed by western blotting using α-MYC antibody. In this way ZFHX3 was shown to interact with EPAS1 when pulling down the ZFHX3-HA fusion protein. (D) MYC-ZFHX3 and REVERBα-V5 or REVERBα-V5 and EV-MYC were co-transfected into HEK293 cells. The ZFHX3 over-expressed protein was pulled down with an α-MYC antibody and the protein lysates probed by western blotting using a-V5 antibody. In this way ZFHX3 was not shown to interact with REVERBα when pulling down the MYC-ZFHX3 fusion protein. (E) In the same way as (A) and (B) ZFHX3 was shown to interact with PER2 when pulling down the MYC-ZFHX3 fusion protein.

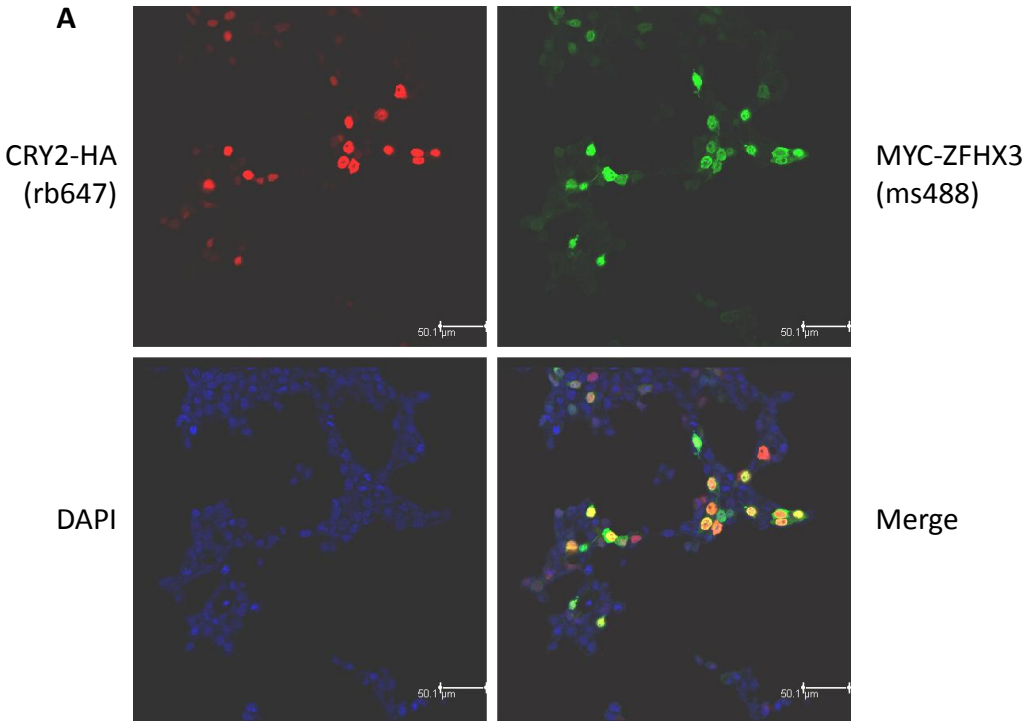

Time [s]	Ch1	Ch2
0	93.3	96.5
1.64	91.2	95.3
3.28	91.8	93.8
4.92	89	93.6
6.56	87.4	92.8
26.68	112.1	48.4
28.32	109.2	48.6
29.96	106.8	48.7
31.6	107.9	48.8
33.24	106.1	48.2

Figure 22: Co-localisation and FRET between MYC-ZFHX3 and CRY2-HA, over-expressed in HEK293 cells. (A) HEK293 cells were transiently transfected with CRY2-HA and MYC-ZFHX3 expression constructs. Protein localisation was visualised by indirect immuno-fluorescence, CRY2-HA pseudo-labelled in far-red (Alexa Fluor® 647) and MYC-ZFHX3 pseudo-labelled in green (Alexa Fluor® 488), DAPI pseudo-labelled the nuclei blue. The merged image shows high overlap between the fluorophores labelling CRY2 and ZFHX3 in the nuclei. Images were taken on Zeiss Axio-observer at X20 objective. (B) FRET technique was used to assess whether the over-lap in fluorescence signal between the CRY2 and ZFHX3 indirect labelling was within protein interaction distance (less than 10 nm). The yellow arrow represents the time of bleaching of the red fluorophore. The transfer of energy, possible at less than 10 nm, is seen in the increased

intensity in the green fluorophore as the intensity of the red fluorophore decreased. The values for the change in fluorescence intensity over time are shown in the table. This result indicates that the two fluorophores, and subsequently the CRY2 and ZFHX3 proteins, are co-localised within physical interaction distance further supporting the co-immuno-precipitation results. Images were taken on Zeiss Multi-photon at X63 objective.

Through immuno-fluorescence, the close proximity (10 nm) of ZFHX3 and CRY2 supports a protein interaction in the nucleus. It is possible that these interactions occur specifically at dense foci within the nuclei to which ZFHX3 appears to localise. These foci may be sites of dense chromatin, consistent with the role of *Zfhx3* in transcriptional regulation and gene activation. Attempts to identify these dense regions of staining to known sub-nuclear structures have so far shown that they do not associate with nuclear speckle or nucleoli markers. These foci are more reminiscent of Cajal bodies, sites of modification and assembly of transcriptional machinery, and this remains to be further investigated. A representative image of the sub-cellular localisation of ZFHX3 within the nucleus (Alexa Fluor® 488, green) together with CRY2 (Alexa Fluor® 647, red) is shown in Figure 23. Z-stack imaging has confirmed these foci to be within the nuclei, however ZFHX3 also appears to form in clusters or inclusions outside the nucleus in some cells, which from later work in this chapter, may be inferred to be mitochondria.

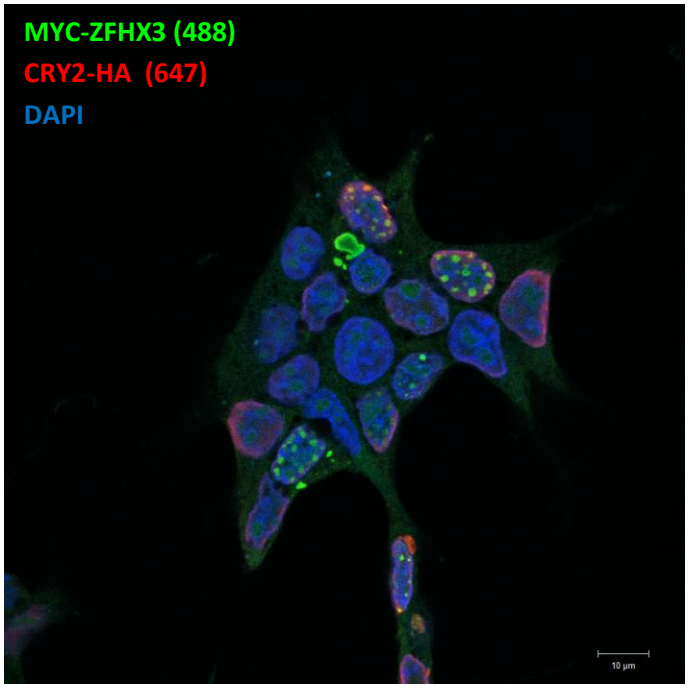

Figure 23: Sub-cellular co-localisation of ZFHX3 and CRY2 within the nuclei of HEK293 cells. CRY2-HA and MYC-ZFHX3 constructs were co-transfected into HEK293 cells. Indirect immuno-fluorescence showed that ZFHX3 may co-localise with CRY2 within the nucleus at distinct dense foci. These may be the sites of dense chromatin and high transcriptional activity. It is possible that it is in these regions that ZFHX3 interacts with CRY2. CRY2-HA, red (Alexa Fluor® 647) and MYC-ZFHX3, green, (Alexa Fluor® 488). Nuclei are labelled with DAPI, blue.

These results show that ZFHX3 can physically bind core clock proteins, indicating that it may play a role in the core circadian oscillator through these interactions. The nature of these interactions in the *Sci* mutant now needs to be determined endogenously once a working ZFHX3 antibody is available. It is possible that a loss or miss-timing of these interactions may be causative of the mutant circadian phenotype, and that these interactions are required for accurate and robust molecular circadian oscillations. The protein interactions between ZFHX3 and CRY1, CRY2, PER2 and EPAS1 are novel interactions involving the circadian clock proteins and may have wide implications on the molecular mechanism of the circadian feedback loop and support a role for ZFHX3 in the negative limb of the feedback loop. Although these interactions have been shown in

one orientation of the immuno-precipitation, co-localisation and preliminary FRET experiments also provide support for these interactions. Additionally, RNA expression analysis by Dr Michael Parsons has also seen effects on *Cry1, Cry2* and *Per1* RNA expression. This further supports an interaction, proteomic and genetic, between *Zfhx3* and these targets. Further investigation into the interaction between *Zfhx3* and *Cry1* and *Cry2* is discussed in Chapter V.

4.4. ZFHX3 protein expression

In order to characterise ZFHX3 across circadian time, an endogenous detection system is required as opposed to over-expression under a constitutive promoter. As such, attempts were made to generate an antibody to detect ZFHX3 in mouse tissue. The generation of a reliable antibody could then be subsequently utilised in a number of assays including determining the relative protein levels between *Zfhx3*$^{+/+}$ and *Zfhx3*$^{Sci/+}$ mutant samples, protein interaction studies and chromatin immuno-precipitation. This is essential for determining the mechanism by which ZFHX3 acts on the circadian clockwork. Although the expression pattern of *Zfhx3* RNA has been characterised, this may not be reflective of where and when functional ZFHX3 protein is expressed and localised. Commercial antibodies proved unsuccessful in detecting ZFHX3 in various cell lines and tissues. Three attempts were therefore made to produce a custom ZFHX3 antibody, each using the rabbit as a host. Two antibodies were generated by 21st Century Biochemicals and a third antibody generated by Eurogentec. The optimisation of these three antibodies is described in this section. The schematic in Figure 24 shows the amino acid antigenic sequence used for peptide generation and antibody production and their relative location within the ZFHX3 amino acid sequence.

Two peptides were generated by 21st Century Biochemicals based upon immunological value. One antigen lay at amino acid 2126-2155 towards the N-terminus (antibody “1”). The second lay at the C terminus of the protein, encoding the last amino acids from 3688-3707 (antibody “2”). In total there were 12 sera and 4 antibodies to optimise for ZFHX3 detection. The first optimisation was to determine whether the ZFHX3 sera could detect an over-expressed full length *Zfhx3*-HA tagged construct, transiently transfected into cell lines. This construct, used earlier in this chapter,

encoded the full length human *Zfhx3* cDNA sequence to which the antibody should have high immuno-reactivity.

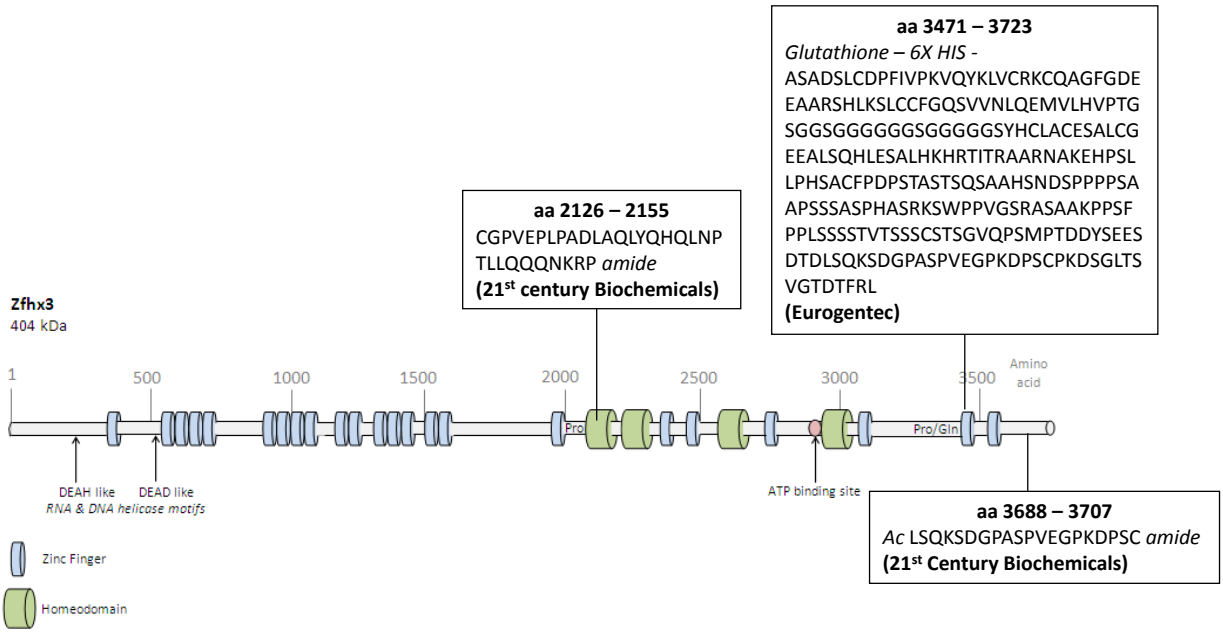

Figure 24: Location of peptide sequences generated for antibody production within the ZFHX3 amino acid sequence. Three peptide sequences were generated for antibody generation. Two peptides were designed and generated externally by 21st Century Biochemicals. The third peptide was self-generated in house and injected by Eurogentec. The *Zfhx3* cDNA fragment was cloned into a pET-32b bacterial expression construct with a 5' 6 X HIS and thioredoxin (TRX) epitope tag. The peptide was expressed in bacterial cells and purified on a cobalt charged column. All three antibodies were generated in rabbits.

Transfected U2OS cells were analysed by indirect co-immunofluorescence, using fluorescent-labelled conjugated secondary antibodies. By this method it was shown that there was an overlap in fluorescent signal between the HA epitope label and α-ZFHX3 antibody number 1, bleed number 6. This was not reproduced for the C terminus antibody (number 2). This demonstrated that the N terminus α-ZFHX3 antibody could specifically detect the over-expressed construct.

There was no additional staining detected endogenously in the U2OS cells. Figure 25 shows the co-immunofluorescence results, with the ZFHX3-HA pseudo-labelled green (Alexa Fluor® 488*),* α-ZFHX3 labelled red (Alexa Fluor® 647) and the cell nuclei labelled blue (DAPI).

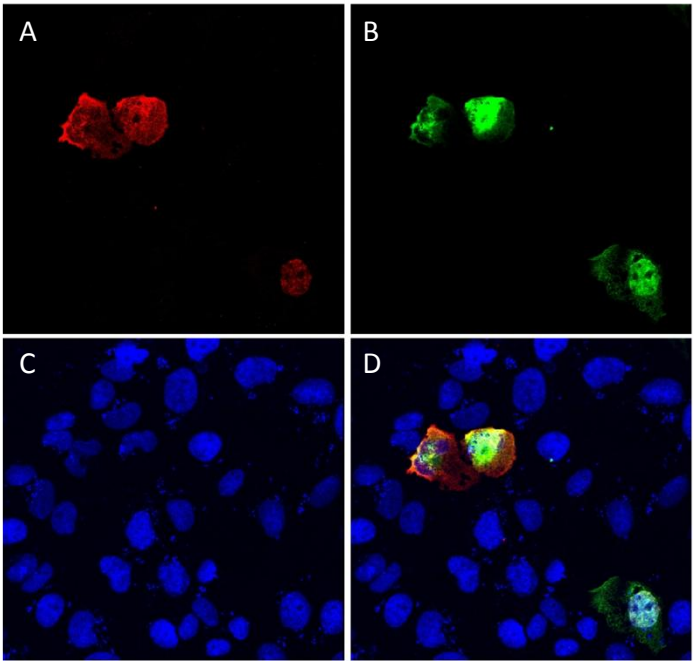

Figure 25: Co-immunofluorescence of U2OS cells transfected with *Zfhx3*-HA full length human construct and labelled with α-HA and α-ZFHX3. Cells were transiently transfected with a mammalian expression construct encoding the full length human *Zfhx3* cDNA sequence. Cells were then co-labelled with α-HA to detect the transfected construct and α-ZFHX3 to look for co-localisation between the endogenous antibody and HA epitope. Indirect co-immunofluorescence was performed using Alexa Fluor® conjugated secondary antibodies. (A) α–ZFHX3, α–rabbit Alexa Fluor® 647 (B) *α-HA,* α–mouse Alexa Fluor® *488* (C) DAPI (D) Merge. The expression of the transfected cDNA co-localised with the staining produced by the endogenous antibody. This indicated that the endogenous antibody had specifically detected the human *Zfhx3* transfected sequence and did not appear to recognise any other endogenous proteins in the U2OS cells.

To confirm these results, HEK293 and U2OS cells transfected with *Zfhx3*-HA were collected and the protein lysate was used for western blotting. Lysates from transfected and un-transfected cells were separated by electrophoresis and probed using α-ZFHX3 (1) bleed 6. A band of a high molecular weight which may correspond to ZFHX3 was weakly detected in the transfected cell

lysates and remained absent from the un-transfected cells (Figure 26). This supports the co-immunofluorescence data that α-ZFHX3 (1) bleed 6 could detect a high molecular weight protein which may correspond to the transfected *Zfhx3*-HA tagged protein, suggesting a specificity for the ZFHX3 protein.

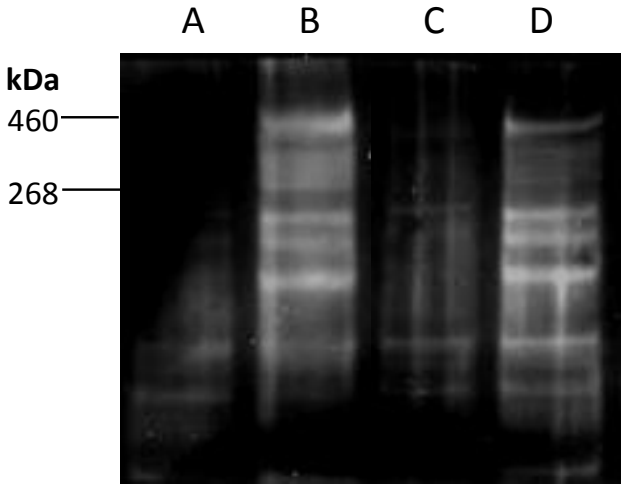

Figure 26: Detection of ZFHX3 in transfected cell lines by western blotting. HEK293 and U2OS cells both transfected with *Zfhx3*-HA and un-transfected were collected and total protein extracted. (A) Untransfected HEK293 cells. (B) HEK293 cells transfected with *Zfhx3*-HA. (C) Untransfected U2OS cells. (D) U2OS cells transfected with *Zfhx3*-HA. 20 μg was loaded and separated on a 3 – 8% tris-acetate gel and western blotting was subsequently performed. Blots were probed with α-ZFHX3 and exposed for 8 minutes using ECL. The antibody detected proteins between 268 – 460 kDa specific to the transfected cells (B & D). It is thought that one of these proteins detected is the expressed ZFHX3-HA construct.

Previous studies have shown that ZFHX3 is highly expressed in neuronal cells (Jung, et al. 2005). It has also been shown that ZFHX3 is up-regulated in P19 carcinoma stem cells upon differentiation with retinoic acid to form neuronal cell lineages (including glia) (Ido, et al. 1994). P19 cells were therefore cultured and induced to differentiate. Once neuronal cells were established, they were harvested for protein. The protein lysate was subjected to western blotting and probed using the α-ZFHX3 sera discussed above. A protein of high molecular weight that may correspond to ZFHX3

(404kDa) was detected in the neuronal differentiated P19 cells however not in the undifferentiated control cells. This is shown in Figure 27. This suggests highly specific expression of ZFHX3 in neuronal cell types and that the protein may be detected using the α-ZFHX3 (1) antibody.

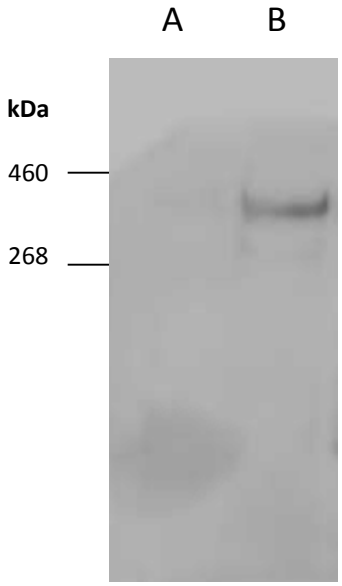

Figure 27: Detection of ZFHX3 in undifferentiated and retinoic-acid differentiated P19 cells. Multi-potent P19 carcinoma cells were differentiated into neural progenitor cells using retinoic acid. Total cell lysate from undifferentiated (A) and differentiated cells (B) was analysed by western blotting for detection of ZFHX3 using α-ZFHX3 (1, sera 6). A protein band of the expected molecular weight was detected in the differentiated P19 cells suggesting an up-regulation of ZFHX3 in neural cell types.

It was next investigated whether ZFHX3 could be detected in adult tissues using the α-ZFHX3 affinity purified antibody from bleed 6 that was shown to detect the transfected *Zfhx3*-HA construct and a high molecular weight protein in P19 differentiated cells. Various adult tissues were collected across circadian time points and total protein lysates were analysed by western blotting and probed using the α-ZFHX3 antibody. Representative western blots are shown in

Figure 28. A protein of the expected molecular weight (404kDa) corresponding to ZFHX3 was not detected in any of these adult tissues across a ZT time course. Smaller proteins however were detected by western blotting. It may be inferred that full length ZFHX3 protein is not highly expressed in adult tissues, or that the α-ZFHX3 antibody was not sensitive or specific enough to detect endogenously expressed ZFHX3 in heterogeneous mouse tissues.

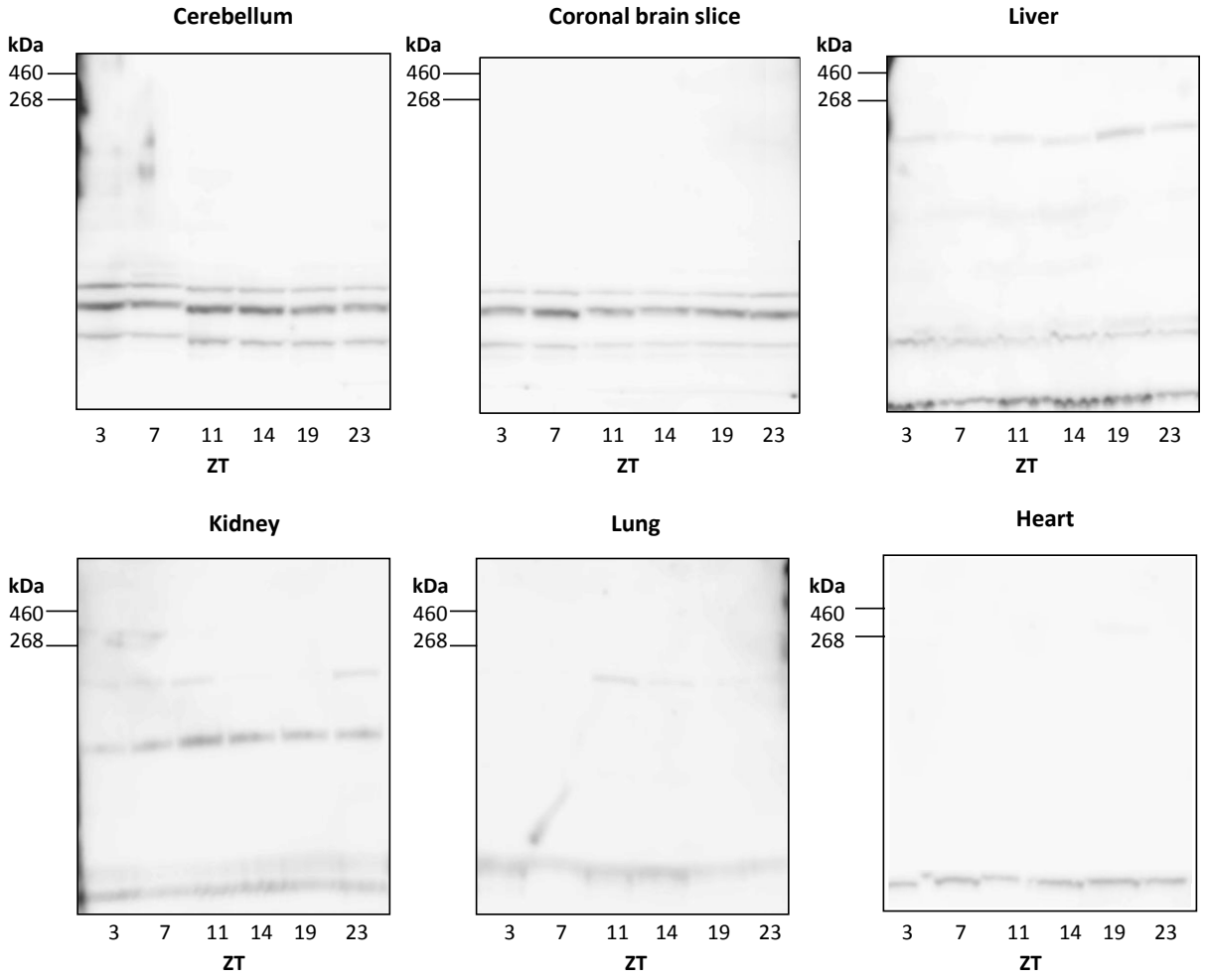

Figure 28: Detection of ZFHX3 in adult tissues across ZT points. Various adult tissues were taken from WT animals across ZT times 3, 7, 11, 14, 19, 23. Total protein lysate was extracted and 50 μg was loaded and separated on a 3 – 8% tris-acetate gel and western blotting was subsequently performed with a 1:1000 primary antibody dilution. Blots were probed with α-ZFHX3 (1). A protein of the expected molecular weight for ZFHX3 (404kDa) was not identified in any adult tissue with this antibody. A lower band of approximately 250 kDa was identified in liver and lung protein lysate and a band of approximately 117 kDa in adult kidney. Blots were exposed for 30 minutes using ECL developing system.

Given RNA data indicating that *Zfhx3* transcript is highly expressed during embryonic development, western blot analysis was repeated using embryonic tissues across 12.5 dpc – 16.5 dpc. Representative images are shown in Figure 29. In this instance a protein was identified of a high molecular weight that could correspond to ZFHX3. The expression pattern of the protein appeared dynamic across organs and developmental time. This protein was particularly sensitive and could only be identified in freshly harvested embryonic tissues that had not been subject to freezing prior to use. Additionally, a lower molecular weight protein was identified at the same height as that identified in adult tissues. This data supports that ZFHX3 may be highly expressed throughout embryonic development, peaking in embryonic brain at 12.5 – 13.5 dpc.

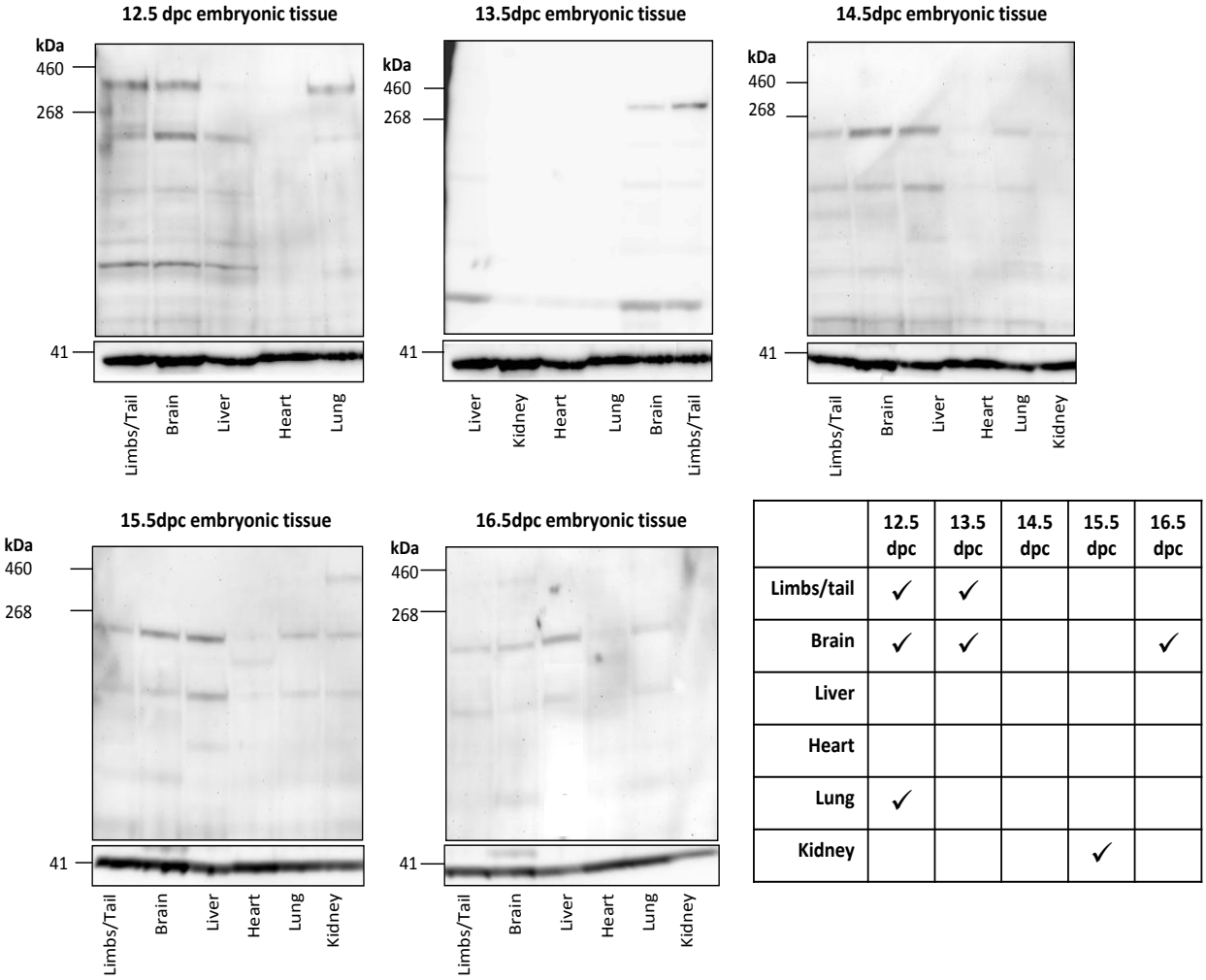

	12.5 dpc	13.5 dpc	14.5 dpc	15.5 dpc	16.5 dpc
Limbs/tail	✓	✓			
Brain	✓	✓			✓
Liver					
Heart					
Lung	✓				
Kidney				✓	

Figure 29: Detection of ZFHX3 in embryonic tissue across developmental stages 12.5 dpc – 16.5dpc. Various embryonic tissues were taken from WT animals across developmental stages. Total protein lysate was extracted and 50 μg was loaded and separated on a 3 – 8% tris-acetate gel and western blotting was subsequently performed with a 1:1000 primary antibody dilution. Blots were probed with α-ZFHX3 (1). A protein of the expected molecular weight for ZFHX3 (404kDa) was weakly detected in various tissues, including limbs/tail, brain, lung and kidney. The overall expression pattern is shown in the bottom right panel. As in adult tissues, a lower band of approximately 250 kDa was identified across most tissues and developmental time points. The lower panel of each western blot shows the actin loading control. Blots were exposed for 10 minutes using ECL developing system.

The specificity of the antibody and the identity of this protein, presumed to be ZFHX3, remained to be identified. Immuno-precipitation reactions were performed in order to enrich and isolate

both the high molecular weight protein (approximately 400kDa) and the lower molecular weight protein (approximately 250 kDa). Enrichment of these proteins was required for mass spectrometry analysis to determine the identity of these proteins for future work. Immuno-precipitation reactions were unsuccessful with this antibody with no enrichment from the 400kDa band in either adult or embryonic tissue. A peptide blocking experiment was set up to determine the nature of the lower molecular weight protein identified in adult tissues and the specificity of the α-ZFHX3 antibody. Peptide blocking demonstrated that the lower molecular weight protein was in-fact being specifically identified by the antibody and it was hypothesised that this may be a novel splice variant or isoform of the ZFHX3 protein that is expressed in adult tissues. Although immuno-precipitation was not able to enrich the larger molecular weight band, the lower molecular weight band appeared enriched and so gels were run and stained using coomassie. The bands that corresponded to the approximate molecular weight were selected for mass spectrometry analysis. The mass spectrometry identified that this band corresponded to fatty acid synthase with no evidence for splice variants or cleaved products of ZFHX3. Further analysis showed that the α-ZFHX3 antibody antigenic sequence had a highly homologous alignment to a region of the fatty acid synthase peptide sequence. Results from this series of experiments are shown in Figure 30. It was therefore determined that this antibody was not specifically detecting endogenous α-ZFHX3 in tissues and could not be reliably used for future downstream experiments including immuno-histochemistry, immuno-precipitation or chromatin immuno-precipitation due to a high affinity for other proteins, including fatty acid synthase.

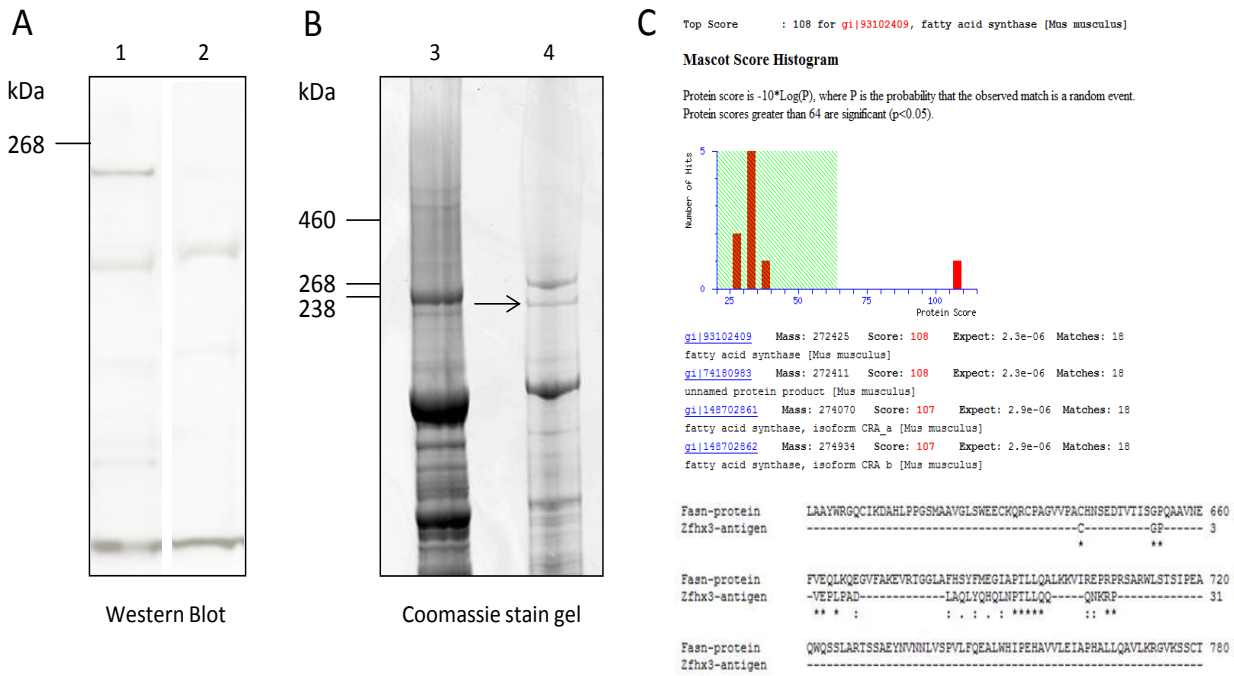

Figure 30: Detection and identification of low molecular weight protein identified by α-ZFHX3. (A) Peptide blocking experiment with α-ZFHX3 and ZFHX3 peptide to determine the specificity of the ≈250kDa protein detected by α-ZFHX3. 30 μg total liver protein lysate was loaded and separated on a 3 – 8% tris-acetate gel and western blotting was subsequently performed. (1) Blot was probed with α-ZFHX3. A protein of approximately 250 kDa previously identified, was detected after 8 minute exposure using ECL. (2) Blot was probed with α-ZFHX3 that had been blocked with ZFHX3 peptide (1:2 ratio in mg). The 250 kDa protein was no longer detected by western blotting suggesting that it was a specific protein detected by the α-ZFHX3 antibody. (B) Coomassie stained gel to detect and select the band corresponding to the lower molecular weight protein identified in A. (3) Total liver protein lysate, 30 μg loaded and separated on a 3 – 8% tris-acetate gel. (4) Immuno-precipitation reaction using α-ZFHX3 aimed to enrich for the lower molecular weight protein. Arrow indicates the band selected for Surface-Enhanced Laser Desorption/Ionization Time-Of-Flight (SELDITOF) mass spectrometry. (C) Results obtained from mass spectrometry on the selected protein band immuno-precipitated by α-ZFHX3 from total liver protein lysate. A highly significant score for fatty acid synthase was identified. The ZFHX3 antigen sequence used for peptide production and antibody generation is highly homologous to fatty acid synthase. These results implicate a non-specific binding of the ZFHX3 antigen to fatty acid Synthase in adult tissues.

Another attempt to generate a custom ZFHX3 antibody was pursued, using a peptide sequence designed and generated in house. A large cDNA fragment of 750 nt at the C-terminus was cloned into a bacterial expression vector, pET-32b with an N-terminus thioredoxin (TRX) and a poly-histadine (6 X HIS) tag. The peptide was then expressed and purified and used for injection for antibody generation in two rabbits. The induction of expression and elution of the peptide is shown in Figure 31 (A-C).

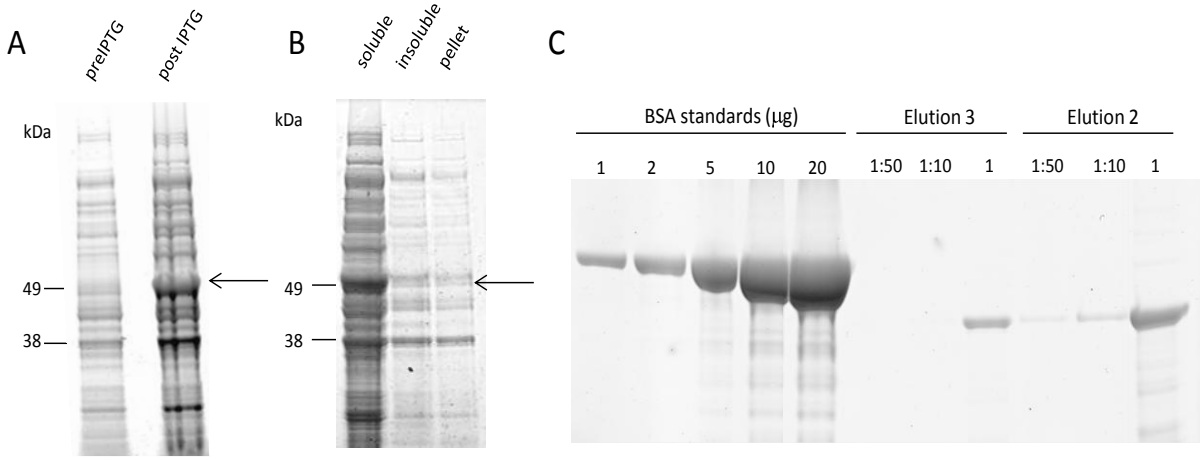

Figure 31: Generation of purified antigenic peptide for α-ZFHX3 generation. A 750 nt cDNA sequence was cloned into pET-32b bacterial expression vector in frame with an N terminus TRX and 6XHIS tag. (A) Plasmids were amplified in BL21 pLysS cells and protein expression induced using IPTG. (B) Protein from bacterial cell lysates was then separated by electrophoresis and the molecular weight and solubility was checked. (C) The His-tagged peptide was then isolated and purified using a charged nickel bead column, the eluates were quantified against BSA standards, and subsequently used for antibody generation by injection into two rabbits (Eurogentec).

A 28 day immunisation protocol using the purified peptide (elution 3) was followed by Eurogentec and four un-purified sera were received for optimisation, two from each rabbit. Optimisations by western blotting using sera from one rabbit are shown in Figure 32 with detection of a protein at the expected molecular weight for ZFHX3 observed in 13.5 dpc embryonic brain lysate and MEF

cell lysate. The sera from the second rabbit failed to detect any proteins of the molecular weight corresponding to ZFHX3. Preliminary results suggest a lower abundance of ZFHX3 in *Zfhx3*$^{Sci/+}$ and *Zfhx3*$^{Sci/Sci}$ MEFs compared to *Zfhx3*$^{+/+}$ when compared to actin loading control. Purification of this serum will follow with subsequent confirmation of the identity of this band.

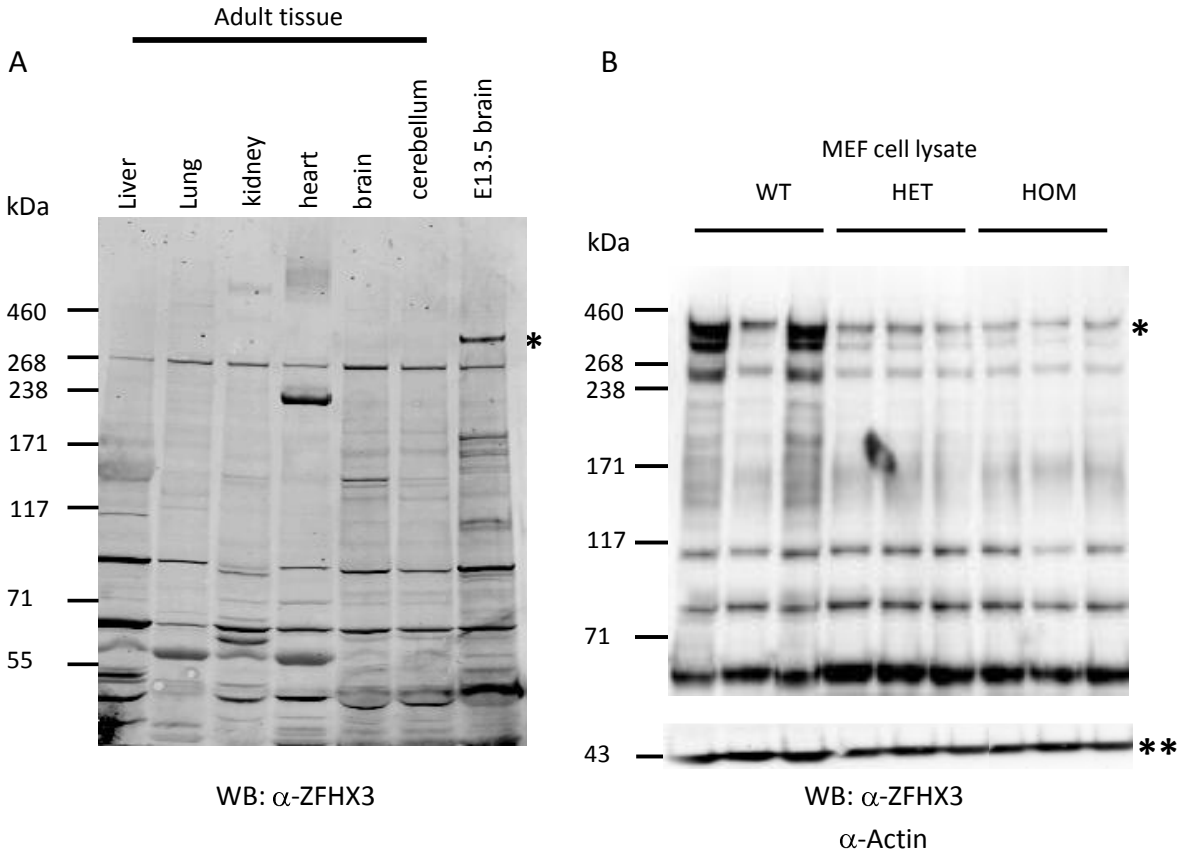

Figure 32: Western blot analysis on adult and embryonic tissue protein lysates using unpurified α-ZFHX3 sera from one injected rabbit. (A) The ZFHX3 antibody was tested against a number of different adult tissue protein lysates and 13.5 dpc embryonic brain. A protein of the expected molecular weight was identified in the embryonic brain lysate, denoted by *. (B) Protein expression was examined across *Zfhx3*$^{+/+}$, *Zfhx3*$^{Sci/+}$ and *Zfhx3*$^{Sci/Sci}$ MEF cell lysates. A protein of the expected molecular weight was detected in MEFs as denoted by *. Actin loading control is shown and denoted by **. From this preliminary result, there appears to be a lower amount of ZFHX3 protein in *Zfhx3*$^{Sci/+}$ and *Zfhx3*$^{Sci/Sci}$ MEFs compared to *Zfhx3*$^{+/+}$. Purification of this antibody and subsequent analysis remains to confirm whether this indentified protein is ZFHX3 and then quantification of protein levels across genotypes may follow.

Three antibodies were generated with the aim of detecting ZFHX3 full length protein in mouse tissue. Out of two antibodies produced by 21st Century Biochemicals, one showed that it could detect a mammalian expression construct for the human full length ZFHZ3 protein, as well as a protein of high molecular weight in differentiated P19 cells and embryonic tissues. The identity of this detected band remains to be confirmed; however it appeared to be expressed at very low levels and to be a very unstable protein, or a sensitive/non robust antibody with which to work. The antibody was unable to be used for immuno-precipitations and other biochemical analyses other than western blotting and therefore was not suitable for further downstream applications. It was also shown that this antibody specifically recognises a non-related protein, fatty acid synthase and that the antigenic sequence used to produce the α-ZFHX3 antibody had high homology to a region of this protein. Based on these results a new antibody was generated using a different antigenic sequence. This peptide was produced in house and used by Eurogentec for immunisations. Sera have been received and are continuing to be optimised. It may be possible to speculate based upon the preliminary data that ZFHX3 is not highly expressed in adult tissues and rather is highly expressed during development as supported by RNA expression studies. *In situ* hybridisation has however detected RNA expression highly localised to the adult SCN and other nuclei within the brain as well as the piriform cortex, however this has not been shown with the custom antibodies so far.

4.5. Stable Isotopically Labelled Amino Acids in Cells Culture assay

With continuing efforts to generate a ZFHX3 antibody, parallel approaches were followed to assess the proteome in *Sci* animals. Stable Isotope Labelling by Amino acids in Cell culture (SILAC) is a method by which the relative levels of proteins in the proteome of two differentially labelled cultures can be analysed. For this experiment, the proteome between *Zfhx3*$^{+/+}$ and *Zfhx3*$^{Sci/+}$ or *Zfhx3*$^{+/+}$ and *Zfhx3*$^{Sci/Sci}$ MEFs were compared. *Zfhx3*$^{+/+}$ MEFs were cultured in "light" media, containing normal isotopes of arginine and lysine. Both the *Zfhx3*$^{Sci/+}$ and *Zfhx3*$^{Sci/Sci}$ MEFs were cultured in "heavy" media, where the arginine and lysine were isotopically labelled. After incorporation of these amino acids during cell division, the two genotypes could be differentiated when pooled together based upon molecular weight. In this way, global differences on a proteomic level could be assessed between genotypes. Additionally, cells were synchronised such that cells could be collected at two time points to assess for any circadian effect between genotype on the proteome. After synchronisation, equal cell numbers were pooled together from the two time points (ZT24 and ZT14) and fractionated into nuclear and cytoplasmic sub-cellular components. A proteasome inhibitor was used for these experiments due to the short half life of the circadian proteins.

The initial aim of this experiment was to directly detect genotypic differences in ZFHX3 and circadian proteins in cultured MEFs. Due to caveats of the approach, these proteins were not detected by mass spectrometry. This is due to the limited dynamic range that the mass spectrometry can detect. However, differentially expressed proteins between genotypes were analysed globally to provide insights into the effects of the *Zfhx3* mutation on other signalling cascades and to give insight into the potential causes of the homozygous lethality in *Zfhx3*$^{Sci/Sci}$. The mass spectrometry was carried out at the University of Oxford by Dr Benedikt Kessler. The

mass spectrometry data was then analysed using Ingenuity Pathway Analysis software and the fold-change threshold of which proteins were considered significantly up or down-regulated was set to < 0.6 or > 1.6 in all cases.

Table 23 shows the top associated networks which are altered with high significance across each SILAC experimental condition. The predominant top associated networks involved DNA replication and cell cycle regulation. These are consistent with the known roles of *Zfhx3* as an anti-mitotic factor and its roles to promote cellular differentiation by halting the cell cycle. The Ingenuity score for each network represented the fit of each network to the user defined set of focus proteins. The ingenuity score is generated through a hyper-geometric distribution, calculated with a right-tailed Fischer's Exact T-TEST. A score greater than 2 indicated at least 99% confidence the network was not generated by random chance. A higher score has a lower probability of finding these proteins together by chance. The score takes into account the number of molecules and the size of the network.

Experimental Condition	Top Associated Networks	Ingenuity Score
Wt v Het Cytoplasmic ZT 0	(1) DNA replication, Recombination, Repair, Protein synthesis, Cellular Development (2) Cellular development, Cellular growth and proliferation, Hair and skin development and function	**52** **48**
Wt v Het Cytoplasmic ZT 10	(1) Nervous system development and function, organ morphology, cancer (2) Cellular assembly and organisation, cellular function and maintenance, lipid metabolism (3) Cellular assembly and organisation, skeletal and muscular system development and function, embryonic development (4) Cellular development, cellular growth and proliferation, tumour morphology	**52** **34** **20** **18**
Wt v Het Nuclear ZT 0	(1) Connective tissue disorders, Dermatological diseases, Developmental Disorders (2) Cell cycle, cellular assembly and organization, DNA replication, Recombination, Repair	**43** **24**
Wt v Het Nuclear ZT 10	(1) Cell cycle, cellular assembly and organization, DNA replication, Recombination and Repair (2) Connective tissue disorders, Dermatological diseases, Developmental Disorders	**41** **37**
Wt v Hom Cytoplasmic ZT 0	(1) Digestive and hepatic system development and function and organ morphology	**46**
Wt v Hom Cytoplasmic ZT 10	(1) Digestive system development and function, hepatic system development, organ morphology (2) Cellular development, embryonic development, organ development	**48** **3**
Wt v Hom Nuclear ZT 0	(1) Antigen presentation, cell morphology, inflammatory response (2) Cell cycle, connective tissue development and function, skeletal and muscular system development and function	**32** **2**
Wt v Hom Nuclear ZT 10	(1) Cell cycle, cellular movement, nervous system development and function	**9**

Table 23: Top associated networks across all SILAC experimental conditions. All proteins detected through the SILAC mass spectrometry within the set threshold were analysed through Ingenuity Pathway Analysis. Top associated networks are listed for all experimental conditions together with the Ingenuity score. The top scored networks involve a number of pathways including DNA replication, cell cycle regulation and cellular development.

Table 24 shows the top associated diseases predicted in association with the affected proteins within each SILAC experimental condition. Cancer and connective tissue disorders (the latter likely associated to using MEFs as the cell model) are predominant associated diseases. A p-value range is generated based upon the number and relationship between the user defined set of focus proteins. All top associated diseases listed are significant with p-values less than 0.05.

Experimental Condition	Top Associated Diseases	Ingenuity Lowest Predicted P-value	Ingenuity Highest Predicted P-value
Wt v Het Cytoplasmic ZT 0	(1) Cancer (2) Reproductive System Disease (3) Cardiovascular Disease (4) Connective Tissue Disorder (5) Dermatological Disorder	**1.98E-3** **1.88E-3** **2.3E-3** **2.3E-3** **2.3E-3**	**0.049** **0.0365** **0.0362** **0.0451** **0.0407**
Wt v Het Cytoplasmic ZT 14	(1) Cancer (2) Endocrine System Disorder (3) Gastrointestinal Disease (4) Inflammatory Disease (5) Neurological Disease	**4.19E-4** **4.35E-4** **4.35E-4** **4.35E-4** **5.64E-4**	**0.0494** **0.0433** **0.0311** **0.0494** **0.0433**
Wt v Het Nuclear ZT 0	(1) Cancer (2) Gastrointestinal Disease (3) Connective Tissue Disorder (4) Developmental Disorder (5) Hereditary Disease	**1.24 E-6** **1.24E-6** **2E-6** **2E-6** **2E-6**	**0.0498** **0.0426** **0.0356** **0.0356** **0.0460**
Wt v Het Nuclear ZT 14	(1) Connective Tissue Disorder (2) Dermatological Disease (3) Developmental Disorders (4) Hereditary Disease (5) Metabolic Disease	**2.77E-8** **2.77E-8** **2.77E-8** **2.77E-8** **2.77E-8**	**0.0267** **0.0433** **0.0309** **0.0105** **0.0128**
Wt v Hom Cytoplasmic ZT 0	(1) Gastrointestinal Disease (2) Hepatic System Disease (3) Cardiovascular Disease (4) Cancer (5) Dermatological Diseases and Conditions	**8.11E-04** **8.11E-04** **8.75E-04** **2.62E-03** **2.62E-03**	**8.71E-03** **4.54E-02** **3.87E-02** **4.54E-02** **6.11E-03**
Wt v Hom Cytoplasmic ZT 14	(1) Connective Tissue Disorder (2) Dermatological Disease (3) Developmental Disorders (4) Hereditary Disease (5) Skeletal and Muscular Disorder	**9.87E-4** **9.87E-4** **9.87E-4** **9.87E-4** **9.87E-4**	**0.0196** **0.0215** **0.0321** **0.0196** **0.0176**
Wt v Hom Nuclear ZT 0	(1) Infectious Diseases (2) Cardiovascular Disease (3) Connective Tissue Disorder (4) Dermatological Disease (5) Developmental Disorders	**5.55E-4** **7.90E-4** **7.90E-4** **7.90E-4** **7.90E-4**	**0.0157** **0.0258** **0.0296** **0.0418** **0.0296**
Wt v Hom Nuclear ZT 14	(1) Infectious Diseases (2) Dermatological Disease (3) Connective Tissue Disorder (4) Gastrointestinal Disease (5) Organismal Injury and Abnormality	**1.58E-3** **0.0106** **0.014** **0.0153** **0.053**	**1.58E-3** **0.0153** **0.014** **0.0153** **0.053**

Table 24: Top associated diseases across all SILAC experimental conditions. Ingenuity pathway analysis identified top associated diseases with the user defined protein dataset. A wide range of associated diseases and disorders were identified from the proteins differentially expressed and detected by the mass spectrometry. Cancer, connective tissue disorders and cardiovascular disease are predominant associated diseases.

Table 25 lists the molecular and cellular functions associated with the differentially expressed protein dataset from each SILAC experiment. A range of p-values has been generated, all significant with p-values less than 0.05. Predominant molecular and cellular functions implicate

regulation of cellular integrity including functions within the cell cycle, morphology, assembly and regulation and cell death.

Experimental Condition	Molecular and Cellular Functions	Ingenuity Lowest Predicted P-value	Ingenuity Highest Predicted P-value
Wt v Het Cytoplasmic ZT 0	(1) Lipid Metabolism (2) Nucleic Acid Metabolism (3) Small Molecule Biochemistry (4) Protein Synthesis (5) Cellular Development	**7.58E-5** **7.58E-5** **7.58E-5** **1.58E-4** **4.61E-4**	**0.0429** **0.0469** **0.0429** **0.0287** **0.0407**
Wt v Het Cytoplasmic ZT 14	(1) Small Molecule Biochemistry (2) Lipid Metabolism (3) Cell Morphology (4) Cellular Function and Maintenance (5) Cellular Development	**6.48E-5** **9.75E-5** **3.82E-4** **3.82E-4** **8.68E-4**	**0.0487** **0.0487** **0.0433** **0.0433** **0.0453**
Wt v Het Nuclear ZT 0	(1) Cellular Assembly and Organization (2) Cellular Function and Maintenance (3) Cellular Development (4) Cellular Growth and Proliferation (5) Cell Signalling	**1.04 E-5** **1.04E-5** **3.03E-4** **3.03E-4** **5.42E-4**	**0.0481** **0.0481** **0.0495** **0.0484** **5.42E-4**
Wt v Het Nuclear ZT 14	(1) Cellular Assembly and Organization (2) Cellular Function and Maintenance (3) DNA Replication, Recombination and Repair (4) Cell Morphology (5) Cell-to-Cell Signalling and Interaction	**2.44E-7** **2.44E-7** **4.89E-5** **4.90E-5** **3.87E-4**	**0.0486** **0.0427** **0.0416** **0.0466** **0.0401**
Wt v Hom Cytoplasmic ZT 0	(1) Cell Morphology (2) Cell-to-Cell Signalling and Interaction (3) Cellular Assembly and Organization (4) Amino Acid Metabolism (5) Post-Translational Modification	**8.75E-04** **8.75E-04** **8.75E-04** **2.62E-03** **2.62E-03**	**4.03E-02** **4.79E-02** **7.85E-03** **2.62E-03** **2.68E-02**
Wt v Hom Cytoplasmic ZT 14	(1) Cell Cycle (2) Cell Morphology (3) Cell-to-Cell Signalling and Interaction (4) Cellular Assembly and Organization (5) Cellular Development	**9.87E-4** **9.87E-4** **9.87E-4** **9.87E-4** **9.87E-4**	**0.0320** **0.0435** **0.0468** **0.0464** **0.0407**
Wt v Hom Nuclear ZT 0	(1) Cellular Development (2) Cellular Growth and Proliferation (3) Cellular Assembly and Organization (4) DNA Replication, Recombination and Repair (5) Cell Cycle	**3.58E-5** **3.58E-5** **1.31E-4** **1.31E-4** **5.80E-4**	**0.0432** **0.0432** **0.0373** **0.0394** **0.0394**
Wt v Hom Nuclear ZT 14	(1) Gene Expression (2) Cell Cycle (3) Cellular Compromise (4) Cell Death (5) Cell Signalling	**3.95E-4** **9.87E-4** **3.35E-3** **9.25E-3** **0.0106**	**3.95E-4** **9.87E-4** **3.35E-3** **0.0128** **0.0106**

Table 25: Top molecular and cellular functions across all SILAC experimental conditions. General associations to cellular integrity, including cellular development, assembly and organisation and cellular function and maintenance have been identified. Additionally, molecular and cellular functions associated with the cell cycle have also been identified. Cellular growth and proliferation, DNA replication, recombination and repair, cell death and cell cycle have all been significantly associated with the differentially expressed protein dataset.

The top canonical pathways with significant p-values identified by Ingenuity are shown in Table 26. Predominant top pathways implicate aspects of the Krebs cycle, oxidative phosphorylation and mitochondrial function. Additionally, canonical pathways implicating the cell cycle and cancer were identified including mismatch repair, Granzyme A signalling (regulating apoptosis), checkpoint regulation and c-MYC mediated apoptosis signalling.

Experimental Condition	Top Canonical Pathways	Ingenuity P-value	Ingenuity Ratio
Wt v Het Cytoplasmic ZT 0	(1) Cyanoamino Acid Metabolism	**6.86E-4**	**0.033**
	(2) Citrate Cycle	**2.01E-3**	**0.035**
	(3) Lysine Degradation	**8.39E-3**	**0.015**
	(4) Sphingolipid Metabolism	**0.016**	**0.018**
	(5) Mismatch Repair in Eukaryotes	**0.0362**	**0.042**
Wt v Het Cytoplasmic ZT 14	(1) Mitochondrial Dysfunction	**6.03E-5**	**0.029**
	(2) Oxidative Phosphorylation	**8.5E-5**	**0.031**
	(3) Citrate Cycle	**1.02E-4**	**0.053**
	(4) Cyanoamino Acid Metabolism	**1.29E-3**	**0.033**
	(5) Methane Metabolism	**1.29E-3**	**0.03**
Wt v Het Nuclear ZT 0	(1) Granzyme A Signalling	**2.51 E-6**	**0.15**
	(2) Intrinsic Prothrombin Activation Pathway	**8.43E-6**	**0.094**
	(3) Protein Kinase A Signalling	**6.31E-4**	**0.023**
	(4) Atherosclerosis Signalling	**1.04E-3**	**0.02**
	(5) Dendritic Cell Maturation	**2.1E-3**	**0.014**
Wt v Het Nuclear ZT 14	(1) Granzyme A Signalling	**3.51E-8**	**0.2**
	(2) Intrinsic Prothrombin Activation Pathway	**1.78E-5**	**0.094**
	(3) Protein Kinase A Signalling	**1.84E-5**	**0.0018**
	(4) Atherosclerosis Signalling	**1.3E-3**	**0.023**
	(5) Hepatic Fibrosis / Hepatic Stellate Cell Activation	**2.12E-3**	**0.02**
Wt v Hom Cytoplasmic ZT 0	(1) CXCR4 Signaling	**7.15E-03**	**0.012**
	(2) Ketolysis	**7.85E-03**	**0.056**
	(3) RhoGDI Singaling	**8.31E-03**	**0.01**
	(4) Ketogenesis	**8.71E-03**	**0.048**
	(5) Glutaryl-CoA Degradation	**9.58E-03**	**0.042**
Wt v Hom Cytoplasmic ZT 14	(1) Pyruvate Metabolism	**2.11E-3**	**0.014**
	(2) Mitochondrial Dysfunction	**7.41E-3**	**0.011**
	(3) Oxidative Phosphorylation	**8.52E-3**	**0.013**
	(4) Synthesis and Degradation of Ketone Bodies	**0.0118**	**0.053**
	(5) Actin Cytoskeleton Signalling	**0.0187**	**0.008**
Wt v Hom Nuclear ZT 0	(1) Endoplasmic Reticulum Stress Pathway	**0.0141**	**0.056**
	(2) DNA Methylation and Transcriptional Repression Signalling	**0.0157**	**0.043**
	(3) One Carbon Pool by Folate	**0.0157**	**0.028**
	(4) Glyoxylate and Dicarboxylate Metabolism	**0.0165**	**0.009**
	(5) Aminophosphonate Metabolism	**0.0188**	**0.018**
Wt v Hom Nuclear ZT 14	(1) Cell Cycle: G2/M DNA Damage Checkpoint Regulation	**8.66E-3**	**0.02**
	(2) Myc Mediated Apoptosis Signalling	**0.0116**	**0.016**
	(3) ERK5 Signalling	**0.0122**	**0.016**
	(4) IGF-1 Signalling	**0.0192**	**0.009**
	(5) 14-3-3-mediated Signalling	**0.0231**	**0.008**

Table 26: Top associated canonical pathways across all SILAC experimental conditions. Oxidative phosphorylation and mitochondrial function canonical pathways are highly represented across SILAC experimental groups suggesting an impact on ATP generation and oxidative stress in mutant cells. Pathways also associated with cell cycle regulation are identified, including check point regulation, mismatch repair and apoptosis. This suggests an impact of mitosis regulation and integrity of transcriptional processes in mutant cells.

4.6. Discussion

This chapter aimed to characterise the molecular role of *Zfhx3* within the context of circadian rhythmic behaviour. The known functions for *Zfhx3* are complex and diverse, as discussed in the Introduction. Although predominantly characterised for its role during development in neurogenesis, its function during adulthood has also been established as an anti-mitotic factor (Ido, et al. 1994; Jung, et al. 2005). There are a number of suggestions from the structure of the transcript, known functions and extrapolation of data from evolutionary conservation, that *Zfhx3* may have the ability to act within the circadian oscillator as a transcriptional regulator. Together with the circadian phenotype of the *Sci* animals, this chapter aimed to investigate the mechanism of *Zfhx3* function with particular focus and relevance to the molecular circadian oscillator.

4.6.1. RNA expression

The *Zfhx3* RNA transcript has been shown to oscillate with a 24 hour period in extra-SCN tissues (Figure 18). The oscillation however is shifted in phase in $Zfhx3^{Sci/+}$ compared to $Zfhx3^{+/+}$ (under a 12:12 LD cycle). This suggests that the mutation in *Zfhx3* results in a miss-regulation of the transcript such that the peak amplitude of expression is phase advanced (or phase delayed). The consequence is that the peak of *Zfhx3* RNA expression, and by implication, the peak of protein expression is mistimed. This may result in downstream targets of *Zfhx3* to be miss-regulated since their peak of expression may be out of synchrony with ZFHX3's activity. As observed in liver, the WT peak of *Zfhx3* RNA expression generally coincides with the peak of *Clock, Bmal1* and *Rev-erb*α. The peak of heterozygous *Zfhx3* RNA expression is shifted to coincide closer to the peak of expression of *Cry1, Cry2, Per1* and *Per2*. It is possible that the peak of ZFHX3 protein expression is also out of phase in heterozygous animals and peaks with the negative limb of the circadian clock

rather than with the positive limb. Co-incidental with this change in timing of peak amplitude of *Zfhx3* in *Zfhx3*$^{Sci/+}$ are effects on *Cry1, Cry2* and *Per1* levels. *Cry2* RNA in the presence of the *Zfhx3*$^{Sci/+}$ has lost robust rhythmicity and perhaps in compensation, *Cry1* has an exaggerated peak of RNA expression. No significant phase shift is observed suggesting that at this time point, when the mutant form of *Zfhx3* is highly expressed, it has a repressive action on *Cry2* transcription or activates *Cry1* transcription. This result may imply that *Zfhx3* regulates or interacts with *Cry1* and/or *Cry2* and that the *Cry* genes are able to compensate for each other. In contrast, the effect of the *Sci* mutation has dampened the peak amplitude of *Per1* RNA although a robust circadian rhythm is still evident. No effect is seen on *Per2*, suggesting that either this effect on *Per1* does not significantly affect protein levels, circadian rhythmicity or PER1 function, or the degree to which *Per2* can compensate for *Per1* is less than that which is observed between *Cry1* and *Cry2*. As discussed in Chapter III, the necessity of *Per1* as a core clock gene may be considered less than that of *Per2*, with more of an involvement in photic entrainment.

Although the effect on *Zfhx3* in *Zfhx3*$^{Sci/+}$ is a phase shift rather than an effect on amplitude, the effect on potential target genes is predominantly an effect on amplitude. This may suggest that *Zfhx3* may form an alternate molecular loop with these proteins that can modulate the expression of clock genes irrespective of CLOCK and BMAL1's transcriptional regulation or acts indirectly on these target clock genes such that the phase shift is not observed downstream. The expression pattern of *Clock* and *Bmal1* is comparable in both the *Zfhx3*$^{+/+}$ and *Zfhx3*$^{Sci/+}$ genetic background and yet effects are still observed on the amplitude of expression of *Cry1, Cry2* and *Per1*. However, it is important to note that these effects on RNA may not necessarily be observed at the protein level, or alternatively they may be more dramatic. The interaction between *Zfhx3* and cryptochromes is discussed in more detail later in this discussion as well as in Chapter V.

The expression of *Zfhx3* RNA was investigated further by *in situ* hybridisation, specifically to determine the expression pattern of *Zfhx3* in the adult SCN. Expression in the adult SCN would further support the hypothesised role of *Zfhx3* as a candidate novel circadian transcription factor. The majority of published data on the expression pattern of *Zfhx3* has focused on expression during development, but little data has shown the expression profile in adult mice. By *in situ* hybridisation, it was shown that *Zfhx3* is expressed almost exclusively in the adult SCN in the adult mouse brain. The qualitative data shows that *Zfhx3* is expressed constitutively across ZT points in both the $Zfhx3^{+/+}$ and $Zfhx3^{Sci/+}$ SCN however it is not possible to conclude whether or not *Zfhx3* oscillates from this data. Further work is required to show if *Zfhx3* oscillates with a circadian period in the SCN, as it does in peripheral tissues. The specific expression of *Zfhx3* in the adult SCN implies a role maintained in adulthood that is unique to SCN function, presumably circadian rhythmicity. Neuronal firing and synchrony however appears normal in SCN slices transduced with a Per2:luciferase reporter. This is a strong indicator that *Zfhx3* acts either within the molecular feedback loop or perhaps in the neural synchrony and integrity of the SCN structure in maintaining normal circadian rhythmicity. Given the effects seen on circadian gene RNA expression in the presence of the $Zfhx3^{Sci/+}$ allele, it is plausible that *Zfhx3* is acting within the core feedback loop and its own gene expression directly impacts on the gene expression of core clock genes.

In situ hybridisation across embryonic time points confirmed the expression of *Zfhx3* from 10.5dpc – 16.5 dpc in the mouse embryo. The expression was shown to be confined almost exclusively to neural tissues, with the highest level of RNA expression in the mid and hind brain. Expression was seen in the developing hypothalamus, thalamus and pre-optic area, consistent with the area of the developing SCN. Other publications have shown that the *Zfhx3* transcript is a transcription factor expressed in the developing SCN (VanDunk, et al. 2011) and therefore it is likely that *Zfhx3*

is involved in the establishment of the SCN as a structure which persists with a role in the adult SCN. The phenotypes observed may therefore be a consequence of developmental alteration in the SCN composition, which is a question that could be addressed through the use of a conditional mutant.

4.6.2. Protein interactions

In an over-expression system, full length *Zfhx3* human cDNA with an epitope tag was co-expressed with full length clock gene constructs in mammalian cell lines. A co-immuno-precipitation screen was performed to identify novel protein interactions between ZFHX3 and clock proteins. A physical protein interaction would indicate a functional role between these proteins and implicate ZFHX3 in the core mechanism of the circadian oscillator. The screen identified four novel protein interactions between ZFHX3 and CRY1, CRY2, PER2 and EPAS1.

Epas1 (Endothelial pas domain protein 1, or *Hif2*α) was initially investigated as a protein interaction partner since it is a basic helix loop helix PAS domain protein with a predicted protein interaction with ZFHX3 (as predicted on www.genecards.org). The super-family of PAS domain proteins broadly function as environmental sensors, providing an adaptive response to environmental stimuli. The most well known PAS domain proteins are the circadian proteins, including PER1-3, CLOCK and BMAL1. As the clock proteins are involved in adaptive sensing such as light detection to regulate the circadian clock, EPAS1 and other hypoxia inducible factor (HIF) proteins are involved in hypoxia sensing (Tian, et al. 1997). Specifically, *Epas1* is a transcription factor involved in the induction of genes regulated by oxygen and its expression is induced when oxygen levels fall. *Epas1* is a paralogue of *Clock* and *Bmal1* and therefore shares to some degree, sequence homology and function. It has also been shown that EPAS1 is able to interact physically with CLOCK and BMAL1 and this raises the possibility of *Epas1* being central to cross-talk between

the circadian clock and the regulation of oxygen homeostasis (Hogenesch, et al. 1998; Maemura, et al. 2000). The protein interaction identified between ZFHX3 and EPAS1 perhaps provides an added link between the circadian clock and hypoxia signalling. ZFHX3 may be an additional "scaffold" between these two processes, enabling a link between oxygen homeostasis and the circadian clock. Importantly, the identification of this protein interaction shows that ZFHX3 is able to bind PAS domain proteins. Although the interacting domain between ZFHX3 and EPAS1 is unknown, it is encouraging that ZFHX3 was predicted and has now been demonstrated to bind to a PAS domain protein, of which this family is central to the molecular circadian oscillator. Furthermore, as will be discussed later, it is interesting to note that the *Zfhx3*$^{Sci/+}$ and *Zfhx3*$^{Sci/Sci}$ mutant MEFs show evidence of oxidative stress as detected by SILAC experiments. *Epas1* knockout mice die at E11.5 dpc due to failures in angiogenesis and metabolism and therefore it is inferred that these knockout animals are unable to adapt to low oxygen levels during development (Tian, et al. 1998). High expression of *Epas1* is detected in the carotid body during embryogenesis and in the adult, further implicating its role in oxygen sensing and control. Taken together, these results suggest a role for *Zfhx3* in oxygen sensing and oxidative stress as well as an interaction with a clock gene paralogue which may suggest further cross-talk and interaction with the molecular circadian clock.

The protein interactions identified between ZFHX3 and CRY1, CRY2 and PER2 provide direct support of a role for ZFHX3 in the central circadian oscillator. Work now ensues to determine how these interactions are affected in the *Sci* mutant and how mechanistically this may result in the short circadian period and other phenotypes observed in the *Sci* animals. Additionally, these novel interactions have been identified in an over-expression approach and now remain to be identified endogenously. It is also not known whether these proteins are in the same phase of expression endogenously within circadian time. With high, regional expression of *Zfhx3* almost

exclusively in the adult SCN, it may be hypothesised that *Zfhx3* has a key role at the site of the core circadian oscillator through these protein interactions. The nature and function of these interactions remain to be determined, which will be facilitated by understanding the nature of the endogenous interaction in the mutant animals. However, it is possible that ZFHX3 is involved in directing CRY and PER proteins toward the CLOCK and BMAL1 complex in order to indirectly regulate transcription. Alternatively, these interactions may be indirect, through the CLOCK and BMAL1 complex at the *Cry* and *Per* promoters. It is known that CLOCK and BMAL1 are sufficient for driving the transcription of *Cry* and *Per*. It is possible therefore that *Zfhx3* acts to enhance or negatively regulate this transcriptional process or plays an additional role within the molecular oscillator that it currently unknown. These results positively support the argument that *Zfhx3* may act as a novel circadian gene, with high expression in the developing and adult SCN, protein interactions with known clock proteins, effects on clock gene RNA expression together with the observed *Sci* phenotype.

4.6.3. Protein expression

To fully determine the mechanism by which ZFHX3 is acting within the circadian clock a reliable antibody is required. RNA expression analysis, by RT-PCR and *in situ* hybridisation, has provided data on the nature of the *Zfhx3* expression pattern, however only assumptions can be made in terms of protein expression from these results. Assuming that the protein expression pattern follows that which has been observed in RNA, ZFHX3 promises to be a strong novel clock protein. On-going attempts have been made to develop and optimise a working antibody to confirm these hypotheses. The aim was to generate an antibody which would allow for immuno-histochemical analyses of protein expression, protein quantification, endogenous protein interactions and chromatin-immunoprecipitaiton (ChIP). Being a transcription factor, experiments such as ChIP

would be informative in identifying whether ZFHX3 interacts with clock gene promoter regions to regulate clock gene transcription. Bioinformatic analyses and preliminary luciferase based assays in an over-expression system have suggested that ZFHX3 may be able to regulate clock gene transcription via AT-like motifs, as previously documented. This may provide an added level of control over clock gene transcription, to create a further robust feedback loop.

Three custom antibodies were generated and trialled with the final antibody generated towards the end of this thesis appearing the most reliable in the detection of ZFHX3. Work continues to purify and validate this antibody and if successful, the aforementioned experimental approaches will be completed. Preliminary data generated using these antibodies confirmed that ZFHX3 is either very weakly expressed or the antibodies may not be able to detect ZFHX3 in adult tissues (as assessed by western blotting). To complete these experiments however, adult SCN tissue needs now to be analysed for ZFHX3 protein expression. ZFHX3 also appears to be highly expressed in embryonic tissue, from E12.5 – 16.5 dpc as well as in neuronal cell lines. The high expression of ZFHX3 in these tissues and cells was expected from previously published data (Jung, et al. 2005) and confirms a developmental role of *Zfhx3* in the mouse embryo.

In parallel, SILAC was used to make a general assessment of the *Sci* proteome whilst antibodies were being generated and optimised. Comparisons of the proteome were made between $Zfhx3^{+/+}$ and $Zfhx3^{Sci/+}$ and $Zfhx3^{+/+}$ and $Zfhx3^{Sci/Sci}$ MEFs. Samples were analysed at two time points, ZT0 and ZT14, in order to make an assessment of whether there were any circadian differences between samples. Although core circadian proteins and ZFHX3 itself were not detected in the mass spectrometry, the proteome analysis provided general insights into the role and function of ZFHX3 and possible reasons towards homozygous lethality in this mouse line.

The analysis readout from Ingenuity Pathway Analysis indicated that predominant pathways, networks and diseases focused on cell cycle and cancer, and oxidative stress and mitochondrial biochemistry. This is consistent with proposed roles of *Zfhx3* in previous publications (Kim, et al. 2010). Numerous proteins involved in mitochondrial function and ATP generation were altered in *Zfhx3*$^{Sci/+}$ and *Zfhx3*$^{Sci/Sci}$ MEFs. One of the proteins identified, peroxiredoxin 6 (PRDX6), was an initial interesting candidate protein to investigate further. It had been recently identified as a conserved marker of circadian rhythms and 24 hour rhythms in peroxiredoxin oxidation have been detected in de-nucleated cells (Edgar, et al. 2012; O'Neill and Reddy 2011; O'Neill, et al. 2011). PRDX6 was up-regulated by 5.249 fold in the *Zfhx3*$^{Sci/+}$ SILAC samples at ZT14 and not at ZT0, confirming the circadian element in its expression in these samples. There was not a significant up-regulation of PRDX6 in the *Zfhx3*$^{Sci/Sci}$ vs *Zfhx3*$^{+/+}$. Further investigation into the relevance of up-regulated PRDX was performed by Dr. John O'Neill (University of Cambridge). The total amount of oxidized PRDX was shown to significantly increase progressively from *Zfhx3*$^{+/+}$ to *Zfhx3*$^{Sci/+}$ to *Zfhx3*$^{Sci/Sci}$ (data not shown). Oxidised PRDX is an indicator of oxidative stress; when peroxide is reduced, the active site of peroxiredoxin is oxidised (Immenschuh and Baumgart-Vogt 2005). Therefore, it is possible to suggest that the mutant MEFs, both *Zfhx3*$^{Sci/+}$ and *Zfhx3*$^{Sci/Sci}$ are experiencing greater oxidative stress compared to *Zfhx3*$^{+/+}$. This may be a contributory or indicative factor of homozygous lethality in *Sci* and as discussed earlier may support a role for *Zfhx3* in the cross talk between the circadian clock and oxygen sensing, perhaps through its interaction with EPAS1.

Another interesting candidate identified through the SILAC was cellular retinoic acid binding protein 1 (CRABP1). CRABP1 was up-regulated in the cytoplasm of *Zfhx3*$^{Sci/+}$ MEFs at both time points investigated, by 2.81 and 3.35 respectively. Interestingly there was again no significant fold change in *Zfhx3*$^{Sci/Sci}$ vs *Zfhx3*$^{+/+}$ MEFs (0.7 fold) but this requires validation by western blotting.

CRABP1 is a vitamin A family member with known roles in retinoic acid mediated differentiation and proliferation (Maden 2007). Aberrant retinoic acid signalling may lead to un-controlled differentiation and proliferation and correlations have been shown between key retinoic acid signalling molecules (including CRABP1) and tumour proliferation (Crowe, et al. 2003; Uhrig, et al. 2008). Similarly, heart-type fatty acid binding protein (FABP3), also involved in retinoic acid signalling as a retinoid carrier protein (Haunerland and Spener 2004), was also found up-regulated (6.2 and 1.8 fold) in *Zfhx3*$^{Sci/+}$ vs *Zfhx3*$^{+/+}$ MEFs at ZT 14 and ZT0. FABP3 is also implicated as a candidate tumour suppressor gene for breast cancer (Haunerland and Spener 2004)..

Overall, a number of proteins implicated in energy production, mitochondrial signalling pathways and retinoic acid signalling have been detected as differentially expressed between the *Zfhx3*$^{Sci/Sci}$, *Zfhx3*$^{Sci/+}$ and *Zfhx3*$^{+/+}$ MEFs. Many of these proteins, including those discussed, also have roles within cellular proliferation and apoptosis and are therefore implicated in diseases such as cancer. Cancer was one of the top diseases identified through the Ingenuity Pathway Analysis, and is again consistent with the known role of *Zfhx3* as an anti-mitotic factor.

Further validation of these preliminary results is now required, with target proteins showing altered levels to be assessed by western blotting. However, a recent model has been hypothesised for a signalling pathway from ataxia telangiectasia mutated (ATM) to ZFHX3 for the expression of beta-type platelet-derived growth factor receptor (PDGFRB) that is required for the activation of ATM in response to oxidative stress in the cytoplasm (Kim, et al. 2010). This model appears to tie together the three components identified in this SILAC experiment: retinoic acid signaling, oxidative stress and DNA damage and checkpoint control via ATM signaling. This model is shown in Figure 33 below and matches the SILAC results.

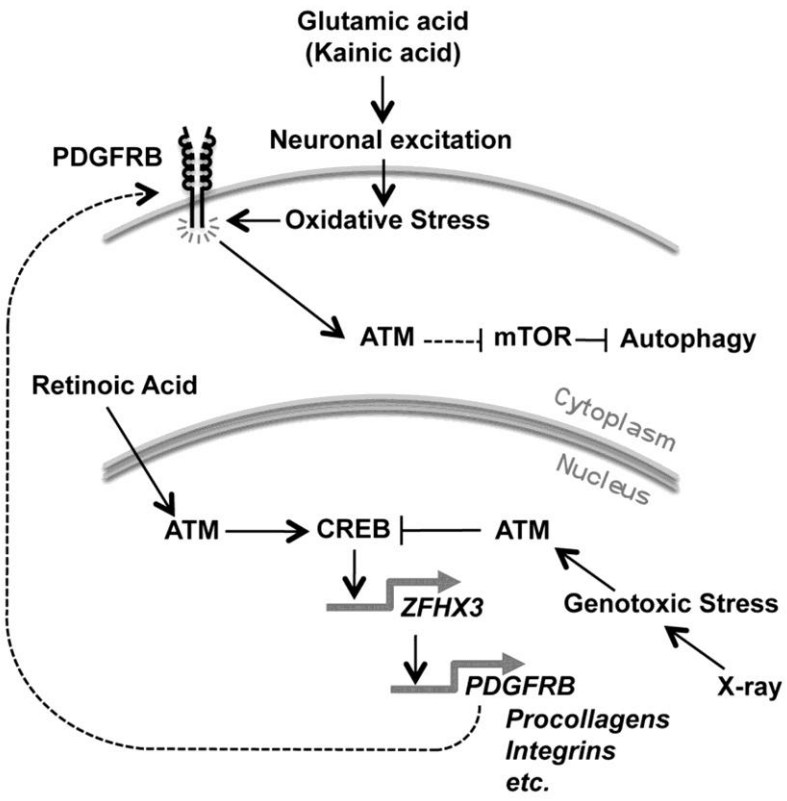

(Kim, et al. 2010).

Figure 33: A model of a signalling pathway from ATM to ZFHX3 required for activation of ATM in response to oxidative stress. Retinoic acid activation of ATM kinase results in the phosphorylation of CREB at Ser133 for the activation of target genes. CREB induces *Zfhx3* expression by binding to CRE (5′-TGACGTCA-3′) in the ZFHX3 (neuron-specific) promoter located 5.5 kb upstream from the initiation site of ZFHX3 transcription. ZFHX3 activates genes for cell adhesion molecules (procollagens, integrins) and PDGFRB for the survival of neurons. By contrast, X-ray irradiation induces activation of ATM at the foci of DNA double strand breaks and this genotoxic stress results in extra phosphorylation of CREB at Thr100, Ser111, Ser121 and causes a decrease in trans-activation potential (Shi et al., 2004). The activation of ATM in the cytoplasm in response to oxidative stress relays signals from PDGFRB to LKB1, AMPK, TSC2 and mTOR to maintain homeostasis of organelles by activating autophagy (Alexander et al., 2010).

4.6.4. Conclusions

The *Zfhx3* transcript is complex, with the potential to bind numerous DNA and amino acid sequences to exert control over gene and protein function. Additionally, the physical size of ZFHX3 may be influential to its function. For example, ZFHX3 may be able to mask E-box or other gene regulatory elements through DNA binding and in this way indirectly modify the molecular oscillator. Whether ZFHX3 is acting predominantly as a transcription factor, perhaps to fine tune to role of CLOCK and BMAL1 or whether it is acting as a scaffold protein, holding protein complexes together for their function, remains to be determined. This may be supported from the data given that ZFHX3 is able to interact with CRY1, CRY2 and PER2. It will be of importance to determine whether it is interacting with these proteins as a complex or individually at different stages of the circadian cycle.

Taking together all the data presented in this chapter, there may be a link between *Zfhx3's* identified role within the molecular circadian clock and its role within the cell cycle, retinoic acid signalling and oxidative stress. Identified from the SILAC experiments, DNA replication and repair and checkpoint control networks and consequently disease states such as cancer have been highly implicated from the *Sci* mutant MEF samples. Together with the *Sci* circadian phenotype, it may be possible to tie together the predominant and characterised role of *Zfhx3* as a tumour suppressor together with this proposed new function within the circadian clock. DNA damage and the impact on the circadian clock is a field of study that is rapidly expanding. DNA damage is known to be a resetting cue on the circadian oscillator but the connection between the circadian clock and the cell cycle is still generally unknown.

The results from this chapter strongly support that *Zfhx3* is a novel gene involved in regulating the circadian clock either directly through protein interactions with CRY1, CRY2 and PER2 or through

genetic interactions and transcriptional control. Additionally, ZFHX3 may be the interface between cell cycle regulation and coordination with the circadian clock through these novel interacting partners. The exact mechanism for *Zfhx3's* function however is yet to be determined and numerous hypotheses may be made regarding its action. The development of new tools such as a ZFHX3 antibody, and even other mutants such as conditional knockout mice, will help facilitate answering these questions.

Chapter V

Results III

Sci^{Zfhx3} Genetic Interaction with Cryptochromes

5. *Zfhx3* interaction with cryptochromes

5.1. Introduction

An important genetic tool to further elucidate gene function is to be able to generate double or triple mutants. This allows for genetic dominance, epistasis and additive effects to be determined. Different mutant strains with well characterised phenotypes may be inter-crossed and the progeny analysed for the interactive effects of the multiple mutations, both phenotypically and genetically. Epistasis experiments such as these allow for genes to be ordered within a given pathway and for genetic interactions to be identified. The availability of well characterised circadian mouse mutants allows for these experiments to be performed such that the role of newly identified genes may be positioned within the molecular pathway of the circadian oscillator and any interactive or additive effects identified. The work presented in this chapter has used this approach by generating *Sci ; Cry1* and *Sci ; Cry2* double mutants to investigate further the role *Zfhx3* may play in the genetic and molecular basis of the circadian clock.

Several lines of evidence from the *Sci* mutant suggest that *Zfhx3* may interact with cryptochromes, either physically or genetically. Firstly, bioinformatic analyses of the *Cry1* and *Cry2* promoters have shown that a motif highly homologous to the AT binding motif, to which *Zfhx3* is predicted to bind, is present within the *Cry1* promoter. Therefore it may be hypothesised that *Zfhx3* is able to interact with and control the transcription of *Cry1* in this way. Secondly, protein-protein interaction studies have indicated that ZFHX3 is able to physically interact with CRY1 and CRY2 in an over-expression system, as previously discussed (4.3). Finally, differential effects on *Cry1* and *Cry2* RNA expression have been observed in *Sci* tissues suggesting that *Zfhx3* is involved in cryptochrome transcription and the *Sci* mutation impairs this function (4.2.1). With these

considerations, *Zfhx3*$^{Sci/+}$ *; Cry1*$^{-/-}$ and *Zfhx3*$^{Sci/+}$ *; Cry2*$^{-/-}$ double mutants were generated in order to assess whether an interaction could be observed at the behavioural level. *Cry1*$^{-/-}$ and *Cry2*$^{-/-}$ knock-out (KO) mice were made available by Gijsbertus T. J. van der Horst (van der Horst, et al. 1999).

Both the *Cry1*$^{-/-}$ and *Cry2*$^{-/-}$ KOs have well defined measurable circadian phenotypes; *Cry1*$^{-/-}$ a significant period shortening and *Cry2*$^{-/-}$ a significant period lengthening in DD. As such, the effect of the *Sci* mutation on the *Cry* mutant phenotype could be readily assessed using wheel-running analysis. It is known that the *Cry1*$^{+/-}$ and *Cry2*$^{+/-}$ heterozygous animals show comparable wheel running activity to wild type animals, with no sex differences presented. Therefore, the aim was to generate *Zfhx3*$^{Sci/+}$ *; Cry*$^{-/-}$ heterozygous-KO mutants and to phenotype both sexes.

5.2. Generation of *Zfhx3 ; Cry1* and *Zfhx3 ; Cry2* Double Mutants

Zfhx3$^{Sci/+}$ mutants were crossed to *Cry1*$^{-/-}$ and *Cry2*$^{-/-}$ homozygous KO animals. The *Sci* mutants were bred on a mixed C3H/C57B/6J F1 background in order to maintain viable breeding within the line. The *Cry1* and *Cry2* KO animals were on a congenic C57B/6J background. Due to a mixed back-ground being used in these crosses, only litter-mate controls were used for phenotypic comparisons. The increased contribution of C57B/6J to the genetic background of the *Zfhx3*-*Cry* double mutants affected mating and offspring viability, but was genotype independent in relation to the presence of the *Cry1* and *Cry2* mutant allele. As such, double mutants of *Zfhx3*$^{Sci/+}$ *; Cry1* $^{-/-}$ and *Zfhx3*$^{Sci/+}$ *; Cry2* $^{-/-}$ could be obtained. The breeding schemes used for generating *Sci ; Cry1* mutants is shown in the Punnett diagrams below (Table 27, Table 28, Table 29) assuming Mendelian inheritance. The equivalent matings were set up for *Zfhx3 ; Cry2* mutants. Since *Zfhx3*$^{Sci/Sci}$ animals are embryonic lethal, it was not expected to obtain any *Zfhx3*$^{Sci/Sci}$ *; Cry*$^{-/-}$ double mutants at post natal day 1 (P1).

1. Original Outcross 1

Genotype 1
Zfhx3 $^{Sci/+}$ ***; Cry1*** $^{+/+}$

Genotype 2
Zfhx3 $^{+/+}$ ***; Cry1*** $^{-/-}$

	Zfhx3 ^{Sci} ***Cry1*** $^{+}$	***Zfhx3*** ^{Sci} ***Cry1*** $^{+}$	***Zfhx3*** ^{Sci} ***Cry1*** $^{+}$	***Zfhx3*** ^{Sci} ***Cry1*** $^{+}$
Zfhx3 $^{+}$ ***Cry1*** $^{-}$	***Zfhx3*** $^{Sci/+}$ ***Cry1*** $^{+/-}$	***Zfhx3*** $^{Sci/+}$ ***Cry1*** $^{+/-}$	*Zfhx3* $^{+/+}$ *Cry1* $^{+/-}$	*Zfhx3* $^{+/+}$ *Cry1* $^{+/-}$
Zfhx3 $^{+}$ ***Cry1*** $^{-}$	***Zfhx3*** $^{Sci/+}$ ***Cry1*** $^{+/-}$	***Zfhx3*** $^{Sci/+}$ ***Cry1*** $^{+/-}$	*Zfhx3* $^{+/+}$ *Cry1* $^{+/-}$	*Zfhx3* $^{+/+}$ *Cry1* $^{+/-}$
Zfhx3 $^{+}$ ***Cry1*** $^{-}$	***Zfhx3*** $^{Sci/+}$ ***Cry1*** $^{+/-}$	***Zfhx3*** $^{Sci/+}$ ***Cry1*** $^{+/-}$	*Zfhx3* $^{+/+}$ *Cry1* $^{+/-}$	*Zfhx3* $^{+/+}$ *Cry1* $^{+/-}$
Zfhx3 $^{+}$ ***Cry1*** $^{-}$	***Zfhx3*** $^{Sci/+}$ ***Cry1*** $^{+/-}$	***Zfhx3*** $^{Sci/+}$ ***Cry1*** $^{+/-}$	*Zfhx3* $^{+/+}$ *Cry1* $^{+/-}$	*Zfhx3* $^{+/+}$ *Cry1* $^{+/-}$

Genotype	Probability
Zfhx3 $^{Sci/+}$; *Cry1* $^{+/-}$	50.00%
Zfhx3 $^{+/+}$; *Cry1* $^{+/-}$	50.00%

Table 27: Punnett square cross for *Zfhx3 ; Cry1* original outcross. Genetic outcomes from out-crossing the *Zfhx3* $^{Sci/+}$ mutant to *Cry1* $^{-/-}$ knockout mice. The equivalent cross was performed for generating *Zfhx3 ; Cry2* double mutant animals and the expected outcomes are shown. 50% animals from the original outcross were expected to be double heterozygotes which could then be used to generate *Zfhx3* $^{Sci/+}$ *; Cry* $^{-/-}$ animals.

2. Double heterozygous intercross from Outcross 1 (Option 1)

Genotype 1

Zfhx3 $^{Sci/+}$; Cry1 $^{-/+}$

Genotype 2 ***Zfhx3 $^{Sci/+}$; Cry1 $^{-/+}$***	***Zfhx3 ^{Sci} Cry1 $^{-}$***	***Zfhx3 ^{Sci} Cry1 $^{+}$***	***Zfhx3 $^{+}$ Cry1 $^{-}$***	***Zfhx3 $^{+}$ Cry1 $^{+}$***
Zfhx3 ^{Sci} Cry1 $^{-}$	*Zfhx3 $^{Sci/Sci}$ Cry1 $^{-/-}$*	*Zfhx3 $^{Sci/Sci}$ Cry1 $^{+/-}$*	***Zfhx3 $^{Sci/+}$ Cry1 $^{-/-}$***	*Zfhx3 $^{Sci/+}$ Cry1 $^{+/-}$*
Zfhx3 ^{Sci} Cry1 $^{+}$	*Zfhx3 $^{Sci/Sci}$ Cry1 $^{-/-}$*	*Zfhx3 $^{Sci/Sci}$ Cry1 $^{+/+}$*	*Zfhx3 $^{Sci/+}$ Cry1 $^{-/+}$*	*Zfhx3 $^{Sci/+}$ Cry1 $^{+/+}$*
Zfhx3 $^{+}$ Cry1 $^{-}$	***Zfhx3 $^{Sci/+}$ Cry1 $^{-/-}$***	*Zfhx3 $^{Sci/+}$ Cry1 $^{+/-}$*	*Zfhx3 $^{+/+}$ Cry1 $^{-/-}$*	*Zfhx3 $^{+/+}$ Cry1 $^{+/-}$*
Zfhx3 $^{+}$ Cry1 $^{+}$	*Zfhx3 $^{Sci/+}$ Cry1 $^{+/-}$*	*Zfhx3 $^{Sci/+}$ Cry1 $^{+/+}$*	*Zfhx3 $^{+/+}$ Cry1 $^{-/+}$*	*Zfhx3i $^{+/+}$ Cry1 $^{+/+}$*

	Genotype	Probability
*	*Zfhx3 $^{Sci/Sci}$; Cry1 $^{-/-}$*	6.25%
*	*Zfhx3 $^{Sci/Sci}$; Cry1 $^{+/-}$*	12.50%
	Zfhx3 $^{Sci/+}$; Cry1 $^{-/-}$	12.50%
	Zfhx3 $^{Sci/+}$; Cry1 $^{+/-}$	25.00%
*	*Zfhx3 $^{Sci/Sci}$; Cry1 $^{+/+}$*	6.25%
	Zfhx3 $^{Sci/+}$; Cry1 $^{+/+}$	12.50%
	Zfhx3 $^{+/+}$; Cry1 $^{-/-}$	6.25%
	Zfhx3 $^{+/+}$; Cry1 $^{+/-}$	12.50%
	Zfhx3 $^{+/+}$; Cry1 $^{+/+}$	6.25%

* *Homozygous lethal*

Table 28: Punnett square cross for *Zfhx3 ; Cry1* double heterozygote intercross. One method by which *Zfhx3 $^{Sci/+}$; Cry1 $^{-/-}$* or *Cry2 $^{-/-}$* double mutants were generated was to intercross double heterozygote animals from the original outcross. The expected frequency of obtaining these animals was 1 in 8 or 12.5%.

3. Double heterozygote (from Outcross 1) backcross to homozygous Cry founder (Option 2)

Genotype 1

Zfhx3 $^{Sci/+}$ **; *Cry1*** $^{-/+}$

Genotype 2: *Zfhx3* $^{+/+}$; *Cry1* $^{-/-}$	***Zfhx3*** ^{Sci} ***Cry1*** $^{-}$	***Zfhx3*** ^{Sci} ***Cry1*** $^{+}$	***Zfhx3*** $^{+}$ ***Cry1*** $^{-}$	***Zfhx3*** $^{+}$ ***Cry1*** $^{+}$
Zfhx3 $^{+}$ ***Cry1*** $^{-}$	***Zfhx3*** $^{Sci/+}$ ***Cry1*** $^{-/-}$	*Zfhx3* $^{Sci/+}$ *Cry1* $^{+/-}$	*Zfhx3* $^{+/+}$ *Cry1* $^{-/-}$	*Zfhx3* $^{+/+}$ *Cry1* $^{+/-}$
Zfhx3 $^{+}$ ***Cry1*** $^{-}$	***Zfhx3*** $^{Sci/+}$ ***Cry1*** $^{-/-}$	*Zfhx3* $^{Sci/+}$ *Cry1* $^{+/-}$	*Zfhx3* $^{+/+}$ *Cry1* $^{-/-}$	*Zfhx3* $^{+/+}$ *Cry1* $^{+/-}$
Zfhx3 $^{+}$ ***Cry1*** $^{-}$	***Zfhx3*** $^{Sci/+}$ ***Cry1*** $^{-/-}$	*Zfhx3* $^{Sci/+}$ *Cry1* $^{+/-}$	*Zfhx3* $^{+/+}$ *Cry1* $^{-/-}$	*Zfhx3* $^{+/+}$ *Cry1* $^{+/-}$
Zfhx3 $^{+}$ ***Cry1*** $^{-}$	***Zfhx3*** $^{Sci/+}$ ***Cry1*** $^{-/-}$	*Zfhx3* $^{Sci/+}$ *Cry1* $^{+/-}$	*Zfhx3* $^{+/+}$ *Cry1* $^{-/-}$	*Zfhx3* $^{+/+}$ *Cry1* $^{+/-}$

Genotype	Probability
Zfhx3 $^{Sci/+}$, *Cry1* $^{-/-}$	25.00%
Zfhx3 $^{Sci/+}$, *Cry1* $^{+/-}$	25.00%
Zfhx3 $^{+/+}$, *Cry1* $^{-/-}$	25.00%
Zfhx3 $^{+/+}$, *Cry1* $^{+/-}$	25.00%

Table 29: Punnett square cross for *Zfhx3 ; Cry1* double heterozygote backcross to homozygous *Cry*$^{-/-}$ knock-out. Double heterozygote animals from original outcross 1 were backcrossed to a homozygote *Cry1* or *Cry2* animal or back to the founder *Cry* knockout animal. The frequency of obtaining the required *Zfhx3*$^{Sci/+}$ *; Cry1* $^{-/-}$ double mutants was 1 in 4, or 25%, however appropriate controls could not all be obtained from this cross as they could be from option 1.

The following numbers of double mutants (shown in Table 30) for each line were obtained for circadian wheel running phenotyping and statistical analysis:

Genotype	n	Genotype	n
***Zfhx3*$^{+/+}$ - *Cry1*$^{+/+}$**	17	***Zfhx3*$^{+/+}$ - *Cry2*$^{+/+}$**	17
***Zfhx3*$^{+/+}$ - *Cry1*$^{-/-}$**	10	***Zfhx3*$^{+/+}$ - *Cry2*$^{-/-}$**	8
***Zfhx3*$^{Sci/+}$- *Cry1*$^{+/+}$**	13	***Zfhx3*$^{Sci/+}$- *Cry2*$^{+/+}$**	13
***Zfhx3*$^{Sci/+}$- *Cry1*$^{-/-}$**	15	***Zfhx3*$^{Sci/+}$- *Cry2*$^{-/-}$**	13

Table 30: Total number of double mutant animals and litter mate controls obtained from *Sci ; Cry* crosses. The total number of animals were screened for circadian phenotypes to assess the modificatory effect of the *Sci* mutant allele on the *Cry1*$^{-/-}$ and *Cry2*$^{-/-}$ phenotype. Both sexes (at an approximately equal ratio) were included.

5.3. *Zfhx3 ; Cry1* Circadian Phenotype in Constant Darkness

Following double mutant generation, all animals were subjected to the same circadian wheel running protocol. No distinction was made between sexes and animals were aged between 2 – 6 months of age when phenotyped. Animals were first subjected to a 12:12 light-dark cycle. Animals then spent 14 days in constant darkness (DD) and 14 days in constant light (LL). Actograms were analysed using MatLab as previously described, with period calculations made under constant dark conditions and an assessment made regarding behaviour under light conditions (during entrainment and LL). Only litter mate control animals were used for comparative analysis. Representative actograms for *Zfhx3 ; Cry1* mutant animals are shown in the panel below (Figure 34).

***Zfhx3*$^{+/+}$; *Cry1*$^{+/+}$**

τDD = 23.21 hours

τLL = 25.20 hours

***Zfhx3*$^{+/+}$; *Cry1*$^{-/-}$**

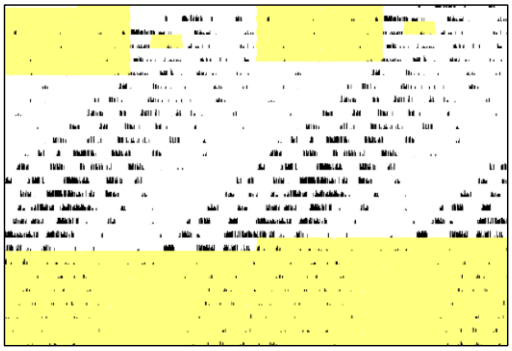

τDD = 22.45 hours

τLL = 23.96 hours

***Zfhx3*$^{Sci/+}$; *Cry1*$^{+/+}$**

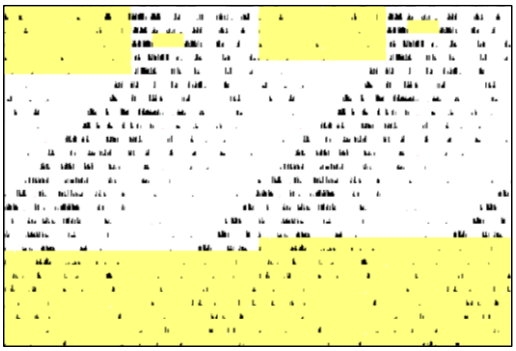

τDD = 22.75 hours

τLL = split / low amplitude

***Zfhx3*$^{Sci/+}$; *Cry1*$^{-/-}$**

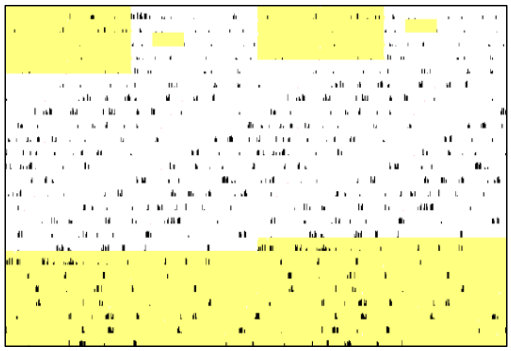

τDD = 21.51 hours

τLL = split / low amplitude

Figure 34: Representative actograms depicting the circadian phenotypes of *Zfhx3 ; Cry1* double mutants. In comparison to WT animals, *Cry1*$^{-/-}$ and *Zfhx3*$^{Sci/+}$ animals both individually had a short period under DD. The *Cry1*$^{-/-}$ DD phenotype is more severe than the *Zfhx3*$^{Sci/+}$ DD phenotype. The combination of the two short-period mutant alleles results in an even shorter period in DD.

A primary assessment of the period length under constant darkness was made on *Zfhx3 ; Cry1* mutant animals. Table 31 indicates the calculated τDD for each *Zfhx3 ; Cry1* animal that was assessed by wheel running circadian screens and is representative graphically in Figure 35.

Period length in hours under constant darkness (τDD) for all *Zfhx3 – Cry1* animals

***Zfhx3*$^{+/+}$ - *Cry1*$^{+/+}$** wt - wt	***Zfhx3*$^{+/+}$ - *Cry1*$^{-/-}$** wt - ko	***Zfhx3*$^{Sci/+}$- *Cry1*$^{+/+}$** het - wt	***Zfhx3*$^{Sci/+}$- *Cry1*$^{-/-}$** het - ko
23.49	22.45	22.98	21.87
23.28	22.47	21.94	22.37
23.28	22.47	22.79	22
23.68	22.47	22.97	21.92
23.51	22.26	22.95	21.61
23.48	22.54	23.46	21.67
23.27	22.52	23.23	22.14
23.63	22.64	23.28	21.67
23.31	23.55	23.16	arrhythmic
23.27	22.61	23.16	arrhythmic
23.56		23.17	21.56
23.55		22.83	22.46
23.37		23.5	21.15
23.35			arrhythmic
23.37			22.24
23.51			
23.16			

n	17	10	13	15
AVERAGE	23.42	22.60	23.03	21.89
STERR	0.04	0.11	0.11	0.11

Table 31: Period length (hours) recorded for all *Zfhx3 ; Cry1* animals analysed by monitoring wheel running activity. Period length calculations were taken using ClockLab software. The gradient of activity was taken from the 2nd full day in DD following entrainment.

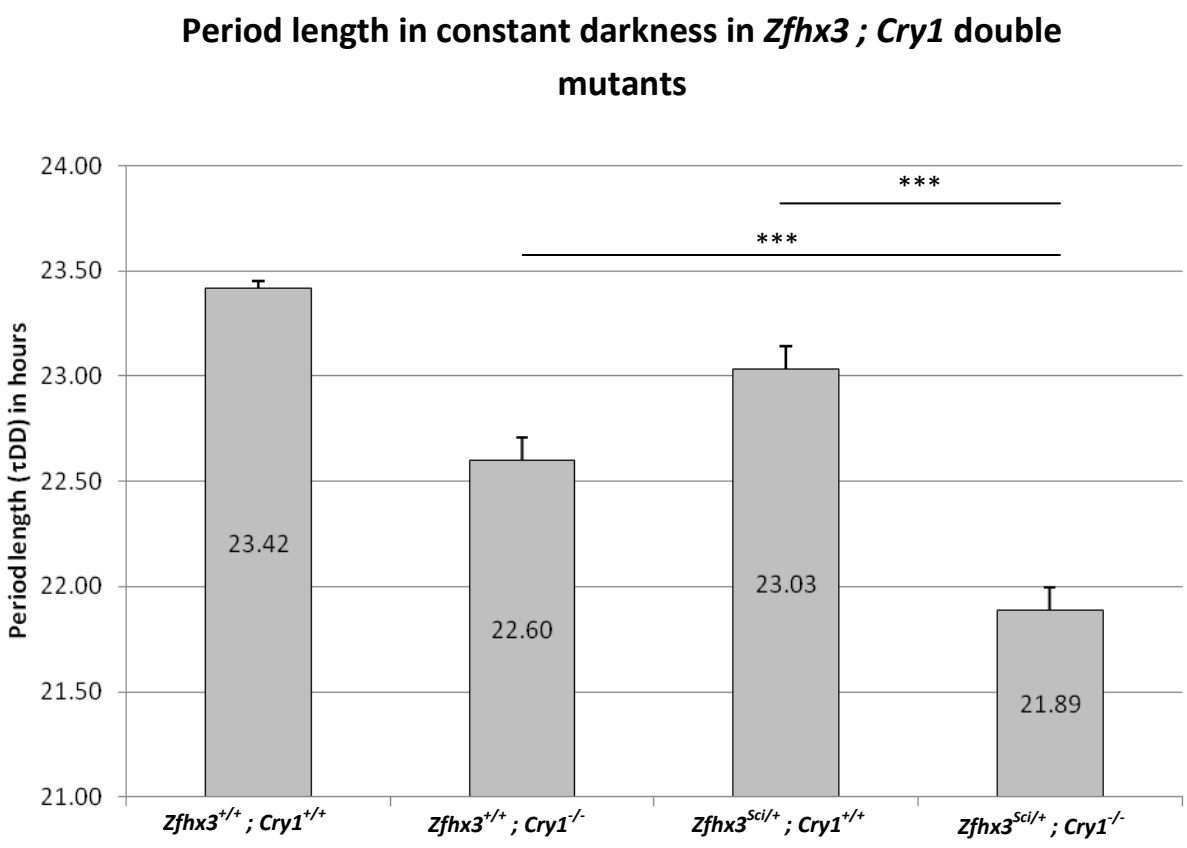

Figure 35: Graphical representation of the period length in constant darkness for *Zfhx3 ; Cry1* mutants. *Cry1*$^{-/-}$ animals have a significantly short period under constant darkness compared to WT animals (22.60 hours). *Zfhx3*$^{Sci/+}$ animals have a significantly short period compared to wild type animals (23.03 hours), but are significantly longer in their intrinsic period compared to *Cry1*$^{-/-}$ mutants. The combination of the two mutant alleles, *Zfhx3*$^{Sci/+}$ *; Cry1* $^{-/-}$, results in a further shortening of the period (21.89 hours). This period is significantly shorter than observed in each individual mutant (T TEST $p < 0.000$ ***).

Cry1$^{-/-}$ and *Zfhx3*$^{Sci/+}$ individually result in a significant shortening of the period in DD compared to wild type litter mates ($p < 0.000$). However, the addition of the *Sci* allele onto the *Cry1*$^{-/-}$ background does not abolish circadian rhythmicity under constant darkness. A significant shortening to τDD 21.89 hours (2-tail T TEST $p<0.000$) was observed in the *Zfhx3*$^{Sci/+}$ *; Cry1*$^{-/-}$ mutant when compared to each other genotype, however this appears to be the additive effect of

the two short period phenotypes (F (1,48) = 3.268, $p < 0.05$, Sci*Cry1 p = 0.077 (n.s)). The statistical analysis is shown in Table 32.

Tests of Between-Subjects Effects

Dependent Variable:scicry1_period

Source	Type III Sum of Squares	df	Mean Square	F	Sig. (p-value)
Corrected Model	17.526[a]	3	5.842	57.292	.000
Intercept	25915.410	1	25915.410	254146.921	.000
sci	3.746	1	3.746	36.733	.000
cry1	12.062	1	12.062	118.294	.000
sci * cry1	.333	1	.333	3.268	**.077**
Error	4.895	48	.102		
Total	27078.274	52			
Corrected Total	22.421	51			

a. R Squared = .782 (Adjusted R Squared = .768)

Table 32: 2 way ANOVA to test for an interaction between *Zfhx3* and *Cry1* based upon τDD. The test statistic, Sci*Cry1 describes the interaction between the $Zfhx3^{Sci/+}$ and $Cry1^{-/-}$ genotypes. The interaction is not significant (p = 0.07) and therefore there is no statistically significant genetic interaction between these two genotypes based upon wheel running activity under constant darkness. The model however, is highly significant, with both *Zfhx3* and *Cry1* having a significantly different τ DD from each other and wild-type ($p < 0.000$ for both).

5.4. *Sci ; Cry1* Circadian Phenotype in Constant Light

Following an assessment of circadian period under constant dark conditions, animals were exposed to 14 days of LL at 100 lux. Behavioural observations under LL were divided up into four main categories: lengthen, split, arrhythmic and low activity. Representative actograms of each type of LL behaviour are shown in Figure 36.

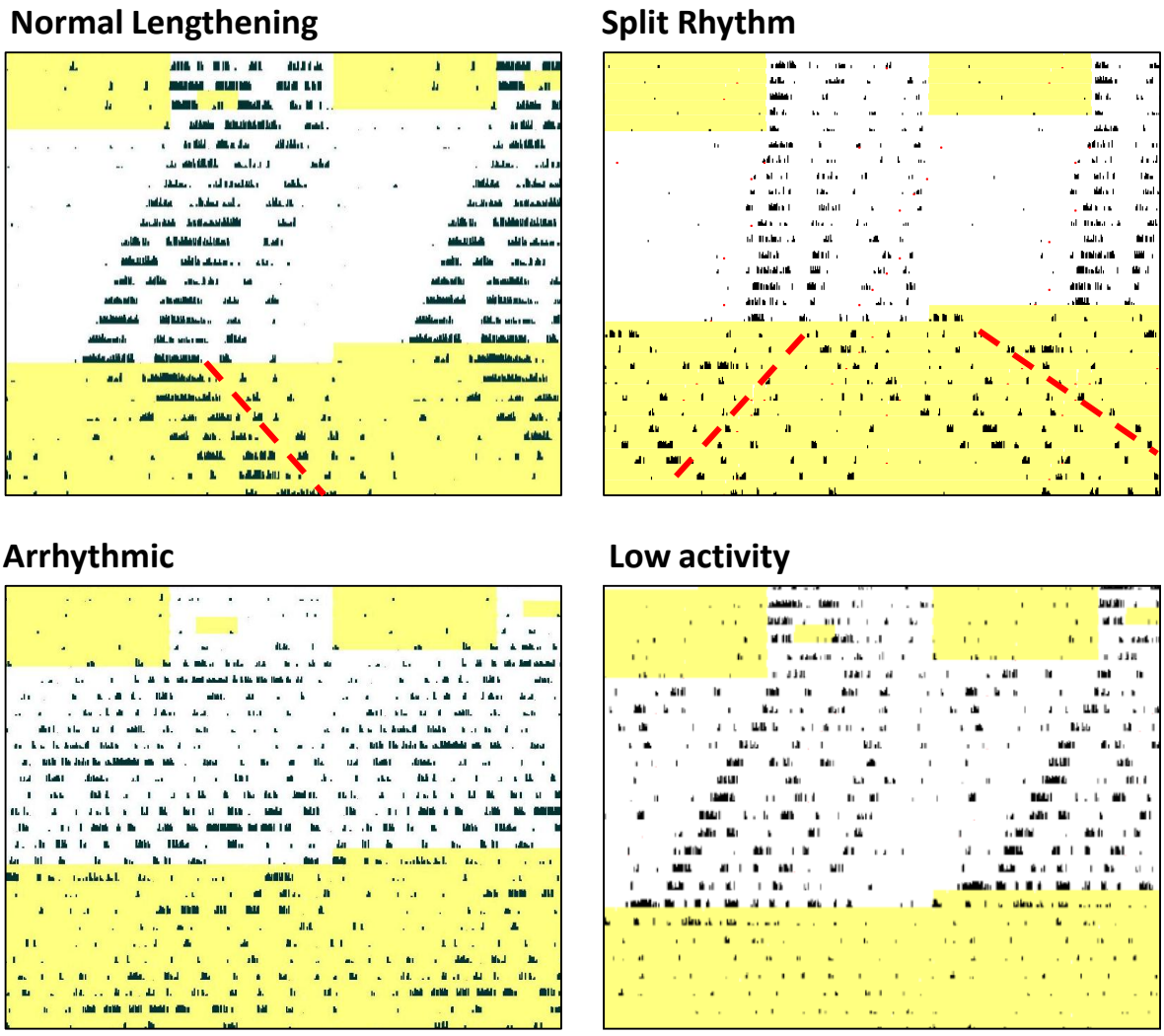

Figure 36: Representative actograms illustrating various behaviours under constant light conditions. The four actograms depict the range of behaviours detected in the *Zfhx3 ; Cry* mutants. Lengthening of the period under constant light is expected in WT animals. Abnormal phenotypes include splitting of the circadian rhythm into two components, arrhythmic behaviour (loss of circadian rhythmicity) and low activity when under constant light.

The percentage of animals expressing each of the four phenotypes was calculated and the data are shown in Table 33 and Figure 37. The phenomenon of "Aschoff's rule" (1960) describes how in addition to the timing of the light exposure, the intensity of light can also modulate cycling periods when organisms are left in constant light. Exposure to brighter light intensities can lengthen the period in some species. Rodents are expected to lengthen their period under

constant light conditions, as per Aschoff's rule. After time, animals will become arrhythmic; however can maintain a constant period for at least 14 days. In the *Zfhx3 ; Cry1* mutants, all wild-type animals exhibited normal lengthening. The majority of *Cry1*$^{-/-}$ animals (80%) *Zfhx3*$^{Sci/+}$ animals (69%) maintained a normal period lengthening. Less than half of the double mutants, *Zfhx3*$^{Sci/+}$ - *Cry1*$^{-/-}$, however had normal period lengthening, 43%, and 50% animals were arrhythmic in LL. This deterioration in the phenotype suggests a possible interaction between *Zfhx3* and *Cry1* under light conditions and the requirement of these two alleles in light-dependent circadian rhythmicity. However, a significant proportion of the double mutants did maintain normal period lengthening; therefore there may be a penetrance effect of the mutant alleles on this phenotype.

	***Zfhx3*$^{+/+}$ *; Cry1*$^{+/+}$** wt-wt	***Zfhx3*$^{+/+}$ *; Cry1*$^{-/-}$** wt-ko	***Zfhx3*$^{Sci/+}$*; Cry1*$^{+/+}$** het-wt	***Zfhx3*$^{Sci/+}$*; Cry1*$^{-/-}$** het-ko
% Lengthen	100	80	69.23	42.86
% Split	0	10	7.69	0
% Arrhythmic	0	10	7.69	50
% Low activity	0	0	15.38	7.14

Table 33: Distribution of behaviours under constant light in *Sci ; Cry1* mutants. The expected activity under constant light conditions is period lengthening, as per Aschoff's rule. This was observed in 100% of all wild type animals examined in this cohort. For *Cry1*$^{-/-}$ animals, 80% maintain normal period lengthening and for *Zfhx3*$^{Sci/+}$ animals, 69%. Less than half, 42.86%, of the *Zfhx3*$^{Sci/+}$*; Cry1*$^{-/-}$ double mutants lengthened their period, and 50%, were arrhythmic.

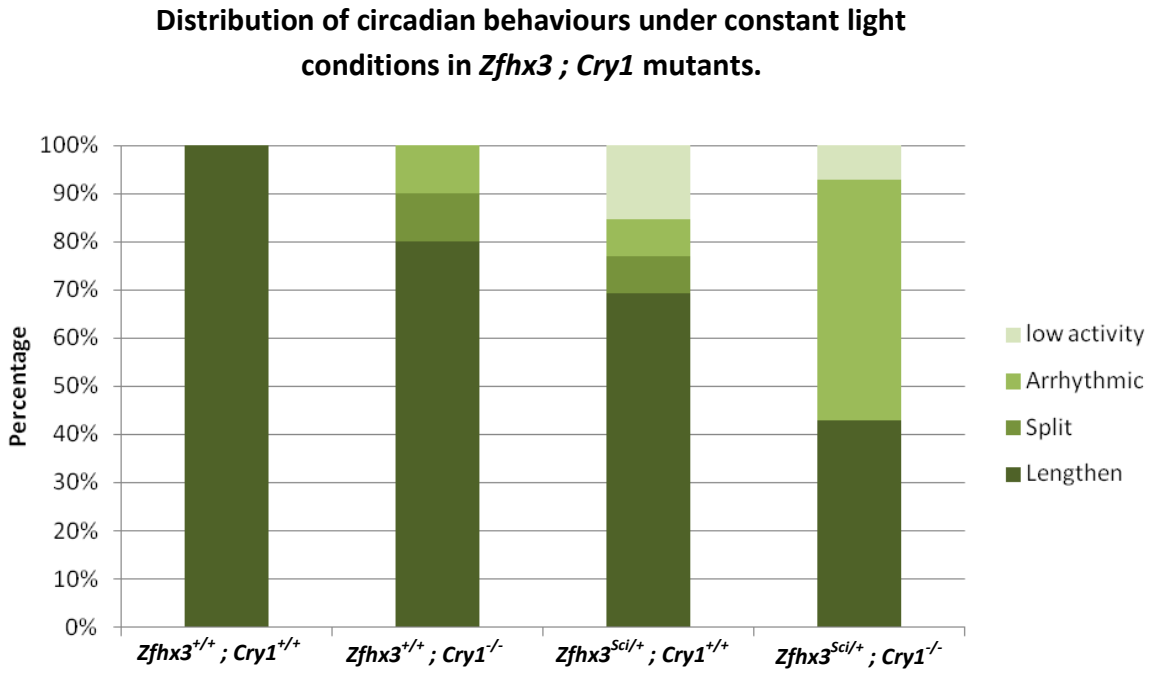

Figure 37: Bar chart of behaviours exhibited by *Zfhx3 ; Cry1* mutants under constant light conditions. Each mutant alone resulted in a proportion of the population exhibiting behaviour that deviates from normal lengthening. However, for both *Cry1*$^{-/-}$ and *Zfhx3*$^{Sci/+}$ mutants, the majority of animals maintained normal circadian lengthening in LL. In the *Zfhx3*$^{Sci/+}$; *Cry1*$^{-/-}$ double mutants, the dominant single behaviour exhibited was arrhythmic activity, seen in 50% animals. This suggests a more severe deterioration of circadian rhythmicity compared to each individual mutant.

5.5. *Zfhx3 ; Cry2* Circadian Phenotype in Constant Dark

All animals were subjected to the same circadian wheel running protocol as the *Zfhx3 ; Cry1* mutants. As before, no distinction was made between sexes and animals were aged between 2 – 6 months of age when phenotyped. Animals were first subjected to a 12:12 light-dark cycle, then 14 days in DD and up to 14 days in LL. Representative actograms for *Zfhx3 ; Cry2* mutant animals are shown in the panel below (Figure 38).

***Zfhx3*$^{+/+}$; *Cry2*$^{+/+}$**

τDD = 23.28 hours

τLL = 25.20 hours

***Zfhx3*$^{Sci/+}$; *Cry2*$^{+/+-}$**

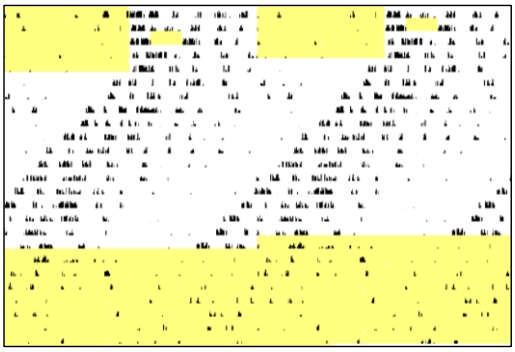

τDD = 22.75 hours

τLL = split / low amplitude

***Zfhx3*$^{+/+}$; *Cry2*$^{-/-}$**

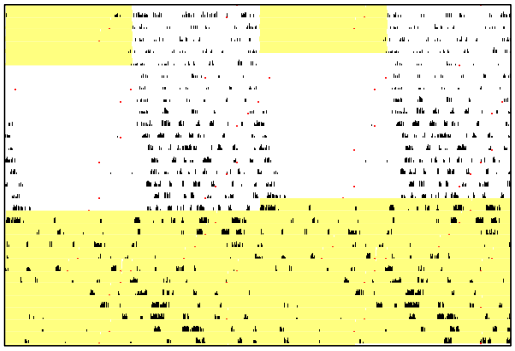

τDD = 24.12 hours

τLL = 25.82 hours

***Zfhx3*$^{Sci/+}$; *Cry2*$^{-/-}$**

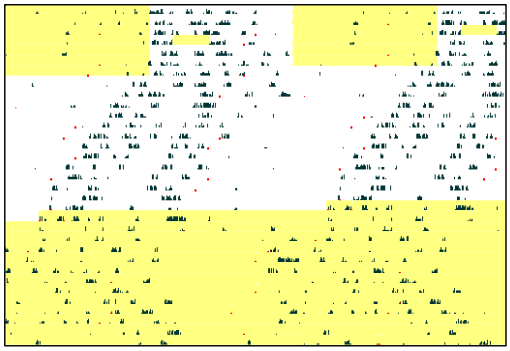

τDD = 23.3 hours

τLL = 24.43 hours

Figure 38: Representative actograms depicting the circadian phenotypes of *Zfhx3 ; Cry2* double mutants. In comparison to WT animals, *Cry2*$^{-/-}$ KO animals have a long period under DD and *Zfhx3*$^{Sci/+}$ mutants have a short period in DD. The combination of the two mutant alleles results in a short period in DD that is not significantly different from that of *Zfhx3*$^{Sci/+}$ alone or WT litter mate animals (2-tail T TEST, $p > 0.05$). The double mutants are significantly shorter than *Cry2*$^{-/-}$ animals (2-tail T-TEST, $p < 0.000$).

A primary assessment of the period length under constant darkness was made on *Zfhx3 ; Cry2* mutant animals. Table 34 indicates the calculated τDD for each *Zfhx3 ; Cry2* animal that was assessed by wheel running circadian screens and is represented graphically in Figure 39.

Period length in hours under constant darkness (τDD) for all *Zfhx3 – Cry2* animals

***Zfhx3*$^{+/+}$ - *Cry2*$^{+/+}$** wt - wt	***Zfhx3*$^{+/+}$ - *Cry2*$^{-/-}$** wt - ko	***Zfhx3*$^{Sci/+}$- *Cry2*$^{+/+}$** het - wt	***Zfhx3*$^{Sci/+}$- *Cry2*$^{-/-}$** het - ko
23.49	24.15	22.98	23.25
23.28	24	21.94	22.85
23.28	23.86	22.79	23.04
23.68	23.95	22.97	22.75
23.51	24	22.95	23.03
23.48	23.83	23.46	23.3
23.27	23.98	23.23	22.3
23.63	24.12	23.28	23.69
23.31		23.16	23.2
23.27		23.16	22.61
23.56		23.17	23.43
23.55		22.83	24.27
23.37		23.5	23.71
23.35			
23.37			
23.51			
23.16			

n	17	8	13	13
AVERAGE	23.42	23.99	23.03	23.19
STERR	0.04	0.04	0.11	0.14

Table 34: Period length (hours) recorded for all *Zfhx3 ; Cry2* animals analysed by monitoring wheel running activity. Period length calculations were taken using ClockLab software. The gradient of activity was taken from the second full day in DD following entrainment.

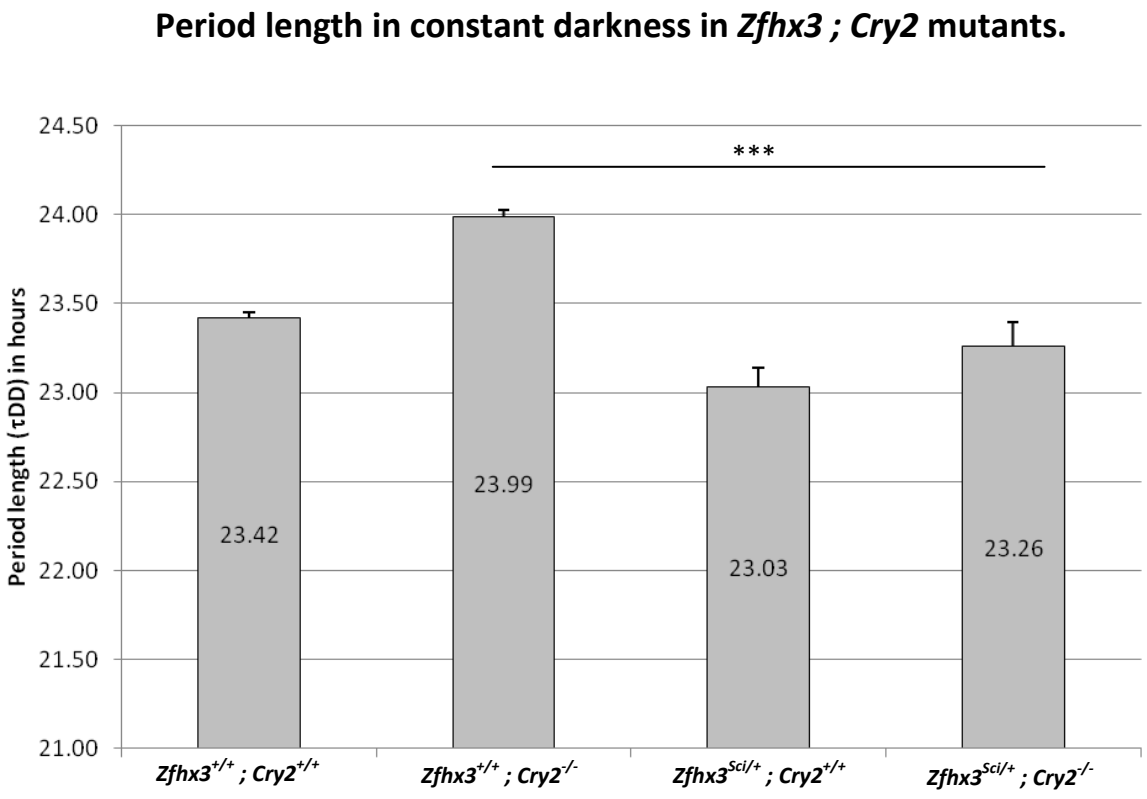

Figure 39: Graphical representation of the period length in constant darkness for *Zfhx3 ; Cry2* mutants. *Cry2*$^{-/-}$ animals have a significantly longer period under constant darkness compared to WT animals (23.99 hours). *Zfhx3*$^{Sci/+}$ animals have a significantly short period compared to WT animals (23.03 hours). The combination of the two mutant alleles, *Zfhx3*$^{Sci/+}$ *; Cry2* $^{-/-}$, results in a short circadian period (23.26 hours) that does not significantly differ from *Zfhx3*$^{Sci/+}$ (2-tail T TEST, p = 0.197) or *Zfhx3*$^{+/+}$ *; Cry2*$^{+/+}$ (2 tail T TEST, p = 0.20) animals but is significantly shorter than *Cry2*$^{-/-}$ animals (p < 0.000 ***).

Cry2$^{-/-}$ and *Zfhx3*$^{Sci/+}$, individually have a long (τDD = 23.99 hours) and short (τDD = 23.03 hours) period length in constant darkness respectively. Both significantly differ from wild type litter-mates (2-tail T TEST, p < 0.000). As with *Zfhx3*$^{Sci/+}$ *; Cry1*$^{-/-}$, the addition of the *Zfhx3*$^{Sci/+}$ allele onto the *Cry2*$^{-/-}$ background did not abolish circadian rhythmicity under DD. *Zfhx3*$^{Sci/+}$ *; Cry2*$^{-/-}$ animals have a τDD that does not significantly differ from *Zfhx3*$^{+/+}$*; Cry2*$^{+/+}$ or *Zfhx3*$^{Sci/+}$ animals. This

suggests that the phenotypic effect of the *Zfhx3*$^{Sci/+}$ mutation is epistatic over the *Cry2*$^{-/-}$ phenotype and therefore would lie upstream of *Cry2* and may be involved in *Cry2* transcriptional regulation. A genetic interaction between *Zfhx3* and *Cry2* has been supported using a 2-way ANOVA test statistic (F (1,47) = 4.344, $p < 0.05$, Sci*Cry2 p = 0.043 (n.s)). The statistical analysis is shown in Table 35.

Tests of Between-Subjects Effects

Dependent Variable:scicry2_period

Source	Type III Sum of Squares	df	Mean Square	F	Sig.
Corrected Model	4.970[a]	3	1.657	14.058	.000
Intercept	25957.200	1	25957.200	220257.973	.000
sci	4.144	1	4.144	35.162	.000
cry2	1.557	1	1.557	13.208	.001
sci * cry2	.512	1	.512	4.344	**.043**
Error	5.539	47	.118		
Total	27814.989	51			
Corrected Total	10.509	50			

a. R Squared = .473 (Adjusted R Squared = .439)

Table 35: 2 way ANOVA to test for an interaction between *Zfhx3* and *Cry2* based upon τDD. The test statistic, Sci*Cry2 describes the interaction between the *Zfhx3*$^{Sci/+}$ and *Cry2*$^{-/-}$ genotypes. The interaction is significant (p = 0.043) and therefore there is a statistically significant genetic interaction between these two genotypes based upon wheel running activity under constant darkness. The model is also highly significant, with both *Zfhx3* and *Cry2* having a significantly different τ DD from each other and from wild-type (p < 0.00 for both).

5.6. *Zfhx3 ; Cry2* Circadian Phenotype in Constant Light

As for the *Zfhx3 ; Cry1* mutants, behavioural observations under LL were divided up into four main categories: lengthened period, split rhythm, arrhythmic and low activity. Representative actograms for each type of LL behaviour is shown in Figure 36. The percentage of animals

expressing each of the four phenotypes was calculated and the data are shown in Table 36 and Figure 40 below. In the *Zfhx3 ; Cry2* mutants, all wild-type and *Cry2*$^{-/-}$ animals exhibited normal lengthening. The *Zfhx3*$^{Sci/+}$ mutants showed only a minor percentage of animals displaying split rhythms, arrhythmia or low activity. The majority, 69%, displayed normal period lengthening. In contrast, only 20% of *Zfhx3*$^{Sci/+}$ *; Cry2*$^{-/-}$ double mutant animals had normal period lengthening and the dominant exhibited behaviour seen in 40% animals, was arrhythmia in LL. This severe deterioration in the phenotype suggests an interaction between *Zfhx3* and *Cry2* under light conditions and as with the *Zfhx3 ; Cry1* mutants, the requirement of these two alleles in light-dependent circadian rhythmicity. The phenotype in these double mutants under LL is more severe than that observed in the *Zfhx3 ; Cry1* mutants, supporting a more important role for *Cry2* and its interaction with the *Zfhx3* allele, in light dependent behaviour.

	***Zfhx3*$^{+/+}$ *; Cry2*$^{+/+}$** wt-wt	***Zfhx3*$^{+/+}$ *; Cry2*$^{-/-}$** wt-ko	***Zfhx3*$^{Sci/+}$*; Cry2*$^{+/+}$** het-wt	***Zfhx3*$^{Sci/+}$*; Cry2*$^{-/-}$** het-ko
% Lengthen	100	100	69.23	20
% Split	0	0	7.69	20
% Arrhythmic	0	0	7.69	40
% Low activity	0	0	15.38	20

Table 36: Distribution of behaviours under constant light in *Zfhx3 ; Cry2* mutants. The expected activity under constant light conditions is period lengthening, as per Aschoff's rule. As with the *Zfhx3 ; Cry1* mutants, this was observed in 100% of all wild type animals examined in this cohort. The addition of the *Cry2*$^{-/-}$ allele had no effect on the circadian behaviour in LL, with 100% animals maintaining normal period lengthening. The majority of *Zfhx3*$^{Sci/+}$ animals (69%) also maintained normal period lengthening, however a small percentage of the cohort exhibited split rhythms, arrhythmic or low activity. A severe deterioration of circadian rhythmicity was observed in the *Zfhx3*$^{Sci/+}$ *; Cry1*$^{-/-}$ double mutants. Only 20% showed normal period lengthening, but 40% animals were arrhythmic in LL.

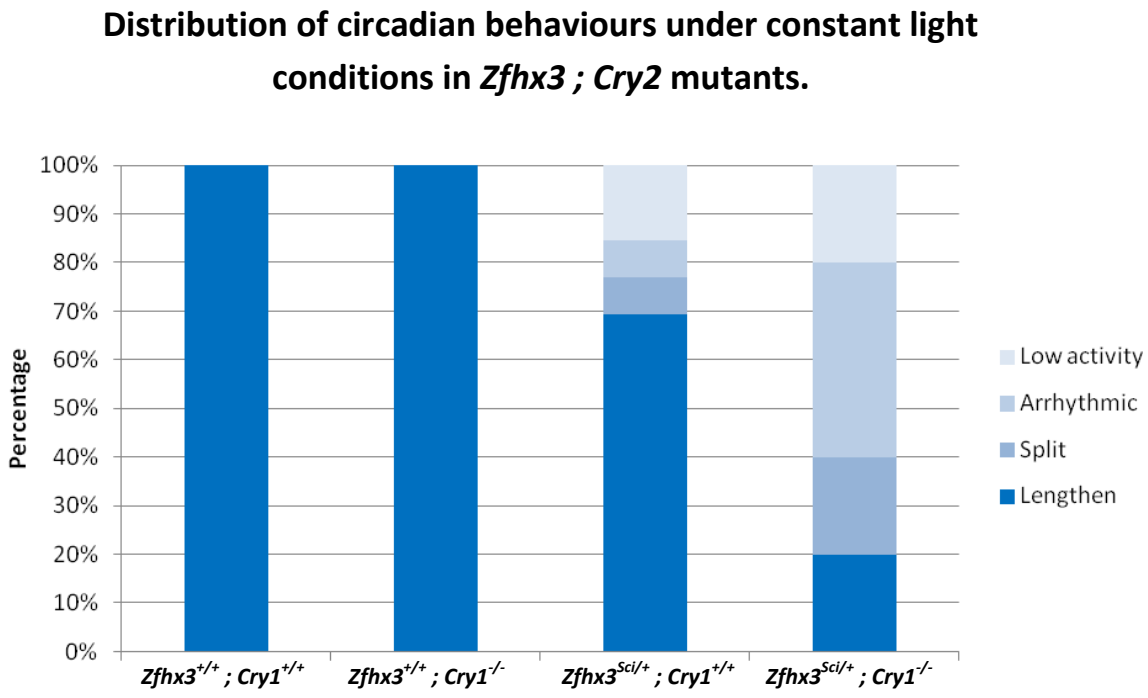

Figure 40: Bar chart of behaviours exhibited by *Zfhx3 ; Cry2* mutants under constant light conditions. Wild-type and *Cry2*$^{-/-}$ animals exhibited normal period lengthening. A small proportion of *Zfhx3*$^{Sci/+}$ animals display behaviours other than lengthening, however, a larger proportion of the cohort did lengthen their period in LL. In the *Zfhx3*$^{Sci/+}$; *Cry2*$^{-/-}$ double mutants, the majority of animals are arrhythmic, 40%, and only 20% animals show period lengthening, suggesting a severe deterioration of circadian rhythmicity in LL in the double mutants.

5.7. Discussion

5.7.1. Purpose of this chapter

The data from this chapter are the result of an *in vivo* epistasis experiment used to determine whether *Zfhx3* acts within the circadian feedback loop and interacts with known clock genes. Epistasis, or dominance, describes the relationship between genes and by determining interactions with other alleles it is possible to define gene order within a pathway. In principal, when two genes of differing phenotypes are combined through creating double mutants, the epistatic gene is the one whose phenotype dominates and is likely acting upstream. The identification of an epistatic interaction implicates non-independence between two genetic loci. This may be a genetic or biochemical interaction, direct or indirect, which would need further experimentation to be determined.

To investigate the epistatic relationships between *Zfhx3* and other clock genes, the *Sci* mutant with its well characterised circadian phenotype, was crossed to known circadian mutants to generate double mutant mice. *Cry1* and *Cry2* knock-out animals which were already generated and available were initially chosen for this experiment. The *Cry1* and *Cry2* KO animals were generated previously and gifted by Gijsbertus T. J. van der Horst (van der Horst, et al. 1999). These two mutant lines have strong phenotypes which facilitate the detection of any perturbations to the circadian clock with the addition of the *Sci* mutant allele. *Cry1*$^{-/-}$ animals have a fast endogenous circadian clock, previously reported as 22.51 hours (± 0.06 hours, $p < 0.000$). In contrast, *Cry2*$^{-/-}$ animals have a slow endogenous circadian clock of 24.63 hours (± 0.06 hours, $p < 0.000$). The τDD obtained from these crosses for *Cry1*$^{-/-}$ and *Cry2*$^{-/-}$ are comparable (τDD 22.60 and 23.99 hours respectively) to this original data, confirming the phenotype and indicating that the genetic background being used is valid for this experiment. These results suggest antagonistic

action of the *Cry1* and *Cry2* genes on the period of the endogenous circadian clock under constant dark conditions. There are no known phenotypes under entrainment (a 12:12 LD cycle) or constant light conditions. This is also observed in $Cry1^{-/-}$; $Cry2^{-/-}$ double knock out animals, however they are arrhythmic in DD. Any perturbation therefore to the entrainment profile or activity under constant light conditions in $Zfhx3^{Sci/+}$; $Cry^{-/-}$ double mutants would be inferred to be due to the added effect of the *Zfhx3* mutation in $Zfhx3^{Sci/+}$ animals interacting with the $Cry^{-/-}$ mutant background. Additionally, no sex differences have been identified in either of the *Cry* KO lines or *Sci* mutant and as such, no distinction was been made between sexes in these experiments.

5.7.2. Hypotheses

The *Cry1* and *Cry2* KO animals were hypothesised to be good candidates for identifying epistatic interactions with *Zfhx3* using the *Sci* allele. Two lines of evidence supported this, the first based upon *in vitro* protein interaction data and the second based upon bioinformatic analyses into cryptochrome transcriptional activity. As previously described, a protein interaction has been identified between the WT ZFHX3 protein and CRY1 and CRY2. It is hypothesised that protein interactions may be disrupted due to the location of the *Sci* mutation which lies in a potential protein interacting domain. Aberrant binding (loss or miss-timed protein interaction) may have an effect on the localisation and activity of CRY1 and/or CRY2 and effect the endogenous period of the circadian clock. With ZFHX3 localised to both the cytoplasm and the nucleus, it is possible that ZFHX3 is involved in directing the localisation of CRY either toward or away from the *Cry* promoter. Alternatively, it may be part of a larger protein complex with the CRY proteins at the *Cry* promoter to facilitate the inhibition of *Cry* transcription. If this protein interaction is important for circadian clock stability, it would be expected that any miss-binding to CRY by ZFHX3

in *Sci* would have an effect on the phenotype of the reciprocal *Cry* KO animals. This would be due to a loss of one functional *Cry* gene as well as a potential loss of function of the remaining reciprocal wild-type CRY protein which is up-regulated to compensate for loss of *Cry*. For example, if ZFHX3 is required to bind CRY2 for CRY2 to function effectively in a wild-type background, *Cry1* KO animals would be expected to have a more severe phenotype since both *Cry1* and CRY2 are affected. CRY2 may be inefficient in compensating for the loss of the *Cry1* allele. The converse may also be applied to *Cry2* and CRY1. In order to verify this hypothesis, protein interaction studies investigating whether the *Sci* ZFHX3 protein is unable to bind CRY and other clock-related proteins need to be performed.

The second hypothesis for an involvement of *Zfhx3* in cryptochrome regulation is based upon a role of ZFHX3 in *Cry* gene transcriptional activity. It is known that ZFHX3 is able to bind to AT sequence motifs in order to regulate transcription of target genes. It is possible that ZFHX3 binds and interacts with other sequence motifs, based upon its complex structure containing multiple zinc fingers and homeodomains, although this remains to be investigated. The predominant and most well characterised mechanism of transcriptional regulation within the circadian clock is by E-box motif binding. *Cry* and *Per* genes both contain E-box elements within their promoters and are regulated by CLOCK/BMAL1 heterodimer binding (Ko and Takahashi 2006). However, it is possible that transcriptional activity may be further enhanced by additional co-factor binding. As discussed in the introduction, AT motifs have been found to be closely associated to E-box elements and binding of a protein to an AT motif may indirectly regulate E-box mediated transcription through masking of the motif (Berry, et al. 2001). Although clock controlled gene (CCG) promoters are characteristically GC rich, bioinformatic analyses have identified putative AT motifs in the promoters of *Cry1* and *Per1* using MotiFSA (performed by Dr Rahul Satija). These are highly homologous to the *Zfhx3* AT binding motif (TATTTAATTAT) and not far dissimilar from the D-box

consensus sequence (TTAYRTAA) (Bozek, et al. 2009). A conserved AT motif was not identified in the *Cry2* promoter however the 10 kb region upstream of the *Cry2* promoter showed less conservation in general. It is possible that there is another transcriptional regulator with an even greater affinity than ZFHX3 as yet unidentified in the *Cry2* promoter. This suggests the possibility of a binding site for ZFHX3 in the *Cry1* and *Per1* promoters. These bioinformatic analyses are shown in Figure 41.

A

AFP		MRF4		Pit1		MUC5AC	
Human	tgattaataattaca	Human	ctaattaaatg				
Rhesus	tgattaataattaca	Rhesus	ctaattaaatg	Human	gattatttaattataa		
Mouse	tgg------gttcca	Mouse	ctaattaaatg	Rhesus	gattatttaattataa	Human	tttattcattaac
Dog	---ttaataattaca	Dog	ctaattaaatg	Mouse	gattatttaattagaa	Rhesus	ttcatccattcac
Elephant	ag-ttaataat----	Platypus	ctaattaaatg	Dog	ggttatttaattataa	Mouse	tttgttcattcat

B

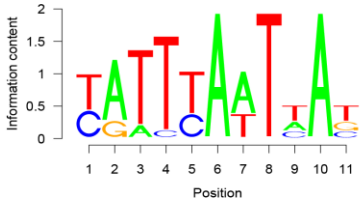

C

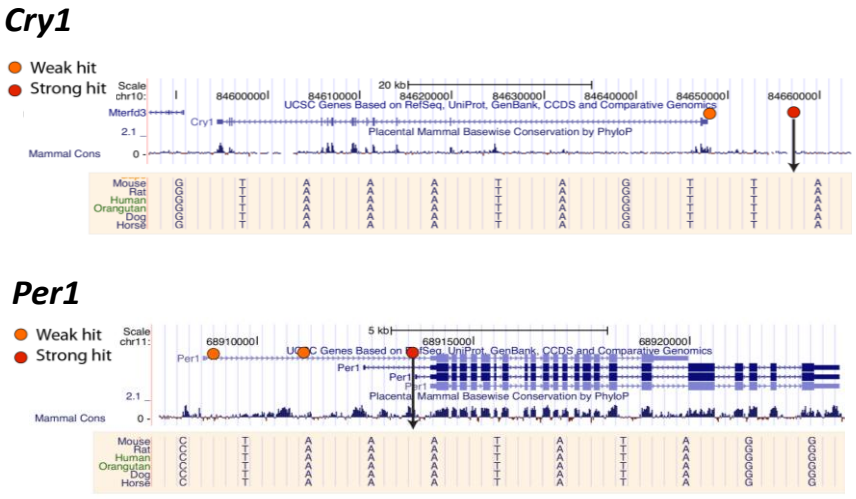

Figure 41: Bioinformatic analyses of the 10kb region upstream of the promoters of known clock genes to identify putative *Zfhx3* AT motif binding sites. (A) Sequences for the AT motifs across a variety of species, to which *Zfhx3* is known to bind and regulate transcription of the target genes. (B) A consensus AT motif for *Zfhx3* was generated using a phylogenetic shadowing based approach based upon the known binding motifs (shown in A) This motif is not too dissimilar from the D-box element (TTAYRTAA). (C) MotiFSA was used to predict the presence of AT motifs in circadian genes. A strong predicted AT motif was found in both *Cry1* and *Per1* upstream of their promoters. (Data courtesy of Dr Rahul Satija).

Due to the size of ZFHX3, it is possible that binding to the AT motif may mask the E-box, approximately 600 nucleotides distal to the putative AT motif in the *Cry1* promoter, and prevent CLOCK/BMAL1 binding. Alternatively, ZFHX3 may directly regulate *Cry1* and *Per1* transcriptional activity through the AT motif. It is also possible that this may be extrapolated to other circadian gene promoters. It should also be considered that *Zfhx3* may be able to bind the E-box together with CLOCK/BMAL1, or other co-factors, to enhance transcriptional activation. If *Zfhx3* is involved in AT motif, E-box or other enhancer element binding to regulate clock gene transcription, it could be hypothesised that the *Sci* mutation may affect ZFHX3's promoter element binding and therefore affect transcriptional activity of the target gene. It is known that CLOCK/BMAL1 alone are sufficient and required to drive *Cry* and *Per* transcriptional activity. *Cry* and *Per* expression can be modified by other factors for example by proteins such as DBP, HLF, TEF and E4BP4 through D-box elements. It is also known that there is competition between transcription factors in binding to E-box and D-box regulatory elements (Gachon, et al. 2004; Mitsui, et al. 2001; Yamaguchi, et al. 2000). It would not be expected that there would be a severe disruption to circadian rhythmicity in the *Sci* mutant since CLOCK/BMAL1 would still be transcriptionally functional to maintain the rhythmicity of the circadian clock. However, the robustness of the clock may be compromised, and this may be more prominent in the presence of other clock mutations.

With a protein interaction identified between CRY1 and CRY2 and a potential consensus AT motif identified in the *Cry1* enhancer, it may be expected that the *Sci* mutation would cause a deteriorated phenotype in the *Zfhx3*$^{Sci/+}$-*Cry2*$^{-/-}$ animals. This is because a ZFHX3/CRY2 protein interaction may be lost together with a potential dis-regulation of *Cry1* transcription due to aberrant ZFHX3 binding to an AT motif or E-box. This may leave CRY1 unable to be fully functional in compensating for CRY2. The converse may also be true. The functional significance of the

ZFHX3/CRY1 and ZFHX3/CRY2 interaction remains to be identified as well as the relevance of the AT motif identified in the *Cry1* and *Per1* promoter.

5.7.3. *Zfhx3*$^{Sci/+}$; *Cry1*$^{-/-}$ and *Zfhx3*$^{Sci/+}$; *Cry2*$^{-/-}$ double mutant phenotypes

Upon generation of the *Zfhx3 ; Cry1* and *Zfhx3 ; Cry2* double mutants, animals were screened for circadian phenotypes using wheel-running screening strategies as previously described. Phenotypes under DD and LL were recorded to identify any significant deviation from each individual mutant allele phenotype. Under constant dark conditions, *Zfhx3*$^{-/+}$-*Cry1*$^{-/-}$ double mutants had a period that was significantly shorter than each individual mutant. Given that both *Cry1*$^{-/-}$ and *Sci* animals have a short intrinsic period under constant darkness, an additive shortening would be expected if there was no genetic interaction. This was the case for *Zfhx3*$^{Sci/+}$-*Cry1*$^{-/-}$, as statistical analysis of the resultant τDD did not identify a significant interaction ($p = 0.07$). This result however showed a strong trend towards significance and it is possible that through screening a larger cohort may become a significant interaction. However, based upon the current data, an epistatic interaction between *Zfhx3* and *Cry1* cannot be statistically confirmed based upon *in vivo* τDD phenotypic data. This would suggest that CRY2 remains functionally capable in maintaining circadian rhythmicity despite the addition of the *Sci* allele. This would imply that ZFHX3 does not have a sufficiently strong affect on CRY2 to affect its ability to compensate for the loss of *Cry1*'s role under constant dark conditions.

An interesting result was identified in the *Zfhx3 ; Cry2* mutants. Under constant dark conditions, the intrinsic period of *Cry2*$^{-/-}$ is long compared to wild-type animals and again, the *Zfhx3*$^{Sci/+}$ period is short. In the case of the *Zfhx3*$^{Sci/+}$; *Cry2*$^{-/-}$ double mutants, the resulting phenotype in DD mirrored that seen in the *Zfhx3*$^{Sci/+}$ mutants alone, with the short τDD dominant over the long τDD of the *Cry2*$^{-/-}$ KO. Statistical analysis supported that there was a significant interaction between

the two genotypes, indicating an epistatic interaction between *Zfhx3* and *Cry2*. The implication of this is that the functional *Cry1* gene is unable to fully compensate for the loss of *Cry2* when on a *Zfhx3*$^{Sci/+}$ background. This would imply that the mutated *Zfhx3* either transcriptionally or physically mis-regulates *Cry1*/CRY1 and as such, CRY1 can no longer act as efficiently in a functionally redundant manner to *Cry2* in the *Cry2* KO background. This may also imply that *Cry1* has a more important role in the molecular clockwork in the SCN (Ruan, et al. 2012). As discussed, with an AT motif identified in the *Cry1* promoter and a physical protein interaction, it remains to be determined by which mechanism (or both) *Zfhx3* is acting to regulate *Cry1*. These results however show that *in vivo,* ZFHX3 is important for *Cry1* function.

Under constant light conditions, the role of *Zfhx3* and cryptochromes becomes more complex. Both *Zfhx3*$^{Sci/+}$ *; Cry1*$^{-/-}$ and *Zfhx3*$^{Sci/+}$ *; Cry2*$^{-/-}$ double mutants exhibited a deterioration of circadian rhythmicity under LL. This may raise the possibility that cryptochromes are involved in light mediated responses, which may be modified by *Zfhx3*. The severity of phenotypes was strongest in the *Zfhx3*$^{Sci/+}$ *; Cry2*$^{-/-}$ mutants where there was a loss of 50% animals with normal behavioural activity compared to the *Zfhx3*$^{Sci/+}$ mutants alone, and a loss of 80% when compared to the *Cry2*$^{-/-}$ and wild-type animals. The majority of the *Zfhx3*$^{Sci/+}$ *; Cry2*$^{-/-}$ mutants became arrhythmic, with an increase by 32% of animals showing arrhythmic behaviour, again in comparison to the *Zfhx3*$^{Sci/+}$ mutants alone (40% increase compared to *Cry2*$^{-/-}$ and wild type animals). The remaining animals showed intermediate phenotypes between split rhythms and low activity/low amplitude rhythms. These results suggest a significant interaction between *Zfhx3* and *Cry2* under constant light conditions, again suggesting impairment in *Cry1* activity due to the *Sci* mutation. A similar trend in the phenotypes under LL was observed in the *Zfhx3*$^{Sci/+}$ *; Cry1*$^{-/-}$ mutants, with 50% animals becoming arrhythmic. However, a larger proportion of the double mutant animals maintained normal circadian rhythmicity under LL compared to the *Zfhx3*$^{Sci/+}$ *; Cry2*$^{-/-}$ mutants (42.86%).

Although the role of type II cryptochromes in mammals in light perception is strongly debated, these results may implicate a role of *Zfhx3* and cryptochromes in prolonged light mediated circadian responses. In both plants and *Drosophila*, cryptochromes (Type I) are involved in light perception through flavin radical formation. In mammals however, Type II cryptochromes act upon the circadian clock independently of light. Recent studies have reopened the debate on whether there is a functional role for Type II mammalian cryptochromes in light responsivity (Vieira, et al. 2012). Studies using cell cultures over-expressing human cryptochrome have shown that this cryptochrome can undergo photoreduction from oxidized to radical flavin states in vivo. Additionally, light has been shown to rapidly degrade type II cryptochrome in recombinant flies, illustrating sensitivity to light in its lability (Hoang, et al. 2008). Finally, type II cryptochrome from the Monarch Butterfly and from humans can rescue light-dependent magneto-reception in transgenic flies (Gegear, et al. 2010).

Since no overt phenotypes were identified under a 12:12 light-dark cycle, it would appear that the circadian clock maintains normal entrainment from photic input pathways. Instead, it may be that *Zfhx3* and cryptochromes are involved in maintaining the stability of SCN neuronal activity under constant light and an involvement in local neuronal synchrony both in and between the two SCN nuclei.

Further work is required to isolate the mechanism by which *Zfhx3* is acting upon cryptochromes. This is the first *in vivo* evidence to suggest that *Zfhx3* may be involved within the same genetic pathway as *Cry1* and *Cry2*, as well as a role for *Cry1, Cry2* and *Zfhx3* in light mediated circadian responses. Future work will aim to identify whether protein interactions between *Zfhx3* and *Cry1* and *Cry2* are affected in the *Sci* mutant as well as the functional importance of the protein interactions. Biochemical and genetic analyses will be required for these studies and current on-

going work includes reporter gene assays, protein interaction studies and ChIP analyses. It would also be valuable to investigate other double mutants by crossing the *Sci* animals to other known circadian mutants. With a protein interaction identified between ZFHX3 and PER2 and an AT motif identified in the *Per1* promoter, another hypothesis would be that the Period genes are also a target for regulation by *Zfhx3*. Epistatic interaction studies using *Per1*$^{-/-}$ and *Per2*$^{-/-}$ would advance this work in the same manner by which these *Zfhx3 ; Cry* double mutants have further confirmed a role for *Zfhx3* in cryptochrome regulation.

Chapter VI

Results IV

Characterisation of Ophthalmological Phenotypes and Functions of *Zfhx3* in the Visual System

6. *Zfhx3* Interaction with the Visual System

6.1. Introduction

The mammalian circadian clock is dependent upon external synchronizers or z*eitgeber*s in order to maintain accurate coordination between the internal (endogenous) and external environment. The suprachiasmatic nucleus (SCN), the master pacemaker in mammals, receives external input for entrainment from various sources however predominant innervations comes from the retino-hypothalamic tract (RHT), direct from the intrinsically photosensitive retinal ganglion cells (ipRGC's) of the retina (Panda, et al. 2005). With strong input from the visual system and a dependency on non-image forming photic information, the circadian clock is often considered an extension or component of the greater visual system. Given this known interplay between these two systems, it was decided to investigate whether any ophthalmological phenotypes were present in the *Sci* animals which may contribute to the observed circadian phenotypes. Additionally, phenotypes had been detected in *Sci* under the light phase of entrainment, constant light conditions and re-entrainment. This suggested an interaction in *Sci* between photic input and detection at the SCN and has been discussed in Chapter III.

The data in this chapter presents an assessment of ophthalmological phenotypes in *Sci* and a molecular characterisation of the involvement of *Zfhx3* in the visual system. RNA profiling by *in situ* hybridisation and RT-PCR showed that *Zfhx3* RNA is expressed in the adult retina and is therefore a good candidate gene for an involvement in retinal function. Additionally, differential effects on retinal candidate genes were seen at the RNA level in the $Zfhx3^{Sci/+}$ animals. A morphological characterization of the adult eye was performed and although there was an apparent normal retinal structure, a corneal dystrophy was identified which may impact on the

proportion of light reaching the retina as well as an effect on refraction and thereby on visual acuity. Further phenotypic characterization on the visual capacity of the *Sci* animals identified an abnormal pupil reflex phenotype indicative of photo-phobia and a decrease in visual acuity which was assessed behaviorally by monitoring head tracking movements.

The results from this chapter would suggest that *Zfhx3* plays a role in the adult visual system, both molecularly at the level of the retina as well as in the formation and maintenance of normal corneal structure and function. Additionally, the effects on the pupillary light reflex response may implicate an involvement in the relay of non-image forming photic information and it may be inferred that there is an effect on SCN afferents.

6.2. *Zfhx3* expression in the adult eye

6.2.1. *In situ* hybridisation

In situ hybridisation was used to assess whether *Zfhx3* RNA was expressed in the adult eye. This technique was used to determine whether *Zfhx3* may be a candidate transcription factor involved in retinal molecular pathways or photic transduction genetic cascades. Previous studies have shown expression of *Zfhx3* RNA in the developing retina (Ishii, et al. 2003) and the studies presented here have gone on to investigate whether *Zfhx3* is expressed in the adult visual system. Since an antibody was not available for immunological analysis of the ZFHX3 protein, RNA analyses have been utilised. Sense and antisense DIG labelled RNA probes generated against the *Zfhx3* transcript were hybridised against adult mouse whole eye cryo-preserved sections. A schematic of the locations where *in situ* hybridisation images were taken in relation to the whole eye section are shown in Figure 42. Representative images of *in situs* showing both retinal and corneal staining are shown in Figure 43.

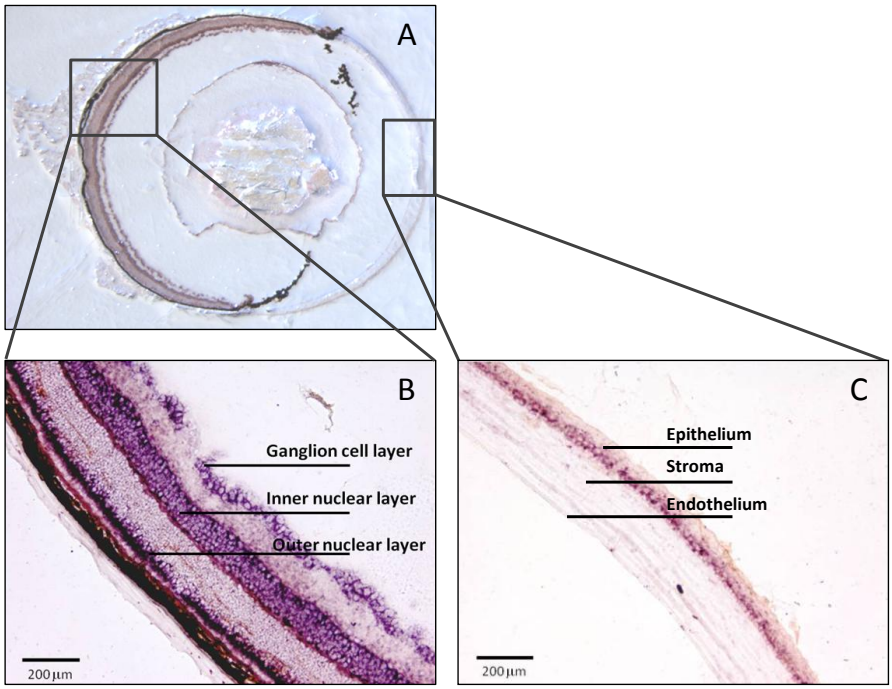

Figure 42: Schematic to illustrate the location of retinal and corneal *in situ* hybridisation images in relation to the entire eye. (A) Sagittal section throughout the centre of the adult mouse eye. (B) Retinal section showing the ganglion, inner and outer nuclear cell layers as observed in *Zfhx3* RNA *in situ* hybridisation. (C) Corneal section showing epithelium, stroma and endothelium cell layers. Staining is detected in the epithelial cell layer with a *Zfhx3* riboprobe.

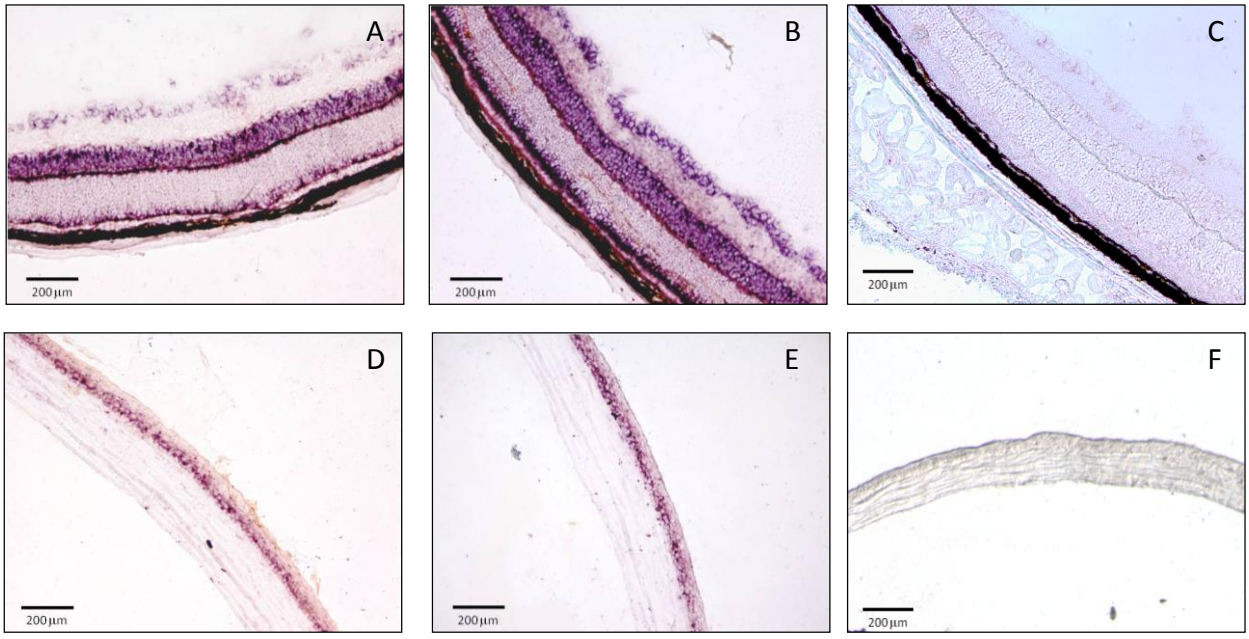

Figure 43: RNA expression of *Zfhx3* in adult retina and cornea. *In situ* hybridisation using DIG-labelled RNA probe generated against an exonic region of *Zfhx3*. Positive staining is represented by purple stain using NBT/BCIP. (A-C) Representative images of in situ hybridisation on adult retina. (A) *Sci* $^{+/+}$ (B) *Sci* $^{M/+}$ (C) Negative control using sense RNA probe. (D-F) Representative images of in situ hybridisation on adult corneas. (D) *Sci* $^{+/+}$ (E) *Sci* $^{M/+}$ (F) Negative control using sense RNA probe. Strong staining was identified in the retina, including the outer and inner nuclear layers and ganglion cell layer as well as the outer epithelium of the cornea. This implicates a role for *Zfhx3* in retinal and corneal function.

Results from the *in situ* hybridisation RNA expression analysis showed that there was high specific expression of *Zfhx3* in the adult eye. Staining was observed in the inner and outer nuclear layers of the retina, the retinal ganglion cell layer and the outer epithelial layer of the cornea. From these results it could be hypothesised that there is an involvement of *Zfhx3* in the visual system. There is wide-spread expression of *Zfhx3* in the ganglion cell layer. It is therefore likely that *Zfhx3* is expressed in melanopsin containing ipRGC's which project directly to the SCN to provide non-image forming photic information, as well as being involved in the pupillary response. This suggests that *Zfhx3* may have a role within the circadian visual system at the level of entrainment

pathways and behavioural responses to light. Additionally, *Zfhx3* RNA is expressed in the outer epithelial layer of the cornea, which is responsible for refraction of light and image formation on the retina.

6.2.2. Retinal RNA expression analysis by quantitative real-time PCR

Following the determination of the RNA expression pattern of *Zfhx3* in the adult eye by *in situ* hybridisation, further analyses and quantification of the *Zfhx3* RNA transcript were performed by quantitative real-time PCR (qRT-PCR). In addition to *Zfhx3*, retinal candidate genes specific to the cell layers in which *Zfhx3* is expressed and circadian transcripts were analysed. Retinas were isolated from adult eyes (at ZT 8) which were removed immediately from animals culled under Schedule 1 in accordance with the Home Office regulations. Relative abundance of RNA transcripts were calculated based upon the $\delta\delta$CT method by comparing the expression to that of a house keeping gene.

The relative expression of mammalian retinal opsins in $Zfhx3^{+/+}$ and $Zfhx3^{Sci/+}$ retinas are shown in Figure 44. Out of six opsins studied, a significant up-regulation of *Opn3* (Encephalopsin) was detected in the $Zfhx3^{Sci/+}$ animals. Encephalopsin is a photoreceptive protein expressed predominantly in the brain and testes, hypothesized to be an extra-retinal opsin, however it is also expressed in the retina (Halford, et al. 2001). Currently, little is known about its function in the retina. The relative expression of *Opn3* was then compared to the $Opn4^{-/-}$ knock-out animals in order to assess whether it may act to compensate for *Opn4* in the knock-out animal. A further up-regulation of *Opn3* expression was identified in these animals and is shown in Figure 45. This suggests a possible redundant mechanism or interaction between *Opn3* and *Opn4*, which is also observed to a lesser degree in the $Zfhx3^{Sci/+}$ mutants and shows a potential functional role for *Opn3* in the retina in the absence of *Opn4*.

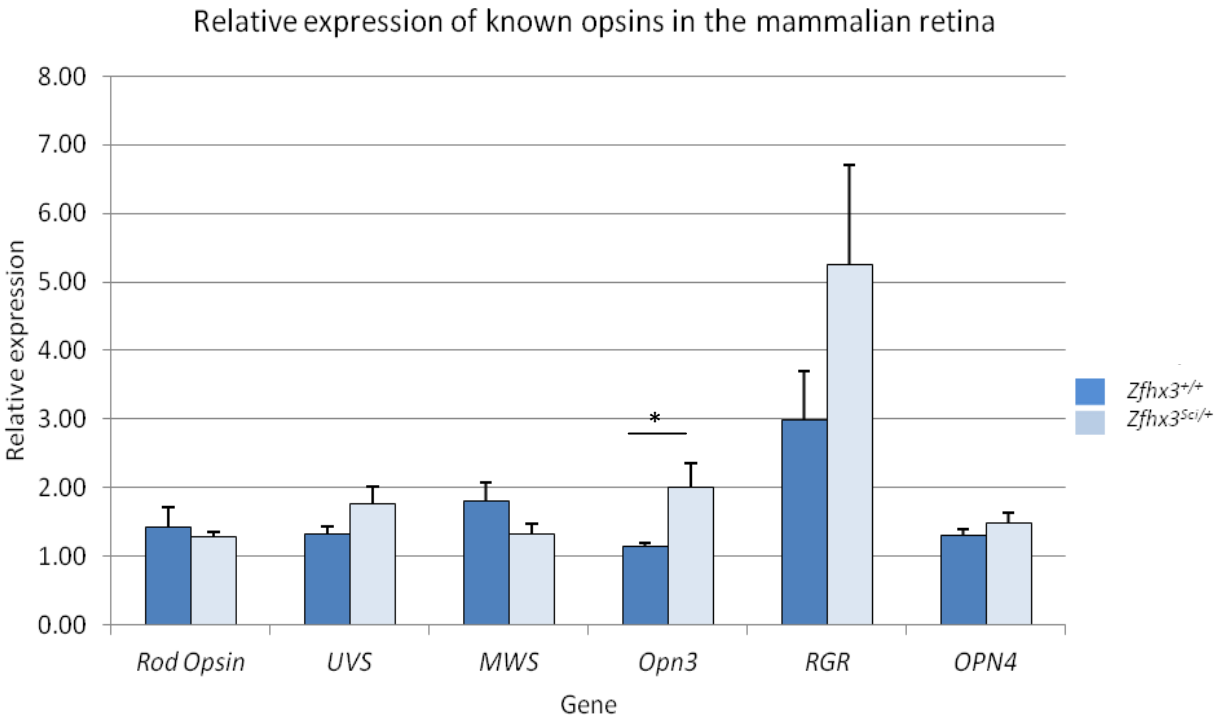

Figure 44: Relative expression of mammalian opsins in *Sci* retinas. Six opsin genes were analysed by qRT-PCR to detect differences in relative expression between *Zfhx3*$^{+/+}$ and *Zfhx3*$^{Sci/+}$ animals. These included: rod opsin, ultra-violet sensitive *(UVS),* middle wave-length sensitive *(MWS)*, encephalopsin (*Opn3*) retinal G protein coupled receptor (*RGR*) and melanopsin (*Opn4*). Out of all opsins investigated, there was a significant up-regulation of *Opn3* (2-tail T TEST, p = 0.03). Error bars show standard error of the mean.

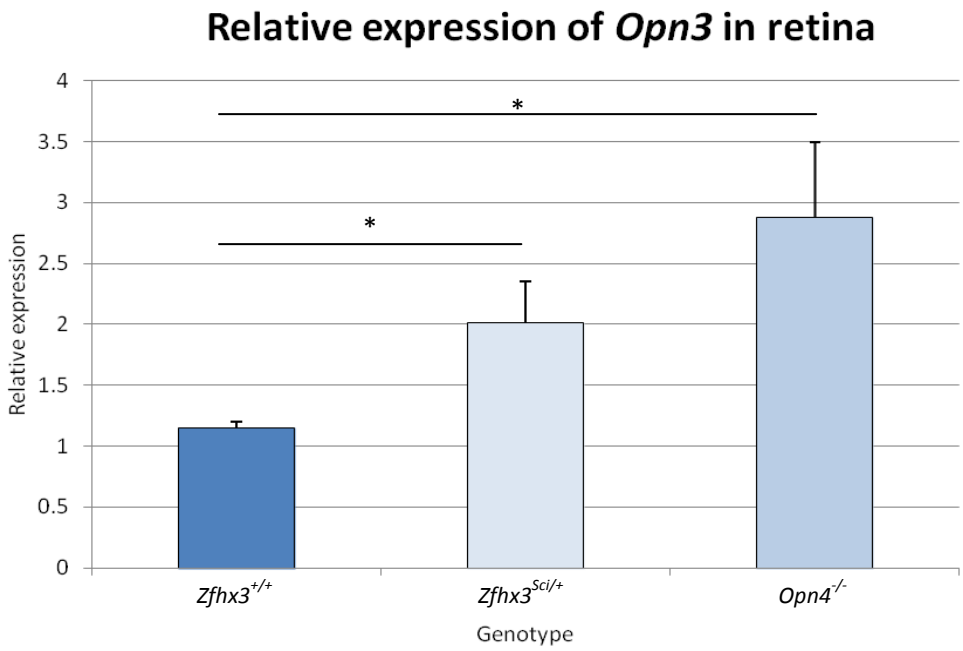

Figure 45: Comparison of relative expression of *Opn3* in the retina between *Opn4*$^{-/-}$ and *Sci* animals. *Opn3* is significantly up-regulated in *Zfhx3*$^{Sci/+}$ and *Opn4*$^{-/-}$ animals compared to WT litter mate controls in total RNA from retinas isolated at ZT8 (2-tail T-TEST, p = 0.03 and p = 0.012 respectively). Although there is no significant difference between the relative expression of *Opn3* between *Opn4*$^{-/-}$ and *Zfhx3*$^{Sci/+}$ animals (p = 0.23), there is a trend to a further up-regulation of *Opn3* relative expression. Error bars show standard error of the mean.

Additional candidate genes were next analysed by RT-PCR to compare relative expression between *Sci* genotypes, including *Zfhx3* itself. These genes were selected based upon their known expression within the cell layers that *Zfhx3* RNA expression had been observed. Genes analysed included *Zfhx3,* glutamate decarboxylase 1 and 2 *(Gad1, Gad2),* tyrosine hydroxylase *(TH)*, pituitary adenylate cyclase-activating polypeptide (*PACAP),* D-site albumin promoter binding protein *(Dbp) and Cry1 and Cry2*. *Gad1* and *Gad2* are precursor enzymes for GABA synthesis, expressed predominantly by amacrine cells of the inner nuclear layer of the retina (Cherry, et al. 2009). Additionally there are dopaminergic amacrine cells, and previous studies have shown that ZFHX3 is highly expressed in dopaminergic neurons (Ishii, et al. 2003). As such, tyrosine hydroxylase was studied as a dopamine precursor enzyme to indirectly examine dopamine

production in the retina. PACAP is a protective neuropeptide that is expressed in amacrine, horizontal and ganglion cells of the retina, as well as throughout the CNS. Melanopsin is exclusively expressed in PACAP containing retinal ganglion cells, therefore implicating a role of PACAP signaling in melanopsin mediated light responses (Colwell, et al. 2004). Results from these RNA expression analyses are shown in Figure 46.

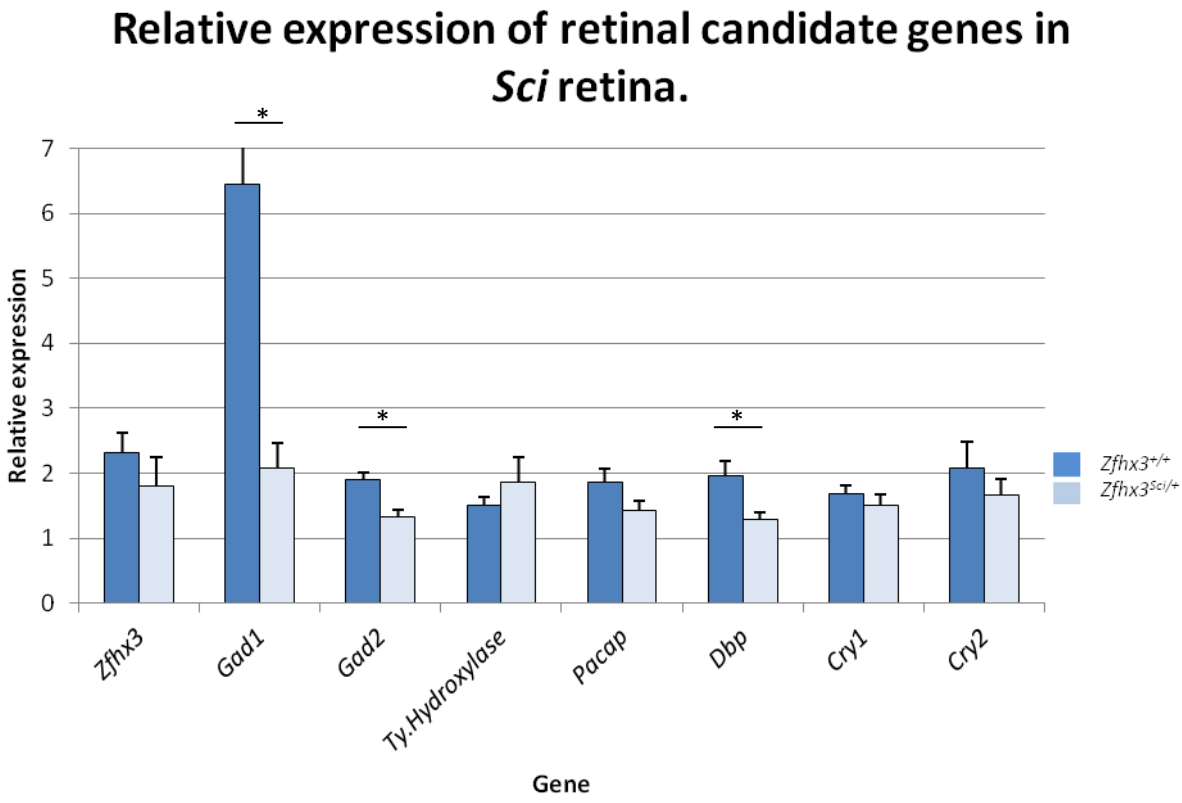

Figure 46: Relative expression of retinal candidate genes in *Sci* retinas. Retinas were isolated from *Sci* animals at ZT 8 and total RNA was extracted. Retinas were isolated from both eyes of six individual animals per genotype. RT-PCR analysis was performed to examine the relative expression of various signaling candidate genes in the retina that are co-expressed in the cell layers where *Zfhx3* had been shown to be expressed. Genes examined included*: Zfhx3, Gad1, Gad2,* tyrosine hydroxylase*, Pacap, Dbp, Cry1* and *Cry2*. A significant down-regulation of *Gad1* and *Gad2* was observed in the $Zfhx3^{Sci/+}$ retinas ($p < 0.05$). Additionally, a significant decrease in *Dbp* relative expression was observed ($p < 0.005$). Error bars show standard error of the mean.

Real time expression analysis from *Sci* retinas showed an up-regulation of *Opn3* and a down-regulation of *Gad1, Gad2* and *Dbp*. Relatively little is known about the function of *Opn3* in the retina, and whether it does have a functional role in photoreception in the mammalian retina or instead has a more predominant role as an extra-ocular, deep brain photoreceptor remains to be determined. Since *Opn3* expression is further up-regulated in $Opn4^{-/-}$, this suggests that perhaps it

is able to compensate partially for *Opn4* in a genetically redundant manner. Decreased *Gad1* and *Gad2* expression may be indicative of a reduction of GABA neurotransmission in the retina. Since *Gad1* and *Gad2* are predominantly expressed in the inner nuclear layer of the retina by amacrine cells (Hoffpauir and Gleason 2005; Jiang and Xiang 2009; Menger and Wassle 2000), it is possible that there is a reduction in GABAergic amacrine cell numbers which would be expected to have the consequences of disinhibition of the inner nuclear layer of the retina.

6.2.3. Startle and Pre-pulse Inhibition Assessment

Startle and pre-pulse inhibition (PPI) behavioural tests were used to assess whether the down-regulation of *Gad1* and *Gad2*, as observed in the *Zfhx3*$^{Sci/+}$ retina, may be indicative of similar effects in the rest of CNS. Overt behavioural phenotypes would be expected if effects on the GABAergic system were attenuated in the entire CNS. The pre-pulse inhibition of the startle response in rodents has been classically used as an endophenotypic marker of psychiatric illness, in particular schizophrenia, in which GABA neurotransmission is implicated (Swerdlow, et al. 1990; Wassef, et al. 2003).

Thirteen *Zfhx3*$^{Sci/+}$ and 12 *Zfhx3*$^{+/+}$ control male animals were tested for their startle response and PPI. Animals were assessed at 10 weeks of age in order to avoid the possibility of age related hearing loss, inherited from the C57BL/6J inbred strain. The startle and PPI was performed on all animals between 10 – 11am in order to eliminate any circadian effects in behavioural response between trials.

The startle reflex was first determined in order to determine whether there was a difference in response to a sound stimulus of 110 dB. The calculated startle response is shown in Table 37 with the averaged data shown graphically in Figure 47. There was no significant difference between

Zfhx3$^{+/+}$ and *Zfhx3*$^{Sci/+}$ (T TEST, p = 0.21). Given an equal startle response to a 110 dB tone, it was then possible to analyse the percentage PPI in both groups of animals as an assessment of sensorimotor gating. The percentage PPI was calculated using the equation shown in Equation 1. The raw data is shown in Table 38 and the calculated percentage PPI in Table 39. The averaged data is shown graphically in Figure 48. There was no significant difference in the percentage pre-pulse inhibition between *Zfhx3*$^{+/+}$ and *Zfhx3*$^{Sci/+}$ animals (2-tail T-TEST, 65dB p = 0.35, 70dB p = 0.45, 75dB p = 0.7).

% pre-pulse inhibition = 100 * ((av. response to pulse alone) – (av. response with pre-pulse)) / av. response to pulse alone

Equation 1: Calculation of percentage pre-pulse inhibition. The average response to a single pulse is also the startle response at 110 dB. This value is used to subtract the background response to a single tone played alone.

	Startle - 110	
	Zfhx3 $^{+/+}$	***Zfhx3*** $^{Sci/+}$
	1499.1	1688.8
	1038.9	894.2
	1526.8	1154.7
	1975.4	1411.1
	2022.7	1892.3
	1858	737.8
	1543.1	1620
	1413.3	1062.1
	1548.9	565.9
	1816.4	1607.5
	1906.6	1955.1
	694.6	1535.8
		1516.6
AVERAGE	**1570.32**	**1357.07**
STDEV	**393.96**	**437.60**
STERR	**113.73**	**121.37**
T TEST	**0.21**	

Table 37: Comparison of the startle reflex response between *Zfhx3*$^{+/+}$ and *Zfhx3*$^{Sci/+}$. There was no significant difference in startle response between *Zfhx3*$^{+/+}$ and *Zfhx3*$^{Sci/+}$ to a 110 dB tone, as analysed by 2-way T TEST (p=0.21). The startle response is measured in arbitrary units.

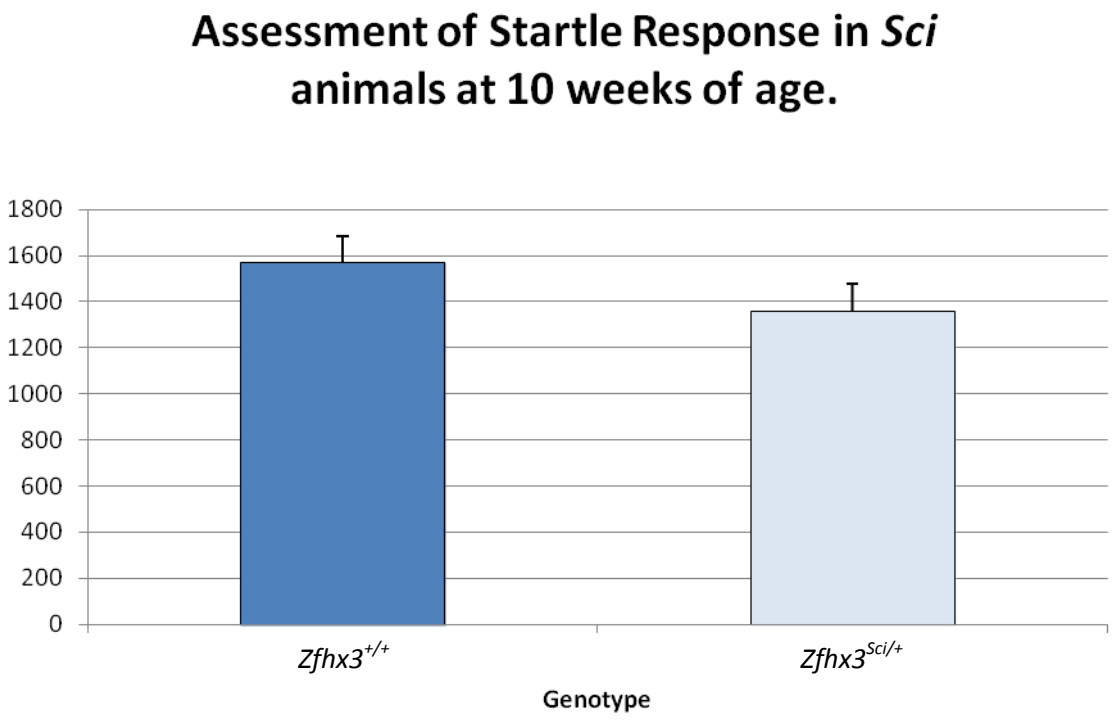

Figure 47: Bar chart representation of the average startle response for *Zfhx3*$^{+/+}$ and *Zfhx3*$^{Sci/+}$. The average values have been plotted with error bars showing standard error of the mean. There was no significant difference between *Zfhx3*$^{+/+}$ and *Zfhx3*$^{Sci/+}$ mice (T TEST, p = 0.21).

***Zfhx3*$^{+/+}$**

pulse alone (dB)	pre-pulse followed by tone (dB)		
0-110	**65-110**	**70-110**	**75-110**
1499.1	1037.5	956.9	700.7
1038.9	862.1	881.2	867
1526.8	447.3	278.7	299.4
1975.4	1631	1274.9	1171.3
2022.7	1099.8	781.8	859.2
1858	777.7	738.8	766.8
1543.1	1308.5	1571.3	1427.7
1413.3	971.8	1085.9	755.1
1548.9	1307	911.2	1117.8
1816.4	1220.4	1569.9	1129.4
1906.6	1291.5	1060.1	425.5
694.6	645.8	537.2	437.2

***Zfhx3*$^{Sci/+}$**

pulse alone (dB)	pre-pulse followed by tone (dB)		
0-110	**65-110**	**70-110**	**75-110**
1688.8	1279	950.4	739.9
894.2	420.1	521.2	363.2
1154.7	470.1	487.7	679.7
1411.1	683.7	638.5	404
1892.3	1161.1	1672.8	1262.9
737.8	470.5	202.6	263.8
1620	919	744.6	547.8
1062.1	938	607.9	471.8
565.9	504.7	426.8	575
1607.5	893.1	759.8	838.8
1955.1	861.7	704.7	394
1535.8	1137.5	1164.8	1117.7
1516.6	951.8	1355	1050.5

Table 38: Raw data for the startle reflex response to a 110 dB tone with or without being preceded by a pre-pulse. Animals were subjected to 15 trials of each combination of tone, in a randomized order. The maximal value was recorded and converted to an arbitrary unit.

	Zfhx3 $^{+/+}$	*Zfhx3* $^{Sci/+}$	*Zfhx3* $^{+/+}$	*Zfhx3* $^{Sci/+}$	*Zfhx3* $^{+/+}$	*Zfhx3* $^{Sci/+}$
% PPI	**65 dB**		**70 dB**		**75 dB**	
	30.79	24.27	36.17	43.72	53.26	56.19
	17.02	53.02	15.18	41.71	16.55	59.38
	70.70	59.29	81.75	57.76	80.39	41.14
	17.43	51.55	35.46	54.75	40.71	71.37
	45.63	38.64	61.35	11.60	57.52	33.26
	58.14	36.23	60.24	72.54	58.73	64.25
	15.20	43.27	-1.83	54.04	7.48	66.19
	31.24	11.68	23.17	42.76	46.57	55.58
	15.62	10.81	41.17	24.58	27.83	-1.61
	32.81	44.44	13.57	52.73	37.82	47.82
	32.26	55.93	44.40	63.96	77.68	79.85
	7.03	25.93	22.66	24.16	37.06	27.22
		37.24		10.66		30.73
AVERAGE	**31.16**	**37.87**	**36.11**	**42.69**	**45.13**	**48.57**
STDEV	**19.00**	**15.87**	**23.61**	**19.60**	**22.12**	**22.10**
STERR	**5.49**	**4.40**	**6.81**	**5.44**	**6.39**	**6.13**
T TEST	**65 dB**	**0.35**				
	70 dB	**0.45**				
	75 dB	**0.70**				

Table 39: Pre-pulse inhibition calculated as a percentage of the initial startle response. The percentage PPI was calculated using the formula described in Equation 1. There was no significant difference between *Zfhx3*$^{+/+}$ and *Zfhx3*$^{Sci/+}$ (T TEST, $p > 0.05$ for each dB).

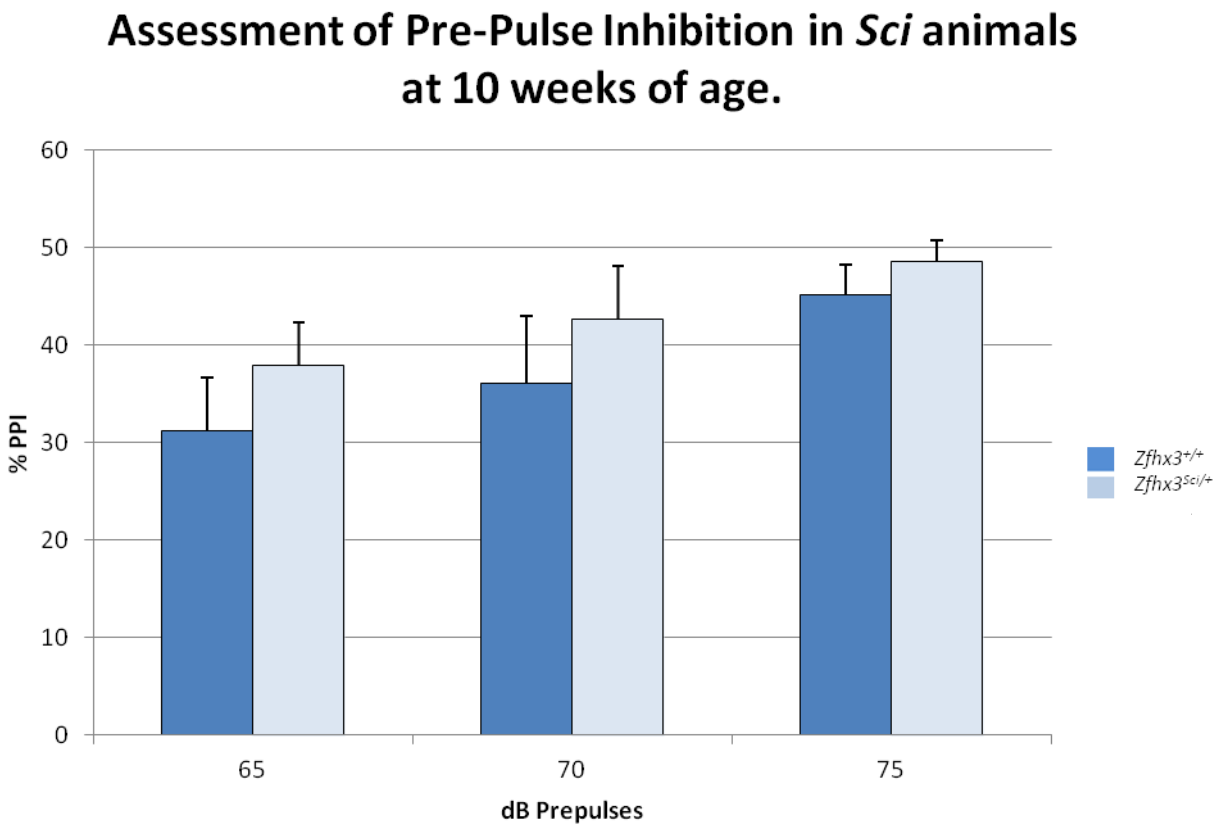

Figure 48: Bar chart representation of the percentage pre-pulse inhibition. The data shown is based upon the calculated averages in Table 2, with error bars representing the standard error of the mean. There was no significant difference between *Zfhx3*$^{+/+}$ and *Zfhx3*$^{Sci/+}$mice in pre-pulse inhibition at 10 weeks of age. As expected, as the pre-tone increased from 65 – 70 – 75 dB, an increase in inhibition was observed.

6.3. Morphological analysis of *Sci* eyes

6.3.1. Retinal Histology

Histological assessment of *Zfhx3*$^{+/+}$and *Zfhx3*$^{Sci/+}$eyes was performed in order to determine whether there were any physiological abnormalities between the two genotypes that may contribute to the circadian behavioural phenotype. Whole eye sagittal sections were cut and then stained using haematoxylin and eosin (H&E) to label the nuclei (blue) and cytoplasm (pink).

Three *Zfhx3*$^{+/+}$ and *Sci*$^{M/+}$ eyes were analysed. Six slides for each animal were taken from along the same axis, which included sections that transected the optic nerve, from which a total of six images were taken. Images were collected from either side of the fovea as shown in Figure 49. In order to assess the integrity of the retinal physiology, images were taken and measurements made throughout the inner nuclear layer (INL) and outer nuclear layer (ONL) (Figure 50 A, C). Six measurements of the INL and ONL were taken from each image and these were averaged in order to account for variations throughout the retinal layer within each image (Figure 50 B, D). A ratio of the INL:ONL was calculated to compensate for any variation in INL and ONL thickness depending on where in the retina the image was taken, making the assumption that the thickness of each layer compared to each other remained constant. The summarised data and graphical representation is shown in Table 40, Figure 51 Figure 52. There was no significant difference in the thickness of the INL, ONL or the INL:ONL between *Zfhx3*$^{+/+}$ and *Zfhx3*$^{Sci/+}$.

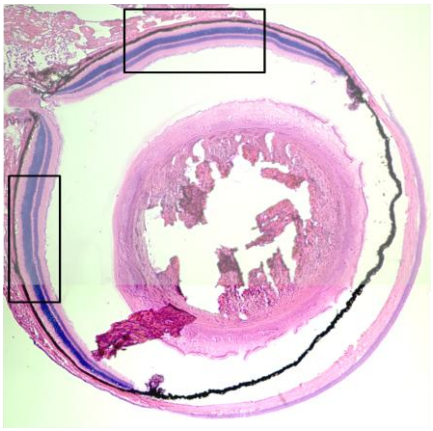

Figure 49: Bright-field image taken of H&E stained whole eye section. The image shows a sagittal section through the whole eye, with all structures maintained. The black boxes indicate areas where images were taken in relation to the fovea for assessment of the retinal layers. Blue/purple = nuclei, pink = cytoplasm.

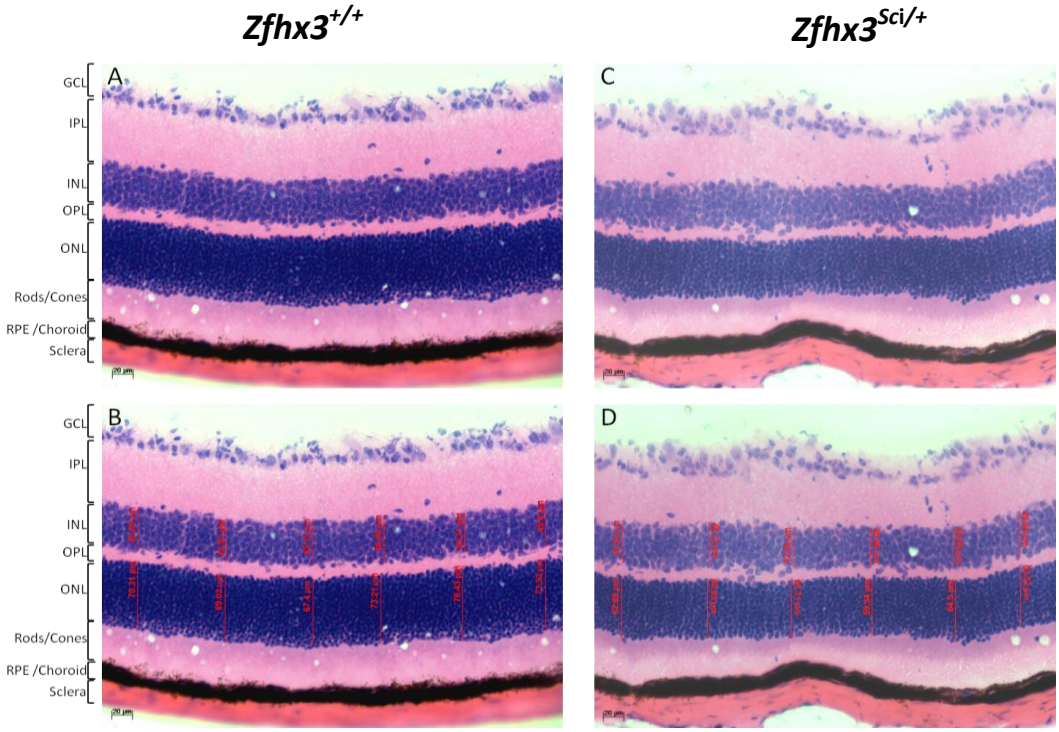

Figure 50: Representative images taken of *Zfhx3*$^{+/+}$ and *Zfhx3*$^{Sci/+}$ retinas on X20 objective. (A) *Zfhx3*$^{+/+}$ retina and (B) corresponding measurements taken throughout the INL and ONL of the same image. (C) *Zfhx3*$^{Sci/+}$ retina and (D) corresponding measurements taken throughout the INL and ONL of the same image. GCL: ganglion cell layer. IPL: Inner plexiform layer. INL: Inner nuclear layer. OPL: Outer plexiform layer. ONL: Outer nuclear layer. RPE: Retinal pigmented epithelium.

***Zfhx3*$^{+/+}$**

	INL (μm)	ONL (μm)	INL:ONL
Average	39.51	62.29	0.63
Stdev	5.29	7.87	0.06
Sterr	1.25	1.85	0.01

***Zfhx3*$^{Sci/+}$**

	INL (μm)	ONL (μm)	INL:0NL
Average	36.37	57.98	0.63
Stdev	6.52	10.30	0.06
Sterr	1.81	2.86	0.02

Table 40: Combined data of INL and ONL retinal thickness and INL:ONL ratio in Sci animals. Six individual measurements from one field of view were taken of the INL and ONL from three separate H&E stained sections of one individual animal. All measurements were then averaged and combined to produce an average INL or ONL thickness in μm. The INL:ONL was then calculated to take into consideration differences in thickness across the retina.

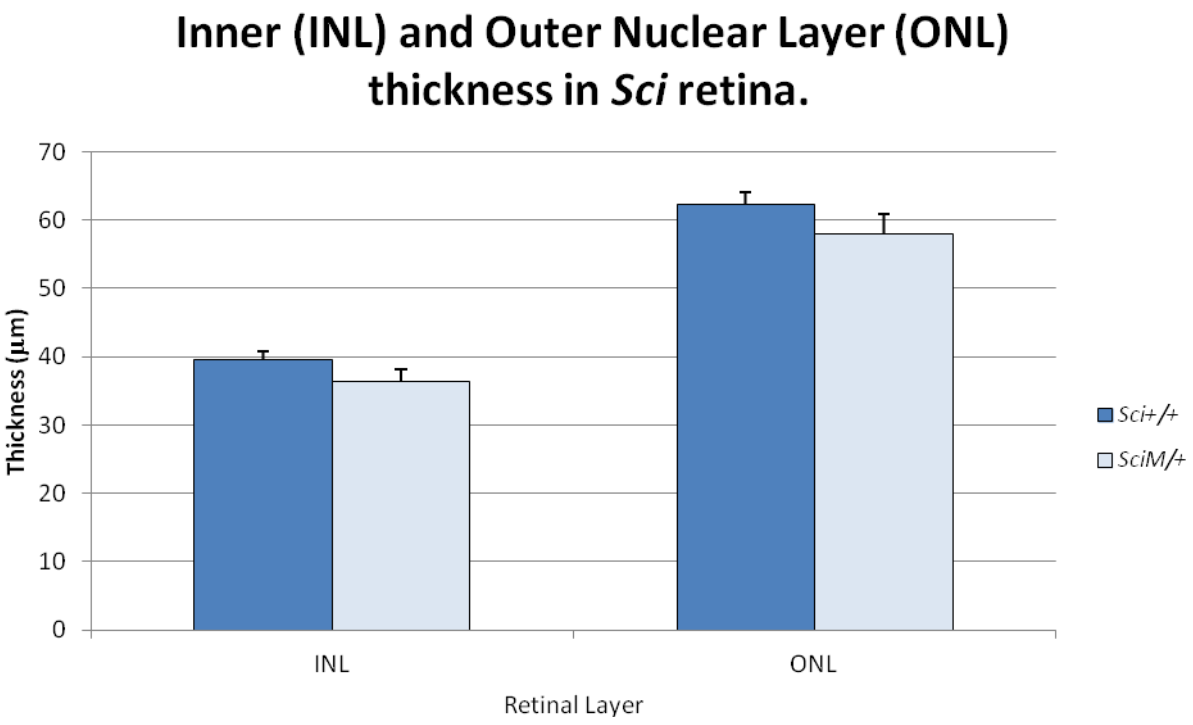

Figure 51: Bar-chart comparison of INL and ONL between *Zfhx3*$^{Sci/+}$ and *Zfhx3*$^{+/+}$ retinas. Measurements of the INL and ONL were taken from sections taken through the whole eye stained using H&E. These measurements were used as an indicator of normal retinal morphology. There was no significant difference between *Zfhx3*$^{+/+}$ and *Zfhx3*$^{Sci/+}$ in INL and ONL thickness (µm) (2-tail T TEST INL: p = 0.15, ONL: p = 0.33). Three individual animals were analysed, six separate sections imaged for each animal and six measurements taken per image. Error bars show the standard error of the mean.

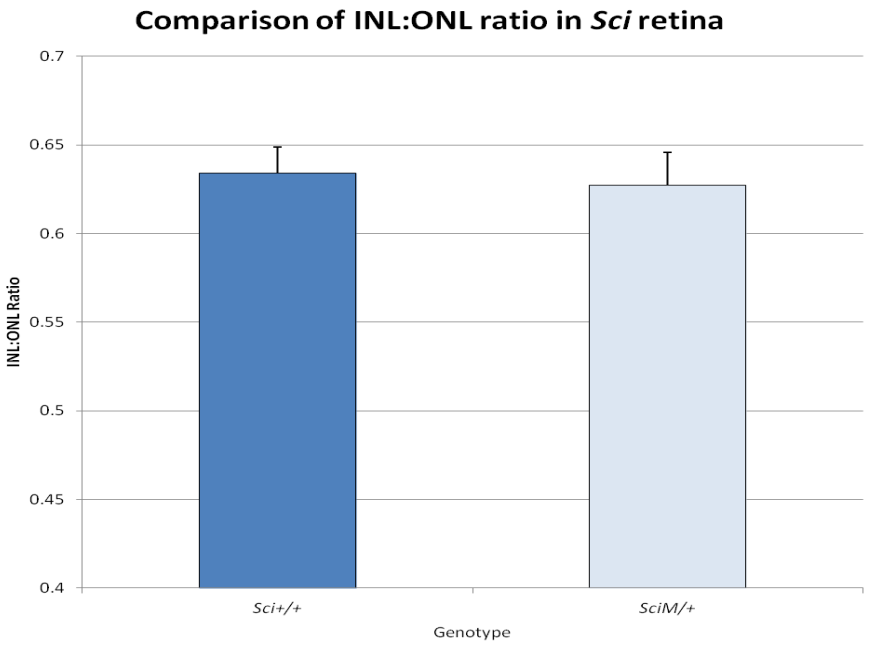

Figure 52: Bar chart representation of INL: ONL ratio between *Zfhx3*$^{Sci/+}$ and *Zfhx3*$^{+/+}$ retinas. A ratio of INL:ONL was calculated in order to control for retinal layer thickness variations depending on where in the retina the image was taken. The retina varies in thickness throughout the eye – tapering at the fovea and towards the front of the eye where it meets the cornea. There was no significant difference in INL:ONL between *Zfhx3*$^{+/+}$ and *Zfhx3*$^{Sci/+}$ (2-tail T TEST, p = 0.75).

6.3.2. Corneal histological assessment

The cornea is the first cell layer of the eye where light first enters and is refracted and absorbed and focused onto the retina. The cornea represents approximately two thirds of the entire refractive power of the eye (MAURICE 1957). Since *Zfhx3* RNA expression was detected by *in situ* hybridisation in the cornea, corneal measurements and morphological analysis was also performed as with the retina. Corneal thickness was analysed in the same way as the retina as described above. Measurements were taken around the mid-point of the cornea, measuring the upper epithelial cell layer and the total corneal thickness (epithelium – stroma – endothelium). The same adult eye sections stained using H&E, from which retinal measurements were taken, were used for corneal measurements.

Representative images of the H&E stained corneas of $Zfhx3^{+/+}$ and $Zfhx3^{Sci/+}$ are shown in Figure 53. The averaged data of the epithelium and total corneal thickness for both $Zfhx3^{+/+}$ and $Zfhx3^{Sci/+}$ is shown in Table 41 and shown graphically in Figure 54.

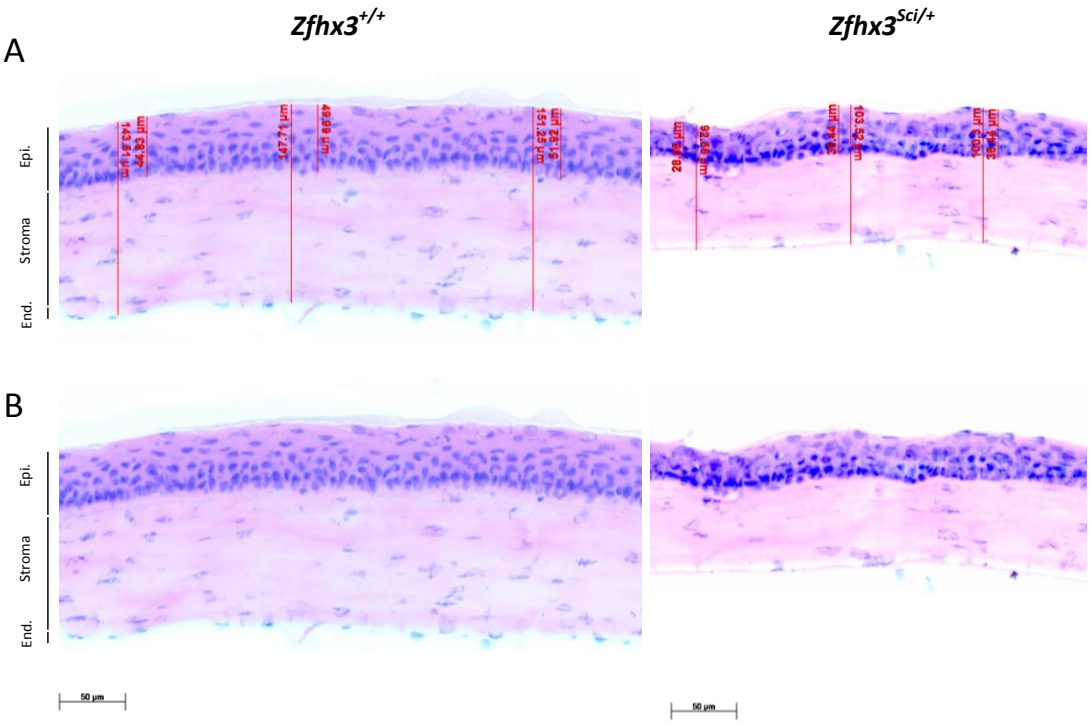

Figure 53: Images taken of H&E stained corneas from *Sci* animals. (A) Measurements taken across the cornea of *Zfhx3*$^{+/+}$ and *Zfhx3*$^{Sci/+}$ H&E stained sections. (B) Raw images of corneas before measurement. Images show the Epithelium (Epi), Stroma and Endothelium (End).

***Zfhx3*$^{+/+}$**

	Average (μm)	STERR
Epi - Endo	157.06	3.23
Epithelium	45.56	0.52
Ratio	0.29	0.00

***Zfhx3*$^{Sci/+}$**

	Average (μm)	STERR
Epi - Endo	111.35	1.85
Epithelium	38.64	0.81
Ratio	0.35	0.01

2-Tail T TEST

Epi-Endo	3.98E-19
Epithelium	6.36E-10
Ratio	9.38E-09

Table 41: Comparison of corneal thickness from H&E stained adult eye sections. Three measurements were taken per field of view with four sections examined per animal. Three *Zfhx3*$^{+/+}$ and three *Zfhx3*$^{Sci/+}$ were analysed. The epithelial cell layer and the total thickness (Epi-Endo) was measured and a ratio of the two was calculated. 2-Tail T TESTs showed that there was a significant difference between *Zfhx3*$^{+/+}$ and *Zfhx3*$^{Sci/+}$ total corneal thickness, epithelium thickness and the ratio. The *Zfhx3*$^{Sci/+}$ mutants have significantly thinner corneas, the majority due to a thinning of the stromal layer as implicated by the larger Epi: Epi-Endo ratio.

A

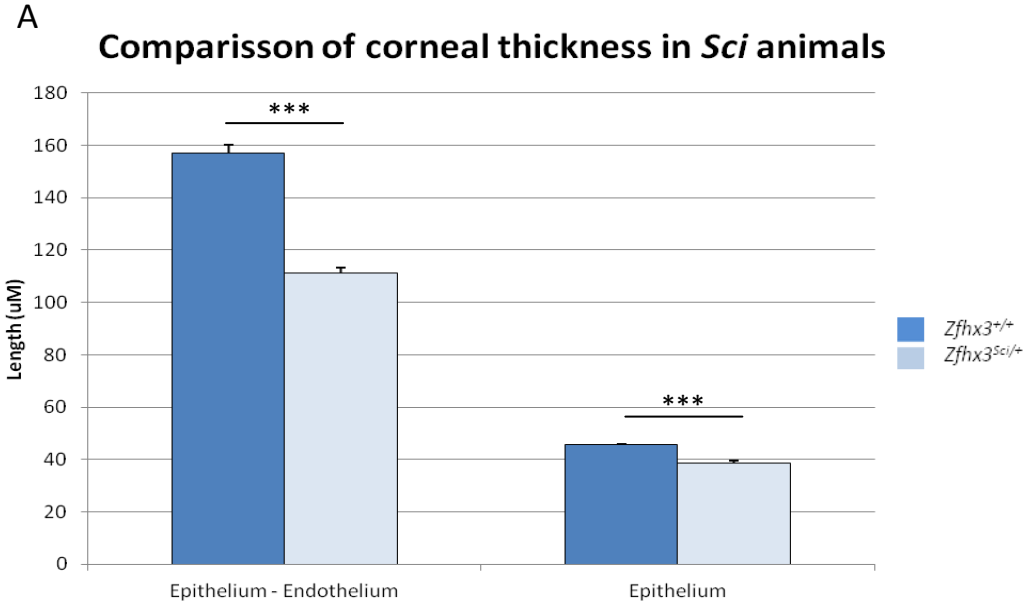

B

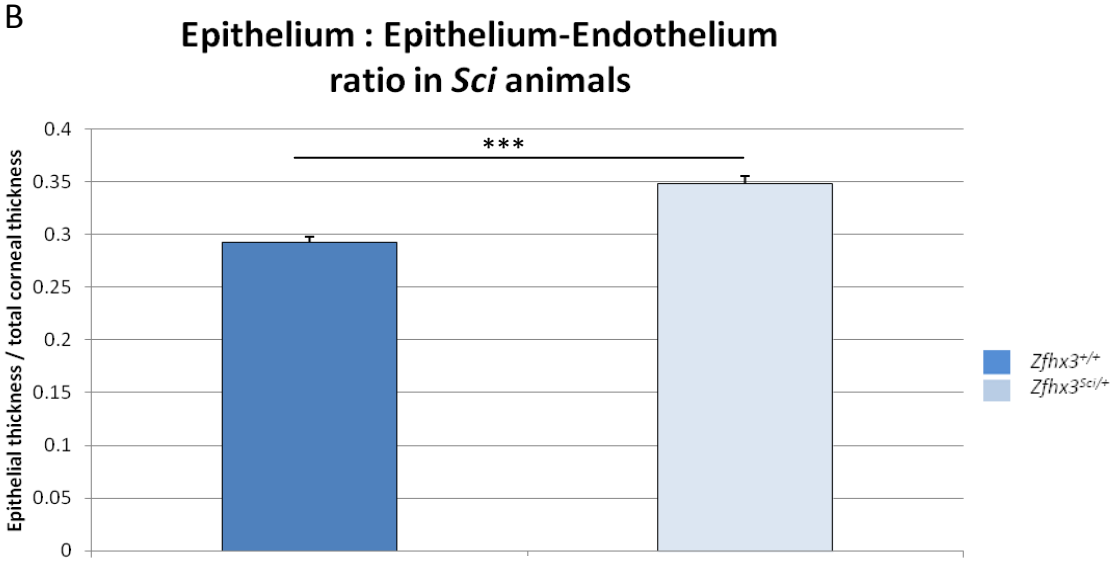

Figure 54: Measurements of corneal thickness in *Sci* mutants. (A) Measurements taken of the total corneal thickness from sagittal whole adult eye sections stained using H&E. Total corneal thickness spanned from the epithelial layer to the endothelial layer. The epithelial cell layer was measured independently. Average lengths are shown in μm. (B) Calculated ratio of Epithelium : Epithelium-Endothelium. This measure demonstrates a skew in the proportions between the epithelial cell layer and the total thickness of the cornea. The data shows that the *Zfhx3*$^{Sci/+}$ animals have significantly thinner corneas compared to *Zfhx3*$^{+/+}$. (2-Tail T TEST Epi-Endo, Epithelium, Epithelium: Epi-Endo: $p < 0.0001$). Error bars show the standard error of the mean.

A significant reduction in corneal thickness was identified in the *Zfhx3*$^{Sci/+}$ animals compared to *Zfhx3*$^{+/+}$. This may impact on the visual capacity of the *Zfhx3*$^{Sci/+}$, in particular in light refraction and acuity, as well as potentially increased light reaching the retina due to reduced absorption. This may also cause photophobia in the *Zfhx3*$^{Sci/+}$ mutants which affect circadian behaviour under light conditions. This would be consistent with the disrupted behaviour during entrainment and constant light conditions observed in wheel running screens in the *Zfhx3*$^{Sci/+}$ mutants discussed in Chapter III.

While a molecular role for *Zfhx3* in the cornea remains unknown, however the close homologue *Zeb1 (Zfhx1a)* has known functions in the cornea with mutations known to associate with various corneal dystrophies (Liskova, et al. 2007). *Zeb1* null mice display a thickened corneal phenotype reminiscent of the human condition Posterior polymorphous corneal dystrophy (PPCD) (Liu, et al. 2008b). Conversely, over-expression of *Zeb1* shows a mirrored phenotype, with a corneal thinning from an increased epithelial-mesenchymal transition (Liu, et al. 2008a). Extrapolation from this data it may suggest that *Zfhx3* also has a role in the maintenance of the corneal epithelial and stroma layers and given its known role as an anti-mitotic factor, it may be similarly involved in the balance of cellular turnover. The outer epithelial cell layer undergoes rapid turnover due to exposure to external environmental damage whereas the cellular turnover of the stromal layer is slow. One mechanism may be that in *Zfhx3*$^{Sci/+}$ mice, cells of this layer are being degenerated more quickly or replaced at a slower rate as a result of the mutation to *Zfhx3*.

6.4. Visual and image forming capabilities in *Sci* animals

6.4.1. Slit lamp, ophthalmoscope and optokinetic drum head tracking

Sci mice were assessed for deficits in eye morphology, retinal structure and visual acuity using three phenotyping tests; slit lamp, ophthalmoscope and optokinetic drum. A cohort of 10 *Zfhx3*$^{+/+}$ and 8 *Zfhx3*$^{Sci/+}$ male animals, all aged between 10 – 12 weeks were phenotyped. The animals, progeny from a cross between C3H-BL6/J F1 animals, may have inherited the C3H linked mutation for retinal degeneration (rd), at a frequency of 25%. In these instances, homozygous animals for the C3H rd mutation would be retinally degenerate by 3 - 4 weeks of age and therefore if any of the cohort analysed were homozygous for this allele, retinal degeneration would be detected at this age. Of the 18 animals tested, one *Zfhx3*$^{+/+}$ animal showed mild retinal degeneration, as assessed using an ophthalmoscope. This animal was removed from the subsequent analyses with the optokinetic drum.

The slit lamp allowed for a rapid assessment of pupil constriction, which was later analysed in more detail and is discussed later in this chapter. As expected, all animals displayed a normal pupil response when presented with a broad slit beam in a dark external environment. No dysmorphologies were observed in the anterior segment of the eye, including structural abnormalities in the lens or opacities or cataracts. The ophthalmoscope was then used to evaluate the fundus of the eye. A drop of 1% tropicamide was used as a local anesthetic to dilate the pupil to avoid the pupil response interfering with assessment of the eye. Under these observations, the single retinal degenerate mouse was identified. All other animals showed normal retinal morphology and blood vessels. From both these tests, it was concluded that the structure of the eye appeared grossly normal, using non-invasive procedures.

Following the assessment of eye for signs of disease, dysmorphia or retinal degeneration, all animals were phenotyped for visual acuity by monitoring optomotor movements using the virtual reality optokinetic drum. This apparatus (shown in Figure 55) was used to determine the threshold at which animals were unable to resolve a pattern presented by monitoring the reflexive head-tracking response. It is known that retinally degenerate mice show no head tracking and therefore score 0 for this test (Thaung, et al. 2002). The one animal identified as retinally degenerate was used as a negative control and as predicted, scored 0 for the optokinetic drum and was removed from subsequent analyses. Monocular acuity could be determined by changing the rotation direction of the visual field, clockwise for the left eye and anti-clockwise for the right eye. The results indicated that for the right eye individually, and left and right eyes combined, the *Zfhx3*$^{Sci/+}$ had significantly decreased visual acuity by 25% (right eye) and 16 % (combined). This trend was observed for the left eye although it was not significant (10.5% decrease). The data is shown in Table 42 and Figure 56.

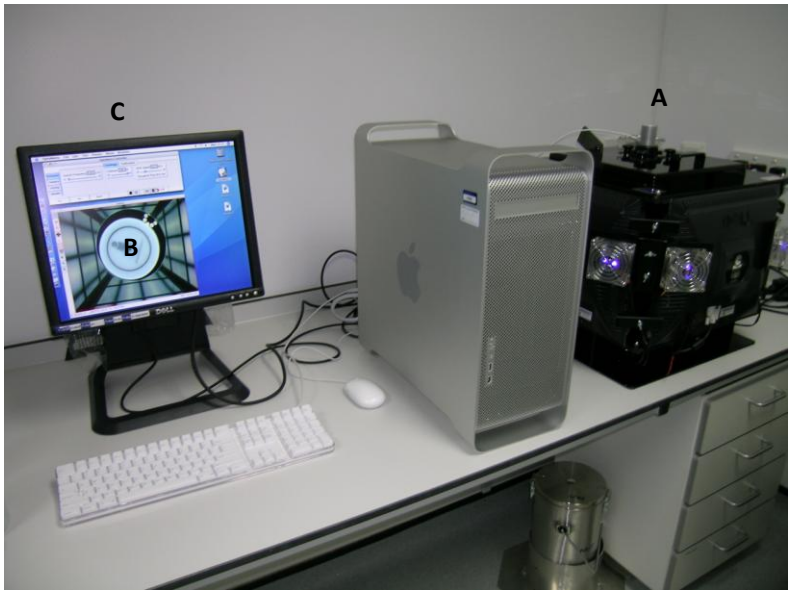

Figure 55: Photograph of the Optokinetic drum and computer set up. The animals were placed within the enclosed apparatus which consisted of 4 computer screens arranged as an enclosed square, with a black lid on top to control the external environmental light (A). In the centre of the 4 surrounding screens was a raised circular platform on which the mouse could freely move (shown in B in the video image). A camera was positioned above the apparatus and the live image was portrayed on the computer screen (C). From the computer, the pattern that was presented on the computer screens within the drum apparatus could be controlled. The mouse was monitored throughout for evidence of head-tracking, as well as a continual assessment of the well-being of the animal.

(A)

Zfhx3$^{+/+}$	Visual Acuity c/d	
	Left eye	**Right eye**
SCI-B6-C3/36.3b	0.300	0.397
SCI-B6-C3/36.3c	0.217	0.328
SCI-B6-C3/42.1g	0.214	0.264
SCI-B6-C3/35.12f	0.328	0.333
SCI-B6-C3/35.12g	0.364	0.364
SCI-B6-C3/35.12h	0.328	0.431
SCI-B6-C3/35.12i	0.197	0.281
SCI-B6-C3/35.10k	0.136	0.253
SCI-B6-C3/35.13j	0.300	0.361
Average	**0.265**	**0.335**
sterr	**0.025**	**0.020**
Combined average (left and right)	**0.300**	
Combined sterr	**0.018**	

(B)

Zfhx3$^{Sci/+}$	Visual Acuity c/d	
	Left eye	**Right eye**
SCI-B6-C3/37.3d	0.137	0.192
SCI-B6-C3/37.3g	0.289	0.350
SCI-B6-C3/37.3i	0.139	0.31
SCI-B6-C3/42.1h	0.286	0.256
SCI-B6-C3/35.12j	0.253	0.233
SCI-B6-C3/35.12k	0.225	0.314
SCI-B6-C3/35.12l	0.275	0.200
SCI-B6-C3/35.13i	0.275	0.272
AVERAGE	**0.235**	**0.268**
sterr	**0.022**	**0.021**
Combined average (left and right)	**0.252**	
Combined sterr	**0.015**	

(C)

T TESTS	
Left eye	0.394
Right eye	0.037
Combined	0.051

Table 42: Visual acuity (cycles/degree ; c/d) of each eye in *Zfhx3*$^{+/+}$ and *Zfhx3*$^{Sci/+}$ animals. The data values represent the threshold at which animals displayed reflexive head-tracking to a rotating visual stimulus. (A) Visual acuity for *Zfhx3*$^{+/+}$ animals left and right eyes. (B) Visual acuity for *Zfhx3*$^{Sci/+}$ animals for left and right eyes. A summation of the left and right eye visual acuity was generated as a marker of binocular visual acuity. (C) 2-tailed T-Tests comparing the left eye and right eye separately between the two genotypes. No significant difference was observed in the left eye but significantly decreased acuity in the right eye (p = 0.394 and p = 0.037 respectively). A significant difference was observed for combined vision, with a significant decrease in visual acuity in the *Zfhx3*$^{Sci/+}$ animals (p = 0.051).

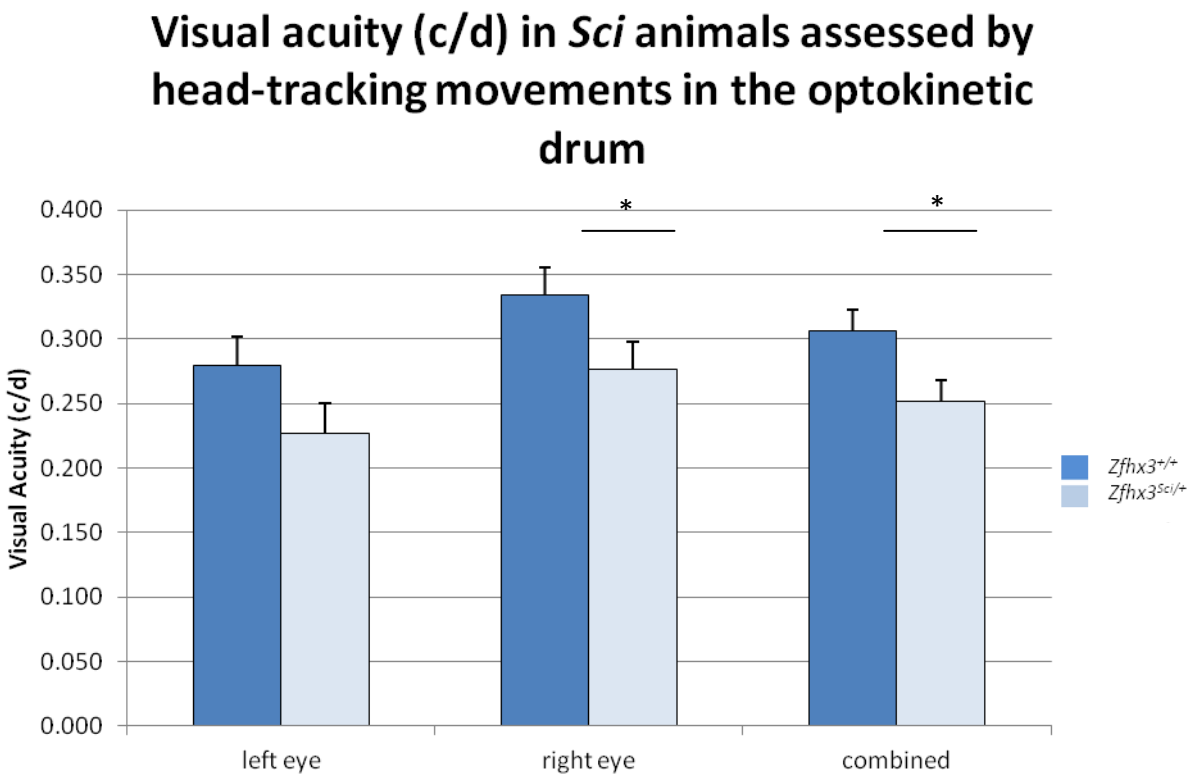

Figure 56: Comparison of visual acuity between *Zfhx3*$^{+/+}$ and *Zfhx3*$^{Sci/+}$ using the Optokinetic drum to monitor head tracking. No significant differences were observed between *Zfhx3*$^{+/+}$ and *Zfhx3*$^{Sci/+}$ when assessing the visual acuity of the left eye individually, although there is a trend in decreased visual acuity in *Zfhx3*$^{Sci/+}$. There was a significant difference in the visual acuity between *Zfhx3*$^{+/+}$ and *Zfhx3*$^{Sci/+}$ when comparing the right eye individually and the averaged visual acuity of both the left and right eyes ($p = 0.037$ and $p = 0.051$ respectively).

It is hypothesized that this reduction in visual acuity is due to the thinning of the cornea as previously discussed due disrupted optical refraction. From the phenotyping performed it is possible to rule out any retinal or grossly abnormal eye morphologies and any conditions such as glaucoma or cataracts. There may be a molecular component to this phenotype which remains to be analysed. Since the slit lamp and ophthalmoscope assessment did not identify any morphological deficits, differences observed in head-tracking may be either due to cortical responses, alterations in the optic nerve transmission or functionality of the retina that is not

apparent visually. However, it is known that a thinning of the cornea would result in a decrease in visual acuity, commonly identified in human patients and other animal models of corneal dystrophy (Krachmer, et al. 1984). The function of the cornea is to refract the majority of light entering the eye, allowing for it to be focused and produce an image on the retina.

6.4.2. Pupillary Response of *Sci* Animals

Assessment of the pupillary light reflex was carried out by Dr's Stuart Peirson and Carina Pothecary (Department of Ophthalmology, University of Oxford). A cohort of eight *Zfhx3*$^{+/+}$ and eight *Zfhx3*$^{Sci/+}$ female animals were phenotyped between 6 - 9 months of age. None of the animals phenotyped had retinal degeneration.

The pupillary light reflex was assessed in order to determine the accurate functioning of the retina. Signaling of the pupillary reflex begins at the melanopsin ganglion cells and goes via the optic tract fibers to the superior colliculus which terminate in the pretectal area of the midbrain. Axons from here are sent bilaterally to terminate in the Edinger-Westphal nucleus of the oculomotor complex. Axons of parasympathetic pre-ganglionic neurons project and terminate in the ciliary ganglion and axons finally terminate on the iris sphincter. The pupillary response to light is consensual since the optic tract carries visual information from both the left and right eyes and the projections from the pretectal area are bilateral. Figure 57 illustrates this signaling pathway. Therefore by measuring the consensual pupillary reflex, the entire reflexive pathway is assessed. Defects identified may attribute the involvement of *Zfhx3* within this signaling cascade that produces this pupillary response.

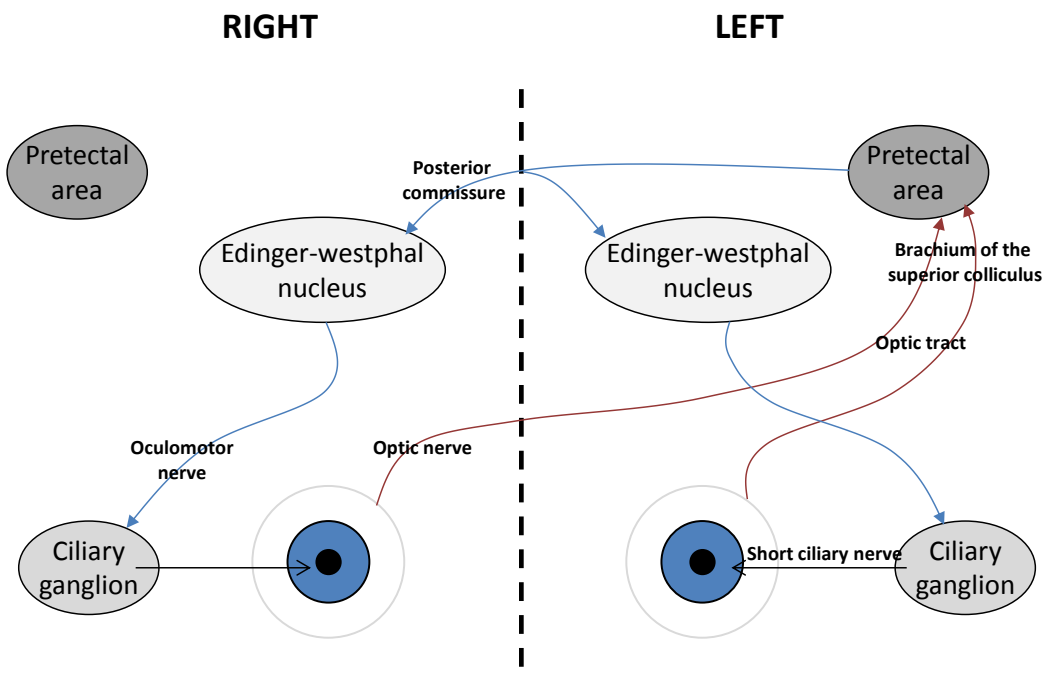

Figure 57: Pupillary light reflex pathway. Arrow heads indicate the structure where axons terminate. The reflexive pathway starts with the optic nerve carrying photic information originating from the intrinsically photoreceptive ganglion cells. The optic tract carries visual information from both the left and right eyes and the pretectal area projects to both Edinger-Westphal nuclei. As a result of the nature of this pathway, the normal pupillary response to light is consensual. When a light is directed to one eye, it results in constriction of the pupils of both eyes. (Figure adapted from Neuroscience Online, Valentin Dragoi, Ph.D).

Animals were dark adapted to ensure full pupil dilation. Animals were then manually restrained without use of any anesthesia and presented with a light stimulus to one eye. The consensual pupillary constriction of the alternate eye was then video recorded and later analysed. The light stimulus duration was 10 seconds, and the stimuli presented were at approximately 14.6, 11.6, 10.1 and 9.1 log quanta/cm^2/s and repeated over separate occasions. Each experiment was conducted at minimum three times independently. Figure 58 shows the results of these experiments performed at each light intensity.

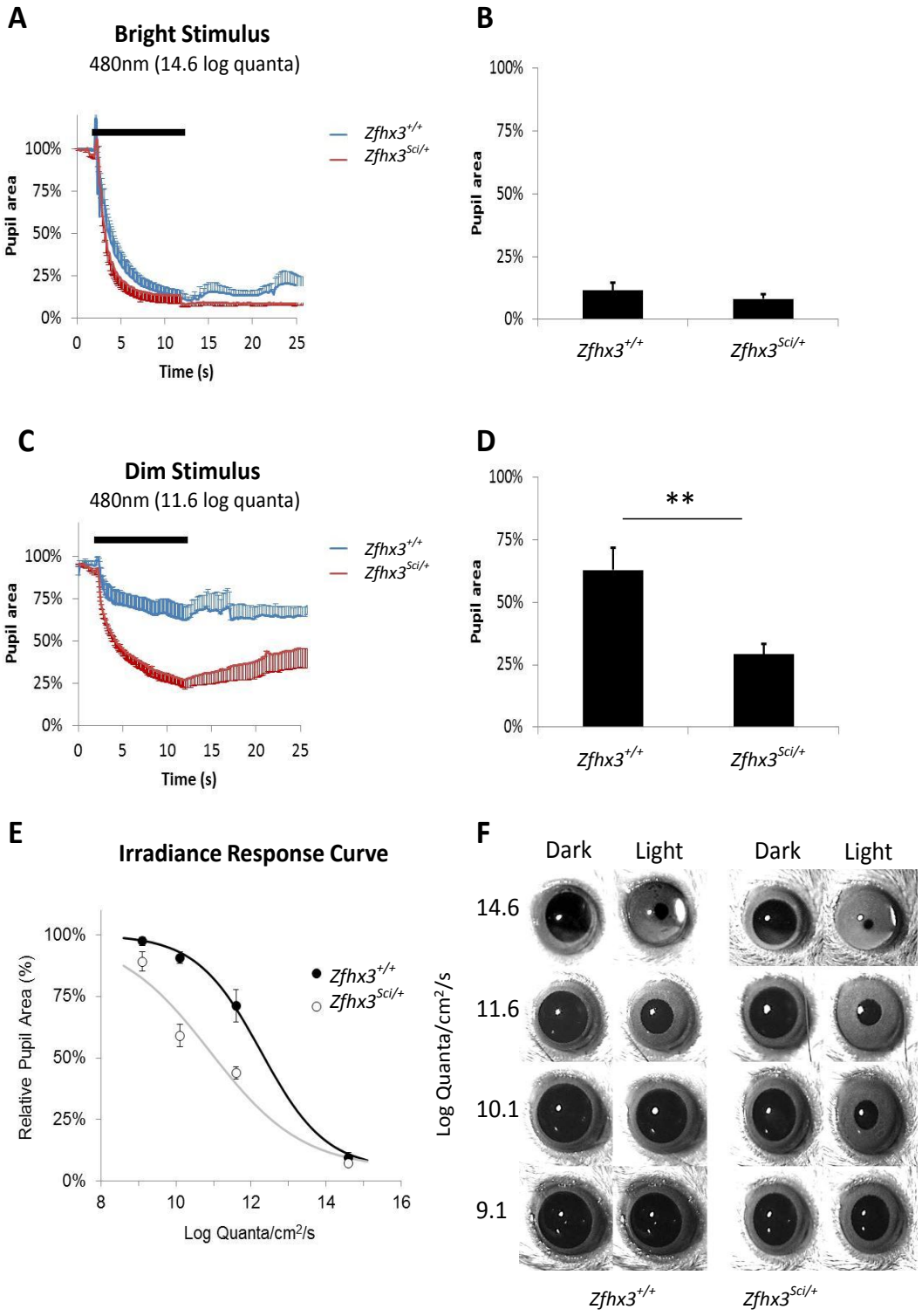
A
Bright Stimulus
480nm (14.6 log quanta)
Pupil area
100%
75%
50%
25%
0%
0
5
10
15
20
25
Time (s)
Zfhx3+/+
Zfhx3Sci/+
B
Pupil area
100%
75%
50%
25%
0%
Zfhx3+/+
Zfhx3Sci/+
C
Dim Stimulus
480nm (11.6 log quanta)
Pupil area
Time (s)
Zfhx3+/+
Zfhx3Sci/+
D
**
Pupil area
Zfhx3+/+
Zfhx3Sci/+
E
Irradiance Response Curve
Relative Pupil Area (%)
100%
75%
50%
25%
0%
8
10
12
14
16
Log Quanta/cm2/s
Zfhx3+/+
Zfhx3Sci/+
F
Dark
Light
Dark
Light
14.6
11.6
10.1
9.1
Log Quanta/cm2/s
Zfhx3+/+
Zfhx3Sci/+

Figure 58: Characterisation of the pupillary light reflex response in *Sci* animals. Animals were dark adapted to ensure full pupil dilation. One eye was then exposed to a light stimulus and the consensual pupillary constriction was recorded and measured. (A) Change in pupil area over time during and after a bright stimulus (14.6 log quanta/cm^2/s). *Zfhx3*$^{+/+}$ response shown in blue and *Zfhx3*$^{Sci/+}$shown in red. (B) The bar chart represents the pupil size when fully constricted in response to the bright light stimulus. The pupil area is equivalent between *Zfhx3*$^{+/+}$ and *Zfhx3*$^{Sci/+}$ animals at approximately 10%. (C) Change in pupil size during and following exposure to a dim light stimulus (11.6 log quanta/cm^2/s). *Zfhx3*$^{Sci/+}$ show over constriction of the pupil in response to the dim light. (D) Bar chart representation of the pupil area after stimulation with a dim light stimulus. *Zfhx3*$^{+/+}$ animals constrict to approximately 60% whereas *Zfhx3*$^{Sci/+}$ animals constrict to approximately 25%. This is a significant difference in pupil constriction at this light stimulus (2-tail T TEST, p = 0.0078). (E) The relative percentage pupil area performed across four irradiances showing a shift in the irradiance response curve between *Zfhx3*$^{+/+}$ and *Zfhx3*$^{Sci/+}$ animals. *Zfhx3*$^{Sci/+}$ have an approximately twenty-fold increased sensitivity to bright light, a difference of 1.36 log units. (F) Representative images of the pupil size both before (Dark) and after (Light) stimulation from which the pupil area was measured.

With a bright stimulus (14.6 log quanta/cm^2/s), pupillary constriction was equivalent between *Zfhx3*$^{+/+}$ and *Zfhx3*$^{Sci/+}$ animals. At dimmer stimuli (11.6 and 10.1 log quanta/cm^2/s) *Zfhx3*$^{Sci/+}$ showed a significant over-constriction of the pupil compared to *Zfhx3*$^{+/+}$ ($p = 0.0078$). This suggested that *Zfhx3*$^{Sci/+}$ were over-sensitive to dimmer light stimuli, perceiving the light source at a higher intensity in terms of pupillary constriction. With an even dimmer stimulus of 9.1 log quanta/cm^2/s, *Zfhx3*$^{+/+}$ and *Zfhx3*$^{Sci/+}$ appeared equivalent in pupillary constriction. This suggests a shift in the irradiance response curve between *Zfhx3*$^{+/+}$ and *Zfhx3*$^{Sci/+}$ animals, with each opposing end of the scale at saturation for observing differences in pupillary constriction. From the irradiance response curve, a difference in sensitivity of 1.36 log units was shown between the *Zfhx3*$^{+/+}$ and *Zfhx3*$^{Sci/+}$ animals, and this equates to an approximately twenty-fold increased sensitivity to bright light stimuli in the *Zfhx3*$^{Sci/+}$ animals based upon their pupillary response. This phenotype has not been observed in any other animal model to date and appears to be a novel

gain of function response in the *Zfhx3*$^{Sci/+}$ animals. The phenotype is the opposite to that observed in *Opn4*$^{-/-}$ mutants where the pupil fails to fully constrict in response to a light stimulus.

6.4.3. Electroretinogram assessment in *Sci* animals

Zfhx3$^{Sci/+}$ animals were assessed for electrical responses of the retina by electroretinography (ERG) and flash visual evoked potential (VEP) recordings. Dr Alun Barnard (Department of Ophthalmology, University of Oxford) performed ERG and flash VEP measurements on the *Sci* animals. This test measures the electrical responses of cell types of the retina, including the amacrine and bipolar cells of the inner retina, photoreceptors including rods and cones, and the retinal ganglion cells. Measurements were taken from electrodes placed on the cornea and the evoked action potentials in volts were recorded across time in response to a photic stimulus. The pupils were dilated using a local anesthetic such that any differences in pupil area in response to the light would not confound results.

The total ERG recordings show the stages of electrical potentials which are produced by the different cell types of the retina. It is possible to analyse these traces at the level of the cell type and attribute any defects down to the cell type responsible. Different stimuli create different responses and may be used to identify the components of the electrical potentials. ERG recordings were taken on both the dark adapted eye to isolate predominantly rod photoreceptor function and light adapted eyes to investigate cone photoreceptor function.

Overt phenotypes were not detected in the ERG recordings, suggesting overall normal electrical activity of the retina. The dark-adapted recordings however did show slightly larger a-wave amplitude. This wave represents the initial negative deflection and is the electrical component

represented by the photoreceptors, predominantly the rod cells. No clear differences were identified in light-adapted recordings. Results are shown in Figure 59 (A, B, E, and F).

Flash VEP recordings were then taken using electrodes placed sub-dermally over the striate cortex. A white strobe light was flashed and measurements were taken at the cortex. The data reflects the arrival of the visual signal at the cortex and the cortical response. In the dark adapted recordings, across all intensities, a slightly larger p1 to n1 amplitude was detected in the *Zfhx3*$^{Sci/+}$ animals. Results are shown in Figure 59 (C, D, G, and H).

Dark adapted ERG recordings and irradiance response curve

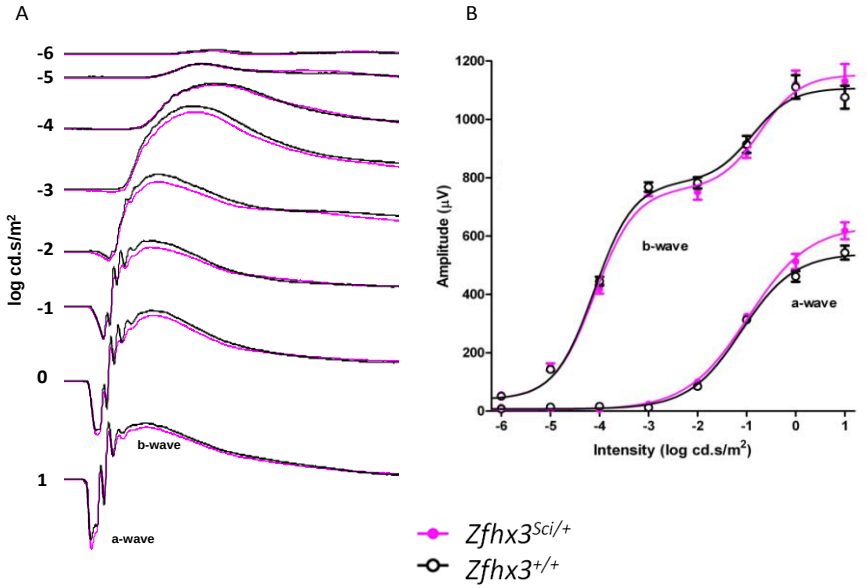

Dark adapted VEP recordings and irradiance response curve

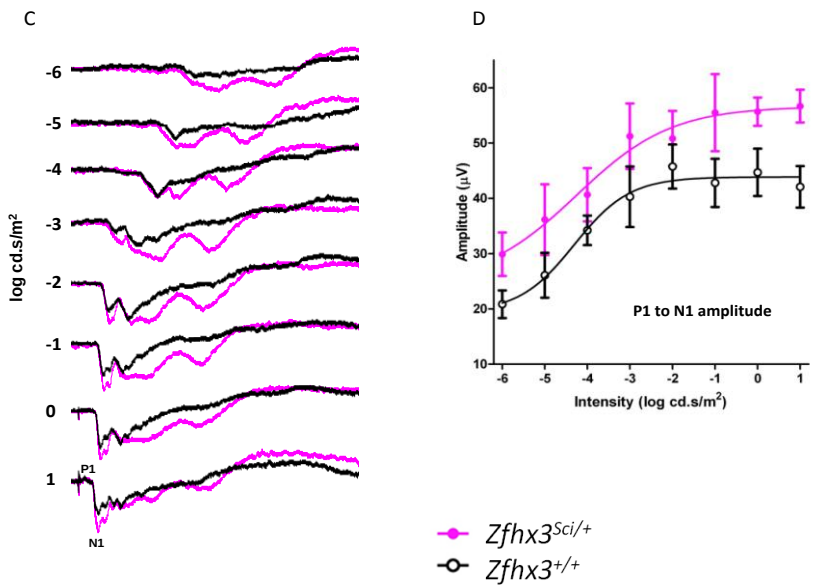

Light adapted ERG recordings and irradiance response curve

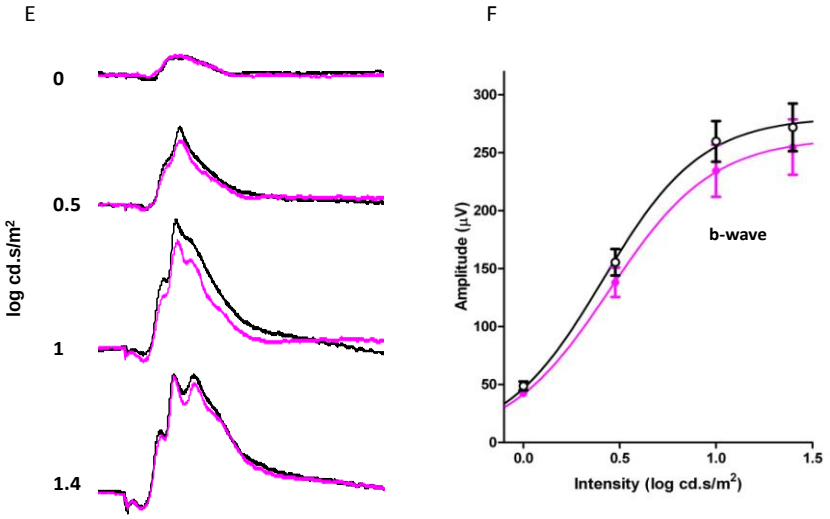

Light adapted VEP recordings and irradiance response curve

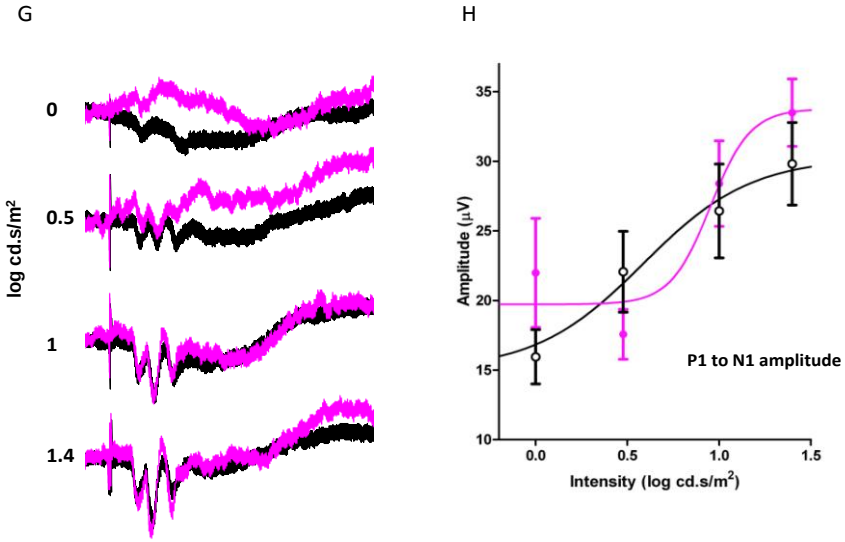

Figure 59: Dark and light adapted electroretinogram (ERG) and flash visual evoked potential (VEP) recordings taken from *Sci* animals. (A, B) Dark adapted ERG data reflecting the electrical activity of the retina. Raw data and the a and b-wave amplitude are shown across light intensities tested. (C, D) Dark adapted VEP recordings and intensity response curve effect on p1 → n1 amplitude. (E, F) Light adapted ERG data reflecting the electrical activity of the retina. Raw data and the a and b-wave amplitudes are shown across light intensities tested. (G, H) Light adapted VEP recordings and intensity response curve effect on p1 and n1 amplitude.

The nature and components of flash VEP recordings remain to be fully understood and the cellular basis of electrical responses is largely unknown. It is however generally accepted that the p1-n1 amplitude reflects either a stronger stimulus or stronger cortical response to the signal (Ridder and Nusinowitz 2006). From these results, the *Zfhx3*$^{Sci/+}$ animals appear to have an exaggerated response to the same photic stimulus presented to *Zfhx3*$^{+/+}$ animals. Although not statistically significant, these differences were consistently observed and with a larger cohort and younger animals, may be more pronounced and may require further investigation with more subtle testing techniques. However, although the neuronal responses and molecular pathways are separate, this may support the pupilometry data that the *Zfhx3*$^{Sci/+}$ animals show an exaggerated response to bright light stimuli, both in pupillary reflex, cortical response and in overt behaviors shown in circadian screens. An additional component in the electrical pattern from the flash VEP recordings was also observed in the *Zfhx3*$^{Sci/+}$ mutants as well as generally less “tight” recordings from the *Zfhx3*$^{Sci/+}$ animals. The nature and consequence of this remains unknown and requires further investigation.

6.5. Discussion

The visual system is a crucial component for modifying normal circadian behaviour. The majority of input to the SCN is derived from photic input pathways from the retina, which act to entrain and synchronise the circadian pacemaker to the external environment. Although the circadian clock persists in the absence of external cues, the circadian period eventually

deteriorates over time under constant light. Light intensity is also a factor that can alter the circadian clock. Constant light conditions will eventually result in a decoupling individual SCN neurons and the paired SCN nuclei, and in most cases, continuous bright light will cause arrhythmicity. In this sense, the master circadian clock is often considered as part of the greater visual system and as such, the two cannot be treated entirely independently of each other (Morin and Allen 2006). Taken together with the behavioural data presented in Chapter III, it was therefore necessary to investigate whether there may be ophthalmological phenotypes in the *Zfhx3*$^{Sci/+}$ mutants which could impact on circadian rhythmicity. Similarly, it was necessary to determine whether *Zfhx3* may be a candidate transcription factor that may play a role in modulating photic input to the SCN or in retinal function, based upon its expression pattern. With numerous phenotypes under light conditions detected in wheel running screens, it was hypothesised that *Zfhx3* may play a wider role in circadian rhythmicity outside of the core circadian oscillator.

6.5.1. Expression analysis

RNA *in situ* hybridisation with a *Zfhx3* riboprobe showed that *Zfhx3* was expressed in the adult retina and cornea. *Zfhx3* expression was shown to be specific to the inner nuclear layer, outer nuclear and ganglion cell layer of the retina. The ganglion cell layer has known roles within the core circadian clock, with melanopsin containing retinal ganglion cells (ipRGC's) projecting axons directly to the SCN forming the RHT (Panda, et al. 2005; Panda, et al. 2003). *Zfhx3* appears to have wide-spread expression throughout the ganglion cell layer and may therefore have a transcriptional role in the function of ipRGC's and their modulation of circadian rhythmicity.

A preliminary morphological analysis of the *Sci* retina did not detect any significant differences in the structure of the layers of the retina. Measurements made of the inner and outer

nuclear layers showed that the *Zfhx3*$^{+/+}$ and *Zfhx3*$^{Sci/+}$ retina were comparable in size. Therefore it is not hypothesised that there would be any retinal dysfunction as a result of aberrant morphology or structure.

Quantitative real-time PCR confirmed that *Zfhx3* was expressed in the adult retina, and no differences in relative expression of *Zfhx3* were observed between *Zfhx3*$^{+/+}$ and *Zfhx3*$^{Sci/+}$ at the 1 time point studied (ZT8). A candidate gene screen was performed investigating various opsins, neurotransmitters and neuropeptides and circadian candidate genes. Significant differences in relative expression between *Zfhx3*$^{+/+}$ and *Zfhx3*$^{Sci/+}$ were identified in *Opn3, Gad1, Gad2* and *Dbp*. *Opn3* (encephalopsin or panopsin) is known predominantly as an extra-retinal photoreceptor (although it is expressed in the adult retina, including the ganglion cell layer). It is hypothesised to play a role in non visual photic processes, including circadian rhythm entrainment and regulation of melatonin production. As with the other opsins, *Opn3* is a G-protein coupled receptor and has a wide expression pattern. It is therefore likely to be involved in the regulation of peripheral circadian rhythms (Kasper, et al. 2002). Although the function of *Opn3* is still unknown, it is interesting to observe from this RNA expression screen that *Opn3* was up-regulated in the *Zfhx3*$^{Sci/+}$ and further up-regulated in *Opn4*$^{-/-}$ mutants. This may suggest that *Opn3* can partially compensate for *Opn4* on an *Opn4*$^{-/-}$ background. The mechanism and consequences of this up-regulation remain to be determined.

Gad1 and *Gad2* are precursor enzymes which catalyse the production of GABA from L-glutamic acid. GABA is the major inhibitory neurotransmitter of the mammalian central nervous system. Within the retina, GABA is predominantly expressed in interneuron amacrine cells (Hoffpauir and Gleason 2005; Jiang and Xiang 2009; Menger and Wassle 2000). As previously identified, *Zfhx3* was shown to be expressed by *in situ* hybridisation in the inner nuclear layer of the retina. The inner nuclear layer consists of bipolar, horizontal and amacrine cells. Amacrine cells form the second synaptic level in the chain from the photoreceptors, bipolar

cells and ganglion cells. The synaptic activity occurs within the inner plexiform layer, although the large cell bodies sit within the inner nuclear layer. They are involved in the modulation of the visual message presented to the ganglion cell layer (Hattar, et al. 2002). Amacrine cells are therefore a target of interest for action of *Zfhx3* given the identified differences in *Gad1/Gad2*. The most common amacrine cell type is the GABAergic A17 cell, which has high sensitivity to scotopic, dim light conditions, driven by rod cells (Menger and Wassle 2000). Decreased GABA from the amacrine cells would impact upon transmission of information to the ganglion cells, hypothesised to cause reduced inhibition of the ganglion cells and a desensitisation of this signalling cascade. As such, the pupillary reflex would be over-stimulated and cause a constriction of the pupil even under dim light conditions. It may be hypothesised that this apparent over-sensitivity to light could result in the variable activity behaviours observed in *Zfhx3*$^{Sci/+}$ under constant light conditions, including an increased proportion of arrhythmic and split rhythm behaviours and the inability to re-entrain.

With a decrease in *Gad1* and *Gad2* expression and therefore a likely reduction in GABA neurotransmission in the retina, the *Sci* animals were phenotyped to determine whether there were any overt behavioural consequences due to a reduction of GABA. A reduction of GABA neurotransmission on a wider scale would be expected to result in severe behavioural abnormalities. Abnormal GABA neurotransmission has long been consistent with schizophrenia, and somatic drug treatment using compounds such as Benzodiazepines (which target GABAergic systems) are common in these patients (Wassef, et al. 2003). Reduced GAD (GAD1/2) and subsequently reduced GABA would result in promotion of dopamine production and this has been frequently observed in schizophrenic patients (Nakazawa, et al. 2012). No significant up-regulation of tyrosine hydroxylase (used to indirectly assess dopamine production) was observed at the RNA level, although there is a weak trend of up-regulation in the *Zfhx3*$^{Sci/+}$ mutants. Behavioural observations due to a reduction of GABA include confusion

and irritability as well as hyperactivity, and reduced startle response and reduced pre-pulse inhibition which are measurable schizophrenia endophenotypes in the mouse (Braff, et al. 1999; Wassef, et al. 2003) . These endophenotypes were not detected in the *Sci* animals, supporting that the reduction in GABA is highly specific to the retina.

6.5.2. Corneal dystrophy and associated phenotypes

As described, *Zfhx3* RNA expression was detected in the cornea by *in situ* hybridisation. This suggests a role for *Zfhx3* at the first point of light input to the adult eye. With a hypothesis that *Zfhx3* may be involved in corneal function, histological analysis was performed in order to detect any aberrant morphology or structure of the *Zfhx3*$^{Sci/+}$ corneas as a result of the mutation in *Zfhx3*. Detection of a phenotype in the morphology would facilitate understanding of a potential new role for *Zfhx3* in corneal function. By H&E staining it was shown that the *Zfhx3*$^{Sci/+}$ corneas were significantly thinner than *Zfhx3*$^{+/+}$ littermates. Preliminary measurements were taken of corneal thickness, measuring the upper epithelial cell layer and the entire thickness of the cornea structure. Aberrant thickness of the cornea would be expected to impact on the curvature of the cornea. This remains to be determined in these animals. However, it is likely that this severe thinning of the cornea observed in the *Zfhx3*$^{Sci/+}$ would impact on curvature. As a result, these two aberrant properties would affect the total amount of light reaching the retina and the focusing of light by the eye.

Although *Zfhx3* has not been implicated in corneal dystrophies previously, a close homologue of *Zfhx3*, known as *Zeb1*, has been implicated in a number of corneal disorders. *Zeb1*, as discussed in the introduction, was previously annotated as *Zfhx1a* and is also known as posterior polymorphous corneal dystrophy gene (*Ppcd*). Numerous studies have shown that mutations in *Zeb1* are causative of a number of corneal phenotypes including PPCD and Fuch's syndrome (Liu, et al. 2008b; Yellore, et al. 2012). Additionally, *Zeb1*$^{-/-}$ mice display abnormal

corneal thickening. Through binding E-box like sequences of target genes, *Zeb1* functions to maintain repression of epithelial specification genes *in vivo* (Liskova, et al. 2007; Liu, et al. 2008a; Liu, et al. 2008b). From this data and the corneal dystrophy identified in the *Zfhx3*$^{Sci/+}$ mutants, it is possible to suggest that *Zfhx3* may also therefore be functional in the maintenance of the cornea and have a role in the epithelial – mesenchymal transition, together with its ancestral homologue *Zeb1*.

Further support for this hypothesis is based upon additional ophthalmological data produced from the *Sci* animals. Based upon the assumption that corneal thinning and miss-curvature would affect light refraction and therefore light-focusing ability, the *Sci* animals were phenotyped for visual acuity. This was assessed by monitoring head-tracking movements to a moving visual field in the optokinetic drum. From this test it was identified that the *Zfhx3*$^{Sci/+}$ animals had reduced visual acuity. This decrease was significant for the right eye and for both the right and left eyes in combination as a measure of overall acuity. This apparent non-symmetric phenotype is common to human corneal dystrophies (Zadnik, et al. 2002), however the overall reduction in acuity is the standard measure by which to analyse this data. This supports the data that the *Zfhx3*$^{Sci/+}$ mutants show the phenotypic consequences of a corneal thinning and abnormal curvature.

The *Zfhx3*$^{Sci/+}$ mutants appear to display some evidence of photo-phobia. This would again be consistent with additional light penetrating the eye to reach the retina in the *Zfhx3*$^{Sci/+}$ animals due to a reduction in cell layer thickness for initial light absorption. This phenotype has been detected by both circadian wheel running screens which has been discussed previously, and through assessment of the pupillary light reflex discussed later in this chapter. From wheel running screens of increasing light intensity, many of the *Zfhx3*$^{Sci/+}$ animals show abnormal wheel running behaviours. The animals appear more sensitive to constant light conditions and become arrhythmic or irregular in their circadian wheel running behaviour more quickly than

Zfhx3$^{+/+}$ littermates. This may be due to effects on the central circadian oscillator, and it can also be hypothesised that the *Zfhx3* mutation has an effect on the coupling and stability of the SCN as a structure under constant light conditions. It may however also be indicative of the effect of additional light input to the SCN compared to *Zfhx3*$^{+/+}$ animals. From pupilometry data, the *Zfhx3*$^{Sci/+}$ animals show increased sensitivity to dim light conditions, as shown through an over-constriction of the pupil in response to a dim light stimulus. This would imply that the differentiation between bright and dim light may be less obvious for the *Zfhx3*$^{Sci/+}$ animals and a much more significant reduction of light intensity would be required for the pupil to remain dilated. As will be discussed later however, this is not the only explanation for this novel phenotype and may be due to the molecular actions of *Zfhx3* elsewhere in the visual system, including a role directly within the retina itself.

Taking these phenotypes together, corneal thinning, decreased visual acuity, photo phobia and an abnormal pupillary light reflex, the *Sci* mutants have a complex ophthalmological phenotype which has implications on the entire visual system which would also impact on circadian entrainment and responses to light. These phenotypes together are consistent with a condition known as Keratoconus. Keratoconus is a corneal disorder characterised by structural changes to the cornea due to cellular degeneration and subsequent thinning (Zadnik, et al. 2002). It has an incidence of approximately 1/1000, usually presenting in adolescence and may affect either one or both eyes (Rabinowitz 1998). The condition leads to severe visual impairment without corrective treatment. The cause of Keratoconus is unknown, but both genetic and environmental factors are likely to contribute (Krachmer, et al. 1984). To address the genetic component, a number of GWAS studies have been performed and two strong loci for the condition have been identified on chromosome 16q and 20q in humans. These studies agree on an autosomal dominant pattern of inheritance (Nowak and Gajecka 2011; Tyynismaa, et al. 2002).

The human homologue of *Zfhx3* lies at 16q22.2 – 16q22.3. This locus has been previously identified in a GWAS study for atrial fibrillation, a cardiac defect causing arrhythmias (Benjamin, et al. 2009b; Li, et al. 2011). A neighbouring locus for Keratoconus has also been identified which over-laps with this region (Tyynismaa, et al. 2002). The locus lies from 16q22.3 – 16q23.1, known as KTCN2. This GWAS study was performed on samples from a Finnish population of individuals affected by Keratoconus and a control group. A high region of linkage, with a maximal LOD score of 4.11 was identified neighbouring the *Zfhx3* human transcript. The *Zfhx3* gene is encompassed by the 6.9 centimorgan locus identified and therefore remains to be a candidate gene for Keratoconus in this population. With the phenotype of the *Sci* animals and the known roles of the highly related protein *Zeb1 (Zfhx1a)* in corneal structure and function, it is therefore hypothesised from the data presented in this chapter that *Zfhx3* may be a Keratoconus candidate gene and the *Sci* mouse may be a good model for this condition. With candidate genes within the GWAS locus previously sequenced and no mutation identified, work has now commenced to sequence *Zfhx3* within the Finnish samples from the GWAS study. This work is being carried out in collaboration with Dr Tiina Alitalo (Department of Medical Genetics, University of Helsinki, Finland) the corresponding author of the GWAS study.

6.5.3. Pupilometry and ERG phenotypes

A novel phenotype was identified in the *Zfhx3*$^{Sci/+}$ mutants. These animals displayed an exaggerated pupillary constriction in response to dim light stimuli compared to litter mate control animals. This phenotype is the opposite to that observed in the well characterised *Opn4*$^{-/-}$ knockout. Melanopsin is known to control the pupillary reflex through a dedicated pathway which goes via the olivary pretectal nuclei in the brain (Chen, et al. 2011b). From these results perhaps there is an enhancement or gain of function to the molecular action by

Zfhx3 within the *Opn4* signaling cascade. Given that the real-time PCR analysis has failed to detect differences in *Opn4* in the *Zfhx3*$^{Sci/+}$ animals, it is likely that *Zfhx3* is either acting further downstream of *Opn4* or independently. To help address this question, *Sci-Opn4* double mutants are being generated and will be phenotyped for their pupillary response in order to detect any genetic or additive interactions using an epistasis phenotyping technique as previously carried out and discussed with the *Sci ; Cry1* and *Sci ; Cry2* mutants.

There is an up-regulation in *Opn3* in the *Sci* mutants as previously discussed, however, a further up-regulation of *Opn3* RNA expression is detected in *Opn4* mutants and therefore cannot account for the opposing phenotypes. One hypothesis for this phenotype may be attributable to the differences in *Gad1* and *Gad2* RNA expression and the consequential decrease in GABA signaling. With a reduction in neuronal inhibition via GABA, it may be hypothesized that there is an overall disinhibition of the retina, likely starting at the GABAergic amacrine cells. The amacrine cells, which synapse with retinal ganglion cells would therefore be sending more action potentials in response to weaker stimuli in the *Zfhx3*$^{Sci/+}$ mutants compared to the *Zfhx3*$^{+/+}$ animals. The result may be an over-activation and stimulation of *Opn4* ipRGC signaling.

A further possibility is that the thinning of the cornea results in additional light entering the eye, with less absorption due to thinner cell layers. It would be expected that a thinning of the cornea would result in photo-phobia, as is a common symptom in human patients with Keratoconus as discussed earlier. Both these hypotheses may be the case, together causing an apparent photophobia phenotype and perturbed pupillary constriction.

ERG data has ruled out electrical responses of the retina being causative of the aberrant pupil reflex response. The data has however indicated that there is again an over-exaggerated response to photic information as detected using flash VEP recordings. The data showed that

there is an increased cortical response to photic stimuli in the *Zfhx3*$^{Sci/+}$ animals compared to *Zfhx3*$^{+/+}$ littermates. Given relatively normal ERG data implicating normal retinal function, the phenotypes detected from the flash VEP recordings would be attributed to defective molecular mechanisms or morphology, after visual processing has occurred within the retina, in photic processing within the brain. It is possible that altered decussation at the optic chiasm, retinotopic mapping or altered inhibition/feedback in the cortex is responsible for this phenotype. This could be answered using tracing studies, looking directly at neuronal connections from the optic nerve to image centers including at the SCN in the brain.

6.5.4. Conclusions

It has been demonstrated in this chapter that there is a functional role for *Zfhx3* in the visual system. Phenotypes have been identified in the *Zfhx3*$^{Sci/+}$ mutants, which suggest that the effects of this heterozygous point mutation in *Zfhx3* have consequences on the ophthalmological function and visual responses in the mouse. Given the pleiotropic nature of *Zfhx3*, it is important to be able to distinguish between which phenotypes are as a result of disruption to the molecular circadian clock, photic input pathways and/or ophthalmology or even roles during development in the establishment of neural networks.

RNA expression analysis has confirmed relatively high expression of *Zfhx3* RNA in the adult eye, both in specific layers of the retina and in the cornea. Very limited *Zfhx3* RNA transcript has been detected elsewhere in the adult organism outside of the eye and the SCN. This implicates a highly specific role for *Zfhx3* in the visual and greater visual (circadian) system. A number of phenotypes together suggest that *Zfhx3* is involved in the perception and response to light. *Zfhx3*$^{Sci/+}$ animals display an exaggerated pupillary constriction to dim light intensities, abnormal cortical responses to bright light stimuli, and as shown and discussed previously, animals display overt behaviours suggestive of photophobia under constant bright light. The

mechanism behind these phenotypes may follow two suggested hypotheses. The first hypothesis is based upon aberrant GABA neurotransmission in the *Zfhx3*$^{Sci/+}$ retina. Reduction of *Gad1/Gad2* RNA transcript in the retina implies that there is a subsequent reduction in GABA and therefore reduced neural inhibition of the retina.

The second hypothesis arises from the reduction in visual acuity of the *Zfhx3*$^{Sci/+}$ mutants. Visual acuity is 80% governed by the cornea. With co-expression of *Zfhx3* in the cornea, together with a thinning of the corneal epithelium and stroma layer and known roles of *Zfhx3* homologues in corneal dystrophies, *Zfhx3* has been identified as a strong candidate transcription factor involved in corneal structure and function. A reduction in corneal thickness would impact on visual responses to light.

Both these hypotheses may be concurrent and further analysis may be employed to dissect the role and mechanism of *Zfhx3* in the visual system. Targeted gene knock-out techniques or retina specific RNAi may be used to assess the effects of a loss of *Zfhx3* on the visual system whilst maintaining functional *Zfhx3* in the SCN and circadian system. This would help to isolate the roles that *Zfhx3* appears to play in these two systems. The generation of *Zfhx3-Opn4* double mutants and subsequent pupillary reflex phenotyping will help position *Zfhx3* in the pupillary response molecular cascade, determining whether there is any interaction between these two genes. Additionally, a GAD-GFP reporter may be utilised to generate an indirect GABA reporter line on the *Sci* background. Differences in the amount of GAD may be assessed by immuno-fluorescence techniques to determine whether the reduction of *Gad1* and *Gad2* is specific only to the retina or to other areas of the CNS, in particular, the SCN. Although wide-spread reduction of GABA is not expected due to normal behavioural responses shown by startle and PPI phenotyping, it is possible that the differences in GABA may be affecting the communication and coupling at the SCN level. This remains to be determined by RT-PCR and immunological methods. Further behavioural characterisation may also be employed.

Chapter VII

Discussion

7. Introduction

7.1. Summary of main aims

This thesis describes the characterisation of the circadian and ophthalmological phenotypes of the short circuit (*Sci*) mutant. *Sci* was identified in an ENU mutagenesis dominant screen, displaying overt circadian abnormalities, predominantly a shortened period under constant dark conditions. The causative ENU induced mutation was mapped to a novel circadian locus. Positional cloning and gene sequencing has identified the causative mutation in zinc finger homeobox 3 (*Zfhx3*), a transcription factor with no known roles in circadian rhythmicity, visual processing or behaviour. The objective of this work has been to use molecular and behavioural techniques to determine the role of *Zfhx3* in circadian behaviour and the mechanism of action on the circadian clock. This study has used the *Sci* mutant to facilitate understanding and defining the role of *Zfhx3* within the circadian system. Additionally, *Sci* has been out-crossed to other circadian mutants in order to position *Zfhx3* within the circadian signalling cascade. The experiments presented in this thesis aimed to test the hypothesis that *Zfhx3* is a novel circadian transcription factor with a role within the core circadian clock as well as roles within the wider circadian system. A wide range of approaches have been used to show novel genetic and protein interactions within the circadian clockwork and visual system, and to define the physiological phenotypes as a result of the *Sci* mutation.

7.2. Summary of the main results

Sci heterozygous mutants were behaviourally characterised using wheel running screens, recording activity output as an endophenotype for endogenous circadian rhythmicity. Aberrations to circadian behaviour were detected under entrainment, constant conditions and in responses to light pulses. The range of phenotypes exhibited in *Sci* suggested an

involvement of the causative gene at different levels of the circadian behavioural system. Poor entrainment, absent re-entrainment after constant light and an abnormal phase response curve (PRC) supported a potential involvement in disrupted photic input to the SCN and non image-forming visual perception. Consistent with this hypothesis, physiological phenotypes were identified in the eye as well as molecular and visual abnormalities. These included a thinning of the cornea, reduced *Gad1* and *Gad2* RNA expression in the retina and an abnormal pupillary response to dim light.

The short circadian period of 21.5 – 23 hours recorded in mutant animals suggests that there may be a deficit within the molecular oscillator at the SCN level. Molecular and genetic approaches have been pursued in order to identify an interaction between *Zfhx3* and other clock components. RNA analyses identified changes in expression of *Cry1, Cry2* and *Per1* in *Sci* heterozygous mutant tissue. Additionally, co-immuno-precipitation experiments identified protein interactions between ZFHX3 and CRY1, CRY2 and PER2. These data, together with highly specific RNA expression of *Zfhx3* in the adult SCN, support the hypothesis that *Zfhx3* is a novel circadian regulator acting upon or interacting with the molecular oscillator. Epistasis experiments have further identified an interaction between *Zfhx3* and core clock genes. $Zfhx3^{Sci/+}$- $Cry1^{-/-}$ and $Zfhx3^{Sci/+}$- $Cry2^{-/-}$ double mutants showed phenotypically that there is an additive effect between *Zfhx3* and *Cry1* and an interaction between *Zfhx3* and *Cry2* under constant dark conditions. An epistatic interaction between *Zfhx3* and both *Cry1* and *Cry2* is implicated under constant light conditions.

The *Sci* homozygous mutant fails to survive through late gestation. *Zfhx3* is known to have a role during development in neurogenesis and cellular differentiation (Ido, et al. 1994; Miura, et al. 1995; Watanabe, et al. 1996). The *Sci* mutation significantly impairs *Zfhx3* function such that the later stages of development fail to complete accurately leading to terminated embryos. *Zfhx3* RNA is expressed from E10.5 dpc in the nervous system and developing limbs.

From this point onwards, when *Zfhx3* is most highly expressed, the brain is rapidly developing, the cervical somites are becoming less distinctive and brain vesicles are being formed. The expression of *Zfhx3* therefore coincides with the rapid expansion and advancement of the brain and nervous system. The homozygous *Sci* mutation may therefore be compromising these stages of development to an irreversible degree leading to eventual natural embryo resorption. As well as this apparent general role for *Zfhx3* during these developmental stages, it is hypothesised that *Zfhx3* may be more specifically required in the establishment of the SCN and circadian network system within the hypothalamus. High regional expression has been detected in the developing hypothalamus, as well as transcription factor analysis in previous studies showing that *Zfhx3* is one of a small subset of transcription factors that is discretely expressed in the putative SCN region of the developing embryo and is maintained in expression in the SCN at post-natal day 1 (VanDunk, et al. 2011). This therefore not only supports a potential role of *Zfhx3* in the functioning of the adult circadian oscillator, but also in the establishment of the structure and circadian network formation.

At the protein level, SILAC analysis was used to investigate the proteome of all three *Sci* genotypes in embryonic fibroblasts in culture. Data produced from these experiments implicated *Zfhx3* in a number of processes including mitochondrial metabolism and oxidative stress, DNA replication and cell cycle regulation. A number of proteins involved in these processes were aberrantly regulated as a result of the *Sci* mutation and provided indications as to the reasons for homozygous lethality. Additionally, the SILAC data has also identified other processes in which *Zfhx3* may function and may be involved in linking these peripheral processes to the circadian clock.

7.3. Short circuit Phenotype

7.3.1. Short circadian period and reduced circadian amplitude

The predominant phenotype of the *Sci* mutant is the short period under constant darkness. This period ranges from 21.5 – 23 hours in *Zfhx3*$^{Sci/+}$ animals. A short circadian phenotype implicates that the molecular feedback loop at the central oscillator is running fast in the absence of entrainment signals. The entrainment or input pathway transduces external environmental stimuli to the core oscillator. These signals terminate at the central pacemaker in the SCN where the periodicity and phase is generated based upon the receipt of these cues. The central molecular oscillator therefore governs the period length and a long or short period phenotype identified in a mutant animal would implicate a deficit in the molecular oscillator following the receipt of the external stimuli. The output pathway couples the internal generated rhythm to other processes, such as gene expression, neuropeptide secretion and neuronal firing to generate the appropriate overt behaviours in response to the external environment. Since the *Sci* heterozygous phenotype of a short period has been recapitulated *in vitro* by monitoring the expression of the Per2-luciferase fusion protein in *Sci* SCN slices, this may suggest a lesser involvement of the input and output pathways as being contributory to this phenotype. Due to the pleiotropic nature of *Zfhx3*, potential functions in modulating the circadian oscillator through SCN afferent signalling may contribute to the short circadian period phenotype.

A number of clock gene animal knock-out models have been shown to produce a short circadian period (Cermakian and Boivin 2003). One of the first circadian mutants identified was the *tau* mutant in the golden hamster (Lowrey, et al. 2000; Ralph and Menaker 1988b). This spontaneous mutation resulted in a 22 hour rhythm under constant darkness and a 4 hour early activity onset, a phase advance in LD. One outcome of even a minor shortening of

period is earlier sleep onset relative to the light-dark environment. In human subjects, the shortest period that has been recorded is 23.3 hours together with an abnormal advanced sleep phase, in correlation with the short period (Xu, et al. 2007). This has been described in human patients as advanced sleep phase syndrome (ASPS), and in familial cases a mutation in *Per2* has been identified as causative (Vanselow, et al. 2006; Xu, et al. 2007). A phase advance is detected in the *Sci* mutants and therefore an analysis of sleep-wake rhythm and biomarkers of sleep, including melatonin secretion and core body temperature would be informative as to whether *Sci* models similar sleep conditions observed in (F)ASPS.

7.3.2. Post-transcriptional modification by ZFHX3 on the circadian clock

Zfhx3 could be acting pre or post-transcriptionally to modulate the circadian clock and cause a shortened period when mutated. Although it's predominant function is as a transcriptional activator and repressor, the complex transcript encoding various domains and motifs also lend ZFHX3 to various roles outside of transcriptional regulation.

Data presented in this thesis has identified protein interactions with CRY1, CRY2 and PER2. The purpose of this protein complex may be in directing these proteins sub-cellularly. This may facilitate the availability of these protein substrates to other proteins for post-translational modification. It is not considered that ZFHX3 uses this protein interaction directly for post-translational modification since no known kinase or phosphatase activity is reported or predicted by the ZFHX3 amino acid sequence. It remains to be determined whether the mutated ZFHX3 still maintains these protein interactions, and this data will facilitate the understanding of the function of these interactions. If lost, it may be inferred that this interaction is responsible for delaying the circadian clock and therefore when functional, the interaction may temporally gate post-translational mediated degradation of cryptochrome and period proteins. An investigation into the rate of degradation of these proteins in the

presence of the *Zfhx3* mutation would be informative as to whether there is an indirect effect of ZFHX3 on post-translational events such as increased phosphorylation or ubiquitination. These interactions may be impaired either directly due to the mutation interfering with the protein binding site or indirectly due to the mutation affecting post-translational modification of ZFHX3 itself.

7.3.3. Transcriptional manipulation by ZFHX3 on circadian clock gene expression

ZFHX3 is one of hundreds of substrates of ataxia telangiectasia mutated (ATM), a serine/threonine protein kinase that becomes activated by DNA double-strand breaks (Lavin and Kozlov 2007; Lee and Paull 2005). It becomes phosphorylated by ATM to induce stabilisation and activation of the protein. An impairment of ATM activation of ZFHX3 may alter the kinetics of ZFHX3 transcriptional ability. If ZFHX3 is involved in transcriptional activation or repression of clock genes, an alteration in its own activation state would impact on the circadian clock. Additionally, the *Sci* mutation may cause an effect on the binding ability of ZFHX3 to promoter or enhancer elements. Electrophoretic mobility shift assays (EMSA) could be used to show whether the mutant and wild type ZFHX3 protein have the same affinity for either clock gene promoter binding or E-box or AT motif consensus sequences. Extrapolation from evolutionary orthologues and homologues of *Zfhx3* may suggest that ZFHX3 has the ancestral ability to bind an E-box consensus sequence. *Zfhx3* is closely related to the *Zeb* family of genes, zinc-finger E-box binding homeobox, both belonging to the zinc finger class (Holland, et al. 2007). ZEB1 represses transcriptional activity by binding to E-box motifs therefore it is possible that the distantly related ZFHX3 may also possess this functional ability (Postigo and Dean 1997).

Zfhx3 is known to act as both a repressor and an activator of transcription (Jung, et al. 2005; Qi, et al. 2008a; Yasuda, et al. 1994a). RNA data produced from the *Sci* mutant may suggest

that *Zfhx3* acts normally as a transcriptional activator on *Cry2*, either direct or indirect. In *Sci* mutant tissue, *Cry2* RNA expression appears to have lost its peak amplitude of expression and is minimally expressed. It is possible therefore that ZFHX3 cooperates with CLOCK and BMAL1 to activate the transcription of *Cry2* and the *Sci* mutation has caused a loss of function of this role of *Zfhx3*. A similar effect is seen on *Per1*. In parallel, an increase in Cry1 RNA expression is observed which may support that under wild-type conditions, *Zfhx3* acts to repress *Cry1*. This repression may be lost as a result of the *Sci* mutation and therefore CLOCK and BMAL1 alone, are sufficient to over-activate *Cry1* transcription without balancing regulation by ZFHX3.

How these scenarios would directly impact on causing a shortened circadian period remains to be determined. The involvement of redundant and compensatory proteins adds complexity to the interpretation of this data. From analysis of the relative expression, there is an approximate overall three-fold increase in *Cry1* RNA and a corresponding decrease in *Cry2* RNA. If the cryptochrome proteins are acting as efficiently as each other in the context of the molecular oscillator, this exact balancing may not cause an imbalance on the speed of the circadian feedback loop. However, it is known that the *Cry1* and *Cry2* genes have opposing roles in terms of phenotype as observed in the $Cry1^{-/-}$ and $Cry2^{-/-}$ knock-out animals. If the RNA data can be translated into protein and these effects observed in peripheral tissues are expressed genome wide, *Sci* is in effect modelling a *Cry2* knock-down since the *Cry2* RNA expression has flattened at basal levels. Data from generating the *Sci ; Cry1* and *Sci ; Cry2* double mutants has shown that $Zfhx3^{Sci/+}$-$Cry2^{-/-}$ double mutants have a short circadian period despite $Cry2^{-/-}$ alone causing a long period, consistent with the *Sci* period alone. This supports an epistatic interaction between the two alleles. In addition to the effects on *Cry* RNA, there is the three-fold loss of peak expression of *Per1*, with no apparent compensatory effect observed in *Per2*. A *Per1* knockout is known to show a shortening of free-running period by approximately 1 hour (Cermakian, et al. 2001; Tischkau, et al. 2003). The *Per1* RNA transcript

in *Sci* however still oscillates and therefore does not model the knock-down effect as is seen on *Cry2*. How these effects, together with the shift in *Zfhx3's* RNA expression, cause a shortening of circadian period remains to be determined as well as whether these effects are observed also at the protein level.

7.4. Phenotypes under altered lighting conditions

In addition to a short circadian period, abnormal phenotypes were detected in *Sci* mutants under various light conditions. This would suggest a disruption to the transduction of photic information from the retina to the SCN. There are a number of potential hypotheses that would explain abnormal behavioural responses to light. The mutation may affect the detection of light, perhaps affecting the sensitivity of the retinal ganglion cells or later cells of the retinal signalling cascade, before relaying light information to the SCN via the retino-hypothalamic tract. Abnormal structuring and morphology of this pathway and decussation at the optic chiasm may also affect the transduction of photic information. Mild phenotypes detected by ERG recordings showed indications of an abnormal neural circuitry between the retina, SCN and visual processing centres, although these data are not significant. Given known roles of *Zfhx3* during development in neuronal establishment and differentiation, it is possible that the establishment of the retino-hypothalamic network has been affected as a result of the *Sci* mutation.

7.4.1. Effects of *Zfhx3* on photic signalling cascades to the SCN

RNA localisation analyses detected specific expression of *Zfhx3* in the retinal ganglion, inner and outer nuclear layers of the retina. An involvement in retinal function based upon the localisation of the *Zfhx3* RNA transcript to these layers of the retina is therefore assumed although this needs to be validated at the protein level. The expression of *Zfhx3* in the retinal

ganglion cell layer appeared ubiquitous and was not restricted to intrinsically photosensitive retinal ganglion cells (ipRGC's). Therefore a specific effect solely on melanopsin (*Opn4*) signalling is not expected. Despite this broad expression pattern within this cell layer, an effect on the pupillary responses of the *Sci* mutants was identified. *Sci* mutants showed an increased sensitivity to scotopic light by an over-constriction of the pupil in response to the dim light stimulus. This is a novel identified phenotype, the opposite to that of *Opn4*$^{-/-}$ knockouts (Panda, et al. 2005; Panda, et al. 2003; Panda, et al. 2002). The method by which the pupillary response was measured, recording the consensual pupil constriction after stimulating the opposing eye, ensured the complete pupillary reflex circuit was being assessed. This suggests that the *Sci* mutants are sensitive to dim light conditions, perceiving them in their reflexive response as a bright light stimulus. This would impact on interpretation of the external environment when light intensity becomes more scotopic as night-fall approaches. From this result, it may be expected that in nature *Sci* may produce a prolonged period of negative masking by light since light intensity would continue to be perceived later into the evening as a higher intensity. This however would be more consistent with phase delays and a longer period, which is not observed under laboratory conditions. A gradual decrease in light intensity is not a laboratory scenario which has been observed since light levels remain constant for 12 hours of the day and do not reflect the gradual change in external environment. A key adaptation in all animals is to adapt visual sensitivity to function optimally under changing light intensities. Mechanisms to achieve this process start at the retina, relying upon different photo-pigment spectral sensitivities (Golombek and Rosenstein 2010). Additional mechanisms such as coupling retinal processes to the circadian system have evolved in order to be able to anticipate changes in light intensity across environments and time. Other afferents from the brain to the retina exist to fine tune and modulate retinal sensitivity. In the *Sci* mutant it would appear that one of these processes is impaired such that the retina perceives light intensity wrongly resulting in a shifted irradiance response curve.

Given that the pupillary reflex response is known to be governed by *Opn4* (Lucas, et al. 2003), an investigation into *Opn4* expression and other candidate genes was performed. No significant effects were seen on *Opn4* RNA expression. Interestingly an up-regulation of *Opn3* was detected. Relatively uncharacterised, the data in this thesis shows that *Opn3* is further up-regulated in *Opn4*$^{-/-}$ knockouts which would indicate a semi-redundant or compensatory mechanism. A significant up-regulation of *Opn3* is seen in *Sci* animals although to a lesser extent, perhaps suggesting an intermediary phenotype or a similar functional aberration between the *Sci* and *Opn4*$^{-/-}$ mutant animals. The role of *Opn3* in visual processing is unknown and has been largely uncharacterised. Its function and role is complicated by its wider spread expression compared to the other classical photo-pigments, as it is also highly expressed in the brain, testis, liver and lung and has known roles in the immune response (Blackshaw and Snyder 1999; Halford, et al. 2001; Nissilä, et al. 2012).

Considering the changes observed in *Opn3* and *Opn4*, it may now also be worth investigating *Opn5* expression. It has been shown to be expressed in the retina of the rat, in the inner nuclear layer and ganglion cell layer similar to *Zfhx3*. It has been hypothesised that *Opn5* is able to contribute to non-image forming photic responses, perhaps responsible for a residual pupillary light reflex observed in non-rod, non-cone, non-melanopsin animals. It has been proposed that *Opn5* may be a new photoreceptor of the mammalian retina that can partially compensate for *Opn4* and encompass a different wavelength range at 420 nm maximal efficiency compared to 480 nm of *Opn4* (Nieto, et al. 2011).

7.4.2. Involvement of *Zfhx3* in retinal neurotransmission

The expression of *Zfhx3* in the inner nuclear layer of the retina is consistent with expression in amacrine cells. *Zfhx3* is known to be predominantly expressed in dopaminergic neurons in the adult and amacrine cells are the only characterised cell type of the retina to use dopamine as a neurotransmitter (Eglen, et al. 2003; Jung, et al. 2005). Additionally, it is the cells of the mammalian inner retina which contain circadian clocks. *Zfhx3* therefore may be co-expressed in dopaminergic clock cells of the mammalian retina with roles in modulating photosensitivity via circadian coupling mechanisms. Dopamine was indirectly assessed by analysing the relative expression of tyrosine hydroxylase, the precursor enzyme to dopamine synthesis, in total retina RNA. Additionally, clock gene RNA relative expression was investigated. No significant differences were observed between $Zfhx3^{Sci/+}$ and $Zfhx3^{+/+}$ retinas, however only one time point was investigated (ZT8). Given the known circadian oscillation of both dopamine and the clock genes in the retina, a conclusive analysis should be performed by investigating relative expression across circadian time points. It is therefore not possible to exclude differences in tyrosine hydroxylase and circadian gene expression in *Sci* mutant retinas at different time points.

Dopamine is known to regulate inner retinal network properties and additionally these inner retinal dopaminergic amacrine cells are circadian clock cells (Eglen, et al. 2003; Hampson, et al. 1992; Ruan, et al. 2008). Dopamine accumulates during the day time and decreases during darkness. These changes are thought to be under circadian control. By altering the levels of dopamine within the retina, the sensitivity of the retina shifts to becoming more rod (night) or cone (day) dominant. In this way, the photosensitivity of the retina may be manipulated in order to anticipate the external environment. Given the differences observed in the *Sci* pupillary response, it may be that this process is affected in the *Sci* retinas; although no differences have been shown so far in tyrosine hydroxylase.

As well as dopamine mediated mechanisms, other processes exist within the vertebrate eye to modify and adapt the visual system over time. Intraocular pressure, mechanical movements of photoreceptors, dopamine synthesis and visual sensitivity are all modified over circadian time (Ruan, et al. 2008). The way in which visual sensitivity is modified requires further investigation in the context of the *Sci* mutant, however data presented in this thesis supports an involvement in neurotransmission at the level of the amacrine cells. Both *Gad1* and *Gad2* GABA precursor enzymes, in *Sci* show a decrease in expression and as a result, reduced GABA neurotransmission would be expected. A dis-inhibition of the inner retina may exert the observed effects on the pupillary response. An over-exaggerated response to a dim light stimulus would be produced due to a reduced inhibition of this neural network. Indeed, GABA is also documented to be involved in manipulating the circadian responses of the inner retina. GABA(A) receptors have been shown to modulate the responsiveness of the circadian system to light (Ehlen and Paul 2009). The *Sci* mutant displays a number of aberrant behaviours under varying light intensities and it may therefore be through this mechanism of altered GABA neurotransmission that these behaviours are manifested. Although *Zfhx3* has not previously been associated with GABA neurotransmission, the *Sci* mutation has shown a direct effect on *Gad1* and *Gad2* expression in the *Sci* retina. The overall effect may be due to a circadian oscillator effect in the retina or involved in neurotransmission. There may however be a reduction of GABAergic cells in the retina which remains to be investigated.

Retinal GABA and Dopamine regulate the amplitude and phase respectively of the retinal circadian molecular rhythm. Therefore a time course based experiment to investigate any effects on the retinal clock should be performed. Additional behavioural phenotypes that would be expected of a reduction in GABA neurotransmission have not been detected in the *Sci* animals. Startle and PPI, endophenotype tests for schizophrenia spectrum disorders and reduced GABA neurotransmission, did not detect any significant differences between *Zfhx3*$^{Sci/+}$

and *Zfhx3*$^{+/+}$. As such, it may be inferred there is not a ubiquitous change in *Gad1* and *Gad2* expression and it is specifically localised such that overt behavioural deficits are not detected. Whether *Gad1* and *Gad2* RNA expression is affected in the SCN remains to be determined. It may be that these effects on *Gad1* and *Gad2* also affect SCN neuronal firing and coupling and causes the *Sci* circadian phenotype in this way. It may be that the differences in GABA alter the amplitude of the circadian rhythm, which is a role that GABA is known to perform in the retina. The *Zfhx3*$^{Sci/+}$ mutants do display significantly reduced amplitude of the circadian rhythm and therefore this phenotype could be attributed to a GABA deficit.

7.4.3. *Zfhx3* as a candidate gene for Keratoconus phenotypes

A significant thinning of the corneas was detected by histological analyses. A thinning of the cornea presents in human Keratoconus patients for which the hereditary component remains to be identified. One locus from a genome-wide association study (GWAS) on affected patients in a Finnish population has identified one Keratoconus locus which encompasses the human *Zfhx3* gene (Tyynismaa, et al. 2002). This gene remains to be fully sequenced but it is possible that a mutation in *Zfhx3* is causative of Keratoconus in humans and the *Sci* mouse may be an animal model of this condition. Any tightly linked genes to *Zfhx3* that remain in synteny between human and mouse may also be involved in this Keratoconus phenotype.

The consequences of a thin cornea have not been studied in terms of the impact on the pupillary response and circadian responses to light. Human patients do not appear to have been monitored routinely for disturbances in sleep wake pattern or pupillary reflex, only annotations made that pupillary responses are often abnormal in these patients. Additionally, Keratoconus patients exhibit photophobia presumably due to extra light reaching the retina and not being absorbed by the cornea. This is in part consistent with the *Sci* mutant, displaying an abnormal pupillary reflex suggestive of increased sensitivity to dim light

conditions. However it is unlikely that a corneal thinning would solely produce sensitivity to dim light since the majority of light absorption occurs after the cornea. It would therefore be interesting to investigate whether any of the molecular aberrations observed in the *Sci* mutants in neurotransmission, are replicated in human subjects and whether this also affects additional phenotypes in Keratoconus patients. Further concordance between *Sci* and the Keratoconus condition is a reduction in visual acuity, as expected by a miss-curvature and thinning of the cornea. Together, the data would suggest that the *Sci* mutant would be a valuable model for both a Keratoconus type condition and also the effect that an abnormal structural eye physiology plays on the circadian visual system.

7.4.4. *Sci* mutants display less plasticity of the SCN in responses to light

The *Sci* animals show poor entrainment responses, both under normal conditions, after constant light and under shifted LD cycles in a jet-lag mimicked experiment. There may be a number of reasons for this phenotype in *Sci* animals. Firstly, the masking effect of light may be reduced such that there is increased activity under day-light hours. Secondly, the inability to re-entrain indicates that the decoupling effect of constant light on the circadian oscillator produces a far more profound effect on *Zfhx3*$^{Sci/+}$ animals than *Zfhx3*$^{+/+}$ such that a permanent inability to re-entrain is produced. This would not only indicate that the SCN is more sensitive to prolonged light exposure, but that it shows less plasticity to re-adapt to normal entrainment conditions such that the effects on SCN coupling are permanent. This is also the case in the shifted LD cycles where the *Zfhx3*$^{Sci/+}$ animals are entrained to a 12:12 light dark cycle and consistently maintain an advanced phase angle despite the shift in time in the onset and offset of light. The *Zfhx3*$^{Sci/+}$ animals appeared more resistant to a shift in the light dark cycle and perhaps required a longer time period in which to adapt. In the same experiment, the *Zfhx3*$^{Sci/+}$ animals showed reduced sensitivity to light in which to entrain. Under dim light conditions of 1 lux, *Zfhx3*$^{Sci/+}$ mice were unable to entrain and were observed to free-run,

illustrating that they were unable to detect sufficient light intensity to entrain the circadian oscillator. This is either a deficit at the level of photic processing in the retina, and perhaps specifically the rods or ipRGC's, or it is the receipt of photic information at the SCN which is not detected or integrated. This data appears contradictory to that of the pupillary data suggesting that the *Zfhx3*$^{Sci/+}$ animals are over-sensitive to dim light. For this reason, it may be unlikely that the responses observed in wheel running activity are due to a deficit in the ipRGC processing involved in pupillary constriction but in a later processing mechanism, perhaps at the SCN. However, caveats in both approaches, including differences in light source and timing, make these data incomparable. Additionally, the behavioural output of the circadian oscillator and the pupillary reflex pathway both use independent and distinct neural pathways via different brain nuclei and therefore may still exert different effects on overt behaviour.

7.4.5. Involvement of *Zfhx3, Cry1* and *Cry2* in light mediated circadian responses

A final involvement for *Zfhx3* in light mediated responses has been shown from the generation of double mutants between *Sci* and *Cry1*$^{-/-}$ and *Cry2*$^{-/-}$ knock out animals. A deterioration in circadian behaviour under constant light conditions was exhibited in both *Zfhx3*$^{Sci/+}$-*Cry1*$^{-/-}$ and *Zfhx3*$^{Sci/+}$-*Cry2*$^{-/-}$ double mutants. Individually, *Cry1*$^{-/-}$ and *Cry2*$^{-/-}$ do not show phenotypes under constant light, however when in combination with the *Sci* mutation, an increased proportion of split or arrhythmic behaviour is observed. This not only suggests an interaction between *Zfhx3* and *Cry1* and *Cry2* under constant light conditions, but may implicate a role for these genes together in contributing to normal circadian behaviour under constant light.

The role of cryptochrome in photoreception remains controversial but studies are starting to elucidate the function that cryptochrome plays in the mammalian retina. Studies have shown that in *Cry1*$^{-/-}$; *Cry2*$^{-/-}$ knock-out mice, the optic nerve fibres have decreased photosensitivity during the night and reduced neuronal firing activity in the SCN in response to retinal

illumination in night-time recordings. Additionally, a circadian variation in frequency of response types in the SCN is observed in WT animals, but is abolished in the *Cry1*$^{-/-}$; *Cry2*$^{-/-}$ animals (Nakamura, et al. 2011). This suggests that cryptochromes are involved in the sensitivity of circadian photoreception in mammals. As discussed, the mammalian retina contains a circadian clock including the retinal ganglion cells which express the cryptochrome genes as well as other core clock genes. Data suggests that the melanopsin containing ganglion cells also contain an autonomous circadian clock, and a loss of *Cry1* and *Cry2* results in low photosensitivity of optic nerve fibres. Additionally, differential effects on the loss of *Cry1* or *Cry2* have been observed between the retina and SCN circadian oscillator. *Cry1*$^{-/-}$ retinas show weak, low amplitude rhythms with a short period. Fairly robust circadian rhythmicity however is observed at the level of the SCN. *Cry2*$^{-/-}$ retinas and SCN show sustained periods of rhythmicity, with a longer period compared to WT. This implicates a more important function for *Cry1* in the retinal circadian clock, and an antagonistic regulation of period in the retinal clock between the two cryptochromes (Ruan, et al. 2012).

Since the identification of *Opn4*, it has been widely assumed that there is no functional role for *Cry1* and *Cry2* as photoreceptors in the mammalian retina. The data from the *Sci ; Cry* double mutants may suggest that at least *Cry1* and *Cry2* require genetic and/or molecular signalling via *Zfhx3* to maintain a normal circadian oscillation under light. This again may be required for the manipulation and plasticity of the retinal clock and does not necessarily implicate a direct role of *Cry1* or *Cry2* as a photoreceptor. However, there does appear to be some role for both *Zfhx3* and the cryptochrome genes in light mediated responses based upon the data from these double mutants.

7.5. Wider roles of *Zfhx3*

ZFHX3 and EPAS1 interaction mediates circadian responses to oxygen levels

SILAC based studies have helped to uncover wider roles of *Zfhx3* in normal physiology and provided an indication as to the reasons behind *Sci* homozygous lethality. The characterisation of the proteome in all three genotypes identified a number of proteins that were deregulated in heterozygous and homozygous mouse embryonic fibroblasts. Common pathways involved in oxidative stress and mitochondrial metabolism implicating ATP production were identified. The protein interaction between ZFHX3 and EPAS1 also suggests a role for *Zfhx3* in regulating genes involved in oxygen responses. *Epas1* is a transcription factor that binds the hypoxia response element in target gene promoters to induce transcription of oxygen regulated genes (Tanaka, et al. 2002; Tian, et al. 1998; Tian, et al. 1997). It is known that *Epas1* requires co-activators for transcriptional activity (Warnecke, et al. 2004) and the protein interaction between ZFHX3 and EPAS1 may suggest that ZFHX3 is also a co-activator of EPAS1 required for transcriptional activity in response to changes in oxygen level and hypoxic conditions. To further investigate this hypothesis, oxidated peroxiredoxin enzyme levels were investigated in *Sci* MEFs in order to determine whether the $Zfhx3^{Sci/+}$ and $Zfhx3^{Sci/Sci}$ cells were undergoing oxidative stress. Peroxiredoxin (PRX) is an antioxidant enzyme detoxifying reactive oxygen species. Signalling via PRX enzymes protects cells from oxidative induced death. A significant increase in over-oxidised peroxiredoxin was identified in $Zfhx3^{Sci/Sci}$ MEFs which would suggest an increase in free-radical accumulation and could result in cell death. This could be one contributory factor to *Sci* homozygous lethality and suggests a role of *Zfhx3* in oxidative stress pathways.

A further link between the circadian oscillator and oxidative phosphorylation may be drawn in cellular responses to DNA damage. The major source of DNA damage is reactive oxygen and

nitrogen species (ROS and RNS) (Wiseman and Halliwell 1996). The circadian clock is involved in the regulation of ROS homeostasis and as discussed previously, this again has been shown in *Sci* mutants and could be partly mediated through *Zfhx3*. ROS and RNS are produced primarily at mitochondria, an organelle where *Zfhx3* is also known to co-localise. Uncontrolled levels of ROS within the cell cause damage to macromolecules and various structures. The precise balance of ROS and energy production is therefore crucial for cell viability. The antioxidant system is required for the elimination of ROS, using for example superoxide dismutases, peroxiredoins and thioredoxins (Nordberg and Arnér 2001). An excess of ROS will result in oxidative stress and therefore impacts on pathogenesis. It has been shown that there are circadian oscillations in peroxiredoxins, with a 24 hour circadian period (Edgar, et al. 2012; O'Neill and Reddy 2011; O'Neill, et al. 2011). This would also be expected of other antioxidant enzymes to oscillate in phase with the generation of ROS and RNS over a 24 hour period. The circadian clock is the ideal system in which to anticipate the periodic variation in ROS. It has already been shown that when *Bmal1* is knocked down, mice experience chronic oxidative stress and accelerated aging (Kondratov, et al. 2006). Therefore the interconnection between the circadian clock, redox control and the cell cycle are strong and the mechanisms that connect these processes continue to be elucidated. From the total data produced in this thesis, *Zfhx3* seems to be a likely candidate to be involved in this process.

7.5.1. Retinoic acid signalling and Hox gene expression

Other signalling pathways identified from the SILAC data involved retinoic acid signalling and vitamin A metabolism. Retinoic acid signalling pathways are required for cell-cell signalling during organogenesis and are essential during development as a permissive signal for neuroectoderm, endoderm and mesoderm differentiation (Langston and Gudas 1994). Retinoic acid acts through Hox genes to control anterior/posterior patterning of the embryo

during early development (Boncinelli, et al. 1991). RNA seq analysis (Dr Rahul Satija, data not presented) in *Sci* embryonic brain tissue has also identified differences in Hox gene expression and embryonic patterning and segment identity genes. In particular, Hox genes involved in the patterning of the neural tube, including *HoxA2, Phox2b, Hoxb3, Msx3* and *Lbx1* have been shown to be down-regulated in RNA expression in homozygous embryos. After gene ontology (GO) enrichment analysis, embryonic patterning genes have been shown to be highly enriched together with those involved in retinoic acid metabolism. Together, this would be consistent with an impairment of neural differentiation. With the SILAC data and previous studies showing that ZFHX3 is highly up-regulated after multi-potent stem cell (P19) differentiation by retinoic acid application, the data indicates a role of *Zfhx3* in hox gene regulation and retinoic acid signalling.

7.5.2. *Zfhx3* functions in DNA damage responses through ATM signalling

The predominant category of proteins miss-regulated in *Sci* mutant MEFs detected by SILAC were those involved in DNA replication, cell division and DNA damage repair. Correspondingly, the most common implicated disease condition in the *Sci* mutant was cancer. *Zfhx3* is a well characterised anti-mitotic factor, implicated in various cancers and frequently mutated in prostate, breast and gastric cancers (Cho, et al. 2007; Kai, et al. 2008; Sun, et al. 2005; Sun, et al. 2007; Xu, et al. 2006; Zhang, et al. 2005). It has been proposed that *Zfhx3* acts as a tumour suppressor gene, by one method negatively regulating *c-Myb* and trans-activating the cell cycle inhibitor cyclin-dependent kinase inhibitor 1A (Kaspar, et al. 1999). Its predominant function is to promote neuronal differentiation and halt proliferation during neurogenesis.

The SILAC data showed that the *Zfhx3* mutation had affected its anti-mitotic function and impacted upon controlled cellular differentiation in *Sci* mutants. Although cancers have not

been detected in the heterozygous animals, it is possible that uncontrolled cellular differentiation is another contributory factor to homozygous lethality in this line. Since nuclear localisation of ZFHX3 is associated with cell cycle arrest, it would be of interest to investigate whether differences in localisation in target cell types are identified between the three *Sci* genotypes. Additionally, fluorescence-activated cell sorting (FACS) analysis to investigate the phase of the cell cycle and how it correlates to expression levels of *Zfhx3* and BrdU incorporation studies would be informative for investigating proliferation in correlation with *Zfhx3* expression. This has been previously shown in pregnant rats, investigating the cellular proliferation and localisation of *Zfhx3* in E13.5 dpc embryos (Ishii, et al. 2003). Cells with *Zfhx3* detected in the nucleus did not show BrdU incorporation and were arrested in post-mitotic phase. An embryonic map was generated to show where BrdU and *Zfhx3* co-localised in the developing embryo.

Zfhx3 was originally identified as binding an AT rich enhancer element in the *Afp* promoter (Yasuda, et al. 1994a). Binding to this enhancer resulted in suppression of *Afp* expression. *Afp* is often used as a biomarker for cancer, foetal abnormalities and Ataxia-Telangiectasia (AT). AT is a neurodegenerative disease caused by mutations to the ataxia-telangiesctasia mutated (ATM) gene. AT patients suffer from cerebellar degeneration. *Zfhx3*-mediated neuronal death has been shown to be dependent on ATM since blockade of ATM, by inhibitors such as caffeine, abolishes this activity (Jung, et al. 2005). Studies have shown that the use of DNA-damaging drugs result in an increase of *Zfhx3* expression in cortical neurons in turn causes an activation of ATM signalling (Jung, et al. 2011). Upon DNA damage, ATM becomes active through auto-phosphorylation on Ser1981 and can then regulate proteins involved in DNA repair, apoptosis and checkpoint control. ATM has a number of targets through which it acts, including *p53, Chk1* and *Chk2*. Co-immuno-precipitation experiments have shown that after DNA damage, ZFHX3 forms a protein interaction with phosphorylated ATM and can then

activate signalling cascades to promote neuronal cell death. Further concordance of function between ATM and ZFHX3 is observed through the *p21* and *p53* genes. ATM activates *p53* to arrest the cell cycle upon DNA damage. *Zfhx3* is known to cooperate with p53 to activate the *p21* promoter together. Data has shown a tight synergistic relationship between ATM and *Zfhx3* through *p53* and *p21*. These data are consistent with mis-regulated proteins identified in the SILAC data, further confirming the link between ATM and DNA damage signalling with *Zfhx3* and aberrant cellular division in the *Sci* mutants.

Links may also be drawn however between ATM, *Zfhx3* and oxidative stress as previously discussed. A novel signalling pathway has been proposed linking ATM to ZFHX3 via cAMP-responsive-element-binding protein (CREB). This pathway promotes the survival of neurons by inducing the expression of platelet-derived growth factor receptor β (*Pdgfrb*). Inhibiting *Pdgfrb* has been shown to suppress ATM activation under oxidative stress but not under X-ray irradiation which implicates the activity of a kinase required to trigger activation of ATM specifically under oxidative stress independent to genotoxic stress. Activating ATM, through ZFHX3 signalling, may be a mechanism of neuronal protection against oxidative stress (Kim, et al. 2010).

7.5.3. Circadian control of the cell cycle through *Zfhx3* signalling

With a fairly complete and robust molecular mechanism generated for the circadian clock, many attempts are now focused on mechanistically linking the circadian clock to other biological processes. The cell cycle is one area where there appears to be a tight association with the circadian clock. 24 hour oscillations have been identified in key cell cycle regulatory components, including cyclins, *c-myc* and *Wee1.* Interestingly, ZFHX3 is known to interact with key cell cycle regulators including p21 (Miura, et al. 2004a). ZFHX3 may be involved in regulating their expression to be in synchrony with the circadian oscillator. This is known to be

the case for *c-myc, cyclin D1* and *Wee1* which are under transcriptional control by CLOCK/BMAL1. *p21* is also under transcriptional regulation by REV-ERBα, indirectly through CLOCK/BMAL1 (Hunt and Sassone-Corsi 2007). Mutations to clock genes have been shown to produce phenotypes of aberrant cellular proliferation, deficits in mitosis and cancer markers. *Cry* deficient mice show impaired hepatocyte proliferation due to constitutively high levels of WEE1 kinase which affects G2/M progression (Matsuo, et al. 2003). A similar phenotype has been observed in *Bmal1* knock-out mice, which has been shown to be due to the imbalance imposed on *Bmal1* circadian targets, *Reverbα* and *Rorα* (Gréchez-Cassiau, et al. 2008). The result is an up-regulation of p21 and delayed progression through G1 phase. It is therefore apparent that the circadian clock can directly influence cell cycle progression and affects processes with a non-circadian rhythm.

Animals with mutations to core clock components have so far been annotated to have no embryonic defects. *Timeless* mutants are an exception, with animals dying early in embryonic development (Benna, et al. 2000). *Sci* homozygous mutant mice also die in late gestation and considering the SILAC data, known roles of ZFHX3 and evolutionary conservation data, *Zfhx3* may have key roles in regulating the cell cycle and with data from this thesis, also in regulating the circadian clock. As such, *Zfhx3* could be a critical gene that holds these two processes together.

The circadian clock is also involved in checkpoint control. When DNA damage is detected by the cell via sensor proteins, cell cycle check point kinases act to repress or activate the transition through the cell cycle. As discussed, CLOCK/BMAL1 are established cell cycle regulators. Additionally, *Per1* has been shown to link ATM pathways to the circadian clock (Gery, et al. 2006). Similarly, *Timeless* (TIM) in the *Drosophila* system interacts with ATR and check point proteins (Unsal-Kaçmaz, et al. 2005). These interactions facilitate the activation of check point kinases and as such the circadian clock is able to modulate proliferation in

response to genotoxic stress. p53 is activated after the initiation of the ATM DNA damage response pathway. It is the stability of p53, achieved through post-translational modification, that results in its activation and ability to regulate the transcription of many target genes to cause an arrest in the cell cycle or apoptosis. *Bmal1* has already been identified as a clock component that can modulate p53 and is necessary for p53-dependent growth arrest (Antoch and Kondratov 2010). ZFHX3 physically binds with p53 and this interaction may also be able to facilitate the stability and activation of the p53 protein. In this way, ZFHX3 may be providing a strong link between p53 mediated apoptosis and cell cycle arrest and the circadian clock.

7.5.4. Circadian responses to genotoxic and chemotoxic stress

Circadian effects can be observed on cells in culture exposed to ionizing radiation to induce DNA damage. Shifts in the phase of oscillation are observed on cells in culture, with ionizing radiation causing exclusively phase advances rather than phase delays (which are observed with chemical compounds) (Oklejewicz, et al. 2008). The circadian clock mediates radiation-induced phase resetting and this circadian phenotype is lost in AT patients. The effects of ionizing radiation on the circadian clock can also be seen in overt behavioural rhythms and is therefore a circadian mechanism that acts on both the molecular oscillator in the SCN level but also on the periphery. The mechanism by which this occurs is unknown, however the tight correlation between ATM signalling, p53 and circadian clock protein interactions may make *Zfhx3* a good candidate gene to be involved in this process. It would be valuable to test whether fibroblasts from *Sci* animals are able to phase advance in response to ionizing radiation or whether the mutation to *Zfhx3* has affected this mechanism between DNA damage responses and the circadian clock.

7.6. Future work

7.6.1. Protein based studies

Currently, the data produced strongly suggests an involvement of *Zfhx3* on the core circadian clock mechanism. The majority of work has focused on RNA based studies, investigating the expression pattern and localisation. With the generation of a suitable ZFHX3 antibody, protein analysis may then follow to determine whether the protein expression pattern follows that observed in RNA. Although the RNA data is conclusive, it may not be assumed that the protein products follow the same pattern. Over-expression based studies have been predominantly utilised to over-come the lack of antibody resources and low expression of investigated proteins in the cellular systems used. As such, work should continue to confirm these results in an endogenous system in order to avoid any artefacts of over-expression. It would be valuable to determine the timing at which ZFHX3 is binding the identified co-immunoprecipitated protein partners, CRY1, CRY2, PER2 and EPAS1. Additionally, the sub-cellular localisation of these interactions should be determined. With this information, the nature and purpose of these interactions can be identified. For example, with a protein interaction between CRY1/2 or PER2 in the nucleus, ZFHX3 may be involved in the negative feedback mechanism, targeting (or removing) these proteins to the CLOCK/BMAL1 complex. The interaction may occur in the cytoplasm, perhaps as a scaffold protein involved in directing the CRY/PER complex to or from the nucleus or allowing their post-translational modification and degradation. The timing of interactions may have a circadian element and together with localisation studies, would be of importance in understanding the function of these interactions and potential effects of the *Sci* mutation.

7.6.2. Transcriptional-based assays

As a transcription factor, *Zfhx3* may regulate clock gene transcription directly. Chromatin immuno-precipitation experiments were attempted during the production of data for this thesis however antibodies were unsuccessful in immuno-precipitating ZFHX3. In addition, this technique was attempted in an over-expression system and this method was also unsuccessful. Future work requires optimisation of a functional antibody to determine whether ZFHX3 is bound to any regulatory regions, promoter or enhancer elements, within clock genes. Bioinformatic analyses and previous literature has shown that ZFHX3 binds to an AT consensus sequence for regulating transcription (Morinaga, et al. 1991b; Ninomiya, et al. 2002), however it is possible that due to the size and complexity of the ZFHX3 protein it may also be able to bind other sequences. Additionally, its regulation of transcription may be indirect, perhaps through masking the E-box or other enhancer elements due to the nature of ZFHX3's size. It is hypothesised that ZFHX3 is involved in circadian gene transcriptional regulation, either in an indirect or direct manner and this can be conclusively determined through chromatin immuno-precipitation experiments. Further molecular based *in vitro* studies, such as luciferase reporter gene assays using promoter constructs are currently being performed in the laboratory. Circadian gene promoter regions tagged with luciferase have been constructed in order to determine whether luciferase expression can be driven by over-expressed *ZFHX3*.

7.6.3. Alternative models and mutant resources

The use of additional mutants would facilitate the research into *Zfhx3* and its involvement on the core circadian clock. Firstly, a conditional knock out using an SCN and/or retinal CRE lines would provide data as to whether *Zfhx3* is required for normal visual and circadian function when knocked out in the adult animal. A conditional knockout is also vital when working with

a transcription factor which is required for normal embryonic development. An assessment of wheel running activity in adult mice homozygous for a loss of *Zfhx3* in the SCN would provide conclusive support for an effect of *Zfhx3* on circadian rhythmicity. Additionally, it would be interesting and valuable to determine whether there are circadian or visual phenotypes as a result of a down-regulation or loss of *Zfhx3* in the retina – either in the total retina or specific cell layers. This would not only support a link between the visual system and the circadian clock, mediated through *Zfhx3.* Also an investigation into the effects on the cryptochrome genes could be investigated and could add to the debate of the involvement of the cryptochrome genes on light mediated circadian responses.

Further genetic interaction studies may be pursued in epistasis experiments. With a protein interaction with PER2 and effects on the RNA of *Per1* respectively, the next suitable out-cross with *Sci* may be to *Per1*$^{-/-}$ and *Per2*$^{-/-}$ knock-out animals. An investigation into the phenotype by monitoring wheel running activity would identify whether a genetic interaction exists not only between the cryptochrome genes but also the period genes. This data would help support and prove the hypotheses on the involvement of *Zfhx3* on the core clock through these genes.

With an involvement identified between *Zfhx3* with *Gad1* and *Gad2* signalling potentially implicating GABA neurotransmission, it may be useful to investigate additional mutants, either reporter lines or knockout animals. The use of a *Gad1*-GFP reporter has been investigated and crosses between this animal and *Sci* could be generated in order to perform histological analyses to investigate whether there are any differences in *Gad1* expression in various target cells including the SCN and the retina. Further investigation into the effects on GABA neurotransmission could be determined by investigating various *Gad1* or *Gad2* gene-trap or conditional knock-out animals and investigating the molecular consequences on *Zfhx3* and

circadian target genes in both single mutant animals and in double mutants generated by crossing to *Sci*.

7.7. Final Conclusions

Sci was identified in a forward genetics screen using chemical mutagenesis in *M. musculus*. This method has been used to identify novel genes or novel gene functions within the context of the investigated phenotype, circadian behaviour. Work presented in this thesis has aimed to characterise this ENU mouse mutant and the novel gene involved in the circadian system. The data has indicated that *Zfhx3* is a novel circadian gene that is involved across many levels of the circadian system. *Zfhx3* has been shown to affect and function in photic detection and transduction of light entrainment signals to the SCN. Additionally, the short circadian phenotype together with molecular data strongly suggests that *Zfhx3* acts within the core molecular oscillator. Finally, *Zfhx3* appears to be a scaffold gene that has the potential to link the circadian clock to other physiological states that require circadian modification. These include the cell cycle, oxidative stress and ATP synthesis and developmental processes.

Substantial advances continue to be made in circadian research and there are already a number of clock genes identified which have been characterised for their role within the circadian oscillator. A comprehensive molecular mechanism for the core circadian feedback loop has been well developed and studied. The circadian system however is becoming increasingly complex as new genes are detected in both forward and reverse genetic strategies. The identification of new genes impacting on circadian behaviour are expanding the over-lap between the circadian system and other molecular, genetic and physiological systems. Additionally the known degree of complexity and molecular and genetic control over maintaining an accurate circadian oscillation is increasing. There are many aspects to circadian physiology which still remain unknown and mutagenesis screening efforts are

facilitating advancements in these areas with novel genes, such as *Zfhx3* affected in the *Sci* mutant, being identified.

Chapter VIII

Bibliography

Albrecht, U., et al.

2001 MPer1 and mper2 are essential for normal resetting of the circadian clock. J Biol Rhythms 16(2):100-4.

Antoch, M. P., and R. V. Kondratov

2010 Circadian proteins and genotoxic stress response. Circ Res 106(1):68-78.

Antoch, M. P., et al.

1997 Functional identification of the mouse circadian Clock gene by transgenic BAC rescue. Cell 89(4):655-67.

Aschoff, J.

1960 Exogenous and endogenous components in circadian rhythms. Cold Spring Harb Symp Quant Biol 25:11-28.

Atherton, G. T., et al.

1996 Regulation of cell differentiation in C2C12 myoblasts by the Id3 helix-loop-helix protein. Cell Growth Differ 7(8):1059-66.

Aton, S. J., et al.

2005 Vasoactive intestinal polypeptide mediates circadian rhythmicity and synchrony in mammalian clock neurons. Nat Neurosci 8(4):476-83.

Bacon, Y., et al.

2004 Screening for novel ENU-induced rhythm, entrainment and activity mutants. Genes Brain Behav 3(4):196-205.

Bae, K., et al.

2001 Differential functions of mPer1, mPer2, and mPer3 in the SCN circadian clock. Neuron 30(2):525-36.

Balling, R.

2001 ENU mutagenesis: analyzing gene function in mice. Annu Rev Genomics Hum Genet 2:463-92.

Battey, J. F., et al.

1991 Molecular cloning of the bombesin/gastrin-releasing peptide receptor from Swiss 3T3 cells. Proc Natl Acad Sci U S A 88(2):395-9.

Battey, J., and E. Wada

1991 Two distinct receptor subtypes for mammalian bombesin-like peptides. Trends Neurosci 14(12):524-8.

Benezra, R., et al.

1990 Id: a negative regulator of helix-loop-helix DNA binding proteins. Control of terminal myogenic differentiation. Ann N Y Acad Sci 599:1-11.

Benjamin, E. J., et al.

2009a Variants in ZFHX3 are associated with atrial fibrillation in individuals of European ancestry. Nat Genet 41(8):879-81.

Benjamin, E. J., et al.

2009b Variants in ZFHX3 are associated with atrial fibrillation in individuals of European ancestry. Nat Genet 41(8):879-81.
Benna, C., et al.

2000 A second timeless gene in Drosophila shares greater sequence similarity with mammalian tim. Curr Biol 10(14):R512-3.
Berry, F. B., et al.

2001 Positive and negative regulation of myogenic differentiation of C2C12 cells by isoforms of the multiple homeodomain zinc finger transcription factor ATBF1. J Biol Chem 276(27):25057-65.
Blackshaw, S., and S. H. Snyder

1999 Encephalopsin: a novel mammalian extraretinal opsin discretely localized in the brain. J Neurosci 19(10):3681-90.
Boncinelli, E., et al.

1991 HOX gene activation by retinoic acid. Trends Genet 7(10):329-34.
Bowden, N. A., R. J. Scott, and P. A. Tooney

2008 Altered gene expression in the superior temporal gyrus in schizophrenia. BMC Genomics 9:199.
Bozek, K., et al.

2009 Regulation of clock-controlled genes in mammals. PLoS One 4(3):e4882.
Braff, DL, NR Swerdlow, and MA Geyer

1999 Symptom correlates of prepulse inhibition deficits in male schizophrenic patients. Am J Psychiatry 156(4):596-602.
Brown, T. M., et al.

2007 Disrupted neuronal activity rhythms in the suprachiasmatic nuclei of vasoactive intestinal polypeptide-deficient mice. J Neurophysiol 97(3):2553-8.
Bruce, V. G.

1972 Mutants of the biological clock in Chlamydomonas reinhardi. Genetics 70(4):537-48.
Buhr, E. D., S. H. Yoo, and J. S. Takahashi

2010 Temperature as a universal resetting cue for mammalian circadian oscillators. Science 330(6002):379-85.
Burgner, D., et al.

2009 A genome-wide association study identifies novel and functionally related susceptibility Loci for Kawasaki disease. PLoS Genet 5(1):e1000319.
Busino, L., et al.

2007 SCFFbxl3 controls the oscillation of the circadian clock by directing the degradation of cryptochrome proteins. Science 316(5826):900-4.
Caligo, M. A., et al.

1998 A region on the long arm of chromosome 16 is frequently deleted in metastatic node-negative breast cancer. Int J Oncol 13(1):177-82.
Carneiro, B. T., and J. F. Araujo

2009 The food-entrainable oscillator: a network of interconnected brain structures entrained by humoral signals? Chronobiol Int 26(7):1273-89.
Cermakian, N., and D. B. Boivin

2003 A molecular perspective of human circadian rhythm disorders. Brain Res Brain Res Rev 42(3):204-20.
Cermakian, N., et al.

2001 Altered behavioral rhythms and clock gene expression in mice with a targeted mutation in the Period1 gene. EMBO J 20(15):3967-74.
Chen, K. F., et al.

2011a QUASIMODO, a Novel GPI-anchored zona pellucida protein involved in light input to the Drosophila circadian clock. Curr Biol 21(9):719-29.
Chen, S. K., T. C. Badea, and S. Hattar

2011b Photoentrainment and pupillary light reflex are mediated by distinct populations of ipRGCs. Nature 476(7358):92-5.
Cherry, T. J., et al.

2009 Development and diversification of retinal amacrine interneurons at single cell resolution. Proc Natl Acad Sci U S A 106(23):9495-500.
Cho, Y. G., et al.

2007 Genetic alterations of the ATBF1 gene in gastric cancer. Clin Cancer Res 13(15 Pt 1):4355-9.
Cleton-Jansen, A. M., et al.

2008 ATBF1 and NQO1 as candidate targets for allelic loss at chromosome arm 16q in breast cancer: absence of somatic ATBF1 mutations and no role for the C609T NQO1 polymorphism. BMC Cancer 8:105.
Colwell, C. S.

2000 Rhythmic coupling among cells in the suprachiasmatic nucleus. J Neurobiol 43(4):379-88.
Colwell, C. S., et al.

2003 Disrupted circadian rhythms in VIP- and PHI-deficient mice. Am J Physiol Regul Integr Comp Physiol 285(5):R939-49.
Colwell, C. S., et al.

2004 Selective deficits in the circadian light response in mice lacking PACAP. Am J Physiol Regul Integr Comp Physiol 287(5):R1194-201.
Cordes, S. P.

2005 N-ethyl-N-nitrosourea mutagenesis: boarding the mouse mutant express. Microbiol Mol Biol Rev 69(3):426-39.
Crowe, D. L., R. Kim, and R. A. Chandraratna

2003 Retinoic acid differentially regulates cancer cell proliferation via dose-dependent modulation of the mitogen-activated protein kinase pathway. Mol Cancer Res 1(7):532-40.
Daan, S.

2000 The Colin S. Pittendrigh Lecture. Colin Pittendrigh, Jurgen Aschoff, and the natural entrainment of circadian systems. J Biol Rhythms 15(3):195-207.
Dardente, H., et al.

2008 Implication of the F-Box Protein FBXL21 in circadian pacemaker function in mammals. PLoS One 3(10):e3530.
Debruyne, J. P., et al.

2006 A clock shock: mouse CLOCK is not required for circadian oscillator function. Neuron 50(3):465-77.
DeBruyne, J. P., D. R. Weaver, and S. M. Reppert

2007 CLOCK and NPAS2 have overlapping roles in the suprachiasmatic circadian clock. Nat Neurosci 10(5):543-5.
Decoursey, P. J.

1960 Phase control of activity in a rodent. Cold Spring Harb Symp Quant Biol 25:49-55.
Dey, J., et al.

2005 The tau mutation in the Syrian hamster differentially reprograms the circadian clock in the SCN and peripheral tissues. Journal of Biological Rhythms 20(2):99-110.
Ding, J. M., et al.

1998 A neuronal ryanodine receptor mediates light-induced phase delays of the circadian clock. Nature 394(6691):381-4.
Ding, J. M., et al.

1997 Resetting the biological clock: mediation of nocturnal CREB phosphorylation via light, glutamate, and nitric oxide. J Neurosci 17(2):667-75.
Dong, X. Y., et al.

2011 Estrogen up-regulates ATBF1 transcription but causes its protein degradation in estrogen receptor-alpha-positive breast cancer cells. J Biol Chem 286(16):13879-90.
Dong, X. Y., et al.

2010 ATBF1 inhibits estrogen receptor (ER) function by selectively competing with AIB1 for binding to the ER in ER-positive breast cancer cells. J Biol Chem 285(43):32801-9.
Dunlap, J. C.

1999 Molecular bases for circadian clocks. Cell 96(2):271-90.
Ebling, F. J.

1996 The role of glutamate in the photic regulation of the suprachiasmatic nucleus. Prog Neurobiol 50(2-3):109-32.
Edgar, R. S., et al.

2012 Peroxiredoxins are conserved markers of circadian rhythms. Nature 485(7399):459-64.
Edmunds, L. N., D. L. Laval-Martin, and K. Goto

1987 Cell division cycles and circadian clocks. Modeling a metabolic oscillator in the algal flagellate Euglena. Ann N Y Acad Sci 503:459-75.

Edwards, K. D., et al.

2006 FLOWERING LOCUS C mediates natural variation in the high-temperature response of the Arabidopsis circadian clock. Plant Cell 18(3):639-50.

Eglen, S. J., et al.

2003 Dopaminergic amacrine cells in the inner nuclear layer and ganglion cell layer comprise a single functional retinal mosaic. J Comp Neurol 466(3):343-55.

Ehlen, J. C., and K. N. Paul

2009 Regulation of light's action in the mammalian circadian clock: role of the extrasynaptic GABAA receptor. Am J Physiol Regul Integr Comp Physiol 296(5):R1606-12.

Fortini, M. E., Z. C. Lai, and G. M. Rubin

1991 The Drosophila zfh-1 and zfh-2 genes encode novel proteins containing both zinc-finger and homeodomain motifs. Mech Dev 34(2-3):113-22.

Foster, R. G., et al.

1991 Circadian photoreception in the retinally degenerate mouse (rd/rd). J Comp Physiol A 169(1):39-50.

Freedman, M. S., et al.

1999 Regulation of mammalian circadian behavior by non-rod, non-cone, ocular photoreceptors. Science 284(5413):502-4.

Gachon, F., et al.

2004 The loss of circadian PAR bZip transcription factors results in epilepsy. Genes Dev 18(12):1397-412.

Gallego, M., and D. M. Virshup

2007 Post-translational modifications regulate the ticking of the circadian clock. Nature Reviews Molecular Cell Biology 8(2):139-148.

Gegear, R. J., et al.

2010 Animal cryptochromes mediate magnetoreception by an unconventional photochemical mechanism. Nature 463(7282):804-7.

Gekakis, N., et al.

1998 Role of the CLOCK protein in the mammalian circadian mechanism. Science 280(5369):1564-9.

Genetta, T., D. Ruezinsky, and T. Kadesch

1994 Displacement of an E-box-binding repressor by basic helix-loop-helix proteins: implications for B-cell specificity of the immunoglobulin heavy-chain enhancer. Molecular and Cellular Biology 14(9):6153-63.

Gery, S., et al.

2006 The circadian gene per1 plays an important role in cell growth and DNA damage control in human cancer cells. Mol Cell 22(3):375-82.

Godinho, S. I., et al.

2007 The after-hours mutant reveals a role for Fbxl3 in determining mammalian circadian period. Science 316(5826):897-900.

Golombek, D. A., and R. E. Rosenstein

2010 Physiology of circadian entrainment. Physiol Rev 90(3):1063-102.
Gould, P. D., et al.

2006 The molecular basis of temperature compensation in the Arabidopsis circadian clock. Plant Cell 18(5):1177-87.
Gray, P. A., et al.

2004 Mouse brain organization revealed through direct genome-scale TF expression analysis. Science 306(5705):2255-7.
Gréchez-Cassiau, A., et al.

2008 The circadian clock component BMAL1 is a critical regulator of p21WAF1/CIP1 expression and hepatocyte proliferation. J Biol Chem 283(8):4535-42.
Gudbjartsson, D. F., et al.

2009 A sequence variant in ZFHX3 on 16q22 associates with atrial fibrillation and ischemic stroke. Nat Genet 41(8):876-8.
Halford, S., et al.

2001 Characterization of a novel human opsin gene with wide tissue expression and identification of embedded and flanking genes on chromosome 1q43. Genomics 72(2):203-8.
Hampson, E. C., D. I. Vaney, and R. Weiler

1992 Dopaminergic modulation of gap junction permeability between amacrine cells in mammalian retina. J Neurosci 12(12):4911-22.
Hao, H., D. L. Allen, and P. E. Hardin

1997 A circadian enhancer mediates PER-dependent mRNA cycling in Drosophila melanogaster. Molecular and Cellular Biology 17(7):3687-93.
Harmar, A. J., et al.

2002 The VPAC(2) receptor is essential for circadian function in the mouse suprachiasmatic nuclei. Cell 109(4):497-508.
Hashimoto, T., et al.

1992 A new family of homeobox genes encoding multiple homeodomain and zinc finger motifs. Mech Dev 39(1-2):125-6.
Hattar, S., et al.

2002 Melanopsin-containing retinal ganglion cells: architecture, projections, and intrinsic photosensitivity. Science 295(5557):1065-70.
Haunerland, N. H., and F. Spener

2004 Fatty acid-binding proteins--insights from genetic manipulations. Prog Lipid Res 43(4):328-49.
Herzog, E. D., et al.

2004 Temporal precision in the mammalian circadian system: a reliable clock from less reliable neurons. J Biol Rhythms 19(1):35-46.
Herzog, E. D., and R. M. Huckfeldt

2003 Circadian entrainment to temperature, but not light, in the isolated suprachiasmatic nucleus. J Neurophysiol 90(2):763-70.
Hoang, N., et al.

2008 Human and Drosophila cryptochromes are light activated by flavin photoreduction in living cells. PLoS Biol 6(7):e160.
Hoey, T., and M. Levine

1988 Divergent homeo box proteins recognize similar DNA sequences in Drosophila. Nature 332(6167):858-61.
Hoffpauir, B. K., and E. L. Gleason

2005 Modulation of synaptic function in retinal amacrine cells. Integr Comp Biol 45(4):658-64.
Hogenesch, J. B., et al.

1998 The basic-helix-loop-helix-PAS orphan MOP3 forms transcriptionally active complexes with circadian and hypoxia factors. Proc Natl Acad Sci U S A 95(10):5474-9.
Holland, P. W., H. A. Booth, and E. A. Bruford

2007 Classification and nomenclature of all human homeobox genes. BMC Biol 5:47.
Hong, S., et al.

2010 Type II protein arginine methyltransferase 5 (PRMT5) is required for circadian period determination in Arabidopsis thaliana. Proc Natl Acad Sci U S A 107(49):21211-6.
Hughes, S., et al.

2012 Profound defects in pupillary responses to light in TRPM-channel null mice: a role for TRPM channels in non-image-forming photoreception. Eur J Neurosci 35(1):34-43.
Hunt, T., and P. Sassone-Corsi

2007 Riding tandem: circadian clocks and the cell cycle. Cell 129(3):461-4.
Ido, A, Y Miura, and T Tamaoki

1994 Activation of ATBF1, a multiple-homeodomain zinc-finger gene, during neuronal differentiation of murine embryonal carcinoma cells. Dev Biol 163(1):184-7.
Ido, A., et al.

1996 Cloning of the cDNA encoding the mouse ATBF1 transcription factor. Gene 168(2):227-31.
Iitaka, C., et al.

2005 A role for glycogen synthase kinase-3 beta in the mammalian circadian clock. Journal of Biological Chemistry 280(33):29397-29402.
Immenschuh, S., and E. Baumgart-Vogt

2005 Peroxiredoxins, oxidative stress, and cell proliferation. Antioxid Redox Signal 7(5-6):768-77.
Ingram, C. D., et al.

1998 Vasopressin neurotransmission and the control of circadian rhythms in the suprachiasmatic nucleus. Prog Brain Res 119:351-64.

Ingram, C. D., R. K. Snowball, and R. Mihai

1996 Circadian rhythm of neuronal activity in suprachiasmatic nucleus slices from the vasopressin-deficient Brattleboro rat. Neuroscience 75(2):635-41.

Ishii, Y., et al.

2003 ATBF1-A protein, but not ATBF1-B, is preferentially expressed in developing rat brain. J Comp Neurol 465(1):57-71.

Janik, D., and N. Mrosovsky

1994 Intergeniculate leaflet lesions and behaviorally-induced shifts of circadian rhythms. Brain Res 651(1-2):174-82.

Jiang, H., and M. Xiang

2009 Subtype specification of GABAergic amacrine cells by the orphan nuclear receptor Nr4a2/Nurr1. J Neurosci 29(33):10449-59.

Johnson, R. F., R. Y. Moore, and L. P. Morin

1988 Loss of entrainment and anatomical plasticity after lesions of the hamster retinohypothalamic tract. Brain Res 460(2):297-313.

Jung, C. G., et al.

2011 Beta-amyloid increases the expression level of ATBF1 responsible for death in cultured cortical neurons. Mol Neurodegener 6:47.

Jung, CG, et al.

2005 Homeotic factor ATBF1 induces the cell cycle arrest associated with neuronal differentiation. Development 132(23):5137-45.

Justice, M. J., et al.

1999 Mouse ENU mutagenesis. Hum Mol Genet 8(10):1955-63.

Kai, K, et al.

2008 Loss of heterozygosity at the ATBF1-A locus located in the 16q22 minimal region in breast cancer. BMC Cancer 8:262.

Kaspar, P., et al.

1999 Myb-interacting protein, ATBF1, represses transcriptional activity of Myb oncoprotein. J Biol Chem 274(20):14422-8.

Kasper, G., et al.

2002 Different structural organization of the encephalopsin gene in man and mouse. Gene 295(1):27-32.

Kim, T. S., et al.

2010 The ZFHX3 (ATBF1) transcription factor induces PDGFRB, which activates ATM in the cytoplasm to protect cerebellar neurons from oxidative stress. Dis Model Mech 3(11-12):752-62.

King, D. P., et al.

1997a The mouse Clock mutation behaves as an antimorph and maps within the W19H deletion, distal of Kit. Genetics 146(3):1049-60.

King, D. P., et al.

1997b Positional cloning of the mouse circadian clock gene. Cell 89(4):641-53.
Ko, C. H., and J. S. Takahashi

2006 Molecular components of the mammalian circadian clock. Hum Mol Genet 15 Spec No 2:R271-7.
Kondratov, R. V., et al.

2006 Early aging and age-related pathologies in mice deficient in BMAL1, the core componentof the circadian clock. Genes Dev 20(14):1868-73.
Konopka, R. J., and S. Benzer

1971 Clock mutants of Drosophila melanogaster. Proc Natl Acad Sci U S A 68(9):2112-6.
Krachmer, J. H., R. S. Feder, and M. W. Belin

1984 Keratoconus and related noninflammatory corneal thinning disorders. Surv Ophthalmol 28(4):293-322.
Kume, K., et al.

1999 mCRY1 and mCRY2 are essential components of the negative limb of the circadian clock feedback loop. Cell 98(2):193-205.
Langston, A. W., and L. J. Gudas

1994 Retinoic acid and homeobox gene regulation. Curr Opin Genet Dev 4(4):550-5.
Lavin, M. F., and S. Kozlov

2007 DNA damage-induced signalling in ataxia-telangiectasia and related syndromes. Radiother Oncol 83(3):231-7.
Lee, J. H., and T. T. Paull

2005 ATM activation by DNA double-strand breaks through the Mre11-Rad50-Nbs1 complex. Science 308(5721):551-4.
Li, C., et al.

2011 Significant association of SNP rs2106261 in the ZFHX3 gene with atrial fibrillation in a Chinese Han GeneID population. Hum Genet 129(3):239-46.
Li, M., et al.

2009 Alpha fetoprotein is a novel protein-binding partner for caspase-3 and blocks the apoptotic signaling pathway in human hepatoma cells. Int J Cancer 124(12):2845-54.
Liskova, P., et al.

2007 Novel mutations in the ZEB1 gene identified in Czech and British patients with posterior polymorphous corneal dystrophy. Hum Mutat 28(6):638.
Liu, A. C., et al.

2007 Intercellular coupling confers robustness against mutations in the SCN circadian clock network. Cell 129(3):605-16.
Liu, Y., et al.

2008a Zeb1 links epithelial-mesenchymal transition and cellular senescence. Development 135(3):579-88.
Liu, Y., et al.

2008b Zeb1 mutant mice as a model of posterior corneal dystrophy. Invest Ophthalmol Vis Sci 49(5):1843-9.
Loros, J. J., S. A. Denome, and J. C. Dunlap

1989 Molecular cloning of genes under control of the circadian clock in Neurospora. Science 243(4889):385-8.
Lowrey, P. L., et al.

2000 Positional syntenic cloning and functional characterization of the mammalian circadian mutation tau. Science 288(5465):483-491.
Lucas, R. J., et al.

2003 Diminished pupillary light reflex at high irradiances in melanopsin-knockout mice. Science 299(5604):245-7.
Ludolph, D. C., and S. F. Konieczny

1995 Transcription factor families: muscling in on the myogenic program. Faseb Journal 9(15):1595-604.
Lundell, M. J., and J. Hirsh

1992 The zfh-2 gene product is a potential regulator of neuron-specific dopa decarboxylase gene expression in Drosophila. Dev Biol 154(1):84-94.
Mabuchi, M., et al.

2010 Tumor suppressor, AT motif binding factor 1 (ATBF1), translocates to the nucleus with runt domain transcription factor 3 (RUNX3) in response to TGF-beta signal transduction. Biochem Biophys Res Commun 398(2):321-5.
Maden, M.

2007 Retinoic acid in the development, regeneration and maintenance of the nervous system. Nat Rev Neurosci 8(10):755-65.
Maemura, K., et al.

2000 CLIF, a novel cycle-like factor, regulates the circadian oscillation of plasminogen activator inhibitor-1 gene expression. J Biol Chem 275(47):36847-51.
Mann, R. S.

1995 The specificity of homeotic gene function. Bioessays 17(10):855-63.
Mathur, A., D. A. Golombek, and M. R. Ralph

1996 cGMP-dependent protein kinase inhibitors block light-induced phase advances of circadian rhythms in vivo. Am J Physiol 270(5 Pt 2):R1031-6.
Matsuo, T., et al.

2003 Control mechanism of the circadian clock for timing of cell division in vivo. Science 302(5643):255-9.
MAURICE, D. M.

1957 The structure and transparency of the cornea. J Physiol 136(2):263-86.
Mendoza, J.

2007 Circadian clocks: setting time by food. Journal of Neuroendocrinology 19(2):127-37.
Meng, Q. J., et al.

2008 Setting clock speed in mammals: The CK1 epsilon tau mutation in mice accelerates circadian pacemakers by selectively destabilizing PERIOD proteins. Neuron 58(1):78-88.

Menger, N., and H. Wassle

2000 Morphological and physiological properties of the A17 amacrine cell of the rat retina. Vis Neurosci 17(5):769-80.

Minors, D. S., J. M. Waterhouse, and A. Wirz-Justice

1991 A human phase-response curve to light. Neurosci Lett 133(1):36-40.

Mintz, E. M., et al.

2002 GABA interacts with photic signaling in the suprachiasmatic nucleus to regulate circadian phase shifts. Neuroscience 109(4):773-8.

Mitsui, S., et al.

2001 Antagonistic role of E4BP4 and PAR proteins in the circadian oscillatory mechanism. Genes Dev 15(8):995-1006.

Miura, Y, et al.

2004a Susceptibility to killer T cells of gastric cancer cells enhanced by Mitomycin-C involves induction of ATBF1 and activation of p21 (Waf1/Cip1) promoter. Microbiol Immunol 48(2):137-45.

Miura, Y, et al.

1995 Cloning and characterization of an ATBF1 isoform that expresses in a neuronal differentiation-dependent manner. J Biol Chem 270(45):26840-8.

Miura, Y., et al.

2004b Susceptibility to killer T cells of gastric cancer cells enhanced by Mitomycin-C involves induction of ATBF1 and activation of p21 (Waf1/Cip1) promoter. Microbiol Immunol 48(2):137-45.

Molkentin, J. D., et al.

1995 Cooperative activation of muscle gene expression by MEF2 and myogenic bHLH proteins. Cell 83(7):1125-36.

Moore, R. Y., J. C. Speh, and J. P. Card

1995 The retinohypothalamic tract originates from a distinct subset of retinal ganglion cells. J Comp Neurol 352(3):351-66.

Mori, K., et al.

2005 Identification of neuromedin S and its possible role in the mammalian circadian oscillator system. EMBO J 24(2):325-35.

Morin, L. P., and C. N. Allen

2006 The circadian visual system, 2005. Brain Res Rev 51(1):1-60.

Morinaga, T., et al.

1991a A human alpha-fetoprotein enhancer-binding protein, ATBF1, contains four homeodomains and seventeen zinc fingers. Molecular and Cellular Biology 11(12):6041-9.

—

1991b A human alpha-fetoprotein enhancer-binding protein, ATBF1, contains four homeodomains and seventeen zinc fingers. Mol Cell Biol 11(12):6041-9.
Mrosovsky, N.

1988 Phase response curves for social entrainment. J Comp Physiol A 162(1):35-46.
Nagai, N., et al.

1996 Roles of the suprachiasmatic nucleus and vasoactive intestinal peptide in the response of plasma arginine vasopressin to osmotic challenge. Endocrinology 137(2):504-7.
Naidu, P. S., et al.

1995 Myogenin and MEF2 function synergistically to activate the MRF4 promoter during myogenesis. Molecular and Cellular Biology 15(5):2707-18.
Nakamura, T. J., S. Ebihara, and K. Shinohara

2011 Reduced light response of neuronal firing activity in the suprachiasmatic nucleus and optic nerve of cryptochrome-deficient mice. PLoS One 6(12):e28726.
Nakazawa, K., et al.

2012 GABAergic interneuron origin of schizophrenia pathophysiology. Neuropharmacology 62(3):1574-83.
Nelson, R. J., and I. Zucker

1981 Photoperiodic control of reproduction in olfactory-bulbectomized rats. Neuroendocrinology 32(5):266-71.
Nieto, P. S., et al.

2011 Expression of novel opsins and intrinsic light responses in the mammalian retinal ganglion cell line RGC-5. Presence of OPN5 in the rat retina. PLoS One 6(10):e26417.
Ninomiya, T, et al.

2002 Regulation of the alpha-fetoprotein gene by the isoforms of ATBF1 transcription factor in human hepatoma. Hepatology 35(1):82-7.
Nissilä, J., et al.

2012 Encephalopsin (OPN3) protein abundance in the adult mouse brain. J Comp Physiol A Neuroethol Sens Neural Behav Physiol.
Nogami, S., et al.

2005 ZFH4 protein is expressed in many neurons of developing rat brain. J Comp Neurol 482(1):33-49.
Nolan, P. M., et al.

2000 Implementation of a large-scale ENU mutagenesis program: towards increasing the mouse mutant resource. Mamm Genome 11(7):500-6.
Nordberg, J., and E. S. Arnér

2001 Reactive oxygen species, antioxidants, and the mammalian thioredoxin system. Free Radic Biol Med 31(11):1287-312.
Novak, C. M., and H. E. Albers

2004 Novel phase-shifting effects of GABAA receptor activation in the suprachiasmatic nucleus of a diurnal rodent. Am J Physiol Regul Integr Comp Physiol 286(5):R820-5.
Nowak, D. M., and M. Gajecka

2011 The genetics of keratoconus. Middle East Afr J Ophthalmol 18(1):2-6.
O'Neill, J. S., and A. B. Reddy

2011 Circadian clocks in human red blood cells. Nature 469(7331):498-503.
O'Neill, J. S., et al.

2011 Circadian rhythms persist without transcription in a eukaryote. Nature 469(7331):554-8.
Ohdo, S.

2010 Chrono-drug-delivery focused on biological clock: intra- and inter-individual variability of molecular clock. Adv Drug Deliv Rev 62(9-10):857-8.
Oklejewicz, M., et al.

2008 Phase resetting of the mammalian circadian clock by DNA damage. Curr Biol 18(4):286-91.
Panda, S., et al.

2005 Illumination of the melanopsin signaling pathway. Science 307(5709):600-4.
Panda, S., et al.

2003 Melanopsin is required for non-image-forming photic responses in blind mice. Science 301(5632):525-7.
Panda, S., et al.

2002 Melanopsin (Opn4) requirement for normal light-induced circadian phase shifting. Science 298(5601):2213-6.
Pittendrigh, C. S.

1993 Temporal organization: reflections of a Darwinian clock-watcher. Annu Rev Physiol 55:16-54.
Postigo, A. A., and D. C. Dean

1997 ZEB, a vertebrate homolog of Drosophila Zfh-1, is a negative regulator of muscle differentiation. EMBO J 16(13):3935-43.
—

1999 ZEB represses transcription through interaction with the corepressor CtBP. Proc Natl Acad Sci U S A 96(12):6683-8.
Preitner, N., et al.

2002 The orphan nuclear receptor REV-ERBalpha controls circadian transcription within the positive limb of the mammalian circadian oscillator. Cell 110(2):251-60.
Provencio, I., et al.

2000 A novel human opsin in the inner retina. J Neurosci 20(2):600-5.
Qi, Y, et al.

2008a Atbf1 is required for the Pit1 gene early activation. Proc Natl Acad Sci U S A 105(7):2481-6.
Qi, Y., et al.

2008b Atbf1 is required for the Pit1 gene early activation. Proc Natl Acad Sci U S A 105(7):2481-6.
Quwailid, M. M., et al.

2004 A gene-driven ENU-based approach to generating an allelic series in any gene. Mamm Genome 15(8):585-91.
Rabinowitz, Y. S.

1998 Keratoconus. Surv Ophthalmol 42(4):297-319.
Ralph, M. R., and M. Menaker

1988a A mutation of the circadian system in golden hamsters. Science 241(4870):1225-7.
—

1988b A mutation of the circadian system in golden hamsters. Science 241(4870):1225-7.
Reebs, S. G., and N. Mrosovsky

1989 Effects of induced wheel running on the circadian activity rhythms of Syrian hamsters: entrainment and phase response curve. J Biol Rhythms 4(1):39-48.
Reghunandanan, V., and R. Reghunandanan

2006 Neurotransmitters of the suprachiasmatic nuclei. J Circadian Rhythms 4:2.
Reppert, S. M., and D. R. Weaver

2001 Molecular analysis of mammalian circadian rhythms. Annu Rev Physiol 63:647-76.
Ridder, W. H., 3rd, and S. Nusinowitz

2006 The visual evoked potential in the mouse--origins and response characteristics. Vision Res 46(6-7):902-13.
Ripperger, J. A., I. Schmutz, and U. Albrecht

2010 PERsuading nuclear receptors to dance the circadian rhythm. Cell Cycle 9(13):2515-21.
Ruan, G. X., et al.

2008 An autonomous circadian clock in the inner mouse retina regulated by dopamine and GABA. PLoS Biol 6(10):e249.
Ruan, G. X., et al.

2012 Divergent roles of clock genes in retinal and suprachiasmatic nucleus circadian oscillators. PLoS One 7(6):e38985.
Shearman, L. P., et al.

1997 Two period homologs: circadian expression and photic regulation in the suprachiasmatic nuclei. Neuron 19(6):1261-9.
Shibuya, T., and K. Morimoto

1993 A review of the genotoxicity of 1-ethyl-1-nitrosourea. Mutat Res 297(1):3-38.
Shigeyoshi, Y., et al.

1997 Light-induced resetting of a mammalian circadian clock is associated with rapid induction of the mPer1 transcript. Cell 91(7):1043-53.
Shiromani, P. J., et al.

1995 Time course of phosphorylated CREB and Fos-like immunoreactivity in the hypothalamic supraoptic nucleus after salt loading. Brain Res Mol Brain Res 29(1):163-71.
Siepka, S. M., et al.

2007 Circadian mutant Overtime reveals F-box protein FBXL3 regulation of cryptochrome and period gene expression. Cell 129(5):1011-23.
Smeal, R. M., G. B. Ermentrout, and J. A. White

2010 Phase-response curves and synchronized neural networks. Philos Trans R Soc Lond B Biol Sci 365(1551):2407-22.
Sun, X, et al.

2005 Frequent somatic mutations of the transcription factor ATBF1 in human prostate cancer. Nat Genet 37(4):407-12.
Sun, X., et al.

2012 Heterozygous deletion of Atbf1 by the Cre-loxP system in mice causes preweaning mortality. Genesis.
Sun, X., et al.

2007 Infrequent mutation of ATBF1 in human breast cancer. J Cancer Res Clin Oncol 133(2):103-5.
Swerdlow, N. R., D. L. Braff, and M. A. Geyer

1990 GABAergic projection from nucleus accumbens to ventral pallidum mediates dopamine-induced sensorimotor gating deficits of acoustic startle in rats. Brain Res 532(1-2):146-50.
Takahashi, J. S., L. H. Pinto, and M. H. Vitaterna

1994 Forward and reverse genetic approaches to behavior in the mouse. Science 264(5166):1724-33.
Tanaka, T., et al.

2002 Endothelial PAS domain protein 1 (EPAS1) induces adrenomedullin gene expression in cardiac myocytes: role of EPAS1 in an inflammatory response in cardiac myocytes. J Mol Cell Cardiol 34(7):739-48.
Thaung, C., et al.

2002 Presence of visual head tracking differentiates normal sighted from retinal degenerate mice. Neurosci Lett 325(1):21-4.
Tian, H., et al.

1998 The hypoxia-responsive transcription factor EPAS1 is essential for catecholamine homeostasis and protection against heart failure during embryonic development. Genes Dev 12(21):3320-4.
Tian, H., S. L. McKnight, and D. W. Russell

1997 Endothelial PAS domain protein 1 (EPAS1), a transcription factor selectively expressed in endothelial cells. Genes Dev 11(1):72-82.
Tischkau, S. A., et al.

2003 Ca2+/cAMP response element-binding protein (CREB)-dependent activation of Per1 is required for light-induced signaling in the suprachiasmatic nucleus circadian clock. J Biol Chem 278(2):718-23.
Tyynismaa, H., et al.

2002 A locus for autosomal dominant keratoconus: linkage to 16q22.3-q23.1 in Finnish families. Invest Ophthalmol Vis Sci 43(10):3160-4.
Ueda, H. R., et al.

2002 A transcription factor response element for gene expression during circadian night. Nature 418(6897):534-9.
Uhrig, M., et al.

2008 Upregulation of CRABP1 in human neuroblastoma cells overproducing the Alzheimer-typical Abeta42 reduces their differentiation potential. BMC Med 6:38.
Unsal-Kaçmaz, K., et al.

2005 Coupling of human circadian and cell cycles by the timeless protein. Mol Cell Biol 25(8):3109-16.
van der Horst, G. T., et al.

1999 Mammalian Cry1 and Cry2 are essential for maintenance of circadian rhythms. Nature 398(6728):627-30.
Van Hook, M. J., and D. M. Berson

2010 Hyperpolarization-activated current (I(h)) in ganglion-cell photoreceptors. PLoS One 5(12):e15344.
VanDunk, C., L. A. Hunter, and P. A. Gray

2011 Development, maturation, and necessity of transcription factors in the mouse suprachiasmatic nucleus. J Neurosci 31(17):6457-67.
Vanselow, K., et al.

2006 Differential effects of PER2 phosphorylation: molecular basis for the human familial advanced sleep phase syndrome (FASPS). Genes Dev 20(19):2660-72.
Vieira, J., et al.

2012 Human cryptochrome-1 confers light independent biological activity in transgenic Drosophila correlated with flavin radical stability. PLoS One 7(3):e31867.
von Gall, C., et al.

1998 CREB in the mouse SCN: a molecular interface coding the phase-adjusting stimuli light, glutamate, PACAP, and melatonin for clockwork access. J Neurosci 18(24):10389-97.
Wager-Smith, K., and S. A. Kay

2000 Circadian rhythm genetics: from flies to mice to humans. Nat Genet 26(1):23-7.
Wang, L. M., et al.

2008 Role for the NR2B subunit of the N-methyl-D-aspartate receptor in mediating light input to the circadian system. Eur J Neurosci 27(7):1771-9.
Warnecke, C., et al.

2004 Differentiating the functional role of hypoxia-inducible factor (HIF)-1alpha and HIF-2alpha (EPAS-1) by the use of RNA interference: erythropoietin is a HIF-2alpha target gene in Hep3B and Kelly cells. FASEB J 18(12):1462-4.
Wassef, A., J. Baker, and L. D. Kochan

2003 GABA and schizophrenia: a review of basic science and clinical studies. J Clin Psychopharmacol 23(6):601-40.
Watanabe, M, et al.

1996 Developmental changes in expression of the ATBF1 transcription factor gene. Brain Res Mol Brain Res 42(2):344-9.
Weber, E. T., R. L. Gannon, and M. A. Rea

1995 cGMP-dependent protein kinase inhibitor blocks light-induced phase advances of circadian rhythms in vivo. Neurosci Lett 197(3):227-30.
Weger, B. D., et al.

2011 The light responsive transcriptome of the zebrafish: function and regulation. PLoS One 6(2):e17080.
Wehr, T. A., D. Aeschbach, and W. C. Duncan

2001 Evidence for a biological dawn and dusk in the human circadian timing system. J Physiol 535(Pt 3):937-51.
Welsh, D. K., et al.

1995 Individual neurons dissociated from rat suprachiasmatic nucleus express independently phased circadian firing rhythms. Neuron 14(4):697-706.
Welsh, D. K., J. S. Takahashi, and S. A. Kay

2010 Suprachiasmatic nucleus: cell autonomy and network properties. Annu Rev Physiol 72:551-77.
Wiseman, H., and B. Halliwell

1996 Damage to DNA by reactive oxygen and nitrogen species: role in inflammatory disease and progression to cancer. Biochem J 313 (Pt 1):17-29.
Xu, J, et al.

2006 Germline ATBF1 mutations and prostate cancer risk. Prostate 66(10):1082-5.
Xu, Y., et al.

2007 Modeling of a human circadian mutation yields insights into clock regulation by PER2. Cell 128(1):59-70.
Yamaguchi, S., et al.

2000 Role of DBP in the circadian oscillatory mechanism. Mol Cell Biol 20(13):4773-81.
Yasuda, H, et al.

1994a ATBF1, a multiple-homeodomain zinc finger protein, selectively down-regulates AT-rich elements of the human alpha-fetoprotein gene. Mol Cell Biol 14(2):1395-401.

Yasuda, H., et al.

1994b ATBF1, a multiple-homeodomain zinc finger protein, selectively down-regulates AT-rich elements of the human alpha-fetoprotein gene. Molecular and Cellular Biology 14(2):1395-401.

Yellore, V. S., et al.

2012 Analysis of the role of ZEB1 in the pathogenesis of posterior polymorphous corneal dystrophy. Invest Ophthalmol Vis Sci 53(1):273-8.

Yoo, S. H., et al.

2005 A noncanonical E-box enhancer drives mouse Period2 circadian oscillations in vivo. Proc Natl Acad Sci U S A 102(7):2608-13.

Yun, K., and B. Wold

1996 Skeletal muscle determination and differentiation: story of a core regulatory network and its context. Curr Opin Cell Biol 8(6):877-89.

Zadnik, K., et al.

2002 Between-eye asymmetry in keratoconus. Cornea 21(7):671-9.

Zhang, Z., et al.

2005 ATBF1-a messenger RNA expression is correlated with better prognosis in breast cancer. Clin Cancer Res 11(1):193-8.

Zheng, B., et al.

2001 Nonredundant roles of the mPer1 and mPer2 genes in the mammalian circadian clock. Cell 105(5):683-94.

Zheng, B., et al.

1999 The mPer2 gene encodes a functional component of the mammalian circadian clock. Nature 400(6740):169-73.